THE PREPARATION AND CHARACTERIZATION OF HOLLOW FIBRE MEMBRANES FOR GAS SEPARATION.

by

Simon Charles Senn

A thesis submitted in accordance with the requirements for the degree of Doctor of Philosophy under the supervision of Dr. G.C. East and Prof. J.E. McIntyre.

Department of Textile Industries,

The University of Leeds,

Leeds, LS2 9JT.

October 1988.

ABSTRACT.

A dry-jet wet-spinning process developed industrially for the preparation of hollow fibre membranes suitable for gas separation applications, has been reproduced on a laboratory scale. Polysulphone hollow fibres were spun from a variety of solvents and their gas transport properties were characterized using equipment built during the course of the research.

The phase inversion process of membrane formation was studied in order that the best morphological structure could be produced. The spinning parameters were studied to establish their influence on the fibre dimensions. Further relationships were then sought between the gas transport properties and the fibre dimensions and spinning parameters.

The behaviour of the membranes to both single gases and gas mixtures was studied. Both the permeation rate constants and the separation factors determined from the mixture permeation were found to be lower than the values predicted from the single gas permeation experiments. A model was developed to help understand the competitive nature of the adsorption-diffusion process and explain the differences in values recorded from the single gas and mixture studies.

Experiments aimed at improving membrane performance were based on modification of the already established polysulphone hollow fibre. Modification of the selective surface layer of the hollow fibre membranes was considered to be the best approach. Coating of the fibres, other than to repair damage to the skin layer, was found to result in too large a decrease in permeability. Sulphonation of the surface layer was achieved using sulphur trioxide, although little improvement in the membrane performance was recorded. The sulphonation experiment results were, however, sufficiently encouraging to recommend future work.

This thesis is dedicated to Dr. V.

Rogers, whose patience and help enabled a

colour chemist to become a fibre spinner.

Nonumque prematur in annum

Membranis intus positis:

delere licebit

Quod non edideris;

nescit vox missa reverti.

HORACE 65-8 B.C.

ACKNOWLEDGEMENTS.

The author would like to acknowledge the contribution of all who helped him during the course of the research, namely:-

S.E.R.C and British Gas plc for funding the research.

Dr. G.C. East and Prof. J.E. McIntyre for their supervision, guidance and encouragement.

Dr. V. Rogers for his instruction in spinning and other related matters.

Dr. G. O'Hair, Dr. B.Laverty, Dr. R. Fielding, Dr. T. Foley and Mr. M. Dongworth of British Gas London Research Station for their assistance and training in the subject of gas transport measurements.

Mr. T. Buckley for generating the SEM images of the hollow fibres.

Mr. L. Johnson for the TGA data from which the solvent retention results were obtained.

Miss H. Dyson for reproducing the plates for this thesis.

and finally to Dr. J.T. Guthrie who persuaded the author to undertake the research.

CONTENTS.

List of Figures.

List of Tables.

List of Plates.

List of Symbols.

A	Membrane area.
a	Rate of injection of internal coagulant (WIR).
b	Hole affinity constant.
C	Concentration.
C_D	Concentration of normal diffusible species.
C_H	Concentration of permeant molecules sorbed into macrovoids.
C'_H	Hole saturation constant.
C_h	Penetrant concentration at high pressure membrane interface.
C_l	Penetrant concentration at low pressure membrane interface.
D, D_o	Diffusion coefficient.
$D_{(C)}$	Concentration dependent diffusion coefficient.
$D_{(C,t)}$	Concentration and time dependent diffusion coefficient.
D_{eff}	Effective diffusivity.
d_f	Total fibre diameter.
d_i	Lumen diameter.
d_w	Wall thickness.
E_d	Activation energy of diffusion.
E_p	Activation energy of permeation.
F_d	Fractional contribution to solubility parameter of dispersion bonding forces.
F_h	Fractional contribution to solubility parameter of hydrogen bonding forces.
F_p	Fractional contribution to solubility parameter of polar bonding forces.
F_P	Polar molar cohesion constant for a functional group.
F_T	Molar cohesion constant for a functional group.
h	Planck's constant.

J	Rate of diffusion through a unit area or diffusive flux.
K	Henry's law constant.
k	Boltzmann's constant.
l	Effective length of pore; Hollow fibre length.
M	Molecular weight.
N	Avogadro's number.
n	Number of fibres in module.
P, P_o	Permeability Coefficient.
$'P$	Permeation rate constant (permeability per unit of effective thickness of membrane).
P'_o, D'_o, S'_o	Pre-exponential factors.
p	Pressure.
p_h	Pressure at high pressure membrane interface.
p_l	Pressure at low pressure membrane interface.
Q	Permeation rate (total flow rate of permeant through the membrane).
q	Rate of void production.
R	Resistance (to permeate flow or electrical); Universal gas constant.
R_D	Molecular rate of diffusion.
r	Pore radius.
S	Rate of fibre wind up (WUS).
S_o	Solubility coefficient.
$S_{(C)}$	Concentration dependent solubility coefficient.
$S_{(p)}$	Pressure dependent solubility parameter.
T	Absolute temperature.
T_b	Boiling point of solvent.
T_c	Critical temperature of solvent.
T_g	Glass transition temperature.
t	Time.
V	Rate of dope extrusion (PER); Potential difference.
V_m	Molar volume of solvent.

W	Weight.
w_i^h	Partial pressure of component i at the high pressure interface.
w_i^l	Partial pressure of component i at the low pressure interface.
X	Mole fraction; Fractional concentration of polymer in dope by weight.
x	A position within a membrane.
y	Mean diffusion jump distance.
z	Thickness of membrane (Effective thickness).
α	Separation factor.
$\dot{\gamma}$	Shear rate.
ΔC	Concentration gradient.
ΔG^*	Change in free energy of formation of a diffusion transition state.
ΔH_s	Enthalpy of solution.
Δp	Pressure difference across a membrane (differential pressure).
ΔT	Lynderson atomic & group constant for critical temperature.
Δw_i	Partial pressure difference of component i across a membrane.
δ_d	Dispersion bonding solubility parameter.
δ_h	Hydrogen bonding solubility parameter.
δ_p	Polar bonding solubility parameter.
$_T$	Total solubility parameter.
η	Viscosity.
Π	Pseudo permeation rate constant.
ρ	Density.
ρ_d	Density of dope.
ρ_f	Density of fibre.
ρ_p	Bulk density of the polymer.
Φ	Enrichment factor.
Ω	Selectivity.

List of Abbreviations.

aq	Aqueous.
Co.Cf.	Correlation Coefficient.
C.R.G.	Catalytic Rich Gas process.
d_f	Total fibre diameter, outer diameter.
d_i	Internal diameter, diameter of fibre lumen.
DMAc	Dimethyl acetamide.
DMF	Dimethyl formamide.
d_w	Wall thickness.
E.O.R.	Enhanced Oil Recovery.
Fa	Formamide.
GPR	General Purpose Reagent.
GPU	Gas Permeability Units.
KM35	A Victrex sulphonated poly(ether sulphone).
KM36	A Victrex sulphonated poly(ether sulphone).
LER	Linear Extrusion Rate.
Obs	Observed result.
OFN	Oxygen Free Nitrogen.
PAPI	Polymer Assisted Phase Inversion process.
PER	Polymer Extrusion Rate.
plc	Public Limited Company.
Pre	Predicted result.
PSA	Pressure Swing Adsorption.
psi	Pounds per Square Inch (Gauge).
PSf	Polysulphone.
P1700	A Udel polysulphone.
P3500	A Udel polysulphone.
RM	Resistance Model.

rpm	revolutions per minute.
SEM	Scanning Electron Microscopy.
S.N.G.	Substitute Natural Gas.
TGA	Thermo-Gravimetric Analysis.
WIR	Water Injection Rate.
WUS	Wind-Up Speed.
$^{w}/_{w}$	Weight for Weight.
1-Fp	1-Formylpiperidine.
200P	A Victrex poly(ethersulphone).

CHAPTER I

Introduction

1.1 Separation science in the gas industry - the project objectives.

British Gas plc, the co-sponsors of this work, are the leading suppliers of gaseous products in the United Kingdom. Gas separation and purification are fundamental processes in the production of fuel gases and British Gas are currently examining areas in which membrane technology could be used to facilitate practical and economic gas separations. The objective of the autjor's project was to develop a hollow fibre membrane system which could separate the gas mixtures commonly encountered in fuel gas production. This was achieved by an investigation of the hollow fibre spinning process in order that elucidation of the relationships between spinning parameters and fibre morphology, and between fibre morphology and gas transport properties might be determined. Such information could then be used to enable membranes to be produced with superior permselective behaviour. In addition, the effect of acidic and basic groups in the membrane structure on the permselectivity was to be examined.

1.1.1 Specific separations of interest.

Laverty and O'Hair [1] have indicated in a recent paper the two main areas where gas separation is required, namely hydrogen recovery and carbon dioxide removal. Each of these areas is briefly examined below.

Hydrogen Recovery.

A substantial part of the British Gas research effort has been devoted, over the past few years, to the development of processes to produce Substitute Natural Gas (S.N.G.) from light oil fractions and coal. S.N.G. is produced using, for example, the Catalytic Rich Gas (C.R.G.) process. The catalysts used in this process are susceptible to poisoning by sulphur-containing compounds present in the feed stock,

which must be removed by a hydrodesulphurisation stage. For reasons of economy unreacted hydrogen is recycled after separation from the other gases.

Carbon dioxide removal.

Carbon dioxide occurs in some natural gases. Several of the more recently discovered North Sea gas fields contain appreciable percentages of carbon dioxide. Carbon dioxide is undesirable in natural gas streams for three main reasons. Firstly, it reduces the calorific value of a given volume of gas and removal may be necessary if the gas company is to meet the government standards relating to gas supply. Secondly, carbon dioxide will combine with water to produce carbonic acid. This acid is capable of causing corrosive damage to pipelines and other transmission equipment. Finally, the carbon dioxide adds extra volume to the gas which is transmitted. If the carbon dioxide was removed at the well head then considerable amounts of money could be saved from the reduced compression power required and also from the reduction in size of the pipelines.

Carbon dioxide may also be produced in large quantities during the S.N.G. processing. Up to 50% CO_2 may be present after certain stages in the production. At these high levels efficient separation is of the utmost importance to maximise the yield of methane. The term 'slippage' is used to evaluate the amount of methane lost when the carbon dioxide is extracted. The amount of slippage is an important factor in the economic evaluation of a separation process.

Finally, a process has been developed in which underground oil reservoirs with insufficient underground pressure to drive oil to the surface may be tapped. The process is known as Enhanced Oil Recovery (E.O.R.) and a schematic representation of the process is shown in Fig 1.1. Carbon dioxide is pumped into the underground oil bearing rock where it mixes with the oil and forces the oil to the surface through the

Fig 1.1 A schematic representation of enhanced oil recovery.

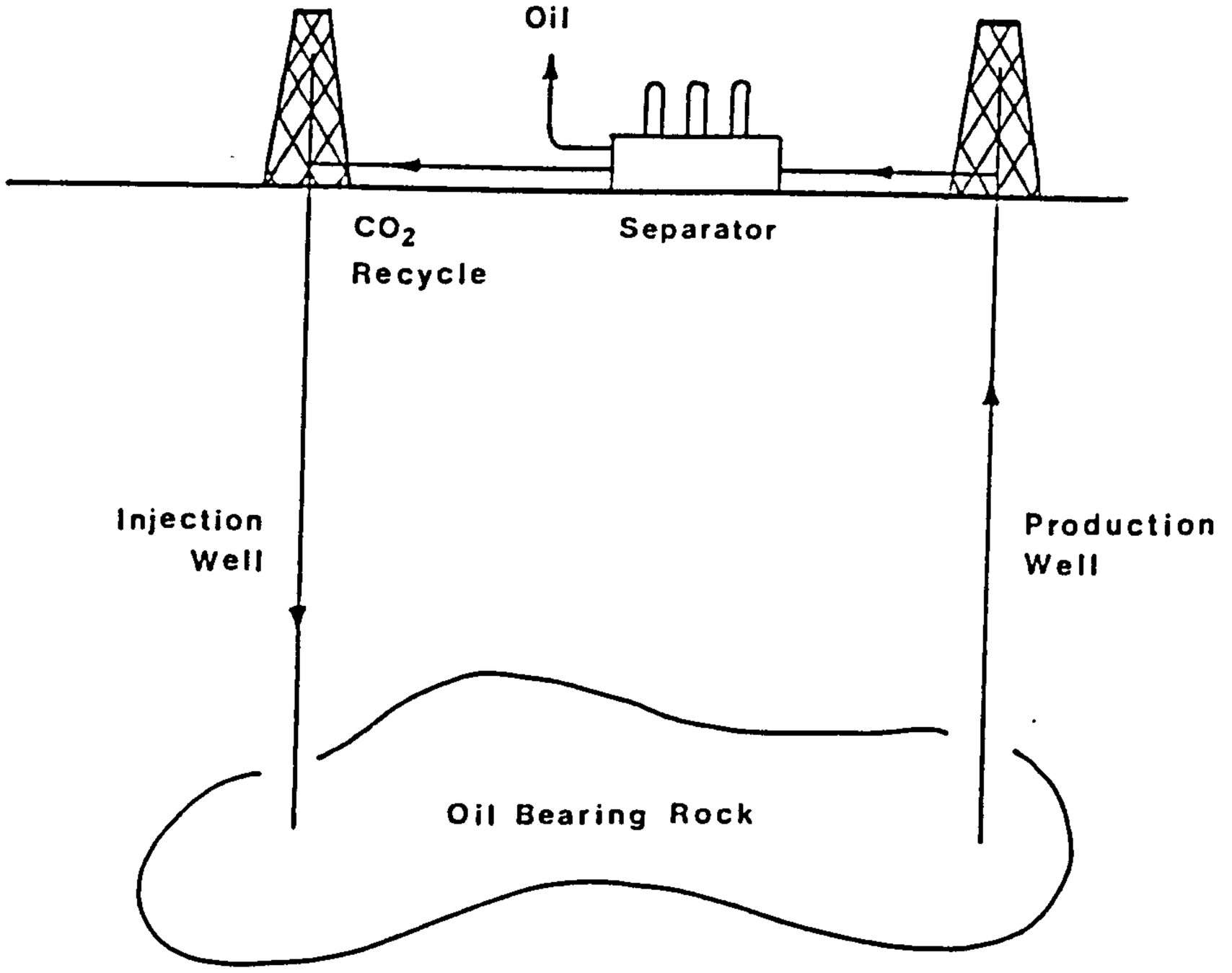

production well. The mixture at the surface contains up to 80% CO_2 which is separated from the oil and recycled back into the injection well. This process was developed for on-shore recovery, but off-shore use could enable presently uneconomic wells to become profitable.

1.1.2 Existing and competing technology.

If membrane technology is to replace existing technology it must be able to outperform the established processes on both economic and technical grounds. To determine the nature of the competition the three main conventional processes are described below, together with their strengths and weaknesses. The details of this section were obtained from Kohn and Riesenfeld [2], MacLean [3], Baldus and Tillmann [4], Kirkby [5], Maddox [6], and Laverty and O'Hair [1]. Further in-depth details may be obtained from these references.

Cryogenic processes [3].

Cryogenic separations involve low temperature distillation techniques. The gas mixture to be separated is cooled to a liquid and then distilled into its component fractions by a series of vaporization and condensation stages. The process has become well established in the last 90 years, evolving its operating systems to high efficiency. The high energy cost required to liquefy the gases is largely recovered by the high degree of heat integration possible in well designed plants. Cryogenic processes have a clear advantage over other methods in that products of highest purity are produced; and the high purity by-products can also be sold profitably. Where the end-product is required in liquid form the cryogenic process is even more attractive as it saves the energy costs incurred for compression that are required by competitive processes.

Cryogenic processing has several drawbacks. The process has a high degree of inherent inflexibility. Each plant is designed for a specific separation and set of operating conditions. Installations are exceedingly expensive and are only viable for very large processing

Absorption [2,3].

Absorption is a process in which a 'sour' gas is 'scrubbed' with a liquid which selectively dissolves the impurities of the sour gas to leave a 'sweet' gas product. Fig 1.2 shows a simplified plant layout. The impurities are absorbed into a liquid solvent in the absorber column. The solution of impurities is then pumped into the stripper column where the solvent is regenerated and the impurities released.

Absorption units are common in the chemical industry. Acid gas removal is commonly achieved by absorption processes. For example, the Benfield process uses hot potassium carbonate at high pressures to absorb carbon dioxide. The carbon dioxide is subsequently stripped from the potassium carbonate at low pressure. Alkanolamines are important absorbers for both carbon dioxide and hydrogen sulphide. The Rectisol process, yet another alternative, uses methanol as the solvent. In any absorption process, the effectiveness of the treatment is governed by the solubility of the constituents in the chosen liquid and by the mass transfer rates in solution.

Adsorption.[3]

Adsorption differs from absorption in that adsorption is a surface phenomenon. Absorption can be either a physical or chemical process whereas adsorption can only be a physical process. Separation occurs by one component of the mixture being preferentially adsorbed onto a fixed solid substrate. Many materials will adsorb small molecules; however, for a potential adsorbent to be considered it must satisfy three criteria. Firstly, it must have a large surface area to volume ratio in

Fig 1.2 A schematic representation of an absorption plant.

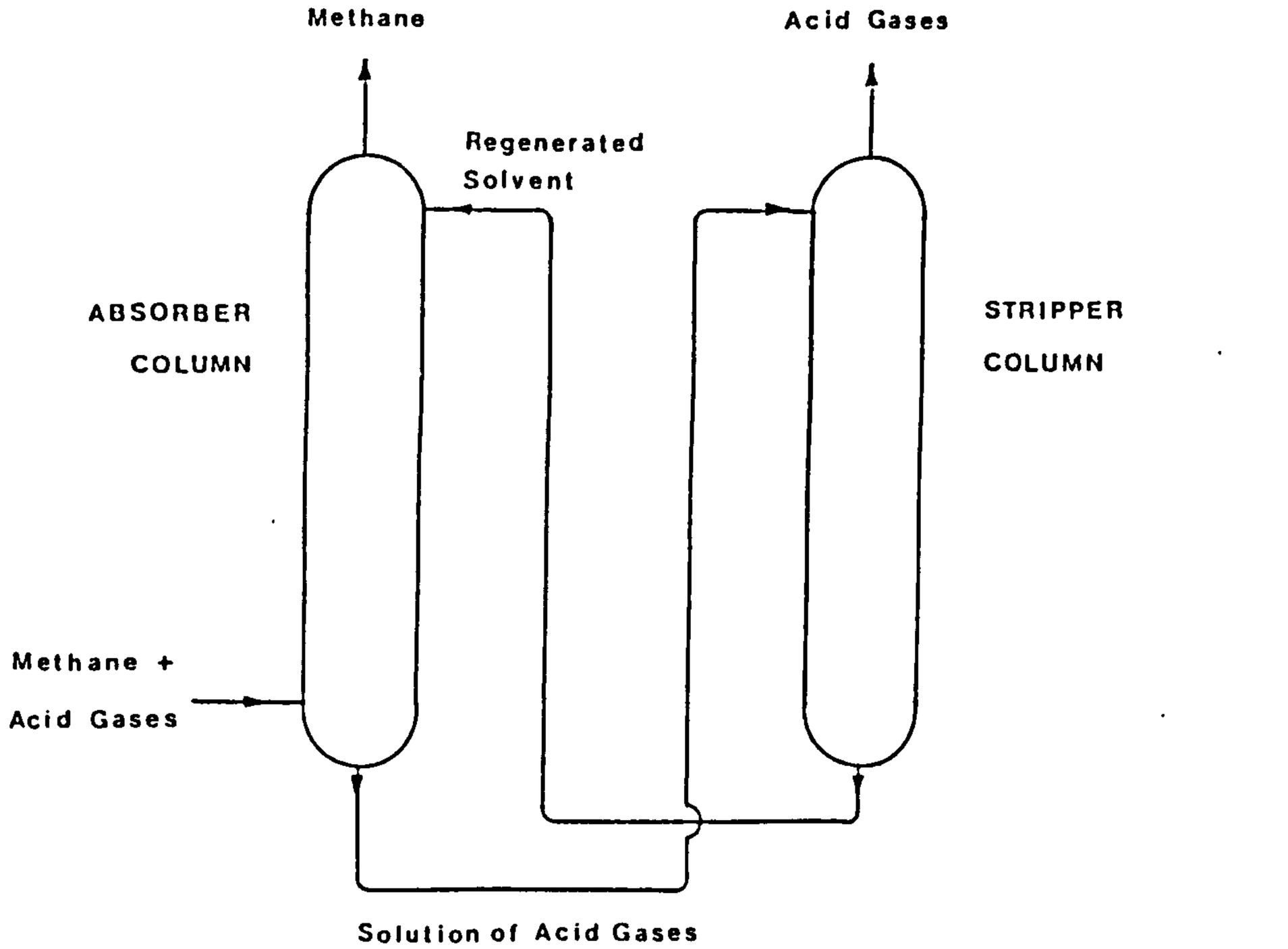

Fig 1.3 A schematic representation of a P.S.A. cycle.

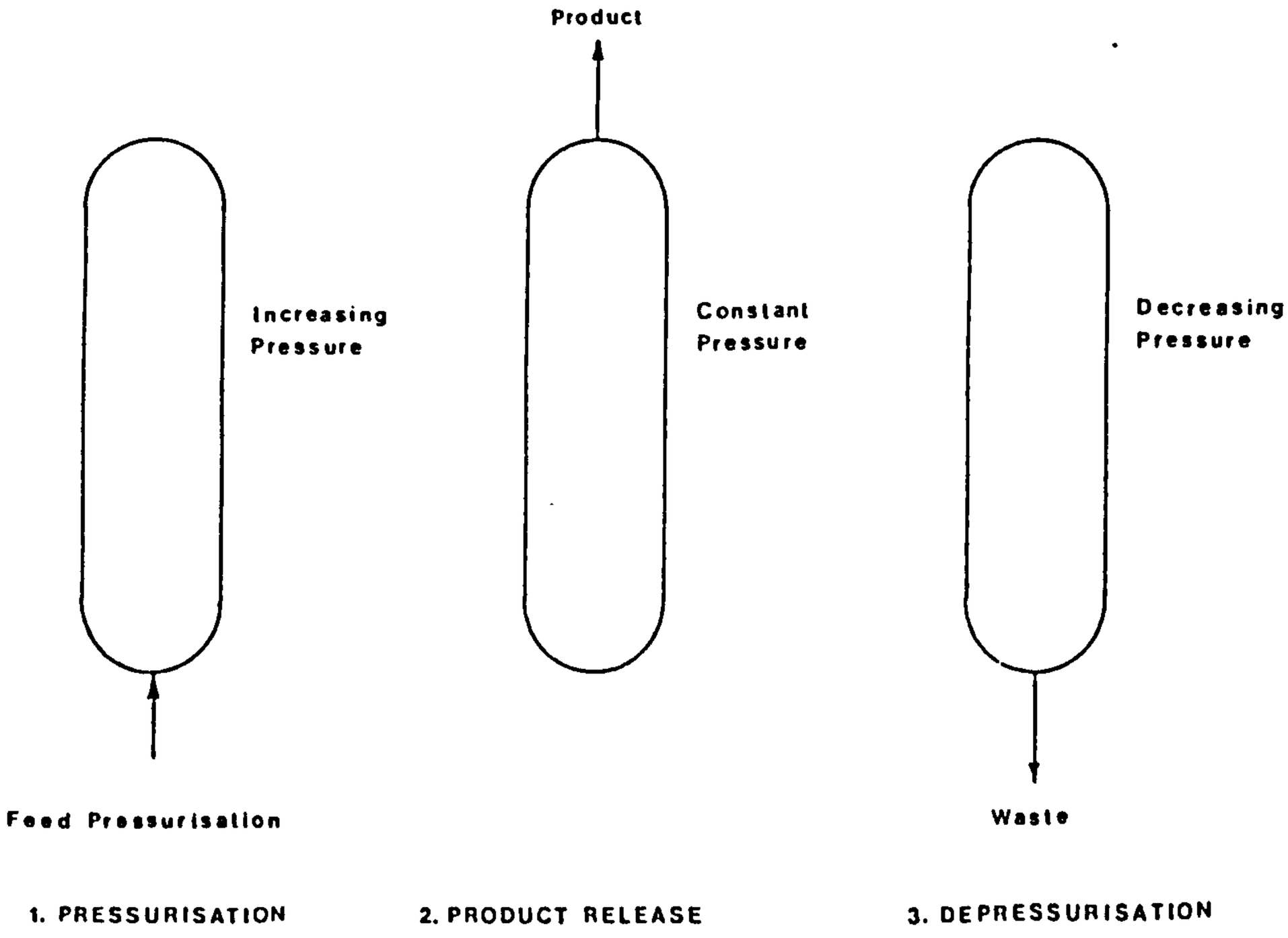

order for it to provide enough active sites for adsorption. Secondly, the process of adsorption must be reversible, i.e. the gas molecules must desorb easily under certain conditions. Finally, the adsorbent must be selective, or a separation would not be possible. Commonly used adsorbents are solids possessing a very high porosity such as activated carbons and zeolites. The adsorption process is governed by the partial pressures of the gases and the operating temperature. The effectiveness is measured in terms of the mass transfer rates.

Parameter swing adsorption processes, such as pressure swing adsorption (P.S.A.) operate in a batch-like manner. Several beds are required, operating out-of-phase with each other, to produce a continuous product flow. Three steps make up most P.S.A. cycles and these are represented in Fig 1.3. There are two fundamental problems with the basic cycle in that both the yield and purity are poor. Enhancement of purity may be achieved with the use of greater pressure in the initial stage, but as the selectivity of most adsorbers is not great this results in a high slippage. Some molecular sieve adsorbers, however, do have excellent selectivity making the process highly efficient. As P.S.A. is relatively cheap to install, many units are in operation throughout the world, many of them separating hydrogen, carbon dioxide and methane.

1.2 Membrane technology.

There has been a rapid explosion in scientific research into membrane science in the last thirty years, so much so that this section does not presume to be a comprehensive review of the progress made in those thirty years. However, a fairly broad knowledge of the field may be obtained from the excellent reviews by Lonsdale [8] and Michaels [9]. Other papers worthy of inspecting are by Matson [10], Henis and Tripodi [11], Cooper [12], Cabasso [13,14], and Vieth [15]. Many books have been written of which the most notable are by Lloyd [16], Kesting [17], Sourirajan [18], Lonsdale and Podall [20], Lacey and Loeb [21], Meares [22], Crank and Park [23] and Comyn [24]. Reviews of patent literature have been produced on hollow fibres by Scott [25] and on reverse osmosis by Hoornaert [26].

1.2.1 A brief history [8].

Membranes have been in use on this earth for over 3000 million years - as long as life itself. As organisms evolved, their need to accomplish more and more complicated biological processes grew. Membranes evolved for this function. Membranes, then, have been in existence for a very long time, but knowledge of their behaviour was only discovered 240 years ago when J.A.Nollet described his observations on the semipermeable nature of animal bladders. Nollet was the first person to describe osmotic pressure, but it was T.Graham and A.Fick who first realised the significance of this phenomena. Both men developed laws of diffusion and additionally Fick prepared the first synthetic membrane from cellulose nitrate called 'collodion' and Graham was one of the first to observe different rates of permeation through rubber of various gases [28]. Working with natural membranes, Graham also

conducted the first dialysis experiments. From these early beginnings synthetic membrane technology has evolved into six main areas namely:-

Microfiltration

Ultrafiltration

Dialysis

Electrodialysis

Reverse osmosis

Gas separation

Fig 1.4, adapted from Lonsdale's excellent review [8] depicts clearly the differences between these six membrane separation processes.

Much research was done following the work of Graham and Fick but industrial usage of membranes was slow to follow. The first major application occurred during World War II [27] in a process developed to isolate U^{235} in the form of its hexafluoride. Due to the high value of the product the costs of the process were relatively unimportant. In order to concentrate the U^{235} to 90%, 4000 separation stages were required involving a power consumption of over 200 MW.

Overall, the early membranes were not suitable for industrial use. They were fabricated into thick, non-porous films and had very poor permeability. Additionally the membranes were not highly selective making a clean separation only possible with multistage processing. Due to low energy costs, distillation was the preferred method for most separation applications.

Membranes were only taken seriously in industry after the work of Loeb and Sourirajan [32] in which they fabricated the first asymmetric porous membranes for reverse osmosis, an asymmetric membrane being a porous polymeric matrix with a thin dense skin layer at the surface. These revolutionary membranes had much higher mass transport rates than conventional membranes and this was attributed to the membrane

Fig 1.4 Membrane separation processes.

Process	Concept	Materials Passed	Driving Force	Materials Retained
Micro-filtration	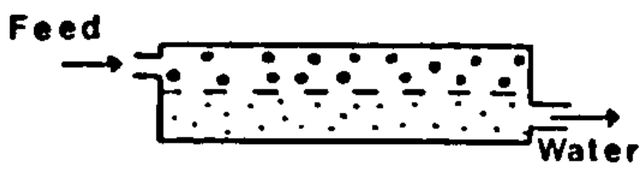	Water and dissolved species	Pressure difference (~10 psi)	Suspended matter (Silica, bacteria, etc.)
Ultra-filtration	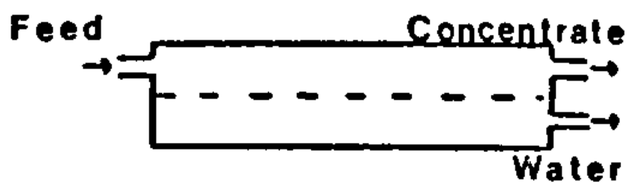	Water and salts	Pressure difference (10 - 100 psi)	Biologicals, colloids and macromolecules.
Dialysis	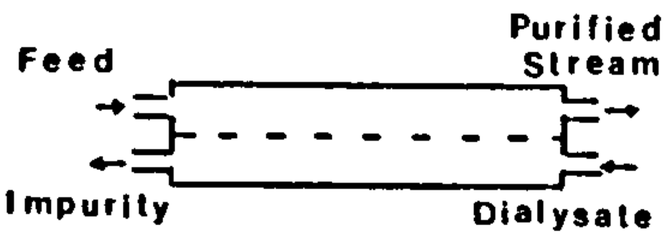	Ions and low Mol.Wt organics. (Urea etc.)	Conc. difference	Dissolved & suspended material with Mol.Wt>1000
Electro-dialysis	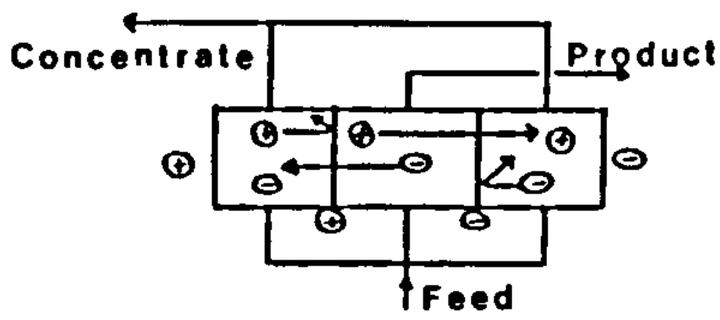	Ions	Voltage (1 - 2 V)	All non-ionic & macromolecular species.
Reverse Osmosis	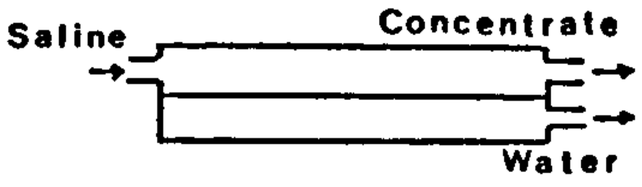	Water	Pressure difference (100 - 800 psi)	Virtually all suspended and dissolved matter
Gas Separation		Gases and Vapours	Pressure difference (1 - 100 atm)	Membrane-impermeable gases and vapours.

morphology. Only the skin layer (0.1-0.2 μm in thickness) held any resistance to mass transport, the bulk of the membrane acting merely as a support for the permselective skin. Conventional membranes of the time were commonly 100-200 μm in thickness whilst the effective thickness of an asymmetric membrane was of the order of a thousand times less.

Another important innovative step in the pathway to profitable membrane based gas separations was the development of the hollow fibre membrane. The first recorded use of tubular membranes was in 1913 when Abel, Rowntree and Turner were working on artificial kidney dialysis. DuPont de Nemours Inc later researched into the possibility of using polyamide hollow fibres to separate gases but it was the Monsanto company who found the first commercial success in membrane gas separation in 1979 when they launched the PRISM separator. The PRISM separators contain hollow fibres spun from polysulphone. Part of their success was due to the composite nature of their asymmetric structure. The fibres were thinly coated with a highly permeable film of silicone elastomer. This outer coating was present not to add a permselective layer but to fill in any defects or surface pores present in the skin layer of the membrane. The result of this was a membrane having the same selectivity as a non-porous dense polysulphone membrane but with the high permeability of a Loeb-Sourirajan asymmetric membrane. The inventors, Henis and Tripodi, refer to these membranes as RM composites after the Resistance Model that they developed [38].

Other composite membranes are presently being investigated, which are mainly of a type designed to add a thin pin hole-free permselective layer to existing membranes. One of the most promising techniques uses plasma polymerization in which a membrane is subjected to a gas or vapour plasma which allows surface polymerization takes place [79].

1.2.2 Theory of gaseous permeation.

The permeation of a gas through an asymmetric hollow fibre membrane involves a set of complex processes. In this section a stepwise approach is made to split up the the various mechanisms of permeant transport. Each of the following theories could be seen to be relevant to the permeation of a gas through a hollow fibre membrane and a knowledge of these theories can help in the selection of suitable membrane materials.

The permeation of a gas through a non-porous rubbery polymer.

The work of Graham [28] in 1866 was sufficiently advanced for it to be still the underlying theory supporting the permeation process today. Since then many people have added refinements to the theory. Stern [29] has presented an excellent paper on the development of the theory and his paper has been used to make up the nucleus of this subsection. Additional information was obtained from Crank and Park [23], Rogers [30], and Rattee and Bruer [31].

There are five stages in the permeation process.

(i) Adsorption of the gas penetrant at one side of the gas-solid interface.

(ii) Solution of the penetrant into the polymer.

(iii) Diffusion of the penetrant in solution to the opposite gas-solid interface.

(iv) Desolvation of the penetrant from the polymer at the interface.

(v) Desorption of the penetrant from that interface.

The permeation process thus involves both diffusion kinetics and solution mechanisms.

Fick's first law of diffusion can be used to account for the diffusion of the penetrant inside the membrane. This law is commonly

expressed in the following form for one-dimensional diffusion.

$$J = -D\left(\frac{\delta C}{\delta x}\right) \tag{1.1}$$

where J is the rate of diffusion through a unit area, or diffusive flux; D is the diffusion coefficient of the particular system; and C is the concentration of penetrant at a point x within the membrane.

Unfortunately the diffusion coefficient is not always a constant. It can behave as a function of penetrant concentration and so Fick's second law is used for time dependent diffusion processes.

$$\frac{\delta C}{\delta t} = D\left(\frac{\delta^2 C}{\delta x^2}\right) \tag{1.2}$$

where $\delta C/\delta t$ is the rate of change of concentration at position x with time.

So far only the kinetics of the diffusional transport of the penetrant within the membrane have been considered as this is often the rate controlling step. However, the concentration of the penetrant in the membrane is a function of the solubility of the penetrant in the polymer. Henry's law relates the equilibrium concentration of dissolved penetrant to the partial pressure, i.e.

$$p = KC \tag{1.3}$$

where p is the pressure and K is the Henry's law constant. Commonly the inverse of K is taken and defined as the solubility coefficient, S_o. Henry's law constant may also be concentration dependent, usually at higher concentrations.

For dilute solutions $C = S_o p$ (1.4)

At higher concentrations $C = S_{(C)} p$ or $C = S_{(p)} p$ (1.5)

Four situations can arise through the dependence of these coefficients on other factors. Detailed examples of the following four situations are given by Stern [29].

(i) $D = D_o$ and $S = S_o$ where both diffusion and solubility coefficients are constants.

(ii) $D = D_{(C)}$ and $S = S_o$ where the diffusion coefficient is concentration dependent but Henry's law is obeyed.

(iii) $D = D_{(C)}$ and $S = S_{(C)}$ where both the diffusion and solubility coefficients are concentration dependent.

(iv) $D = D_{(C,t)}$ and $S = S_{(C)}$ where both the coefficients are concentration dependent and diffusion is also time dependent.

Using the simplest case, (i), the rate of permeation is controlled by the rate of diffusion. Integrating equation (1.1) across the thickness of the membrane (z) produces:-

$$J = D_o \frac{(C_h - C_l)}{z} \qquad (1.6)$$

where C_h and C_l are the penetrant concentrations at the high and low pressure sides of the membrane respectively. Expressing the system in terms of penetrant pressure by combining equations (1.6) and (1.4) gives:-

$$J = D_o S_o \frac{(p_h - p_l)}{z} \qquad (1.7)$$

Commonly the product $D_o S_o$ is expressed as the permeability coefficient, P_o.

$$J = P_o \frac{(p_h - p_l)}{z} \qquad (1.8)$$

Where the diffusion coefficient is concentration dependent, integration of Fick's second law across the thickness of the membrane produces:-

$$J = \frac{1}{z}\int_{C_l}^{C_h} D_{(C)}\, dC \qquad (1.9)$$

and hence;-

$$J = \overline{D} \frac{(C_h - C_l)}{z} \qquad (1.10)$$

$$\text{where } \overline{D} = \frac{1}{(C_h - C_l)} \int_{C_l}^{C_h} D_{(C)}\, dC \qquad (1.11)$$

Rogers [30] has shown that this can be written in terms of pressure:-

$$J = \overline{D} \frac{C_h - C_l}{p_h - p_l} \frac{p_h - p_l}{z} = \overline{\overline{DS}} \frac{(p_h - p_l)}{z} \qquad (1.12)$$

$$\text{where } \overline{S} = \frac{C_h - C_l}{p_h - p_l} \qquad (1.13)$$

For a planar membrane of thickness z and area A:-

$$Q = J\,A = \overline{P}\,A \frac{(p_h - p_l)}{z} \qquad (1.14)$$

where $\bar{P} = \bar{D}\ \bar{S}$ (1.15)

and Q = the total flow of permeant through the membrane.

The permeability coefficient can also exhibit a dependence on temperature. In the simple cases the relationship is of the Arrhenius type:-

$$P_o = P'_o \exp \frac{-E_p}{R\ T} \quad (1.16)$$

where E_p is the activation energy for permeation and the pre-exponential factor P'_o is associated with the free volume of the polymer. P_o can be further expanded to produce Arrhenius type relations for D_o and S_o:-

$$D_o = D'_o \exp \frac{-E_d}{R\ T} \quad (1.17)$$

$$S_o = S'_o \exp \frac{-\Delta H_s}{R\ T} \quad (1.18)$$

where E_d is the activation energy of diffusion and ΔH_s is the enthalpy of solution.

Rattee and Bruer [31] use Eyring's more detailed interpretation of equation (1.17). Eyring assumes that when a molecule diffuses from one position to another it passes through a transition state. The free energy of formation of the transition state (ΔG^*) can be seen to be analogous to the activation energy of diffusion (E_d)

$$D_o = \frac{k\ T}{h}\ y^2 \exp \frac{-\Delta G^*}{R\ T} \quad (1.19)$$

where k is Boltzmann's constant; h is Planck's constant; T the absolute temperature; and y is the average distance of a jump between two holes.

The enthalpy of solution from equation (1.18) is the sum of two further terms, namely the enthalpy of condensation of the penetrant and the enthalpy of mixing of condensed penetrant with polymer molecules.

The overall effect of the temperature is to control the segmental motion of the polymer chains, which in turn controls the formation of holes and thus the diffusion rate.

Permeation of mixtures in non-porous membranes [33].

Where gas penetrants do not interact with each other, the rate of permeation of a particular permeant is the same as for single gas permeation (equation (1.7)) except for the fact that the driving force is the partial pressure difference of the permeant across the membrane thickness.

$$J_i = P_{o,i} (w_i^h - w_i^l) \qquad (1.20)$$

where $P_{o,i}$ is the permeability coefficient of the membrane to permeant i; and w_i^h and w_i^l are the partial pressures of permeant i at the high and low pressure interfaces respectively.

Meares [33] defines the separation factor α_j^i for an experimental separation as:-

$$\alpha_j^i = \frac{w_i^l / w_j^l}{w_i^h / w_j^h} = \frac{J_i / w_i^h}{J_j / w_j^h} \qquad (1.21)$$

and the selectivity Ω_j^i, which is a function only of the membrane material, permeants and temperature as:-

$$\Omega_j^i = \frac{D_{o,i}\ S_{o,i}}{D_{o,j}\ S_{o,j}} \qquad (1.22)$$

Combination of equations (1.20) - (1.22) shows how the separation factor is related to the selectivity:-

$$\alpha_j^i = \Omega_j^i \left\{ \frac{1 - (w_i^l / w_i^h)}{1 - (w_j^l / w_j^h)} \right\} \qquad (1.23)$$

The selectivity represents the best separation achievable, whilst the separation factor is the actual separation encountered during an experiment. Due to this fact, some workers refer to the selectivity as the ideal separation factor.

The above equations relate to situations where permeants do not interact with each other. Where interactions do take place the problems become much more complex. Another complicating factor arises when a permeant is highly soluble in the polymeric material. This tends to plasticize the polymer causing an increase in the chain mobility resulting in an increase in the permeation rate of all penetrants.

Permeation of gas through glassy polymers [15]

Vieth et al. [15] have produced a comprehensive review of the development of theories explaining permeation in glassy polymers.

In experiments on glassy polymers the above theories did not fit the data obtained. Meares [34] discovered that the glassy polymer poly(vinyl acetate) was able to sorb a greater amount of gas than was predicted by Henry's law and postulated that polymers below their glass transition temperature (T_g) contain microvoids immobilised in the polymer structure. These holes adsorb a portion of the permeating gas on their

high energy surfaces. Meares noted that measurements of the diffusion coefficients involved some gas adsorbed by the microvoids which did not contribute to the diffusion process.

Barrer et al. [35], working at the same time as Meares, produced a number of sorption isotherms concave to the pressure axis which they rationalised as being the summation of two mechanisms, namely Henry's law solution and Langmuir-type sorption.

Vieth and Sladek [36] formulated an equation to express the sorption of gases in glassy polymers. This theory has become widely known as the Dual Mode Sorption Theory.

$$C = C_D + C_H = S\ p + \frac{C'_H\ b\ p}{1 + b\ p} \qquad (1.24)$$

where C = total concentration of gas sorbed.

C_D = concentration of normal diffusible species.

C_H = concentration of permeant molecules sorbed into microvoids.

S = Henry's law dissolution constant.

C'_H = hole saturation constant.

p = pressure.

b = hole affinity constant (ratio of the rate of sorption to desorption in the microvoids).

The dual mode sorption equation can be simplified according to the conditions at which permeation takes place. At low pressures where $bp \ll 1$ the sorption isotherm simplifies to :-

$$C = S\ p + C'_H\ b\ p = (S + C'_H\ b)p \qquad (1.25)$$

which implies a linear relationship between concentration and pressure.

At high pressures the saturation limit is reached as $C_H \rightarrow C'_H$. As bp >> 1 the equation simplifies to :-

$$C = S\ p + C'_H \qquad (1.26)$$

This again implies a linear relationship between pressure and concentration. A graph of concentration against a large range of pressures (i.e. bp << 1 to bp >>1) should have a linear region at low pressure and a linear region at high pressure connected by a non-linear region. This graph can then be used to determine the individual sorption modes. The upper slope of the graph (equation (1.26)) has a slope of S, the value of which can be used to determine C_D over a range of pressures as :-

$$C_D = S\ p \qquad (1.27)$$

By subtracting C_D from C the value of C_H can also be obtained over the same range of pressures. The C_H isotherm can then be tested against the Langmuir model in the usual way; i.e. a plot of p/C_H against p will produce a straight line of gradient $1/C'_H$ and intercept of $1/C'_H b$ if the adsorption follows the Langmuir model.

From their work on dual mode sorption Vieth and Sladek [36] went on to develop a diffusion model for gases in glassy polymers. In order to produce their model they set down seven postulates which are reproduced below from the review by Vieth et al [15].

I Two concurrent modes of penetrant sorption are operative in a micro-heterogeneous medium.

II Sorption of mobile or diffusible species obeys a linear law e.g. Henry's law for gas sorption in a glassy polymer.

III The second mode of sorption occurs by immobilization at a fixed number of sites within the medium and can be represented by a non-linear Langmuir expression.

IV Local equilibrium between mobile species and immobilised species is always maintained throughout the medium. In other words, it is assumed that the kinetics of the immobilization process are very rapid compared with the rate of migration of mobile species (i.e. the diffusion process is rate controlling).

V Penetrant sorbed by the second mode is completely immobilized and therefore does not contribute to the diffusive flux.

VI Only diffusion of the mobile species occurs and is driven by its concentration gradient.

VII The true diffusion coefficient is constant, independent of concentration or position in the membrane.

From the postulates Vieth and Sladek derived equation (1.28) for unsteady state diffusion when dual mode sorption occurs.

$$D \frac{\delta^2 C_D}{\delta x^2} = \frac{\delta C_D}{\delta t} \left[1 + \left[\frac{C'_H (b/S)}{(1 + (b/S) C_D)^2} \right] \right] \qquad (1.28)$$

At low pressures ($bp = bC_D/S \ll 1$) where

$$C_H = \left[\frac{C'_H b}{S} \right] C_D \qquad (1.29)$$

equation (1.28) becomes:-

$$D \frac{\delta^2 C_D}{\delta x^2} = \frac{\delta C_D}{\delta t} \left[1 + \frac{C'_H b}{S} \right] \quad \text{or}$$

$$\frac{\delta C_D}{\delta t} = \left[\frac{D}{1 + (C_H' \, b/S)} \right] \frac{\delta^2 C_D}{\delta x^2} \qquad (1.30)$$

The term in parenthesis can be defined as the effective diffusivity (D_{eff})

$$D_{eff} \quad \frac{\delta^2 C_D}{\delta x^2} = \frac{\delta C_D}{\delta t} \qquad (1.31)$$

D_{eff} can be calculated from time-lag diffusion experiments.

At high pressures ($bp = bC_D/S \gg 1$) equation (1.28) reduces to:-

$$D \frac{\delta^2 C_D}{\delta x^2} = \frac{\delta C_D}{\delta t} \left[1 + \frac{C_H' \, (b/S)}{(1 + bp)^2} \right] \qquad (1.32)$$

As $\frac{C_H' \, (b/S)}{(1 + bp)^2}$ is $\ll 1$ the equation further simplifies to Fick's second law (equation (1.2)) i.e.

$$\frac{\delta C_D}{\delta t} = D \frac{\delta^2 C_D}{\delta x^2} \qquad (1.33)$$

Thus at high pressure $D_{eff} = D$.

Permeation through microporous media.

Sourirajan and Agrawal [37] describe three main flow mechanisms which can operate in microporous media, namely:-

(i) Knudsen (free molecular) flow.

(ii) Viscous or hydrodynamic flow.

(iii) Surface flow.

When the diameters of the pores in the microporous media are much less than the mean free path of the permeating gas molecules, Knudsen flow predominates. The mean free path is the distance a gas molecule will move on average between collisions, and is inversely proportional to the pressure of the gas. When Knudsen flow operates, the molecular rate of diffusion (R_D) is governed by:-

$$R_D = (p_h - p_l)\sqrt{\frac{N^2}{2\,\pi\,R\,T\,M}}\;\pi r^2 \qquad (1.34)$$

where N = Avogadro's number.

M = molecular weight of the penetrant gas.

r = pore radius.

In a gas mixture each component, effusing independently along its partial pressure gradient, will move at a rate which is inversely proportional to the square root of its molecular weight. Thus under these conditions the separation factors would be expected to be simply:-

$$\alpha_j^i = \frac{\sqrt{M_j}}{\sqrt{M_i}} \qquad (1.35)$$

e.g For hydrogen/methane, α = 2.821

and for carbon dioxide/methane, α = 0.604

When the pore diameters are much greater than the mean free path of the effusing gases then viscous flow predominates. Sourirajan and Agrawal define for an incompressible, laminar, isothermal viscous flow through a long cylindrical pore:-

$$Q = \frac{\pi r^4}{8 \eta L} (p_h^2 - p_1^2) \qquad (1.36)$$

where Q = the rate of permeation.

η = the coefficient of viscosity of the gas.

L = the effective length of the pore.

In this case the permeation rate is inversely proportional to the gas viscosity, i.e.:-

$$\alpha_j^i = \frac{\eta_j}{\eta_i} \qquad (1.37)$$

e.g. For hydrogen/methane, α = 1.24

and for carbon dioxide/methane, α = 0.735

Surface flow is caused by the sorption of gases at the membrane/gas interface and the subsequent diffusion of the sorped molecules through the membrane pores. The extent to which this mode will affect the separation factor is dependent upon the preferential sorption characteristics of the membrane material. The author's knowledge of surface flow is insufficient to comment further.

Permeation through asymmetric membranes.

The majority of membrane processes in use in the gas industry today utilise the Loeb-Sourirajan type asymmetric membrane. Asymmetric membranes can be considered as being a composite of three different structures. Firstly, a dense skin layer in which gases permeate mainly by the solution-diffusion mechanism. In the microporous layer underneath the skin layer and through any micropores in the skin layer, permeation occurs by the Knudsen flow mechanism. In the bulk of the membrane, consisting of the macroporous network, permeation is likely to occur by viscous flow mechanisms.

In this sub-section only the Resistance Model (RM) composite membranes, developed by Henis and Tripodi [38,39] will be discussed. RM composites are asymmetric membranes which have been coated with a highly permeable polymeric material whose only function is to fill in any pores in the skin layer, to prevent them from allowing gases to permeate through by Knudsen flow. This ensures that permeation through the skin layer is by the solution-diffusion mechanism. Henis and Tripodi have developed a model in which they present their membranes in analogy with electrical resistance. In their analogy the current in a circuit, I, is equivalent to the permeation rate, Q. The driving force for the current is the potential difference, V, which is said to be equivalent to the concentration gradient, ΔC, in a membrane process. The equivalent to electrical resistance, R, is defined as the resistance to permeate flow, R.

In electrical circuits:-

$$R = V/I \qquad (1.38)$$

and in the resistance model:-

$$R = \Delta C/Q \qquad (1.39)$$

Note that ΔC is assumed constant over all the morphological zones of the asymmetric membrane so that the component resistances can be compared. Henis and Tripodi then show how the total resistance to flow is made up from the series and parallel combination of resistances from the various zones within the asymmetric structure. Fig 1.5 illustrates the combination of resistances according to the resistance model.

$$R_t = R_1 + \frac{R_2 R_3}{R_2 + R_3} + R_4 \qquad (1.40)$$

where R_1 is the resistance of the coating to permeate gas flow; R_2 is the resistance of the dense portion of the skin layer; R_3 is the resistance of 'filled' pores in the skin layer; and R_4 is the resistance of the highly porous matrix. By comparison $R_4 << R_3$, R_2 and R_1 and can be considered negligible. Thus:-

$$R_t = R_1 + \frac{R_2 R_3}{R_2 + R_3} \qquad (1.41)$$

Assuming that the coating material fills the voids in the surface to the same depth as that of the skin layer (i.e. $z_2 = z_3$) then the resistance to flow in the filled pores is:-

$$R_3 = \frac{z_2}{P_1 A_3} \qquad (1.42)$$

where P_1 is the intrinsic permeability of the coating material and A_3 is

the area of the surface layer containing pores. Similarly:-

$$R_1 = \frac{z_1}{P_1 A_1} \tag{1.43}$$

$$R_2 = \frac{z_2}{P_2 A_2} \tag{1.44}$$

where P_2 is the intrinsic permeability of the bulk membrane material. Combining the resistances produces an equation for the total permeation rate, Q_t:-

$$Q_t = \Delta p \left[\frac{z_1}{P_1 A_1} + \frac{z_2}{P_2 A_2 + P_1 A_3} \right]^{-1} \tag{1.45}$$

where Δp is the pressure difference across the whole membrane. Thus if the intrinsic permeability to various gases of the coating and membrane material are known then some knowledge of the dimensional composition of the membrane might be obtained.

Fig 1.5 The resistance model of asymmetric membranes.

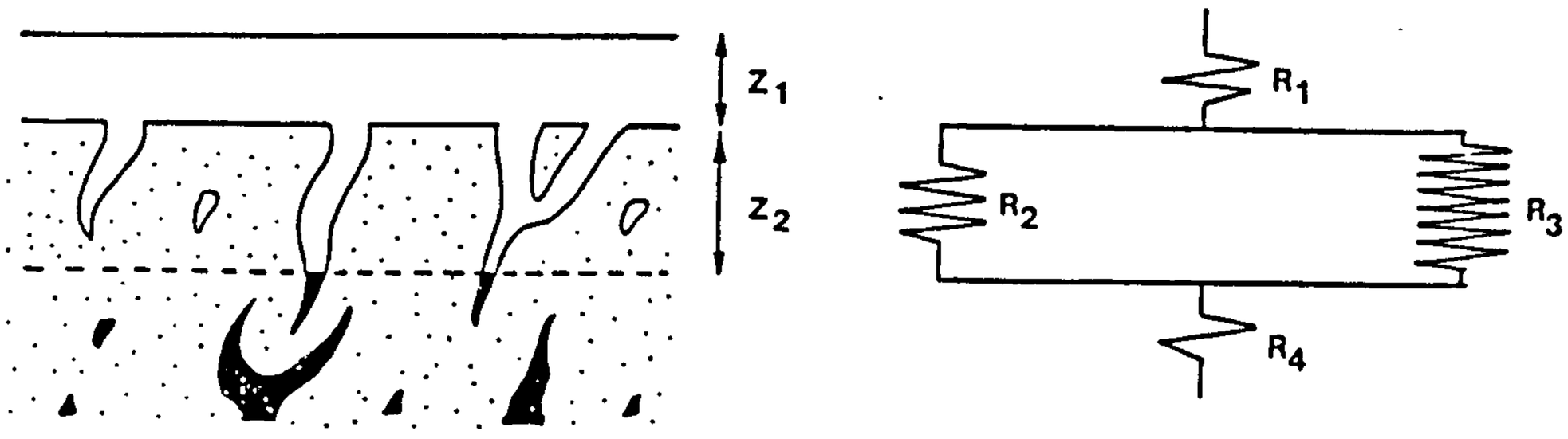

Summary of permeation theories.

The theories presented in this section all apply to some extent to the mechanism of permeation of gases through hollow fibre membranes. These theories help in the process of designing membranes for specific transport requirements. The following sections look at the fundamentals of membrane fabrication and the reasons for selecting certain materials.

1.2.3 The phase inversion process for the fabrication of membranes.

In membrane science the term phase inversion is used to describe the process in which a polymer solution of two or more components is converted into a two phase gel consisting of a solid (polymer-rich) phase and a liquid (polymer-poor) phase. The solid phase produces the rigid macromolecular network and the liquid phase the pores in the structure.

Kesting [40] and Strathmann [41,42] have been the leading investigators in this field and their knowledge together with the work of Frommer and Messalem [43] and Cabasso [44] has been collated here to produce a summary of relevance to this project.

Kesting states that there are four ways in which phase inversion can take place:-

(i) The dry process; in which the solvent evaporates from the polymer solution resulting in precipitation of the polymer.

(ii) The wet process; in which solvent-nonsolvent exchange occurs to form two interdispersed liquid phases leading to gelation.

(iii) The thermal process; in which a polymer solution is cooled to the point at which the solvent and polymer separate into two phases.

(iv) The polymer assisted phase inversion process (PAPI); in which two polymers are dissolved in a solvent system. A film cast from the solution is formed by evaporation of the solvent. Following evaporation

the film is immersed in a liquid which has the capacity to selectively dissolve one of the polymers. The remaining undissolved polymer makes up the porous membrane structure.

The work of this thesis involved the wet spinning of hollow fibre membranes and so only the details of the wet process will be examined here. Strathmann [41] outlines that there are two different methods of wet process phase inversion. The first method occurs when nonsolvent is introduced from the vapour phase. In this case a skinless homogeneous porous membrane is formed. The principle reason for this is that the rate limiting step for the phase inversion is the slow diffusion of nonsolvent vapour adjacent to the surface of the nascent membrane. The consequence of this is that flat concentration profiles develop across the thickness of the casting. This produces a fairly uniform rate of precipitation throughout the casting leading to homogeneity. The second method involves the introduction of nonsolvent from the liquid phase. In this the cast solution is immersed in nonsolvent precipitant with the important difference that the nonsolvent is now permanently in contact with the solution surface. The precipitation in this method is far more rapid resulting in an asymmetric skinned membrane. Steep concentration gradients develop at the polymer solution-nonsolvent interface with the result that there is a rapid removal of solvent from the surface. This results in an increase in the polymer concentration at the surface layer which forms the skin. The newly formed skin layer then acts to hinder the diffusion of nonsolvent into, and of solvent out of, the casting solution slowing down the rate of precipitation resulting in a slow transition in morphology towards that of the vapour phase wet process phase inversion membranes.

The change in composition which takes place during phase inversion is best represented using phase diagrams. Strathmann [41] has produced such a diagram (reproduced in Fig 1.6) for a phase inversion in which

nonsolvent diffuses into the coagulating membrane at the same rate that solvent diffuses out.

Fig 1.6 Phase diagram of typical porous membrane precipitation.

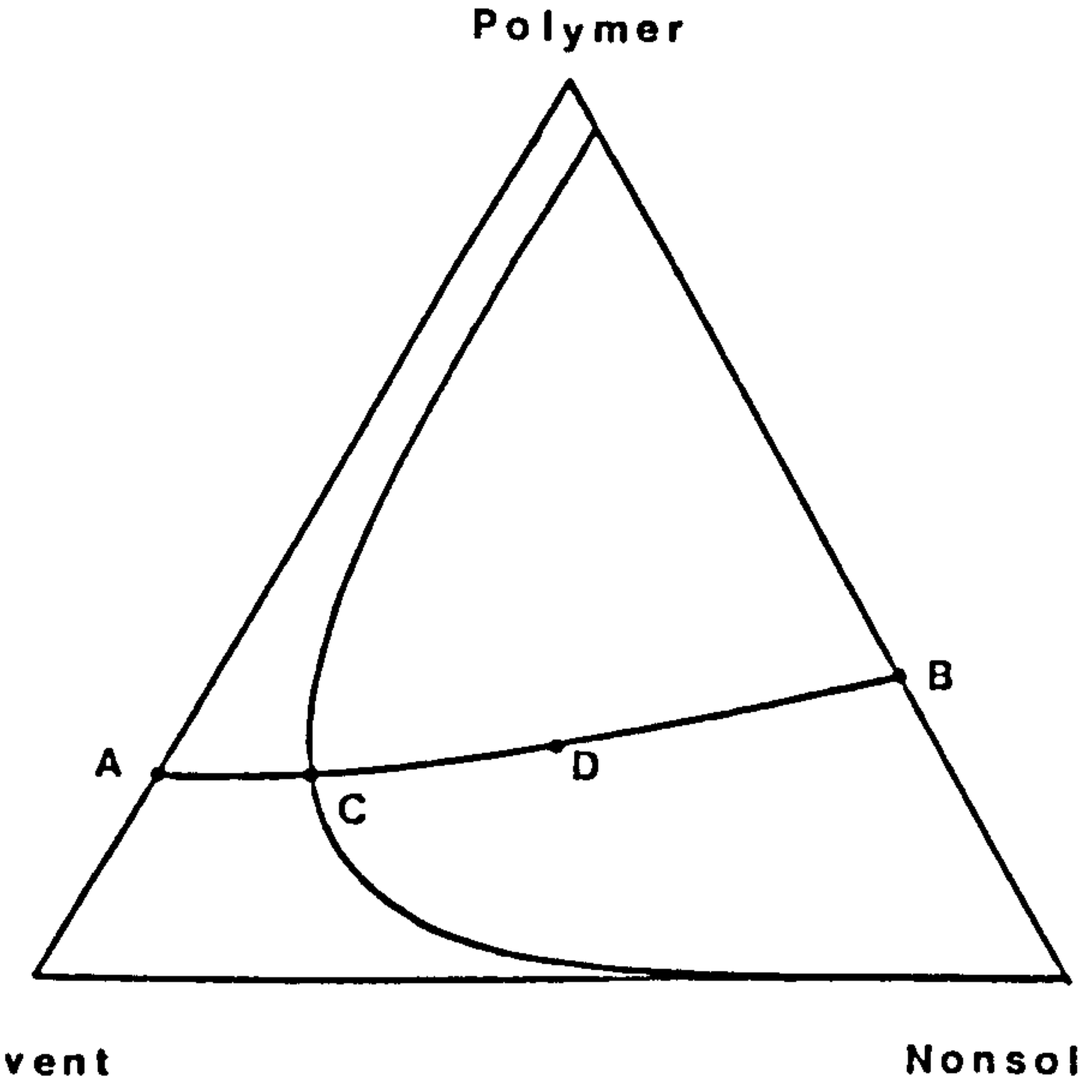

Point A represents the composition of the original casting solution. On immersion in the coagulant solvent-nonsolvent exchange occurs changing the composition from A to B. At point C the miscibility gap is reached and two separate phases begin to form. One phase is rich in polymer and the other phase, represented by the lower boundary of the miscibility gap, becomes the polymer-poor phase. At point D the polymer content of the polymer rich phase has reached a high enough level for the membrane to be considered a solid. The membrane structure is more or less determined from this point onwards. When all the solvent has been removed the final composition of the membrane is reached with a porosity of B.

During the coagulation process three distinct layers can be observed. Firstly, the casting solution layer of composition close to point A. Secondly, the fluid polymer layer which has a composition ranging from C to D. This region has a higher viscosity than A due to the depletion of solvent and influx of nonsolvent. Finally, the region between D and B is known as the solid polymer layer. In this region the nascent membrane undergoes desolvation resulting in shrinkage or syneresis. As the structure is already solid when shrinkage occurs stress builds up in the matrix. If the stress cannot be relieved by creep relaxation then the structure is likely to rupture leading to structural irregularities which are discussed later.

Cabasso [44] describes three mechanisms of coagulation. The first case involves an equal exchange of solvent and nonsolvent, similar to that shown in Fig 1.6. The other two mechanisms occur when the diffusion of one liquid is greater than that of the other. Strathmann [42] has shown how this affects the overall porosity of the membrane. Fig 1.7 illustrates his findings.

Another method of controlling the porosity of the membrane is achieved by the addition of nonsolvent to the polymer solution prior to casting. Strathmann has, again, produced a phase diagram to illustrate this. Fig 1.8 shows this effect for the cellulose acetate system that he and his co-workers were investigating. Kesting [40] explains this effect in the following way. The more nonsolvent added before casting the closer the solution is to the gelation state. Thus when the cast solution is immersed in nonsolvent the gel contracts less than if the solution was more distant from the boundary of the polymer's solubility envelope. As the membrane contracts less with nonsolvent additions, then the porosity of the final membrane must be greater.

Fig 1.7 Effect of precipitation mechanism on membrane porosity.

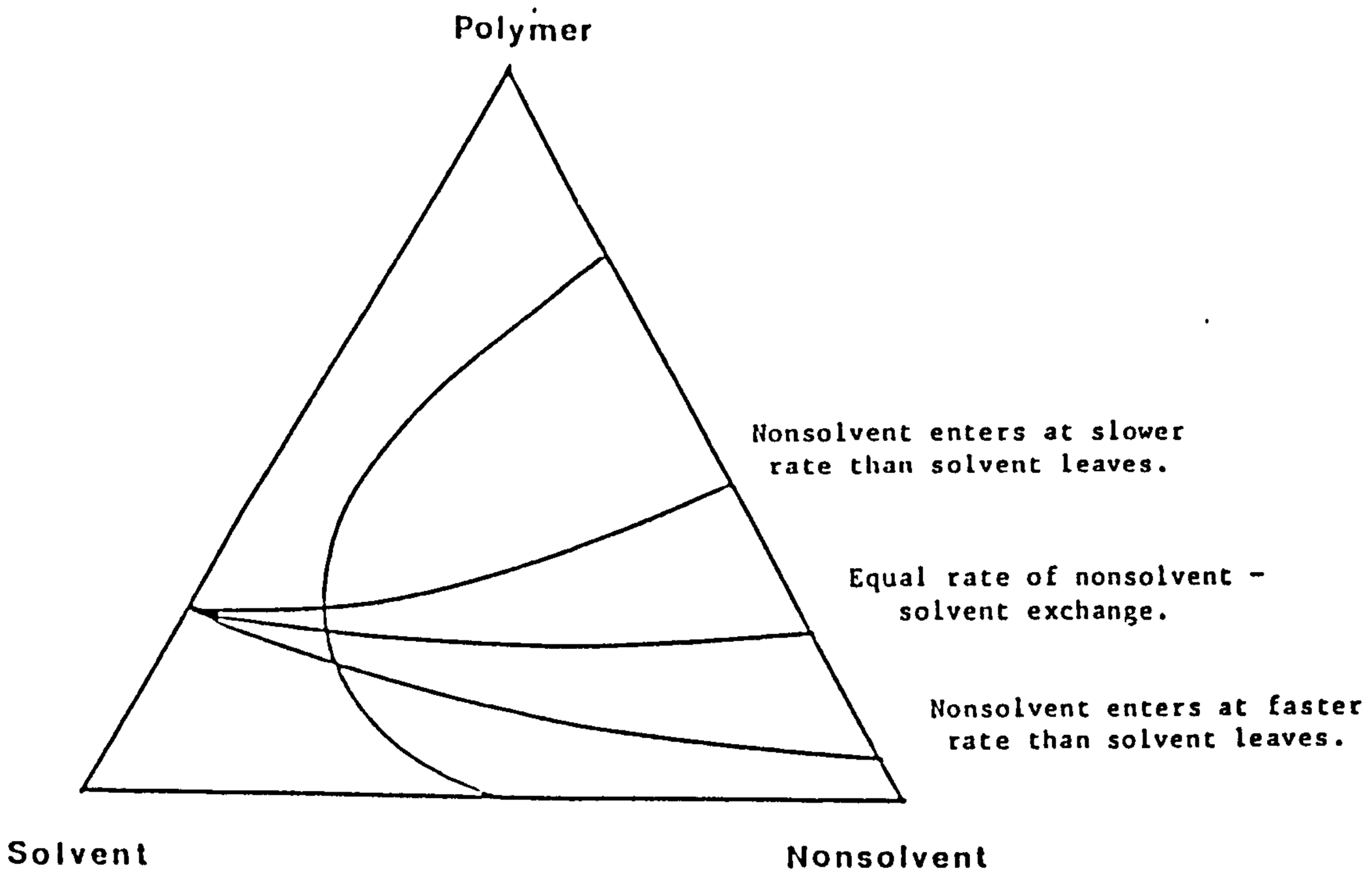

Fig 1.8 Effect of nonsolvent concentration on membrane porosity.

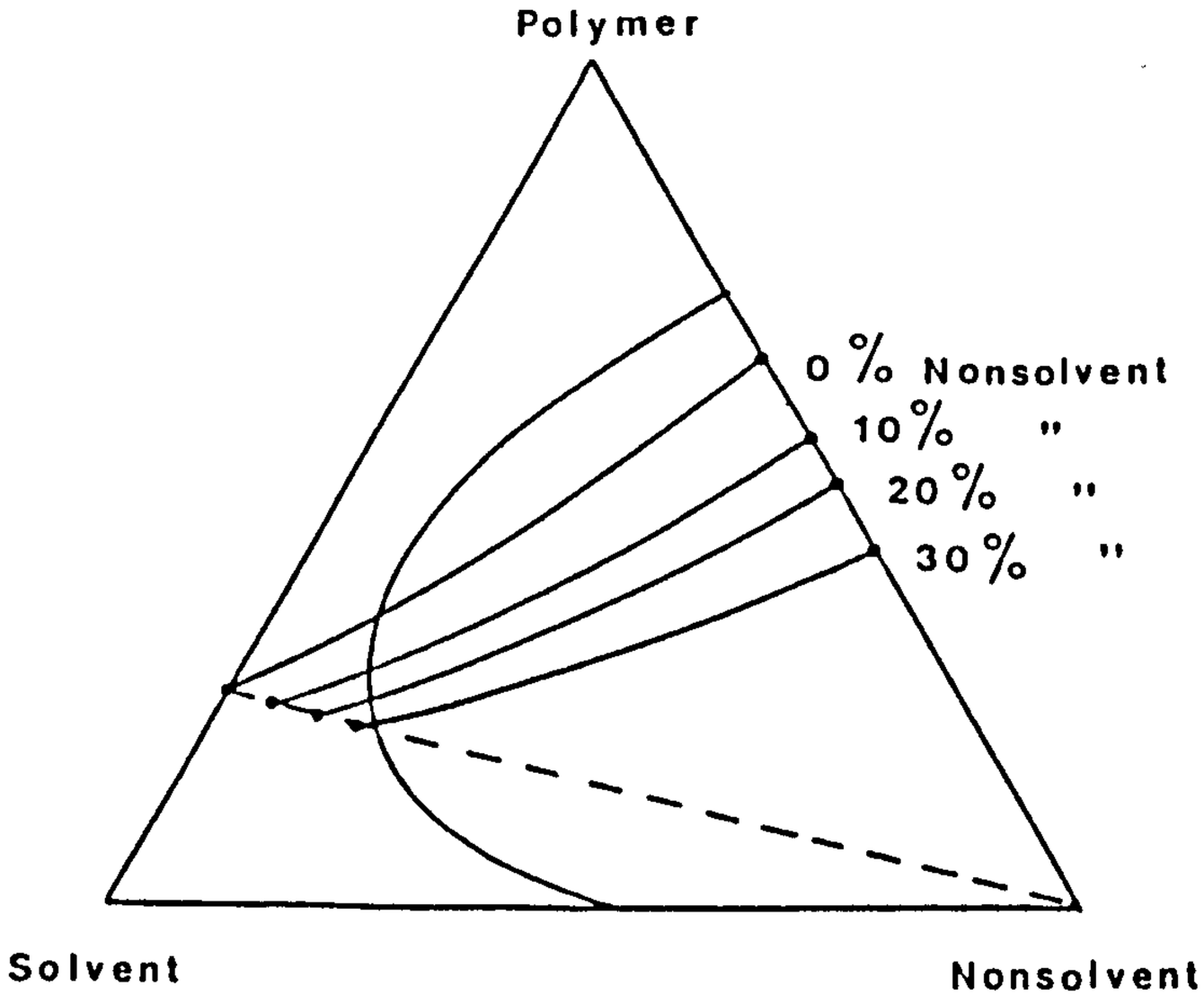

Fig 1.9 Effect of nucleus size on rate of crystallite growth.

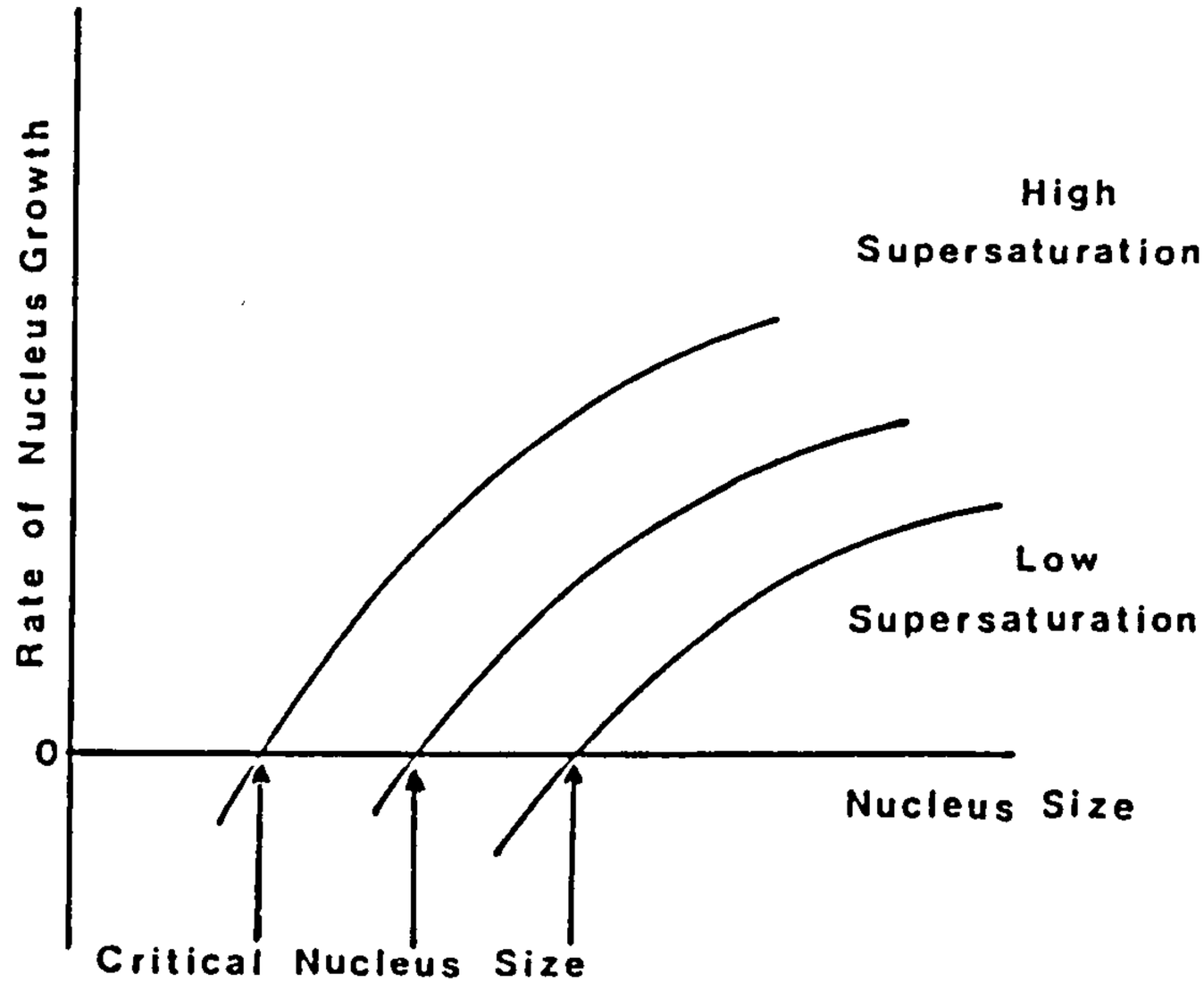

The mechanism of precipitation on a microscopic scale has been investigated by Panar et al [45], and by Kamide and Manabe [46]. Strathmann's [42] explanation using the analogy of crystal growth describes the mechanism clearly and leads to an understanding of the formation of the asymmetric structure. Fig 1.9 shows how the rate of nucleus growth varies with nucleus size for a crystallization process. The point where the curves intercept with the x axis is known as the critical nucleus size, above which a spontaneously formed nucleus will start to grow. The more supersaturated the solution the smaller the critical nucleus size. Panar et al have shown that membranes are made up of micelles. These micelles are formed in a similar manner to that of crystal growth and obey similar laws in respect to supersaturation. Strathmann et al determined that at the solution-nonsolvent interface the degree of supersaturation is extremely high, resulting in a low critical nucleus size. The consequence of this is that many small micelles will form and grow to fuse into a dense polymer-rich skin layer. As the

coagulation front advances the concentration of nonsolvent at the coagulation front progressively falls and the concentration of solvent increases reducing the degree of supersaturation. This results in an increase in the critical nucleus size and a proportional increase in the average pore size on traversing the membrane.

Phase inversion does not always proceed as well as one might like. A great variety of structural irregularities may develop of which the most important is the appearance of macrovoids. Macrovoids are hollow defects found beneath the surface of the membrane. They range in size from a few microns to hundreds of microns and are often described as being 'tear drop' or 'finger like' in shape. Macrovoids are rarely an advantageous feature. Cabasso [47] has shown that permeation pathways avoid macrovoids which represent dead space in the membrane structure. Cabasso believes that macrovoids are created during the formation of skin layers of too-fluid solutions when 'osmotic shock' causes rupture of the newly formed skin. Strathmann has suggested that the rupture results from the inability of a rapidly coagulated membrane to relieve the stress which builds up during the shrinkage stage of the process. Whichever mechanism causes the skin to rupture, the consequence is the same. The point of rupture allows a pathway to the interior for nonsolvent. The nonsolvent which penetrates the interior forms a cavity which is then enlarged by shrinkage of the coagulating polymer-rich phase. Frommer and Lancet [48] have suggested that macrovoid formation is a result of an excessively fast precipitation rate and Frommer and Messalem [43] have described two techniques designed to prevent macrovoid formation by reducing the precipitation rate.

(i) Reducing the propensity of the precipitant to diffuse into the cast solution. This may be achieved in three ways: Firstly, by reducing the temperature of the precipitant,resulting in the diffusivity of the nonsolvent to be reduced. Secondly, the addition of a salt to an

aqueous coagulation bath will reduce the activity of the precipitant. Thirdly, by choosing a solvent and nonsolvent combination with a low enthalpy of mixing. When the enthalpy of mixing is high, the high affinity between the solvent and nonsolvent causes an increase in the rate of precipitation.

(ii) Increasing the viscosity of the cast solution to lower the rates of diffusion in and out of the nascent membrane. This may be achieved in three ways. Firstly, by lowering the temperature of the casting solution to increase its viscosity. Secondly, the viscosity can be increased by increasing the concentration of the polymer in the casting solution. Finally, by promoting evaporation of solvent from the surface of the cast solution before immersion, the viscosity at the surface may be increased.

1.2.4 Material selection for asymmetric hollow fibre membranes.

There are four essential criteria which must be satisfied when choosing a polymeric material for the formation of asymmetric hollow fibre membranes.

(i) The material must have suitable permselective characteristics.

(ii) The material must be suitable for incorporation into the phase inversion process.

(iii) The material must be spinnable into hollow fibres.

(iv) The material must have good mechanical properties and be stable in long term use.

The majority of research is devoted to examining materials for their permselective nature. This criterion is usually the starting point of the selection process. Much data [49,50] is now available to enable a choice to be made without necessarily undergoing lengthy testing

procedures. It is, however, not necessarily a good idea to choose a commercial polymer. It may be advantageous to produce a specific polymer with the exact requirements for a specific separation operation. This section outlines some structural features of polymers and their bearing on the permselective behaviour, and also the requirements of the other criteria.

Ideal permselective materials will have a high permeability to one component and a negligible permeability to another. Seldom are such ideals achieved in designing a membrane material as any factor which promotes the permeability of one component may as easily promote the permeability of the other. However, some guidelines do exist and it is useful to start by examining the gas mixtures which are to be separated.

Examination of the hydrogen/methane system shows that both molecules have similar intermolecular attractive forces and so separation by virtue of a difference in the solubility coefficients of the two gases is difficult. However, the two gases have very different molecular diameters (see Table 1.1). Rogers [30] states in his review that there are correlations between the activation energy of diffusion (see equation (1.17)) and the cross-sectional area of the penetrant. In general, as the size of the penetrant increases the diffusion coefficient decreases. This trend can be incorporated into a membrane system by careful selection of the polymeric material. Pilato et al [51] have shown that there is a good correlation between helium flux and polymer density. This is explicable in terms of free volume.

In free volume theory it is assumed that a certain amount of a polymer's volume exists as holes or voids in which there is an absence of polymer chains. This free volume is not static but moves around the volume contained by the polymer as a consequence of the thermal motion of the polymer chain segments. Permeation is considered to take place by the movement of penetrant molecules within the free volume. This it

accomplishes in a number of diffusion jumps which occur when a pocket of free volume of sufficient size materializes adjacent to a penetrant molecule. Thus the rate of diffusion is governed by the amount of free volume and also by the mobility of the chain segments. If the available free volume is too great then little selectivity will occur as all gaseous permeants will be able to diffuse through the material. But, when there is only sufficient free volume to allow the smaller species to permeate then separation will occur. Factors which affect the amount of free volume and the chain mobility are crystallinity, crosslinking and chain branching. Stannett [52] postulates that crystalline regions act as inert fillers through which gases cannot permeate. Michaels et al [53] have shown that the presence of crystallites leads to more tortuous diffusion pathways and also restrict the segmental motion of the polymer chains. Crosslinking restricts segmental motion as does the presence of side chains on a polymer backbone which tend to increase the number of chain entanglements.

Table 1.1 Molecular diameters of the relevant gases.

Gas	Molecular Diameter (Å)
H_2	2.82
CH_4	3.76
CO_2	3.8

In the case of carbon dioxide/methane systems the permeation is not necessarily diffusion controlled. The solubility coefficient also adds considerably to the overall permeability. Carbon dioxide is a polar molecule with an appreciable dipole moment, unlike methane, and this difference can be utilised by selection of a polymeric material which will interact with CO_2 molecules. Pilato et al [51] have shown that a

sulphone group can facilitate CO_2 solubility via dipole-dipole interaction between the sulphone and CO_2. In section 1.2.2 equation (1.18) shows that the solubility coefficient is dependent on the enthalpy of solution of penetrant in polymer. As stated in section 1.2.2 this enthalpy of solution is attributed to the sum of the enthalpy of condensation of the penetrant and the enthalpy of mixing of condensed penetrant with polymer molecules. The enthalpy of mixing is dependent on the cohesive energy density of polymer and penetrant. As the cohesive energy density of one approaches the other so the solubility of the penetrant in the polymer increases.

There is a drawback involved in using a material which has a very high solubility coefficient for a specific penetrant. The penetrant will tend to plasticize the polymer resulting in a change in the free volume characteristics of the polymer often resulting in an overall increase in permeability to all penetrants and a consequent drop in selectivity. The precise changes in permeability and selectivity associated with structural elements has been studied by Salame [54]. His Permachor method assesses the permeability of a polymer to a specific penetrant from the summation of the individual contributions of the structural elements which are present in the polymer. The main disadvantage with the Permachor method is that it does not assess the permselective nature of the materials.

Once a list of suitable polymers has been drawn up, based on their permselective behaviour, an effective choice can be made by considering the other three criteria. Kesting [55] and Monsanto [56] both give guidelines on how the selection should be made. In summary, the polymer should be amorphous and non-ionic to facilitate the formation of asymmetric membranes. With respect to mechanical properties the polymer should not be brittle within the range of expected operating temperatures. It should be strong, resistant to creep and be able to

maintain these properties for a lifetime of several years. Both Kesting and Monsanto recommend polysulphones (e.g. Udel P3500) for membrane fabrication. The Udel polymer is an amorphous glassy material with a suitably high glass transition temperature of 195 ^{o}C. It has excellent thermal and oxidative stability as well as good strength and flexibility. Johnson [57] quotes permeability values which would give idealised separation factors of 48 for hydrogen/methane and 25 for carbon dioxide/methane. These factors make polysulphone a good choice for the preparation of hollow fibre membranes for the purification of methane.

1.3 Hollow fibre technology.

A hollow fibre membrane is a membrane which has been cast in a cylindrical form. Mass transport proceeds across a hollow fibre membrane by permeation from the outside of the fibre to the fibre lumen (or vice versa). The diameter of a hollow fibre usually lies within the range of 0.1 to 1.0 mm. Hollow fibres have structural advantages over flat sheet membranes. Firstly, hollow fibres are self supporting in a permeator chamber. Flat sheet membranes require complex supports consisting of spacers and porous supports in order to collect the permeate separate from the feed. Hollow fibres merely need potting into a tube sheet (see Fig 2.7) to allow access to be made to the fibre lumen. Secondly, a chamber of hollow fibres may have up to 25 times as much membrane surface area as a chamber of similar dimensions containing a spiral wound flat sheet membrane.

Hollow fibres have been produced in the textile industry for a number of years - mainly for use in thermal insulation applications. These fibres are usually produced by a melt-spinning process. Melt-spinning is a relatively simple process for producing continuous

filaments. The process involves heating a polymer to its molten state where upon it is extruded through a spinneret to produce a fine filament which cools and solidifies into the fibre. Hollow fibres are produced by extruding the molten polymer through an annular shaped spinneret. Fibres produced by melt-spinning have a homogeneous morphology. Pores may be introduced into the structure by incorporating a water-soluble polymer into the base polymer before spinning. Subsequent washing out of the water soluble polymer produces a uniform porous matrix suitable for microfiltration. In order to produce the kind of asymmetric structure suitable for gas separations a wet process phase inversion (or possibly a dry process phase inversion) process is required. Wet-spinning, an established fibre spinning process as used in the production of acrylic fibres, incorporates wet process phase inversion. Wet spinning is a process in which a polymer solution is extruded through a spinneret into a coagulation bath where solvent-nonsolvent exchange occurs to produce a solid filament. Continual washing of the filament removes the residual solvent before winding up of the fibre is commenced. By careful selection of materials, as described in section 1.2.3, the desired asymmetric structure can be produced. Hollow fibres are produced by extruding the polymer solution through a tube-in-orifice spinneret. A tube-in-orifice spinneret is designed so as to allow a coagulant to be injected down the centre of the forming fibre to produce the central lumen.

Monsanto [56, 58 - 62] have developed over the last 20 years a method for the production of anisotropic hollow fibre membranes suitable for gas separation. Monsanto use a derivation of the wet-spinning process known as dry-jet wet-spinning. In dry-jet wet-spinning the spinneret is raised above the surface of the coagulant by a distance (approximately 10 cm) known as the jet gap (or air gap). The jet gap serves three main functions. Firstly, it allows a temperature differential to be

maintained between the spinneret and the coagulation bath. This allows more viscous solutions to be spun by maintaining the spinning solution at an elevated temperature during the extrusion process. Secondly, the jet gap allows greater spinning speeds to be used without continual breakage of the coagulating filament occuring. Nourpanah [63] has shown in his work on acrylic fibres the third reason for incorporating a jet gap. When the polymer solution is extruded through the spinneret a great amount of stress builds up at the point of ejection. The effect of stress is readily seen during dry-jet wet-spinning as the filament bulges outwards as it leaves the extrusion nozzle and this is often refered to as the die-swell. This stress relaxes as the fibre falls through the jet gap but where coagulation occurs immediately after extrusion (i.e. in wet-spinning) these stresses are frozen into the solidifying structure often resulting in cracks appearing in the surface layer. The length of the jet gap is relatively unimportant so long as the filament has time enough to relax before coagulation takes place.

CHAPTER 2

Experimental

2.1 Introduction.

The techniques developed for this research evolved from simple ideas to effective working practice. The procedures have been classified into two main areas; namely preparative techniques (i.e. film casting, fibre spinning etc.) and characterisation methods (i.e. permeation rate measurements, void volume determination etc.).

From the wealth of literature published in this field many patents and research papers outline only brief experimental procedures. The translation of the information in patent literature to working procedures at the laboratory bench proved to be an arduous task and so the procedures detailed below have been given at length for the benefit of future workers.

2.2 Materials.

Membrane forming polymers.

Polysulphone was obtained in chip form from the Union Carbide Co. under the trade name UDEL P3500 and P1700. ICI plc also manufacture a poly(ethersulphone) under the trade name of Victrex 200P. The structures of these polysulphones are given in Fig 2.1. Sulphonated poly(ethersulphone)s were also supplied by ICI, again under the trade name Victrex. Two grades, KM35 and KM36, were obtained.

Solvents used in membrane fabrication.

N,N-dimethylacetamide (DMAc), dimethylformamide (DMF) and formamide (Fa) were obtained from BDH plc. GPR grade was considered sufficiently pure; however, the DMAc was dried with anhydrous magnesium sulphate before use. 1-formylpiperidine (1-Fp), purum grade, was obtained from Fluka AG.

Fig 2.1 Chemical structure of polysulphones.

Udel P3500 (Union Carbide)

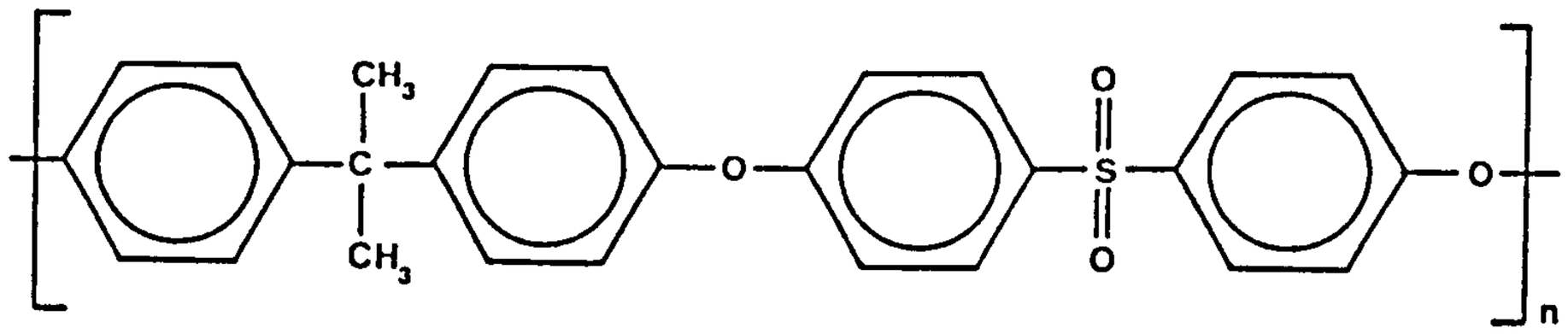

Victrex 200P (I.C.I.)

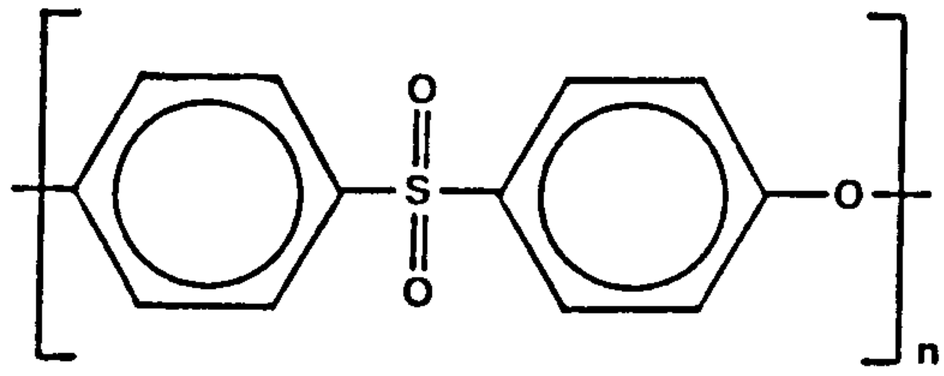

Potting and Coating materials.

Both the epoxy putty and epoxy resin used in the potting of fibres into fibre modules were obtained from RS components plc.

The silicone elastomer used for the coating of the majority of hollow fibres was obtained by courtesy of Dow Corning. The actual elastomer used was the Sylgard 184 kit consisting of the silicone component and a liquid curing agent. Isopentane, GPR, was obtained from BDH plc.

Intex 181, a styrene-butadiene-vinylpyridene latex, was supplied by courtesy of Enichem Ltd.

Test gases.

All gases used during permeation experiments were supplied by BOC Industrial Gases and BOC special gases. The grades were chosen to give the highest purity with the restriction that the cylinder pressure was as high as possible; hence Research grade gases were not used. The gases used were hydrogen (99.99%), methane (99.0%), carbon dioxide (99.995%) and nitrogen (OFN grade). The gas mixtures hydrogen/methane and carbon dioxide/methane were made specially at BOC special gases and were supplied as approx 50:50 mixtures.

Miscellaneous.

Sulphur trioxide (stabilised 99%) was obtained from Aldrich. Sevron Blue BGL, the basic dye used to detect the presence of sulphonic acid groups was obtained from DuPont Nemours Inc.

2.3 Preparative techniques.

2.3.1 Preparation of polymer solutions.

The polymer solutions (dopes) required for spinning and film casting were prepared by dissolving polymer chips or powder in either pure solvent or a solvent/nonsolvent mixture. Concentrations were typically of the order 30-40% by weight of polymer. The high polymer content of the dopes meant that it was often difficult to achieve a non-turbid solution. The procedure below was found to be the most successful method of producing a homogeneous solution for batches of between 400 and 800g of dope.

The polymer to be used was pre-dried in a vacuum oven to remove any water present (quoted levels suggest a level of 0.62% equilibrium water absorption for Union Carbide P3500 [57]). The mixing apparatus was assembled as shown in Fig 2.2. The stirrer (Heidolph RZR2) was chosen for its ability to stir rapidly in low viscosity liquids and also to stir with high torque very viscous liquids, although at lower speeds. The required volume of solvent (and nonsolvent when required) was placed in the reaction flask so as to approximately half fill it. The stirrer was then engaged at its highest speed of rotation (approx. 1500 r.p.m.). The polymer chips were introduced in a steady feed over one minute. The water bath was maintained at room temperature during this period to ensure that each chip was completely wetted and remained discrete from the other chips and the wall of the flask. This was an important step towards cutting down the time required to make a solution. The rate at which the polymer dissolved was related to the surface area of polymer in contact with the solvent and this was best achieved when each chip was discrete from its neighbours.

Fig 2.2 Polymer dope preparation apparatus.

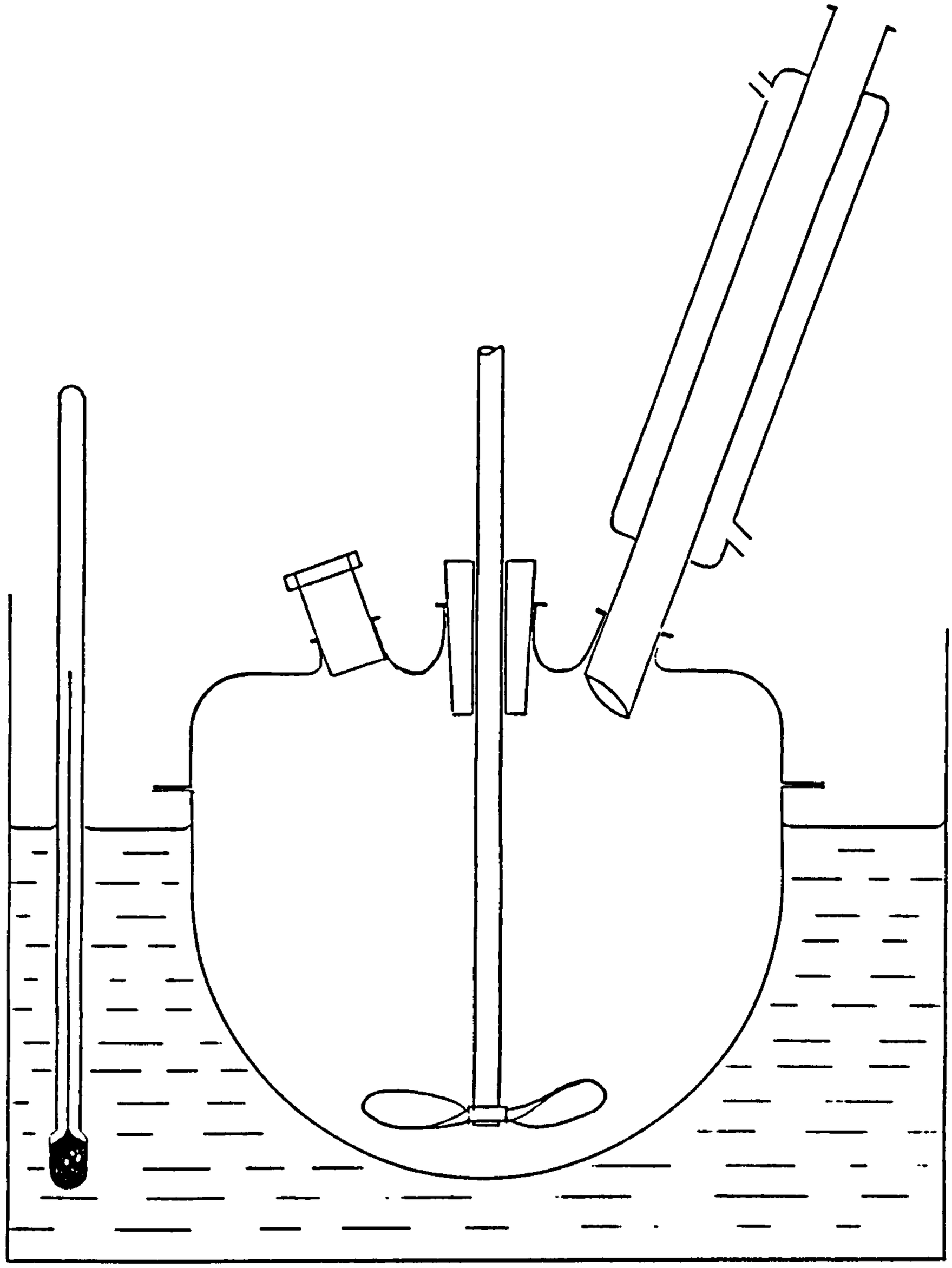

Fig 2.3 Film casting apparatus.

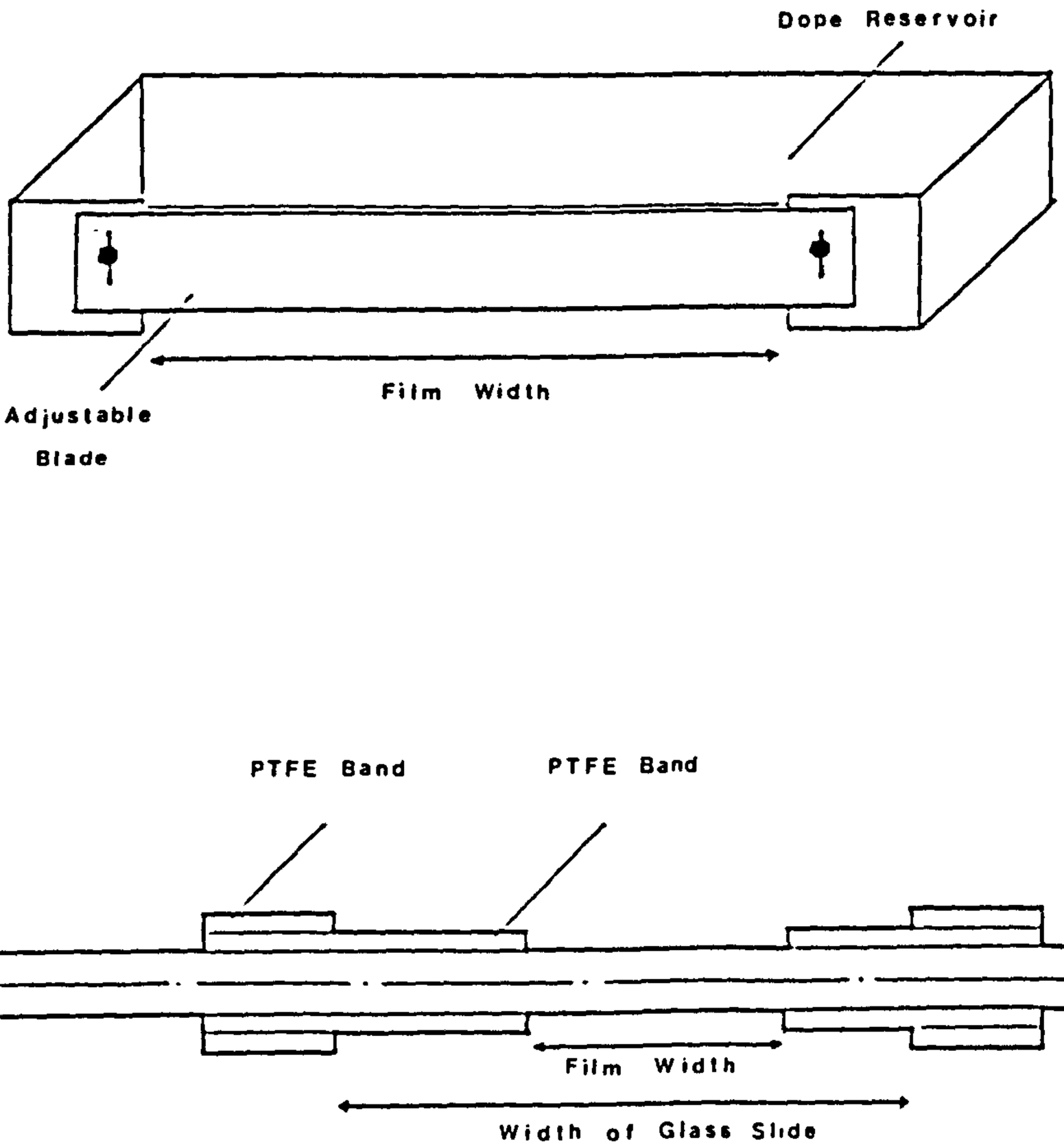

When the chips were thoroughly wetted the temperature of the water bath was raised slowly to 80°C. and the condenser was attached to the flask. As the polymer chips swelled and went into solution the viscosity of the system increased and the stirrer was adjusted accordingly to produce the fastest stirring rate with the necessary torque to compensate for the viscosity increase. At the highest torque the stirrer was still rotating at 350 r.p.m.

Most batches appeared to have dissolved after three hours at 80°C. However, to ensure that the dope was homogeneous, the system was stirred for a total of eight hours at 80°C. After this time the solution was poured hot into a dope reservoir and immediately degassed by application of a vacuum (usually overnight) to remove any bubbles which might interfere with the spinning and casting processes.

2.3.2 Film casting.

Film casting techniques were developed to allow quick assessment of combinations of polymer, solvent and coagulant. Films were cast onto glass plates using a draw down technique similar to that used in the pigments industry. Two devices were constructed to provide both small and large films (Fig. 2.3). The small film caster (glass rod design) allowed films approximately 2 cm wide to be cast onto microscope slides, whilst the large film caster (box design) produced films up to 10 cm wide. The glass plates used, in both cases, were cleaned thoroughly and dried before use. The polymer solution to be cast was poured onto the glass plate either in front of the glass rod or inside the box assembly. Care was taken during pouring to ensure that no air bubbles were introduced in the casting solution, as these would appear as large voids after phase inversion. The draw down was made at a constant rate leaving a film of solution of constant thickness along the length of the

glass plate. The plate was then lowered into the coagulation bath for the required time for phase inversion to form the membrane structure. After coagulation the membrane was washed in water before drying to remove any residual solvent. Drying was carried out at room temperature in a dust free environment.

2.3.3 Spinning of hollow fibres.

All the hollow fibres produced were spun by the dry-jet wet spinning process (Fig 2.4). Rogers, a previous worker, constructed a dry-jet wet spinning unit suitable for producing hollow fibres. Modifications were made to this equipment by the author to enable better control of spinning to be achieved and to allow a wider range of fibres to be spun. The equipment consisted of three sections each controlling one of the three main steps of dry-jet wet spinning, namely; extrusion, coagulation and washing.

Extrusion.

Extrusion describes the delivery of polymer solution to the spinneret and the casting of the uncoagulated filament. A schematic diagram of the equipment is shown in Fig 2.5.

The degassed polymer solution contained in the dope reservoir was fed under a pressure, of approx. 40 p.s.i., to the metering pump. The pressure applied to the reservoir was such as to prevent the formation of bubbles in the supply lines on route to the metering pump. The metering pump (Slack and Parr gear pump) ensured an accurate and constant delivery of dope to the spinneret. Before arrival at the spinneret the dope was passed through a variety of filters to remove any particulate matter which could cause problems during extrusion through the spinneret. The internal coagulant was supplied to the injection capillary of the

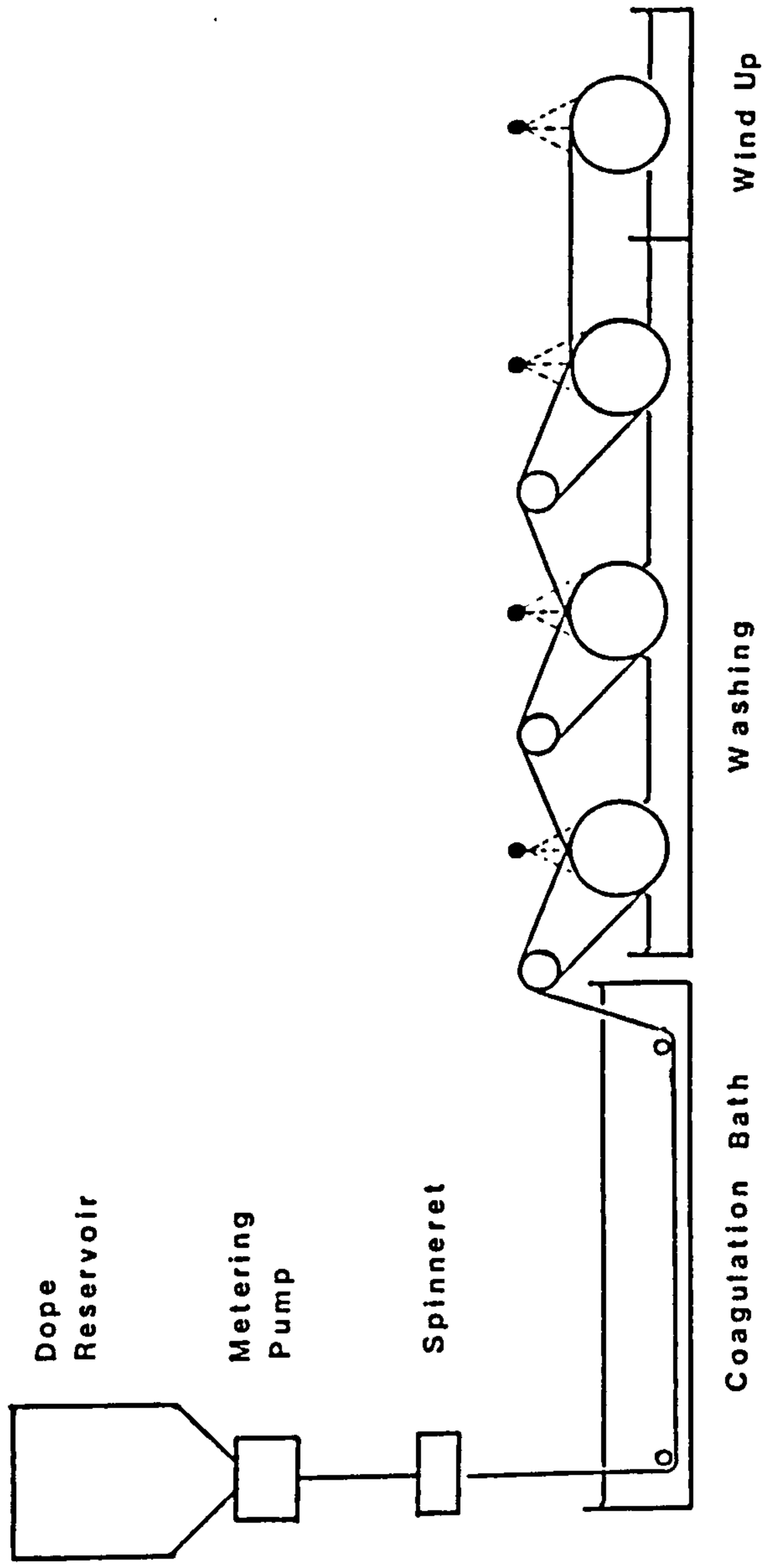

Fig 2.4 The dry-jet wet-spinning process.

Fig 2.5 Extrusion apparatus.

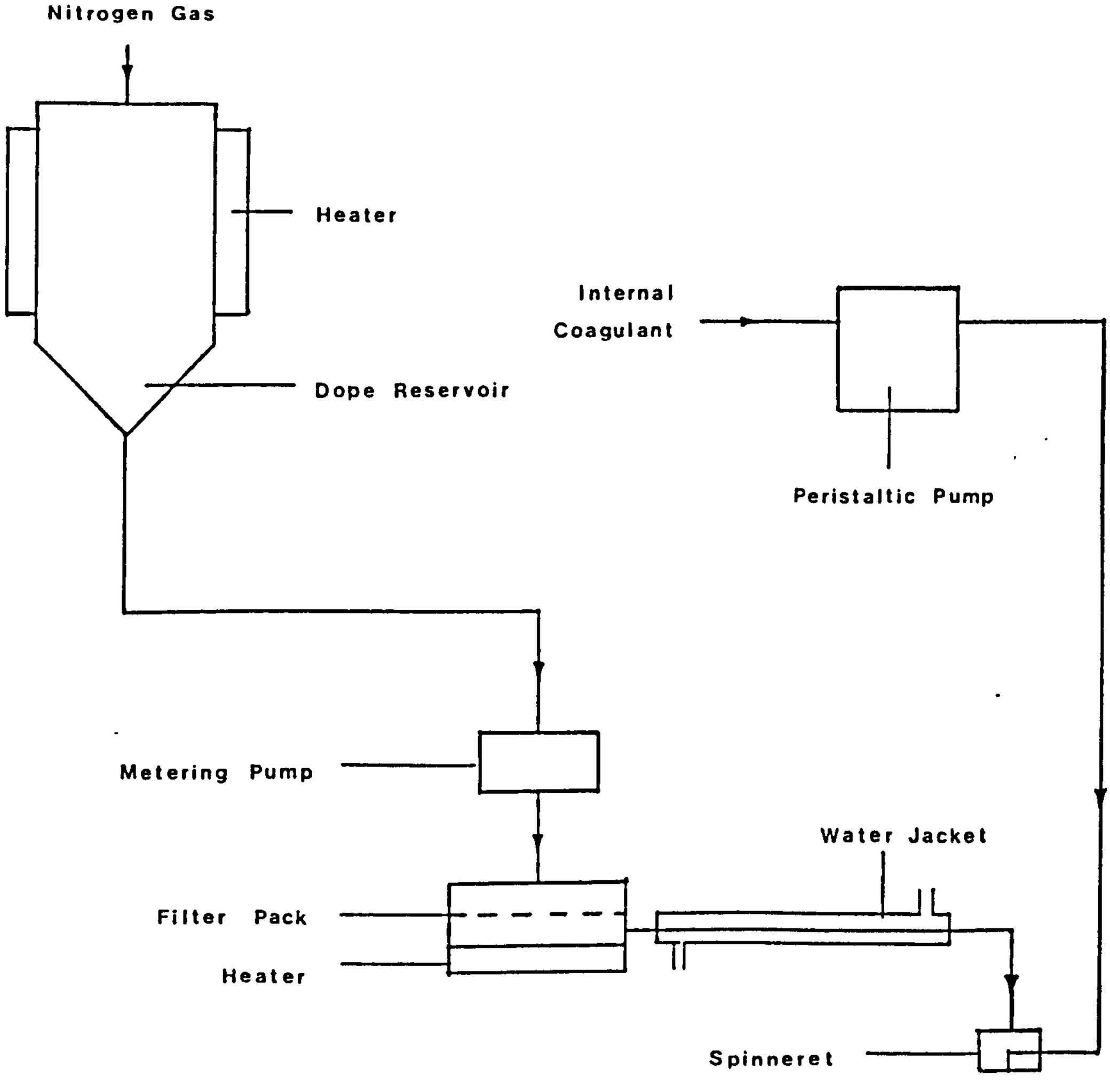

spinneret via a peristaltic pump. This particular kind of pump was chosen for its ability to pump small volumes of fluid with the minimum of pulsing.

Tube in orifice spinnerets were used on all occasions and had the basic design as shown in Fig 2.6. Several spinnerets were used and their dimensions are specified in Table 2.1.

Table 2.1 Tube-in-orifice spinneret dimensions.

Spinneret N^{o}	Orifice diameter (μm)	Capillary diameter (μm)	Capillary Bore diameter (μm)
1	630	305	203
2	820	320	200
3	820	430	340
4	570	225	150
5	630	320	200
6	820	410	200
7	580	330	150

From the spinneret the nascent fibre was extruded, the precise dimensions being governed by the polymer extrusion rate (PER), the linear extrusion rate (LER) and the water injection rate (WIR). The PER is the volume of polymer solution extruded per unit time; the LER is the length of pre-nascent fibre extruded from the spinneret per unit time; and the WIR is the rate of supply of internal coagulant to the spinneret.

During the course of the work, modifications were made to the extrusion unit to allow more viscous solutions to be spun. Installation of heaters helped to lower the viscosity of the dope to allow it to flow through the extrusion unit. A heating jacket surrounding the dope reservoir was used to raise the temperature of the dope. However, due to the poor thermal conductivity of the solutions, several hours were required to raise the temperature of the dope evenly. A second heater was situated in the filter pack to aid the flow of dope through this, the region with the greatest resistance to flow. The metering pump was also in contact with the filter pack heater and so benefited from the input of heat energy. The third heater was a water jacket placed between the filter pack and the spinneret. This allowed final temperature adjustments to be made at the moment of extrusion.

Coagulation.

After extrusion the pre-nascent fibre passed through an air gap of between 5 and 10 cm before plunging into the coagulation bath. Fig 2.7 shows a schematic representation of the coagulation system of which the main component was a 170 cm long stainless steel bath. The solidifying fibre was guided through the bath by two low friction rollers. The bath was adapted to allow the coagulant to be continually refreshed in order to prevent a build up of solvent in the bath. Cooling coils were also fitted to the replenishment system to lower the temperature of the coagulant to below 5^{o}C. when required.

Washing.

On leaving the coagulation bath, the fibre was washed by passing over a series of wash rollers as shown in Fig 2.4. Each successive roller rotated at a slightly higher speed to maintain tension in the fibre. Following washing the fibre was wound up. In a normal textile

Fig 2.6 A Tube-in-orifice spinneret.

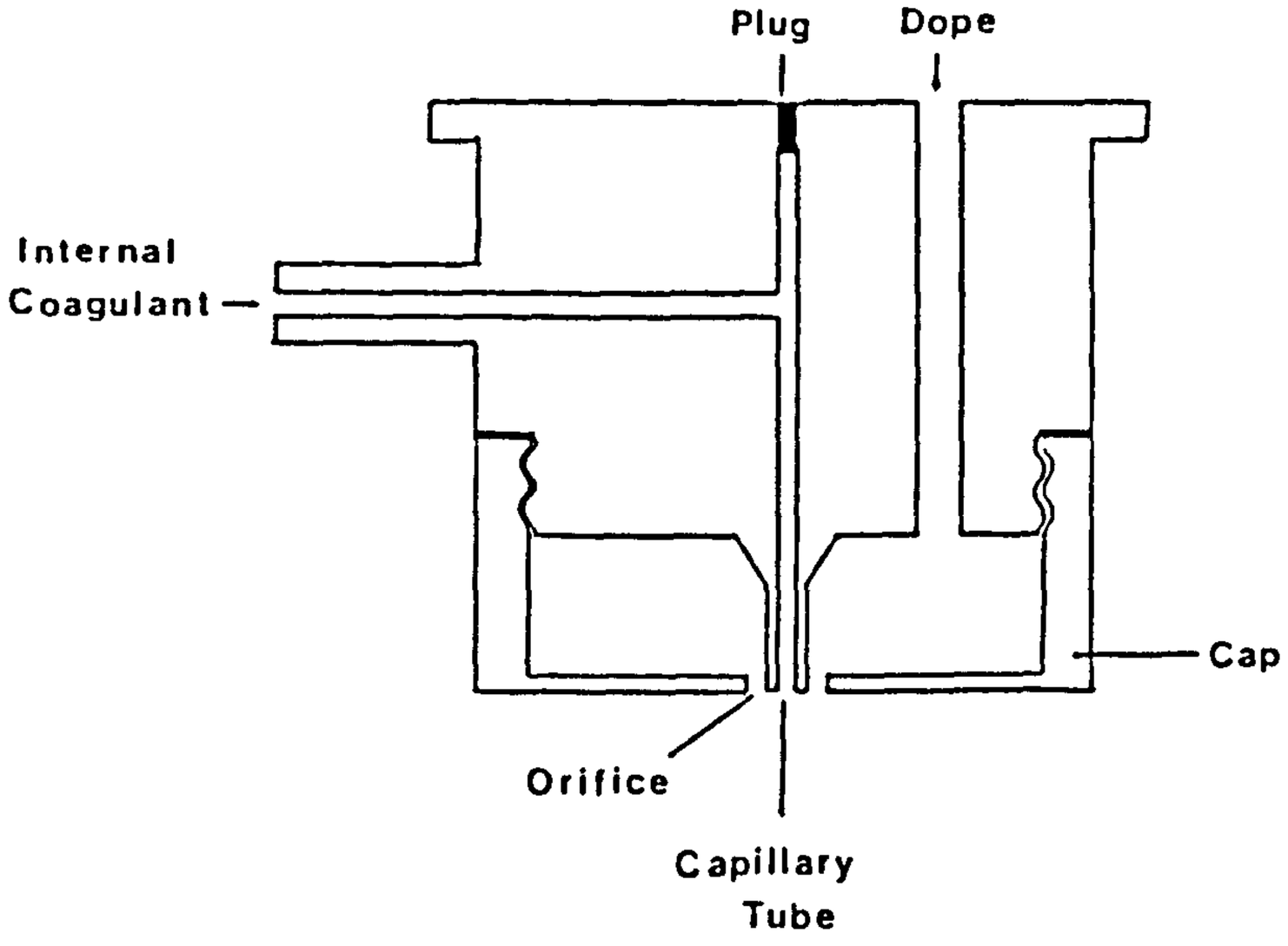

Fig 2.7 Coagulation control apparatus.

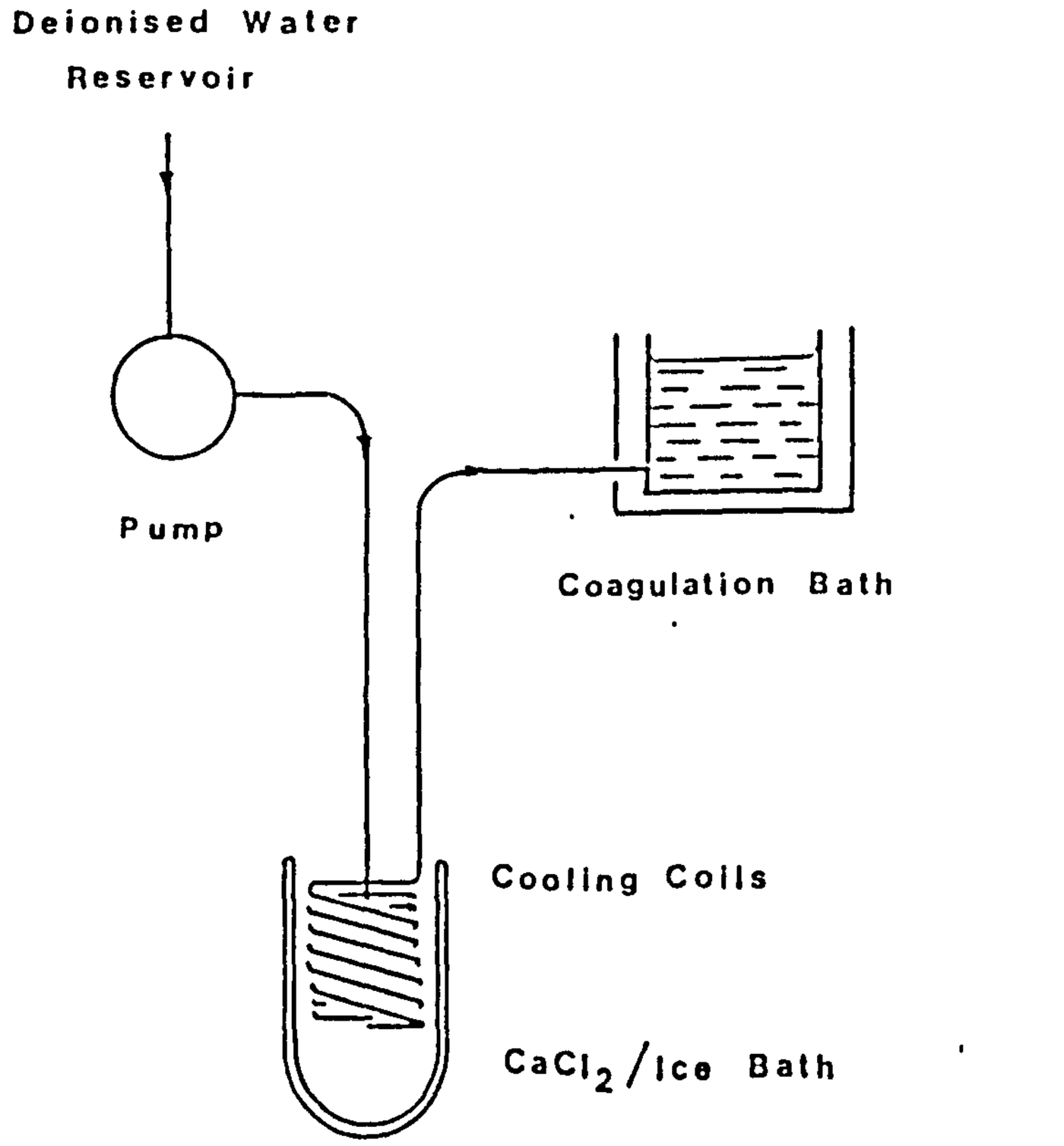

fibre process the fibres would be wound up on a cone; however, this was unsatisfactory as the fibres crushed one another where they overlapped on the cone. A solution was found by winding the fibre (without overlap) on the last wash drum. After collection the fibres were cut from the roller before fibre shrinkage could cause any problem. The only disadvantage of this was that the fibres had a fixed length of 60 cm (the circumference of the wash roller); however, this did not represent a problem as the length was more than sufficient for subsequent processing.

The cut fibres were immersed in water for at least 72 hours to remove the residual solvent trapped in the fibre. The fibres were then dried at room temperature in a dust free environment. To prevent the fibres from curling up during drying they were mounted vertically with small weights hanging from them.

2.3.4 Preparation of fibre modules.

A module was developed to allow easy handling of the hollow fibres once the spinning was complete. The module, shown in Fig 2.8, was specifically designed for fitting into the permeation chamber of the laboratory scale permeation rig. The module is an assembly of ten hollow fibres fitted at one end into a 'tube sheet'. The tube sheet allows access to be made to the fibre bores. At the other end of the fibre bundle the ends of the fibres were potted into an 'end cap' to seal the bores at this, the bottom end.

Hollow fibre membranes are easily damaged, especially during the preparation of the fibre modules. Initially the failure rate of the modules was as high as 60%. The main cause of failure was poor alignment of the fibres away from the centre of the tube sheet. Poor alignment resulted in damage to the fibres when they were fitted into the laboratory permeator rig. The use of small plastic cones (see Fig 2.8b)

to hold the fibres in the centre of the tube sheet proved to be the solution and the failure rate of modules was successfully reduced to below 5%. The detailed assembly procedure is given below:-

(a) The tube sheet was produced in the following way. A 3 cm length of 1/4 inch (6.35mm) outer-diameter copper tubing was cut and reamed. A stainless steel nut was fitted to each end of the tubing using copper ferrules to provide a leak proof compression fitting.

(b) A hollow plastic cone was made of dimensions such as to fit into the end of the tube sheet. The internal dimensions were such as to hold lightly a bundle of ten hollow fibres. The cone was sprayed with a PTFE mould release agent to prevent adhesion to the epoxy resin. The cone was inserted into the end of the tube sheet as shown in Fig 2.8b.

(c) A 1 cm length of 5/32 inch (3.97mm) outer-diameter aluminium tubing was cut and reamed. One end was then sealed with epoxy putty.

(d) Ten fibres were cut to a length of 30 cm and threaded through the cone until 5 cm protruded from the top of the tube sheet. They were then sealed into the tube by injection of epoxy resin into the top of the tube sheet. Sufficient resin was injected to fill the tube sheet to overflowing.

(e) When the resin was firm (not hard) the excess resin was cut cleanly from the top of the tube sheet with a sharp scalpel. This revealed the open bores of the ten hollow fibres (Fig 2.8c). At this stage the plastic cone may be removed by gently pulling it loose from the tube sheet and drawing it off the fibres.

(f) The fibres were cut to a length of just over 20 cm long and then sealed in the end cap with epoxy resin. The finished module was then transferred to a storage rack in a dust free environment.

Fig 2.8a A fibre module.

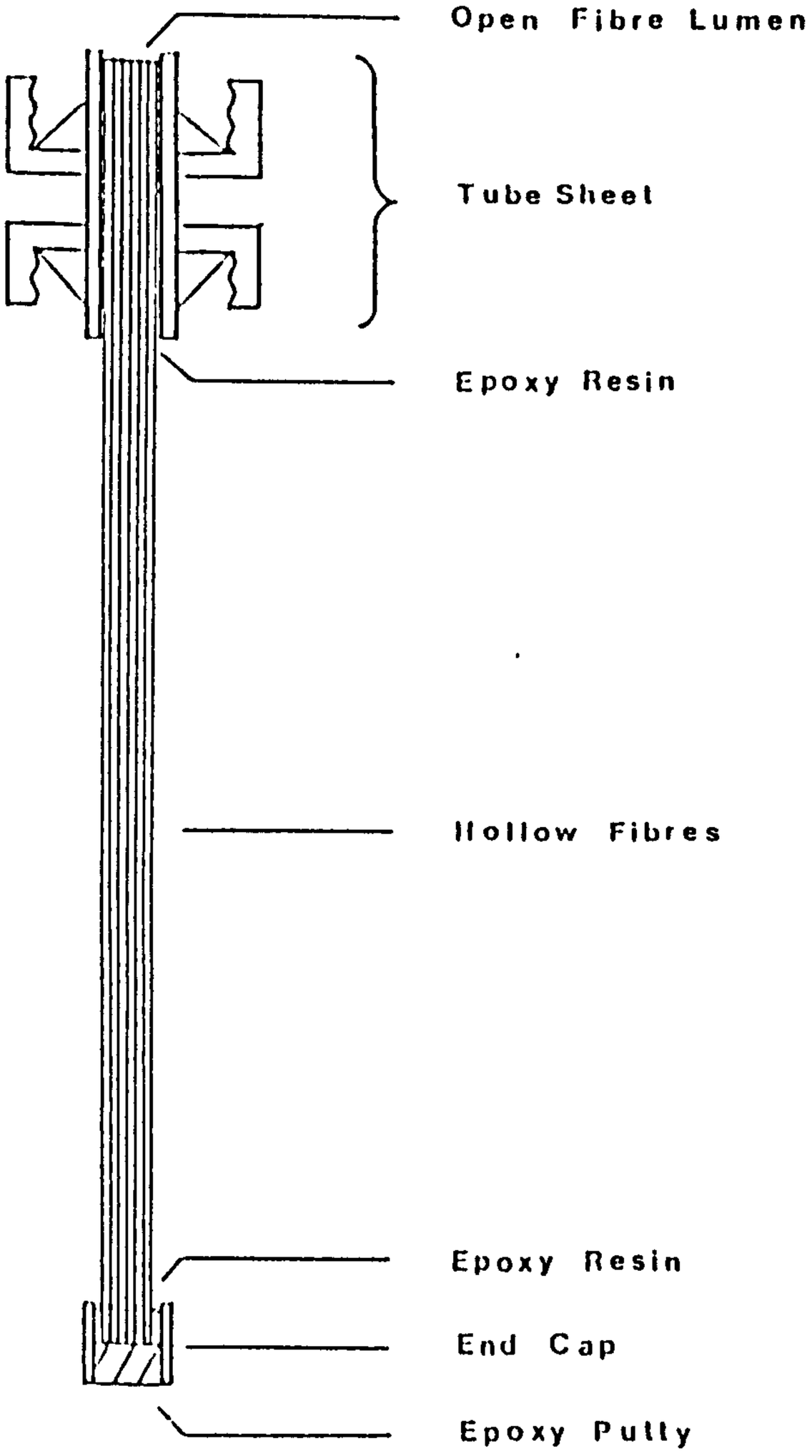

Fig 2.8b Module tube sheet showing plastic cone.

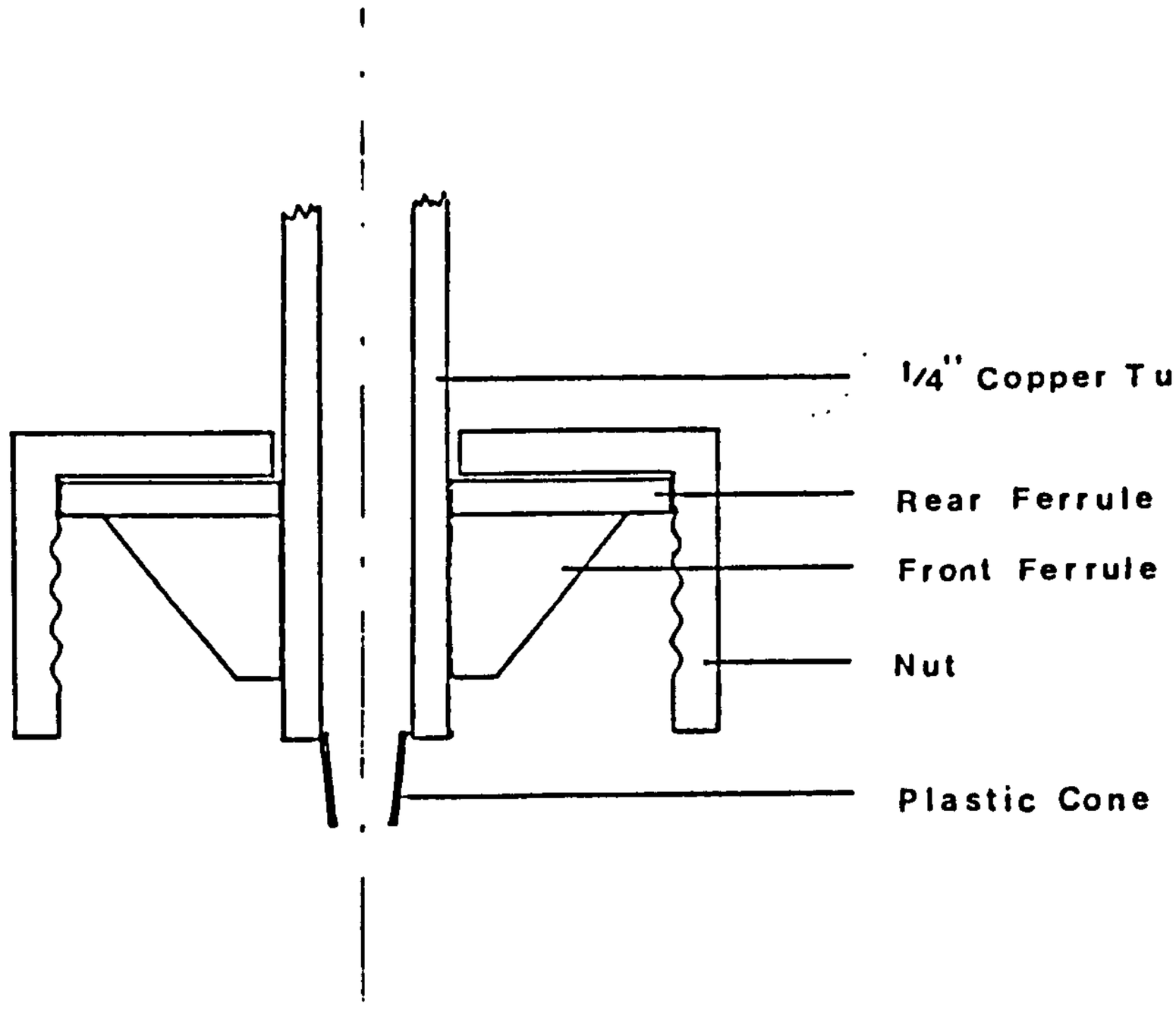

Fig 2.8c Module tube sheet (view from above).

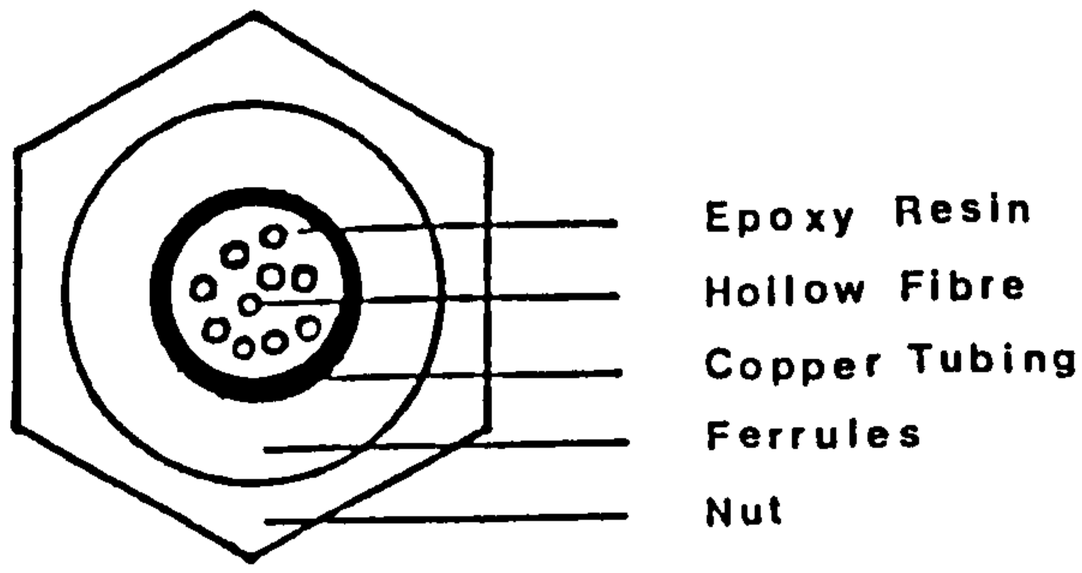

2.3.5 Fibre coating.

For fibres which required a surface coating, the application was made to bundles which were already mounted in the fibre modules. This allowed a vacuum to be applied to the lumen of the fibre, in order that the coating solution could be drawn into any pores or defects in the outer skin layer. Materials used for coatings were elastomeric in nature in order to ensure good film forming properties. This ensured that the coating remained in occluding contact with the fibre and that the coating film was not brittle which might have resulted in the formation of cracks during the lifetime of the fibre. The coating materials were examined by Differential Scanning Calorimetry to ensure that the glass transition temperature (T_g) was well below that of the normal operating temperature for gas permeation processes.

Coating with a solvent based system.

Where a coating material was to be applied from a solution, great care was taken in the choice of solvent to prevent interaction between the polymer (i.e. the fibre) and the coating solvent. Any interaction could damage the surface layer causing a change in the gas transport properties of the membrane.

Fig 2.9 shows the apparatus used in most of the coating experiments. The design incorporates all the features necessary to coat hollow fibres by the method described by Monsanto [64]. The fibre module was attached to the vacuum line by the tube sheet. The level of vacuum applied to the bores was controlled by a needle valve known as the bleed valve. The free hanging fibre bundle was immersed in the coating solution, contained in a 100 cm^3 measuring cylinder, for the required length of time. At the end of this time the solution was removed, but the vacuum was maintained for a further period of time to ensure that any defects were fully sealed by the coating solution. Where the coatings required

Fig 2.9 Fibre coating apparatus.

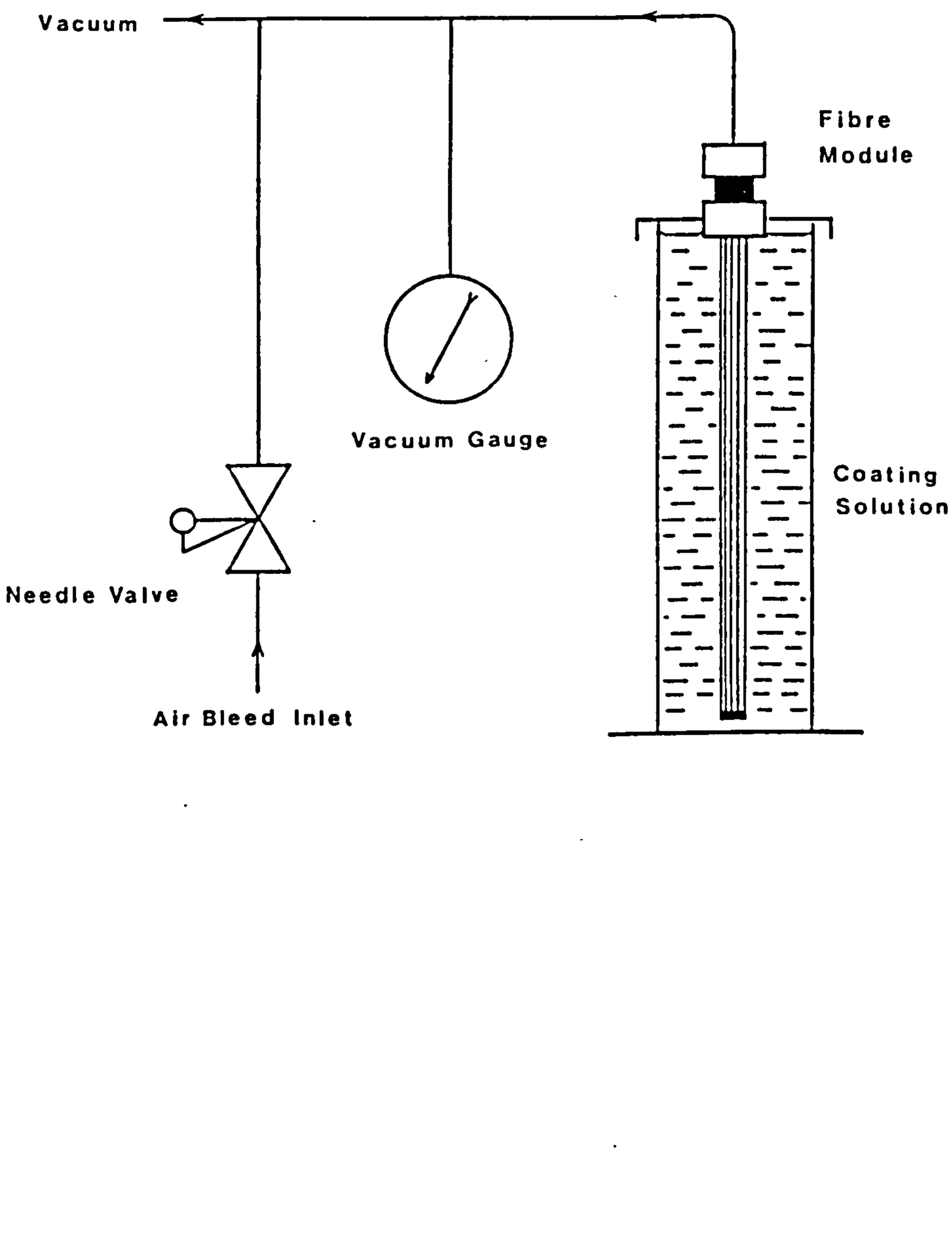

curing, a time of seven days was generally allowed before further testing or treatment was carried out.

Coating with a latex based system.

This method was almost identical to the solvent system except that the coating was applied from a water based dispersion. The latices used were shown to have good film forming properties when the dispersing medium evaporated. Being water based there was no danger of damage to the surface skin. The latex coating was dried at room temperature in a dust free environment for seven days before further testing or treatment.

2.3.6 Sulphonation of hollow fibres.

Polysulphone P3500 has been used successfully to produce hollow fibre membranes of a good engineering standard. It has been reported that sulphonated polysulphones have better gas separation properties than polysulphone [65]. In an aim to benefit from both the engineering properties of the polysulphone and the gas separation properties of the sulphonated polysulphone it was decided to attempt to sulphonate just the surface skin layer, which could result in a well engineered polysulphone fibre with superior gas separation properties.

The following gas phase treatment was used in an attempt to sulphonate the surface without the use of liquid solvents which might have resulted in other changes in the fibre morphology.

Sulphur trioxide vapour is a strong sulphonating agent [66] and was the ideal choice for a gas phase reaction. Sulphur trioxide is supplied in a stabilised form in which it appears as a white crystalline solid of polymerised trioxide. This readily breaks down into a cloudy vapour and a colourless liquid. Passing nitrogen gas over the solid is sufficient to produce copious quantities of dense white vapour. In this manner SO_3 vapour was produced and circulated around a fibre module within a

bell jar for the required length of time. A steady flow of vapour was maintained with residual vapours being passed through a solution of sodium hydroxide before being vented to a fume hood. (See Fig 2.10).

It was possible to test the effect of SO_3 on the fibres by observation of the interaction of a basic dye with the fibres. Unsulphonated, standard polysulphone will not take up a basic dye as the polymer has no acid groups. However, sulphonated polysulphone contains sulphonic acid groups which readily interact with basic dyes resulting in a strong staining of surface sulphonated fibres. It was found that less than 20 seconds exposure to SO_3 was sufficient to produce a strong positive staining with a cold solution of the dyestuff. However, prolonged exposure, of ten minutes or more, still resulted in only the surface layer being sulphonated.

Fig 2.10 Sulphonation apparatus.

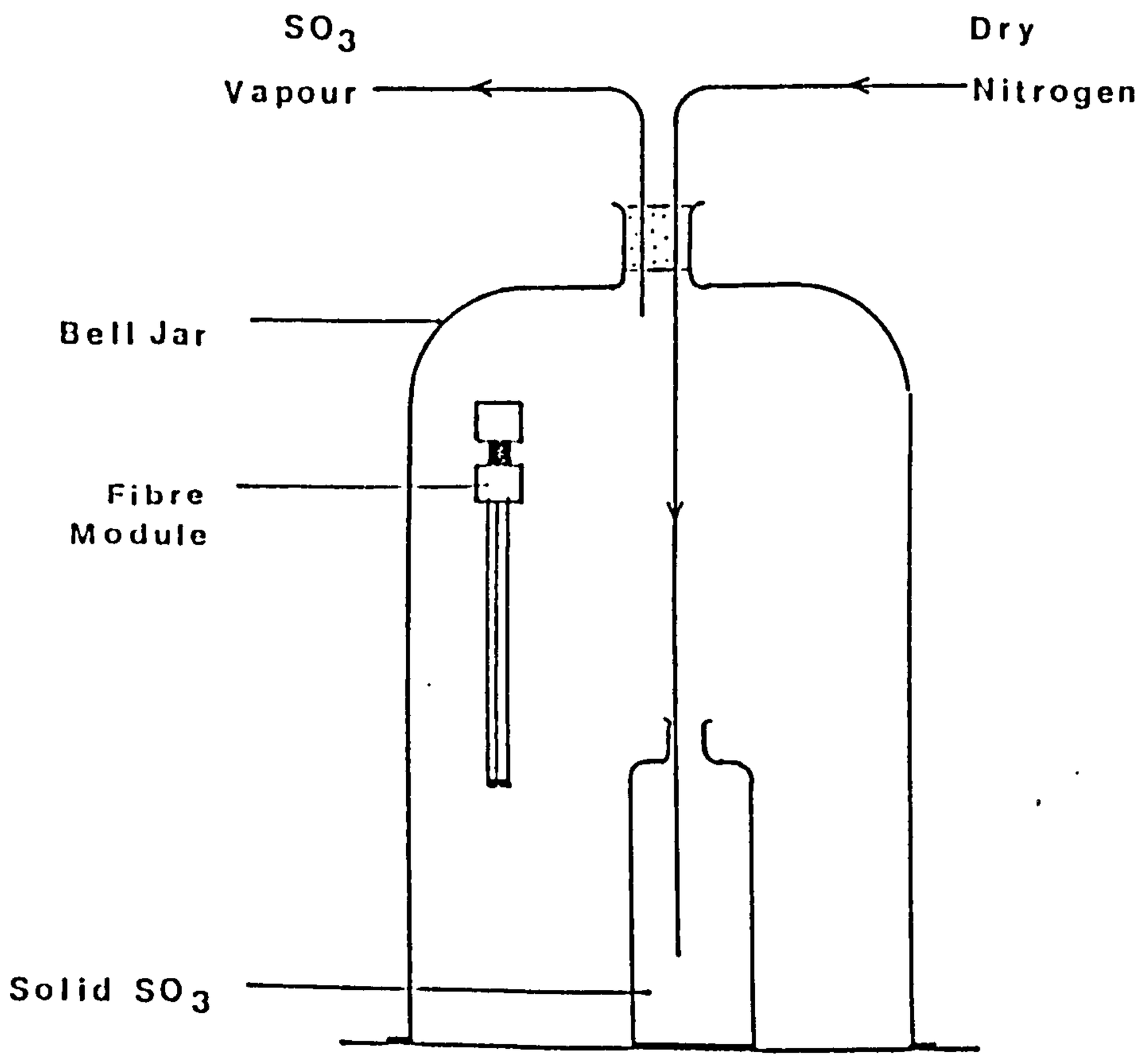

2.4 Characterisation techniques.

So far in this chapter the methods employed in producing membranes have been described. The remaining part of this chapter is concerned with the analytical techniques used to examine the morphology of the fibres and their usefulness for the separation of gases.

2.4.1 Examination of coagulation by optical microscopy.

The coagulation mechanisms of different dope/precipitant combinations were examined using a glass cell as shown in Fig 2.11. The cell was made from two microscope slides sealed together on three sides with a spacer. The polymer solution was injected into the cell from the fourth side. The filled cell was immersed in a petri dish of precipitant and the coagulation front was then observed by placing the entire assembly onto a microscope stage. Viewing the phase inversion process by microscope enabled details of the mechanism of precipitation to be obtained.

2.4.2 Examination of the coagulation mechanism by Schlieren detection of solvent convection.

Cabasso [44] describes this experimental method for detecting which component diffuses fastest during a phase inversion process (see section 1.2.3). The method is based on the detection of convective flow patterns which occur as a result of solvent/nonsolvent exchange. The apparatus shown in Fig 2.12 consisted of a small illuminated coagulation tank. Behind the tank was placed a card which had ruled lines drawn across it with a spacing of less than 2 mm. A sample of polymer solution was placed at the bottom of the tank and the ruled card was then

Fig 2.11 Apparatus for observation of membrane precipitation.

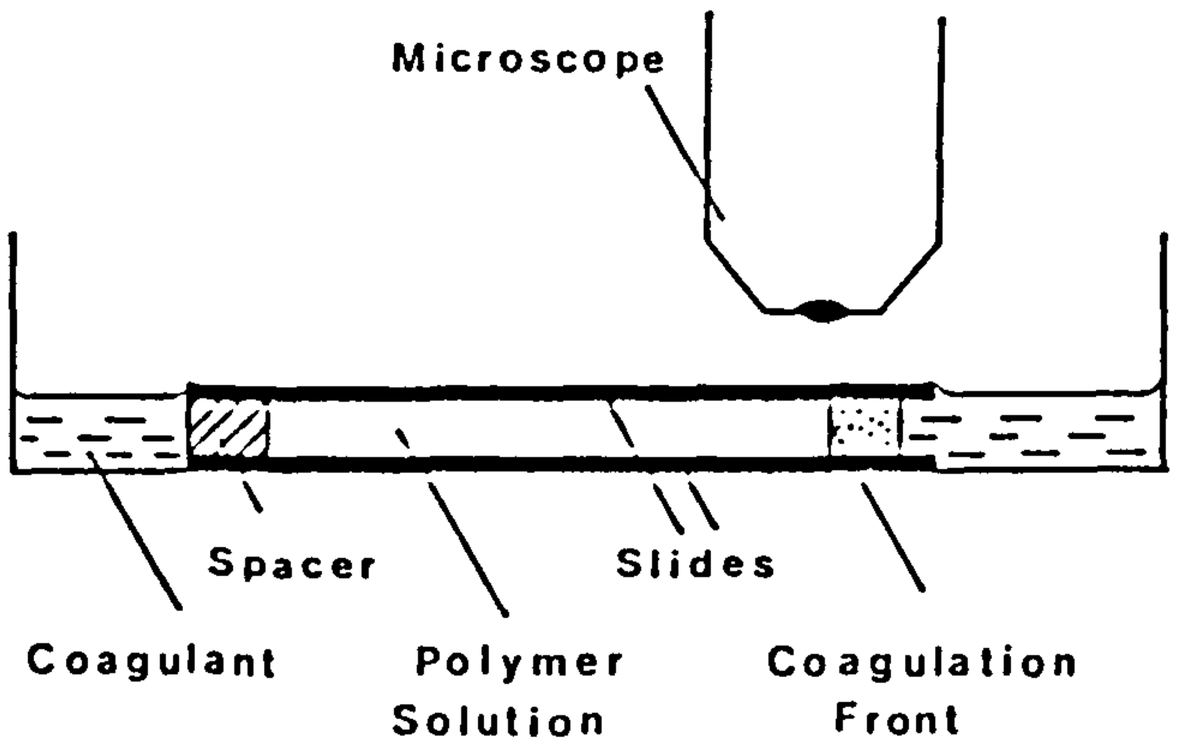

Fig 2.12 Apparatus for Schlieren detection of solvent emission.

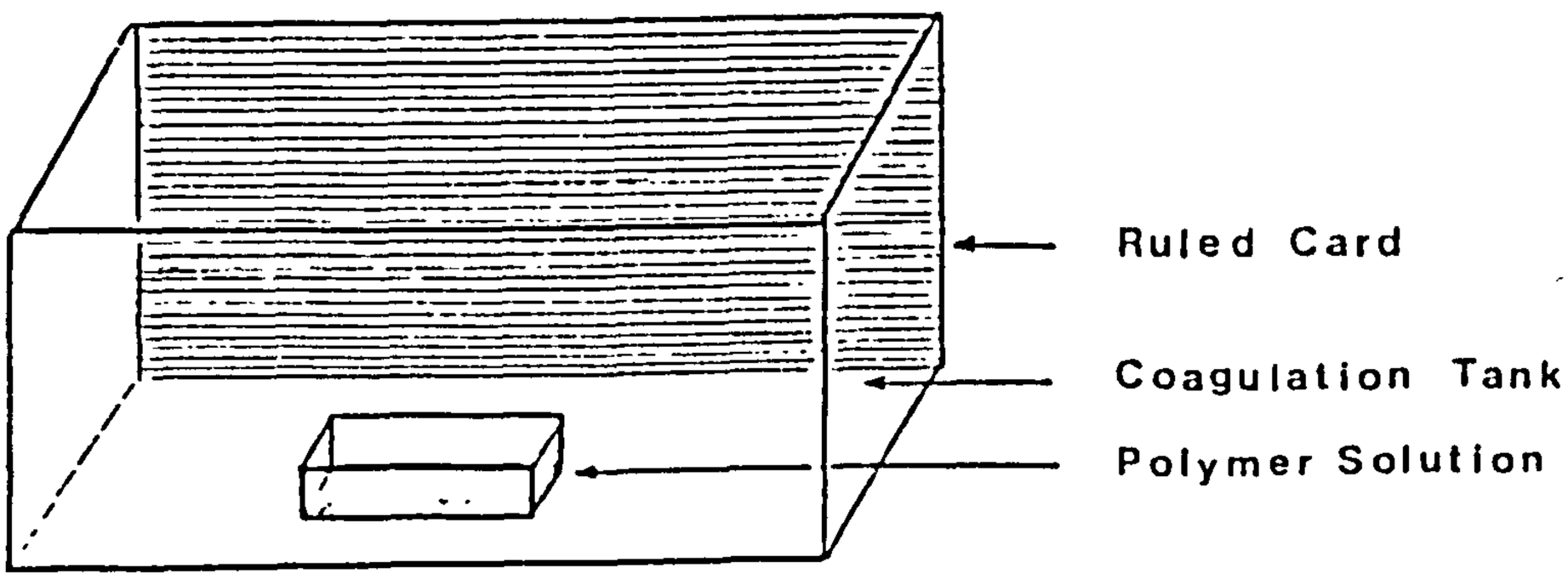

observed through the tank. Any liberation of solvent into the precipitant was detected by the convective flow patterns distorting the image of the ruled lines.

2.4.3 Examination of membrane morphology by Scanning Electron Microscopy.

Scanning Electron Microscopy (SEM) proved to be an invaluable tool for examining the sub-structure of membranes. The detailed morphology of the membranes was beyond the resolving power of light microscopy and so the SEM was indispensible for analysis of structure.

Two different microscopes were used. Firstly, and more often, a Cambridge Stereoscan (150 Mk2) was used for analysis of structural detail and secondly, a Hitachi (S600) complete with an energy dispersive X-ray analyser was used when elemental composition of specific features was required.

The majority of samples examined were cross-sections of membranes. To prepare a clean cross-section the specimen was immersed in liquid nitrogen, to lower the polymer's temperature to below the brittle point (-101 ^{o}C. for polysulphone [57]). The immersed membrane was then fractured to give a sharp, clean cut. The specimen was then mounted on a stub before being sputter coated. The samples examined on the Cambridge instrument were gold coated, which gives the best contrast, whilst the Hitachi samples were coated with carbon graphite which allowed the transmission of the x-ray radiation. Photographic records were kept of all samples examined under the microscopes from which detailed structural analysis was made.

2.4.4 Measurement of fibre dimensions.

There are three important parameters associated with a hollow fibre, namely the total diameter (d_f), the lumen diameter (d_i) and the wall thickness (d_w). For a perfect cylindrical fibre $d_f = d_i + 2(d_w)$.

Three methods of measurement were employed during the course of the research. Each method had its own advantages and disadvantages.

(a) Measurement by micrometer.

A micrometer was used to make measurements of the fibre d_f. By closing the jaws of the micrometer gently against the wall of the fibre a quick, and fairly accurate measurements could be made without damaging the fibre. The advantage of this method was that a large number of measurements could be made quickly allowing a statistical average to be calculated. This method was the only non-destructive measurement method though only d_f could be assessed. Problems were encountered when the fibre had a non-cylindrical cross-section. Elliptical cross-sections tended to align themselves in the jaws such that the minimum d_f was measured instead of a mean value.

(b) Measurement by SEM.

By taking photographs of the SEM images an accurate measurement could be made of the three fibre dimensions. However, the disadvantage was that only one set of measurements could be made for each batch of fibres, due to limited access to the instrument and to the time required for the processing of the photographic film.

(c) Measurement by light microscopy.

The accessibility of light microscopes is not normally a problem and so this technique was generally used when SEM facilities were not available. The fibres were fractured under liquid nitrogen before mounting, as in the case of SEM samples. Difficulties arose in practice due to the poor depth of field associated with light microscopy. In

order to overcome this limitation it was important to mount the samples as near to the vertical axis as possible in order to bring the entire cross-section into the same horizontal plane.

2.4.5 Determination of membrane void volume.

The percentage void volume of a porous membrane was determined by comparing the weight per unit volume of the membrane to that of a similar volume of base polymer.

By using simple geometry it is possible to calculate the % void volume of a perfectly cylindrical hollow fibre:-

$$\% \text{ void volume} = \left[1 - \frac{4\,W}{\rho_p\, l\, \pi\, (d_f^2 - d_i^2)} \right] \times 100 \qquad (2.1)$$

where W is the weight of a hollow fibre of length, l. ρ_p is the bulk density of the polymer (1.24 g/cm^3 for polysulphone P3500 [57]).

2.4.6 Determination of solvent retention in coagulated fibres.

Solvent remaining in coagulated membranes after spinning can have a critical effect on membrane performance. Solvents acting as plasticizer can increase the permeability and lower the permselectivity of a membrane to diffusing species. The amount of solvent retained in a membrane was assessed using Thermo-Gravimetric Analysis (TGA). In this technique the weight of a sample of membrane was monitored against a linear increase in temperature. At a certain temperature the retained solvent escaped from the membrane which was recorded as a weight loss from which the percentage solvent in the membrane was calculated. The instrument used for this study was a Dupont 951 Thermogravimetric

Analyzer controlled by a Dupont 990 Thermal Analyzer.

2.4.7 Determination of gas transport properties.

There are two important parameters which characterise the gas transport properties of a hollow fibre membrane namely, the permeability and the selectivity. However, when a complicated structure, such as an asymmetric hollow fibre membrane, is encountered the permeability and selectivity are difficult to determine. Instead two other parameters are determined. The first parameter is based on the permeability of the membrane to a certain gas and is called the permeation rate constant ('P) and is numerically equal to the permeability per unit thickness of membrane. The reason that the permeability cannot be determined is due to the difficulty in determining the effective thickness of an porous asymmetric membrane. If the permeability of polysulphone to a given penetrant is a constant independent of the morphology of the membrane then the effective thickness of a porous membrane can be calculated as the permeability of a dense membrane of the same material divided by the permeation rate constant of the porous membrane. The second parameter, which replaces the selectivity, is known as the separation factor. Meares [32] has derived the relationship between selectivity and the separation factor which was described in section 1.2.2. The separation factors quoted are the ratio of permeation rate constants of a membrane to two gases. This ratio, however, does not represent the membrane's separation performance when subjected to a gas mixture. In order to express the performance of a membrane to a gas mixture accurately an enrichment factor should be quoted whose value can only be determined by subjecting the membrane to the specific gas mixture, and may well be dependent on the relative composition (i.e. a different enrichment factor may be obtained for a 50:50 mixture from that of a 90:10 mixture).

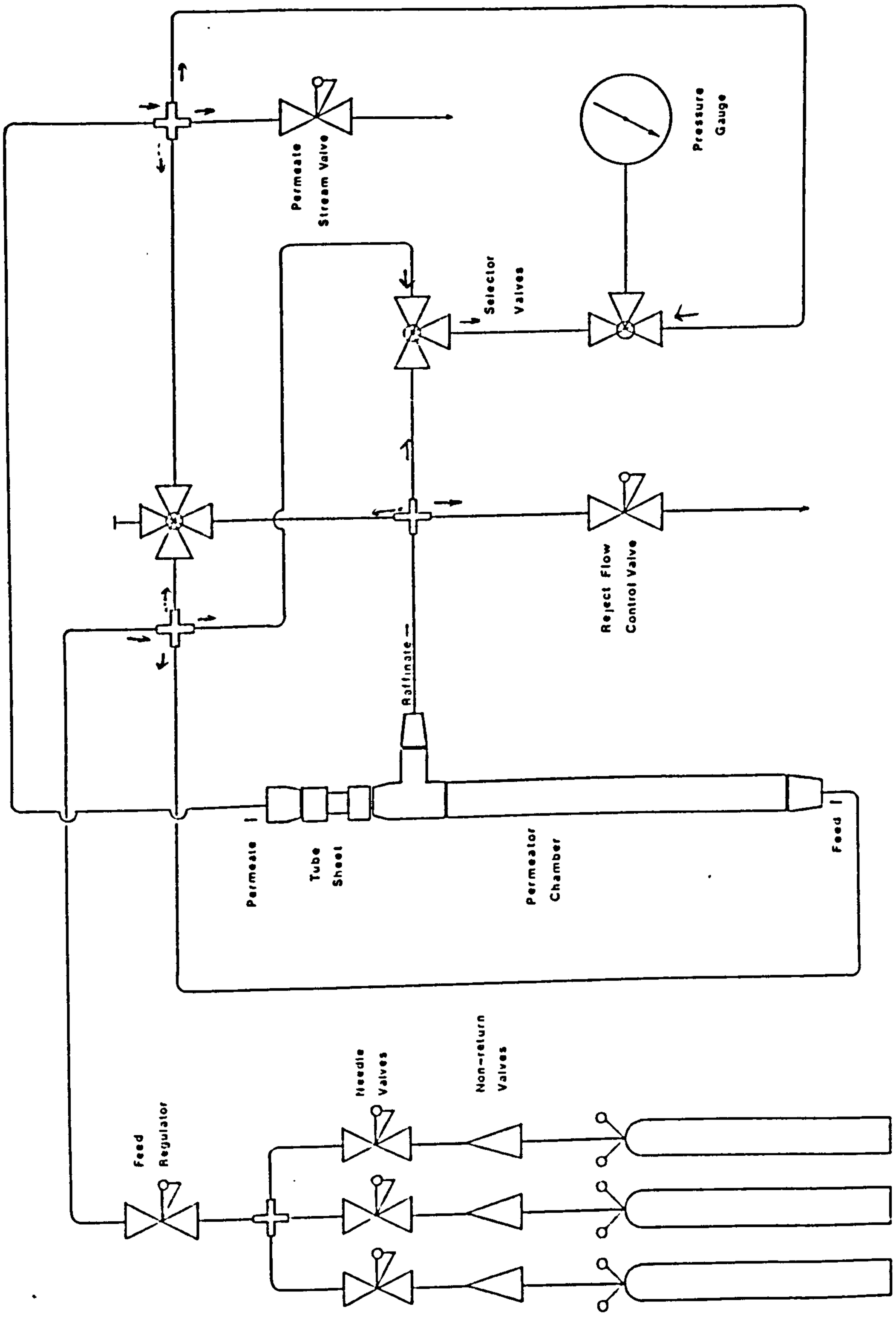

Fig 2.13 The gas permeation rig.

Fig 2.14 A soap bubble flow meter.

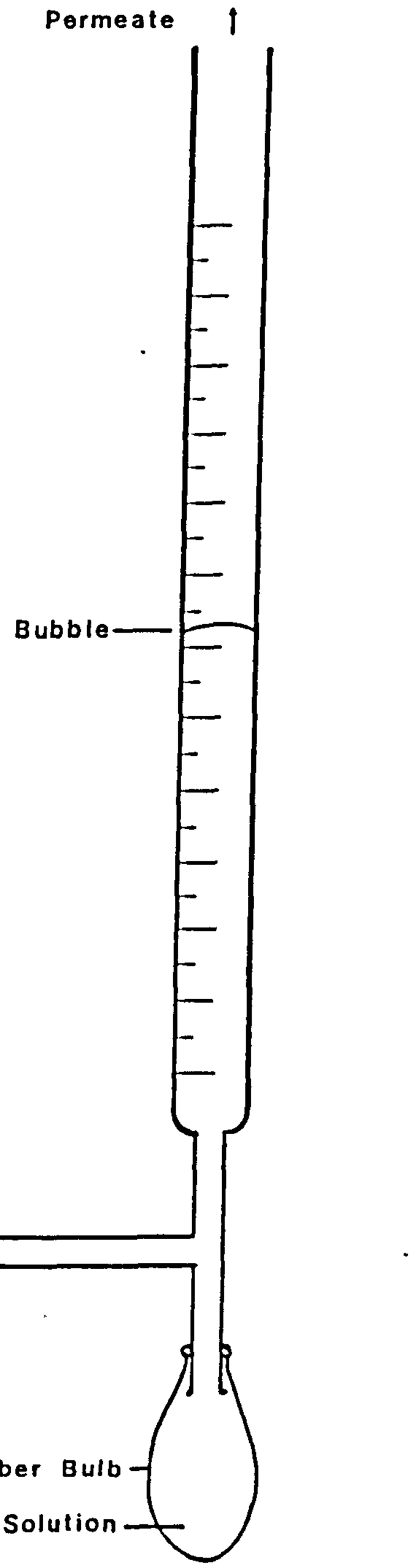

An apparatus was constructed by the author, based on a similar design of apparatus used at British Gas, for the measurement of these parameters.

(a) Construction of the laboratory permeation rig.

Fig 2.13 shows a detailed layout of the permeation rig. The rig was constructed from a mixture of copper, brass and stainless steel fittings. Stainless steel parts are preferable for construction, where costs allow, but essential for fittings that are exposed to high pressures (>1000 psi) and at points which could suffer from wear (i.e. the screw threads where the fibre module was inserted into the permeator chamber). Compression fittings were used on all connections to pipe work and gave leak free seals up to and above 2000 psi. All the fittings in the gas selection section were made of stainless steel as they were exposed to full cylinder pressure. Non-return valves were used to prevent back mixing of the gases which could occur by accident if two cylinders were open at the same time. At the end of the selection section was the main feed regulator. which controlled the pressure delivered to the outer surface of the hollow fibres. The internal pressure (the pressure within the lumen of the fibre) was controlled by the permeate stream valve. This valve was usually kept fully open such that the low pressure side of the membrane was as close to atmospheric pressure as possible.

The permeator chamber was assembled for co-current flow, but was designed so that the chamber could easily be converted to a counter-current configuration. The flow rate along the fibres was controlled by the reject stream valve. Adjustment of this valve had a secondary effect of slightly altering the pressure on the high pressure side of the membrane; thus a careful balancing of the feed regulator and reject stream valve was necessary to achieve particular pressure

differences and flow rates.

All pressure measurements were made on a single pressure gauge, selection being made between feed, raffinate and permeate by use of the selection valves. Due to the small membrane area in the permeator chamber a negligible pressure drop was observed between the feed and raffinate.

Permeate flow rates were measured using soap bubble flow meters attached to the permeate stream valve via neoprene tubing. These flow meters were constructed by modifying borosilicate glass burettes. The burettes were modified by replacing the tap with a 'T' shaped piece of glass tubing as shown in Fig 2.14. The rubber bulb fitted to the base of the 'T' piece was filled with a soap solution. By squeezing the bulb a bubble was introduced to the junction in the 'T' from where it was carried up the graduated column by the permeate gas stream at a constant rate. The permeate flow rate was then calculated by measuring the length of time required for the bubble to pass through a known volume within the burette. Four modified burettes were made (100 ml, 50 ml, 10 ml & 1 ml) to allow a range of flow rates to be measured.

Finally a five-way ball valve was connected to allow sampling to be made from the three gas streams. Although this had little practical use in the rig built by the author, the sister rig at British Gas was linked to a gas chromatography unit via this valve.

(b) Determination of gas transport parameters from single gas studies.

The permeation rate constant of a gas through a hollow fibre membrane was calculated from the following equation:-

$$'P_i = \frac{Q_i}{\pi \; n \; l \; d_f \; \Delta p} \qquad (2.2)$$

where Q_i = Flow rate of gas i across the membrane.

n = number of hollow fibres in the permeator (10 in all cases).

l = length of fibre in the module.

d_f = outer diameter of the fibres.

Δp = pressure difference across the membrane.

It is customary to present permeability in units of Barrer which are:

$$\frac{cm^3\ (STP)\ \ cm}{cm^2\ \ s\ \ cmHg} \times 10^{-10}$$

Monsanto [56] continued this tradition for hollow fibres expressing their permeabilities (permeation rate constants) in terms of gas permeability units (GPU):

$$1\ GPU = \frac{cm^3\ (STP)}{cm^2\ \ s\ \ cmHg} \times 10^{-6} \qquad (2.3)$$

The equivalent S.I. unit for permeability would be:

$$\frac{m^3\ (STP)}{m\ \ s\ \ Pa}$$

where 1 Barrer equals 7.50×10^{-18} of the above S.I. units. The S.I. unit for the permeation rate constant would be:

$$\frac{m^3\ (STP)}{m^2\ \ s\ \ Pa}$$

where 1 GPU equals 7.50×10^{-12} of these S.I units.

In order to maintain tradition in the field all permeation rate constants are given in GPU.

(c) Operation of the permeation rig.

The pressure gauge was adjusted to zero on a daily basis, to compensate for variations in atmospheric pressure. The fibre module to be tested was inserted into the permeator chamber and the compression fittings were leak tested with soap solution. The valves to the desired gas cylinder were opened and the feed regulator was set to 100 psi (0.69 MPa). The rate of flow along the membrane was set to the required level using the reject stream valve before the feed regulator and permeate stream valve were balanced to give a pressure difference of exactly 100 psi. Once the pressures and flow rate were set the rig was left to equilibrate for at least one hour before measurements of gas flux were made. At least five measurements of flux were made at ten minute intervals to ensure that a steady permeation rate had developed.

Each gas was measured in the same manner to give permeation rate constants for a range of gases. Separation factors were then calculated from the ratios of the permeation rate constants.

(d) Determination of gas transport parameters from gas mixture studies.

Membrane performance using a gas mixture was assessed with the aid of a gas chromatography unit. This resource was only available at the British Gas research station and due to limited access to the station only a few measurements were possible.

The gas analysis was made by passing the gas mixture through a Perkin Elmer Sigma 4B gas chromatograph controlled by a Sigma 1 programmer. Separation was made using a two metre porapak QS column at 40^{o}C. with nitrogen as the carrier gas. The permeator rig was operated in the same manner as before with the addition of sampling of the gas feed, raffinate and permeate. Three or more samples were taken from each stream to ensure a steady state had developed and to allow an

estimate of the variance to be made. Output from the Sigma 1 was displayed in terms of percentage composition of the sample taken. Together with the measurements of permeate flux it was possible to calculate the enrichment factor and the 'pseudo'-permeation rate constant.

$$\Phi_j^i = \frac{X_j^1 (1 - X_j^h)}{X_j^h (1 - X_j^1)} \qquad (2.4)$$

where Φ_j^i is the enrichment factor.

X_j^h is the mole fraction of j in the feed supply.

X_j^1 is the mole fraction of j in the permeate.

$$\Pi_i = \frac{Q \; X_i^1}{A \; \Delta w_i} \qquad (2.5)$$

where Π_i is the pseudo-permeation rate constant of component i.

Q is the permeate flow rate.

X_i^1 is the mole fraction of i in the permeate.

A is the membrane area.

Δw_i is the partial pressure difference of component i across the membrane.

(e) Determination of collapse pressures.

In order for a hollow fibre membrane to be useful in industry it must be able to withstand a considerable pressure difference across its wall thickness. As permeate flux is generally proportional to the pressure difference then higher pressures lead to better productivity. However, there is a point above which a hollow fibre's cylindrical structure cannot withstand the pressure acting upon it and this is known

as the collapse pressure.

Determination of the collapse pressure was made using the permeation rig. Nitrogen gas was used as the source gas for reasons of safety. At high pressures the permeate flux may be of the order of several litres per minute and if flammable gases were used this could lead to explosive mixtures being created in the laboratory environment. Carbon dioxide cannot be used as the source gas as the full cylinder pressure is insufficient.

The permeate flux was measured in the usual way but over a range of pressure differences. The maximum feed pressure, governed by the upper limit of the main feed regulator, was 850 psi (5.86 MPa). The data collected were plotted as a graph of permeate flux against pressure difference to show the collapse profile from which the collapse pressure could easily be found.

2.4.8 Measurement of the change in temperature of liquids on mixing.

The temperature change on mixing of two liquids was measured under controlled conditions using a thermometer calibrated in 0.1^{o}C. intervals. The two liquids to be mixed were kept at room temperature before mixing. The first liquid was contained in an insulated beaker, stirred vigorously by a magnetic stirrer. The temperature was noted before an equal volume of the second liquid was quickly injected into the first. The change in temperature was recorded at the point of greatest change.

CHAPTER 3

Results and discussion.

3.1 Material selection.

3.1.1 The prior work of Dr. V. Rogers.

Dr. V. Rogers started the work on hollow fibres at Leeds University. Following the work of Monsanto [56] and Cabasso [67], Rogers based his work on polysulphone, for the reasons outlined in section 1.2.4. Rogers spun his fibres using the dry-jet wet-spinning technique as described in the experimental section. Using DMAc as the solvent for the polymer and water as coagulant, fibres were produced with a morphology similar to that shown in Fig 3.1 and plate 3.1. Five zones were readily identifiable as described by Asahi Kasei Kogyo Kabushiki Kaisha [68]. Zones A_o and A_i were the outer and inner dense skin layers respectively; zones B_o and B_i the void layers containing large finger-shaped macrovoids; and zone C, linking zones B_o and B_i, characteristically had a similar pore structure to zones B_o and B_i but with the absence of macrovoids.

The macrovoids, present in such large numbers, severely reduce the fibre's ability to withstand pressure and failure typically occurred at pressures of less than 2.8 MPa (400 psi). In order for the membranes to be used effectively in industrial separations, a collapse pressure above 4 MPa (600 psi) would be required and preferably of the order of 6.9-10.3 MPa (1000-1500 psi) [69]. To produce fibres with a sufficiently high collapse pressure it was necessary to develop a fabrication technique in which macrovoid formation was not favoured. From the information reproduced in section 1.2.3 it was decided that two approaches could be made:- firstly, to adapt the DMAc/water system and secondly, to use a different solvent-nonsolvent combination for phase inversion.

Fig 3.1 Schematic diagram of a DMAc type fibre.

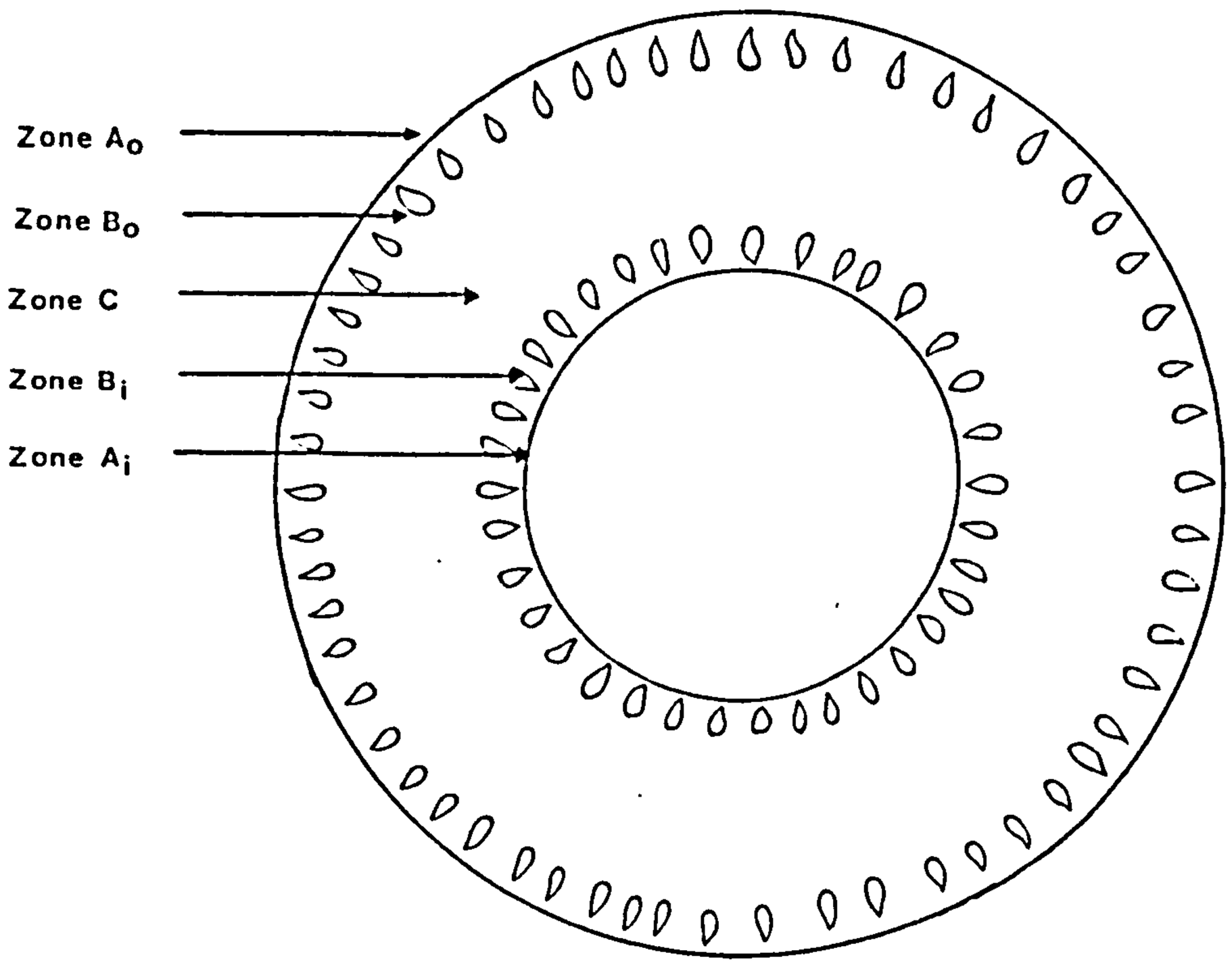

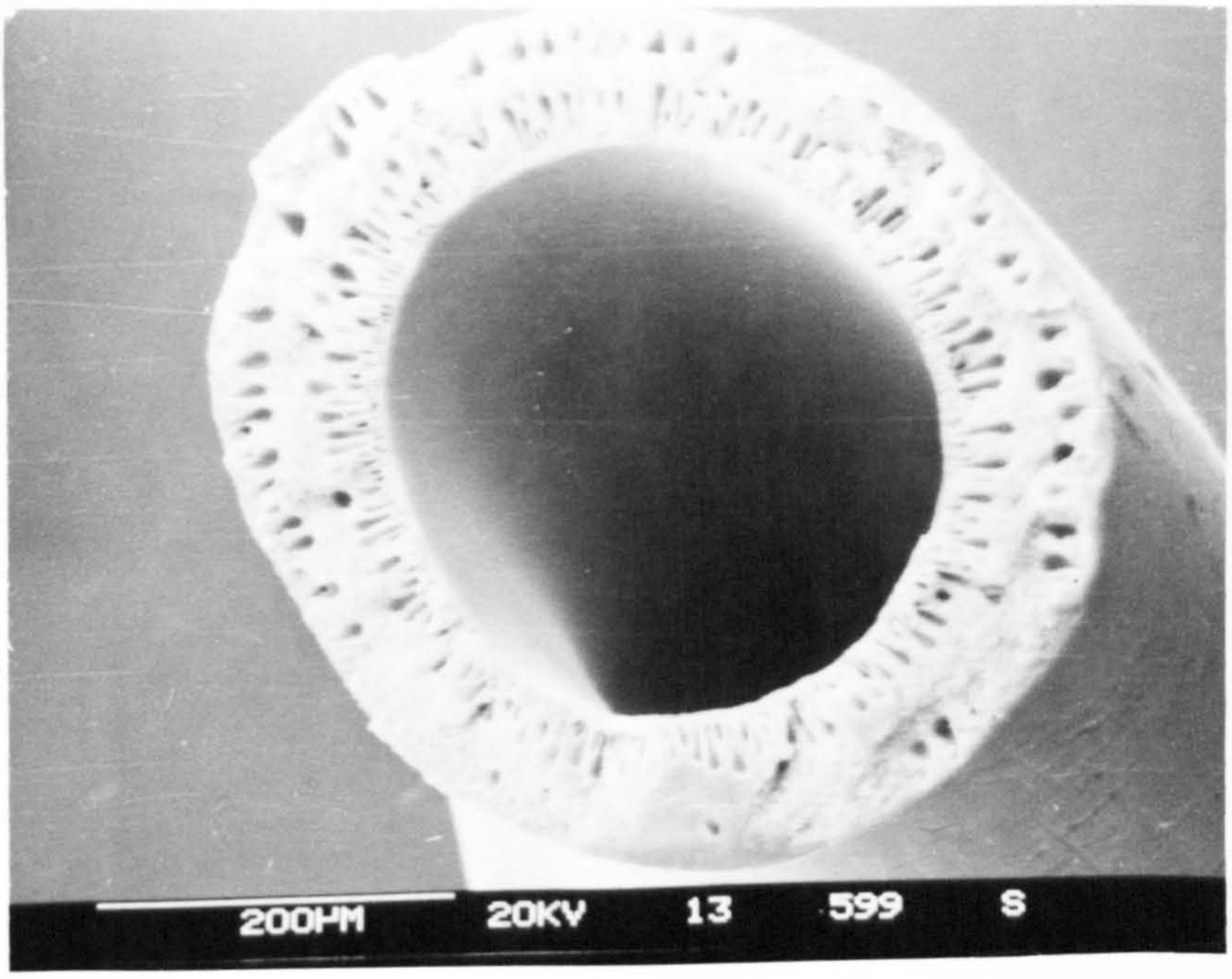

Plate 3.1 Typical DMAc type fibre (30%).

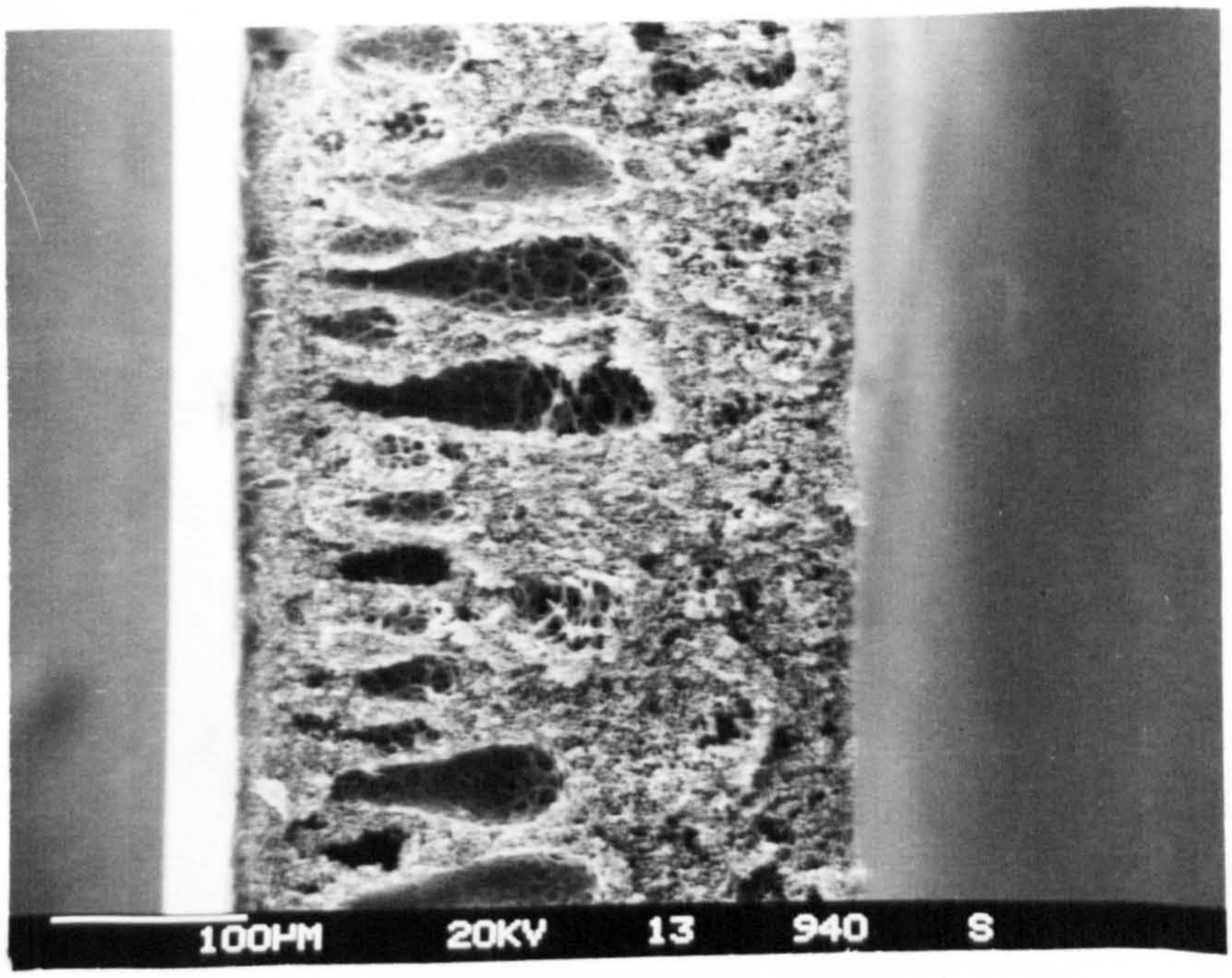

Plate 3.2 DMac type fil, (30%) coagulated in water.

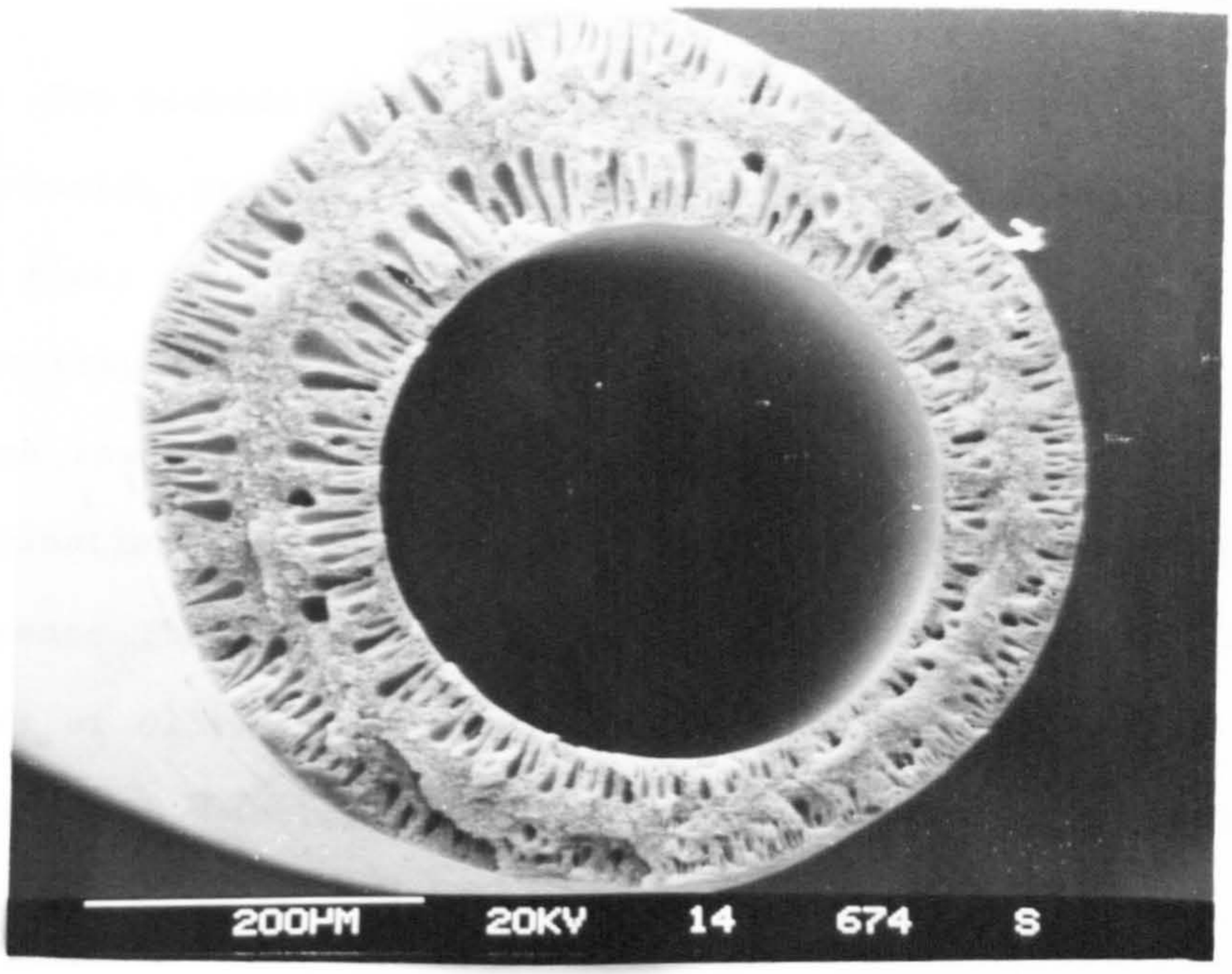

Plate 3.3 DMAc type fibre (35%)

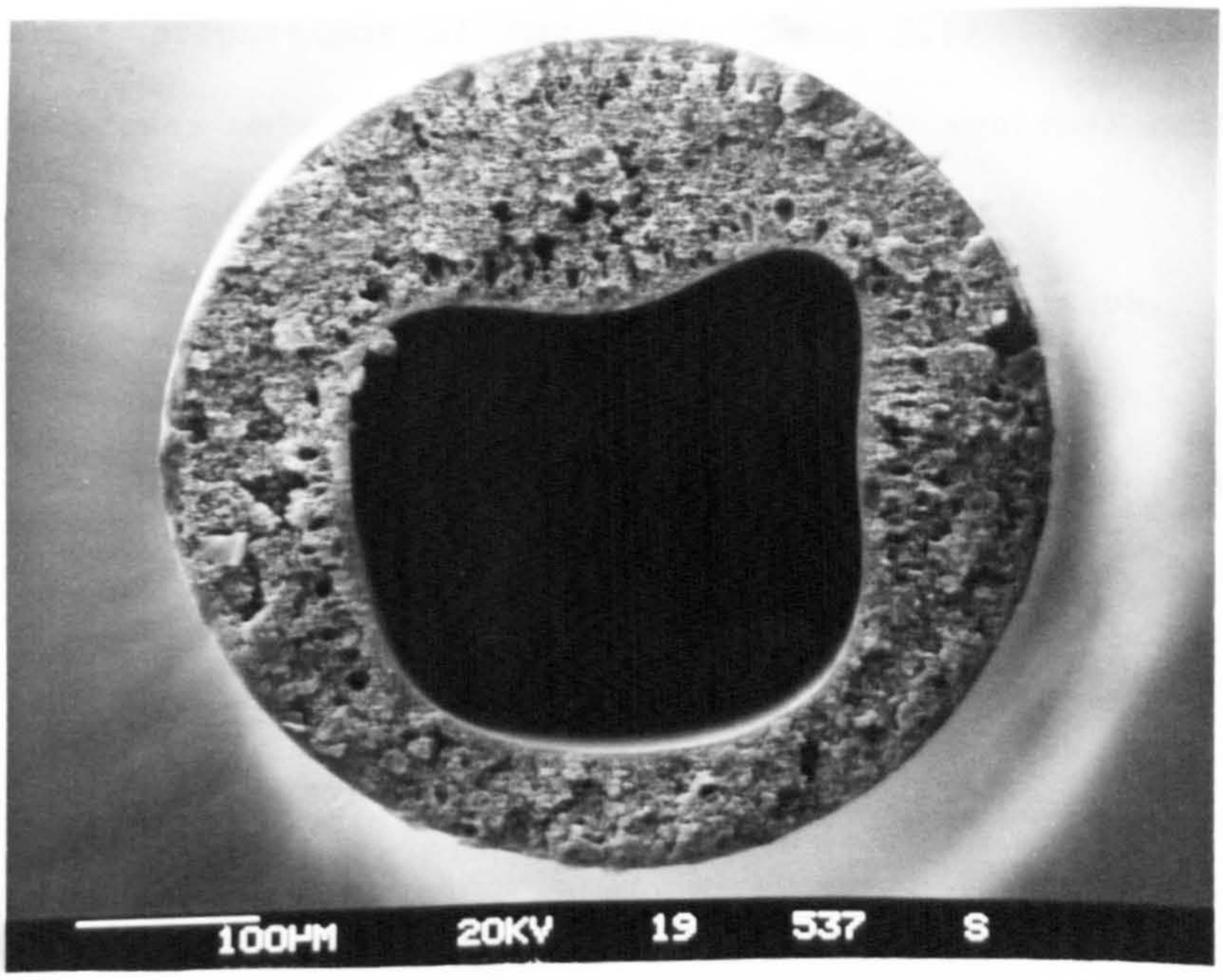

Plate 3.4 DMAc type fibre (40%).

3.1.2 Elimination of macrovoids, I. Improvement of the DMAc/water system.

Two methods were investigated with the aim of reducing the number of macrovoids present in the fibre morphology for the DMAc/water system. The first method involved the addition of DMAc to the coagulation bath in an attempt to lower the rate of exchange of solvent and nonsolvent and hence lower the rate of membrane precipitation. The second method of elimination was as described by Frommer and Lancet [48], i.e., to increase the viscosity of the polymer solution in order to lower the rates of diffusion in and out of the nascent membrane. This was to be achieved by increasing the concentration of polymer in the casting solution.

(a) Effect of the presence of DMAc in the coagulation bath.

Four films were cast from a 30% $^{w}/_{w}$ polysulphone (P3500) - DMAc solution. The films were precipitated in coagulation baths containing different proportions of DMAc (see Table 3.1). Following coagulation the membranes were soaked in water to remove residual solvent, dried and examined by S.E.M.

Table 3.1 Coagulation bath composition.

Bath	% Dimethylacetamide	% Water
1	0	100
2	20	80
3	60	40
4	80	20

Plate 3.2 shows the morphology of the film coagulated in bath 1. The right hand side of the plate shows the bottom surface of the membrane, i.e. that which was in contact with the glass supporting plate.

The morphology of the bottom surface of the membrane would most resemble zone C of a hollow fibre membrane, as this region lies farthest away from the precipitant during coagulation (N.B. A hollow fibre membrane is precipitated with coagulant from inside as well as outside the casting). The top surface, left hand side of plate 3.2, of the film resembles that of the A_o and B_o zones of a hollow fibre. Many large finger shaped voids were seen to be present in the film as was expected from the corresponding spinning runs. The presence of DMAc in the coagulant had a negligable effect on the morphology of the top surface of the film membrane. Macrovoids were still to be found in all the films to more or less the same extent. The DMAc in the bath did, however, affect the bottom surface of the films. The films which had been precipitated in high concentrations of DMAc were observed to contain a second skin layer and a second zone of macrovoids in the bottom half of the film. This was most likely caused by a breaking of the adhesion between the casting solution and the supporting glass plate by the DMAc in the coagulant. The result was that coagulant was able to penetrate between the casting and the glass plate and initiate a second coagulation front. This phenomenon would be of no consequence for a self-supporting hollow fibre.

The main conclusion from the experiment was that the presence of DMAc in the coagulant would have little noticeable effect on the morphology of a hollow fibre membrane, even at concentrations as high as 80%. The affinity of DMAc and water for each other was therefore presumed to be so great that the rate of precipitation was unaffected by the presence of large quantities of DMAc already present in the water in the coagulation bath.

(b) Effect of polymer concentration.

Three spinning dopes were prepared containing 30, 35 and 40% polymer dissolved in DMAc. Fibres spun from these dopes were examined by S.E.M., the results being shown in Plates 3.1, 3.3 & 3.4. At 30%

polymer concentration a large number of macrovoids were found to be present in both B_o and B_i zones. However, increasing the concentration of the polymer resulted in a decrease in the macrovoid content and at a concentration of 40% polymer only a few small tear-shaped voids were observed in the B_i layer, and the B_o layer was virtually macrovoid free. It could well be expected that a polymer solution of 45% polymer would yield a fibre with a complete absence of macrovoids. It was not possible to test this, however, due to the difficulty in producing a homogeneous polymer solution from so high a solids content.

3.1.3 Elimination of macrovoids, II. Examination of alternative solvent -nonsolvent systems.

The work of Dr. V. Rogers was primarily concerned with the DMAc/water system. However, other solvent-nonsolvent combinations could possibly yield a satisfactory asymmetric membrane structure. Monsanto [56], for example, quote the use of N-acylated heterocyclic solvents (such as 1-Formylpiperidine (1-Fp)). Monsanto also give useful guidelines in their patent publications as to the requirements a solvent must fulfil in order for it to be considered as a possible liquid carrier for the polymer. In summary, a solvent must be capable of dissolving the polymer and producing a solution with a viscosity in the range suitable for the hollow fibre spinning (10 - 500 PaS). Adequate viscosity should be obtained without resorting to excessive polymer concentrations in the solution. The solvent chosen must be miscible with the chosen nonsolvent without exhibiting excessive heats of mixing. On contact with the nonsolvent the solution should coagulate readily. Other criteria which may be of importance involve the toxicity of the solvent and its ease of recovery from coagulant and washing fluids.

In this subsection, the experiments discussed were designed to examine various solvents and coagulants in order that a membrane might be produced with a morphology better suited to withstand the operating pressures of a gas separation process than the DMAc/water type membranes.

(a) Solvent selection.

Polysulphone has been reported [57, 70, 71] as being soluble in a large number of solvents. Polysulphone P3500 did not, however, dissolve in all the solvents listed. A number of test-tube scale solubility tests were carried out for a number of potential common solvents. The results are presented in Table 3.2. Solvent miscibility with water was also included as coagulation and/or washing in water necessitates a compatible system.

Table 3.2 Solubility and miscibility of polysulphone P3500.

Key	Solvent	Miscibility	Solubility	Reference
1	Dimethylformamide	yes	soluble	70
2	Dimethylacetamide	yes	soluble	71
3	N-methylpyrolidone	yes	soluble	71
4	Pyridine	yes	soluble	70
5	Epichlorhydrin	no	soluble	71
6	Methylene chloride	no	soluble	70
7	Chloroform	no	soluble	70
8	Dimethylsulphoxide	yes	partially soluble	70
9	Acetone	yes	partially soluble	70
10	Morpholine	yes	soluble	70
11	Formamide	yes	insoluble	70
12	Ethanol	yes	insoluble	70
13	Water	yes	insoluble	70
14	1-Formylpiperidine	yes	soluble	--

Fig 3.2 A solubility diagram of a DMAc type fibre.

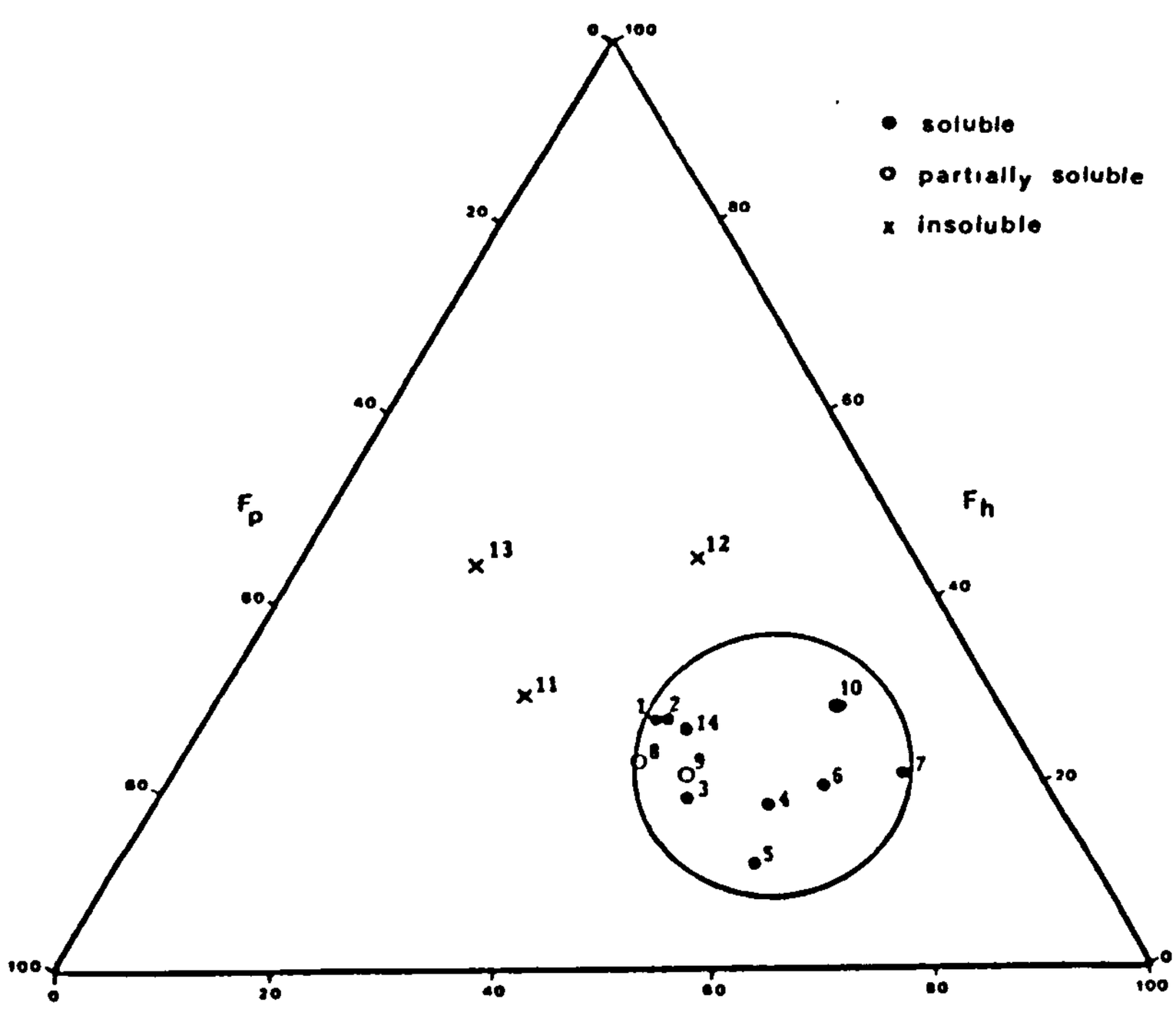

Fig 3.2 is a solubility map for polysulphone p3500. The map uses three co-ordinates to represent the solubility parameters of each solvent. In this method, developed by Hansen [72], the solubility parameter of a solvent is split into three parts each representing an intermolecular force (i.e. dispersion, polar and hydrogen bonding forces). In Fig 3.2 the subparameters are represented as fractional parameters, as developed by Teas [73]. The circle drawn on the map indicates the approximate area of polysulphone P3500 solubility and any solvent falling within that zone should dissolve, or at least partially dissolve, the polymer. The solubility parameter data were obtained from the references cited in Table 3.2. As data were unavailable for the solvent 1-formylpiperidine, the solubility parameters were calculated by Small's method as described by Hoy [74] and are detailed in Appendix 1.

Having produced a list of solvents compatible with the two main criteria the next step was to produce 30% solutions of the polymer in the shortlisted solvents and then to cast some trial films. Films were produced from solutions made with DMAc, DMF and 1-Fp. The morphologies of these films are shown in Plates 3.2, 3.5 & 3.6. Both the DMF and 1-Fp solutions produced films with fewer structural irregularities than with DMAc and consequently it was decided to examine these solvent systems more closely by producing hollow fibres from these 30% solutions. Typical results for the DMF and 1-Fp systems are depicted in Plates 3.7 & 3.8. As can be seen, the fibres spun from DMF appeared to have an almost macrovoid free structure whilst in the 1-Fp type fibres the macrovoids were restricted to the B_i zone. In both cases the structure appeared to be a marked improvement over the DMAc type fibres. It was noted that fibres spun from 1-Fp generally had thicker walls. This was thought to be a consequence of the higher viscosity of the 1-Fp dope.

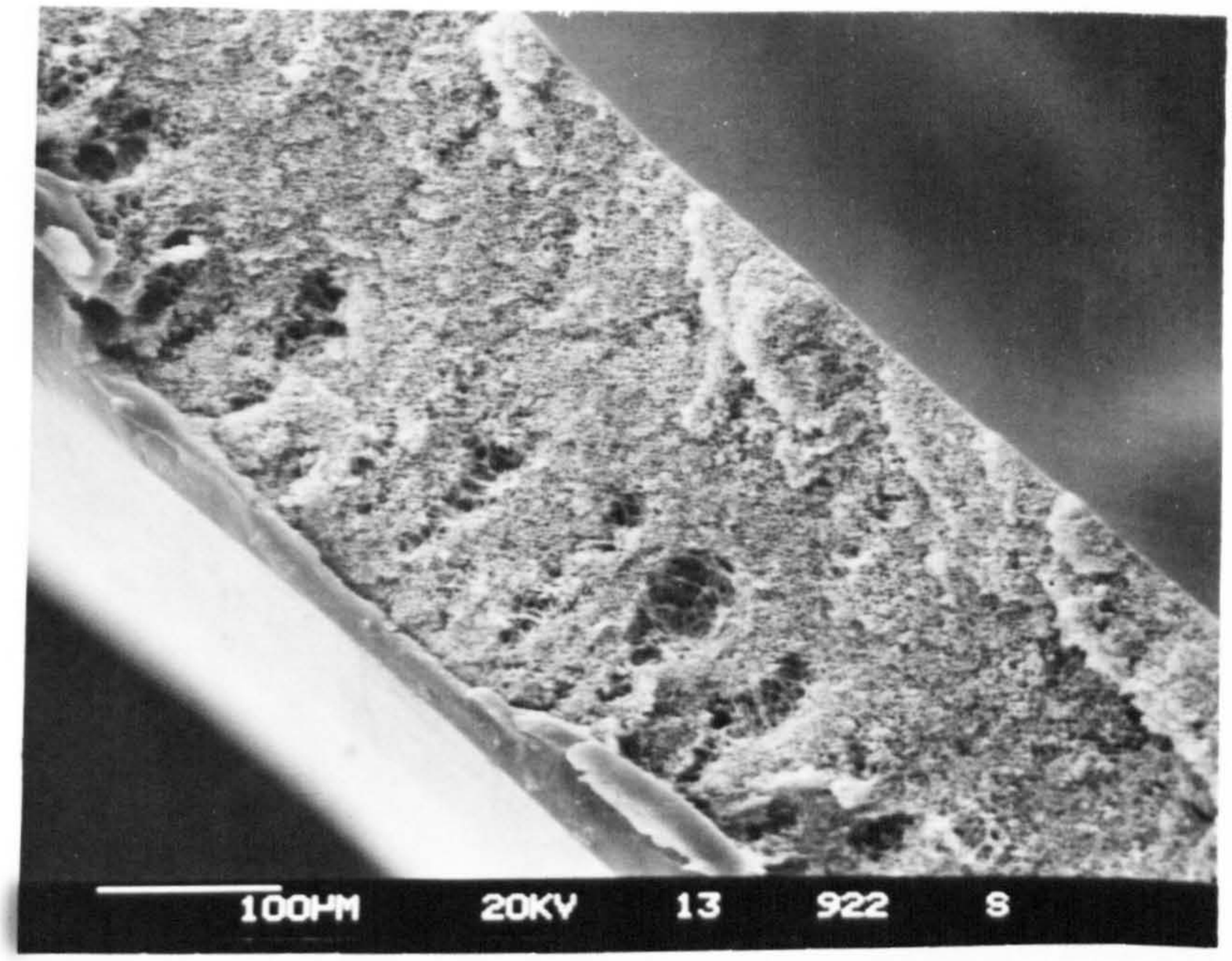

Plate 3.5 DMF type film (30%) coagulated in water.

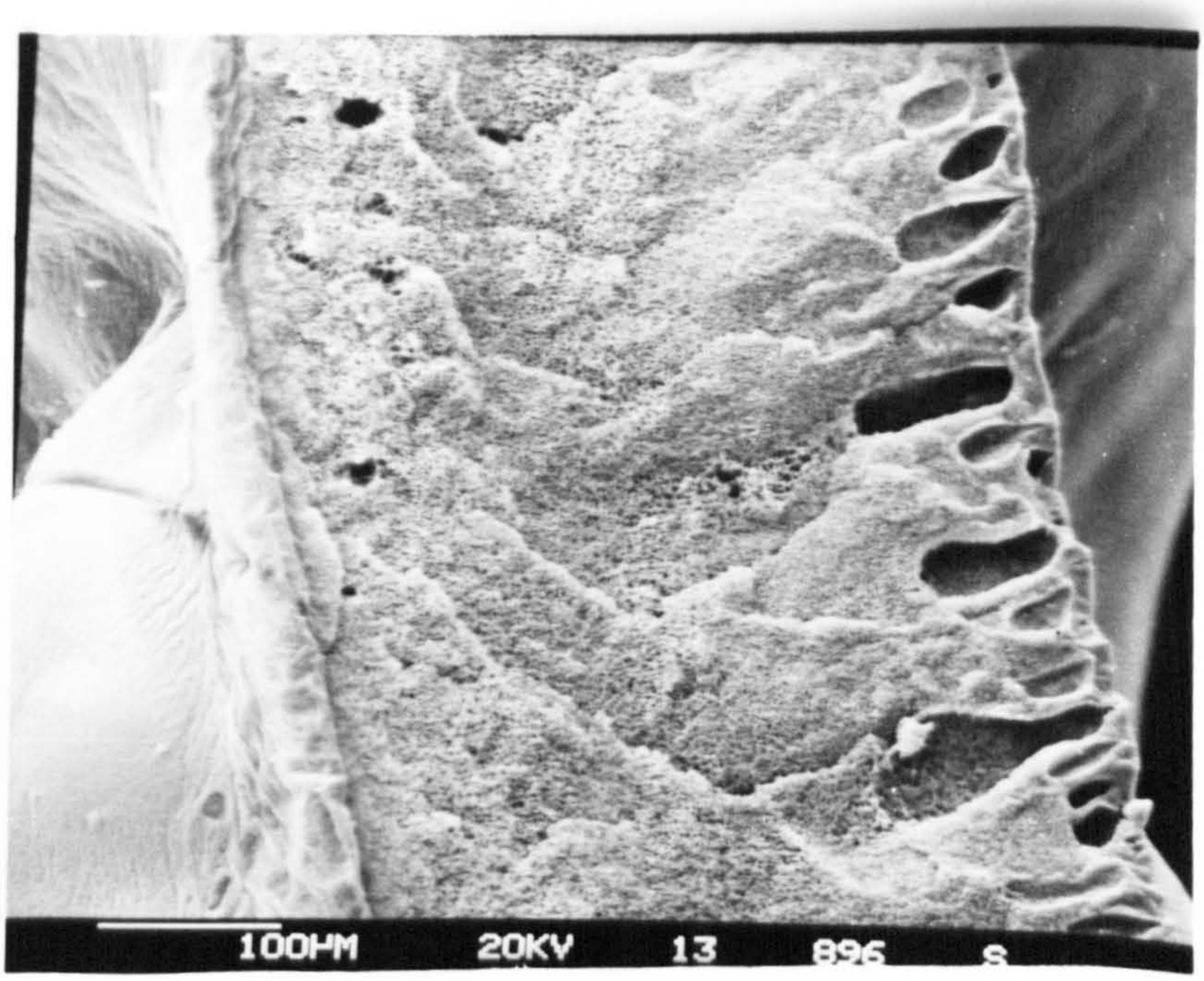

Plate 3.6 1-FP type film (30%) coagulated in water.

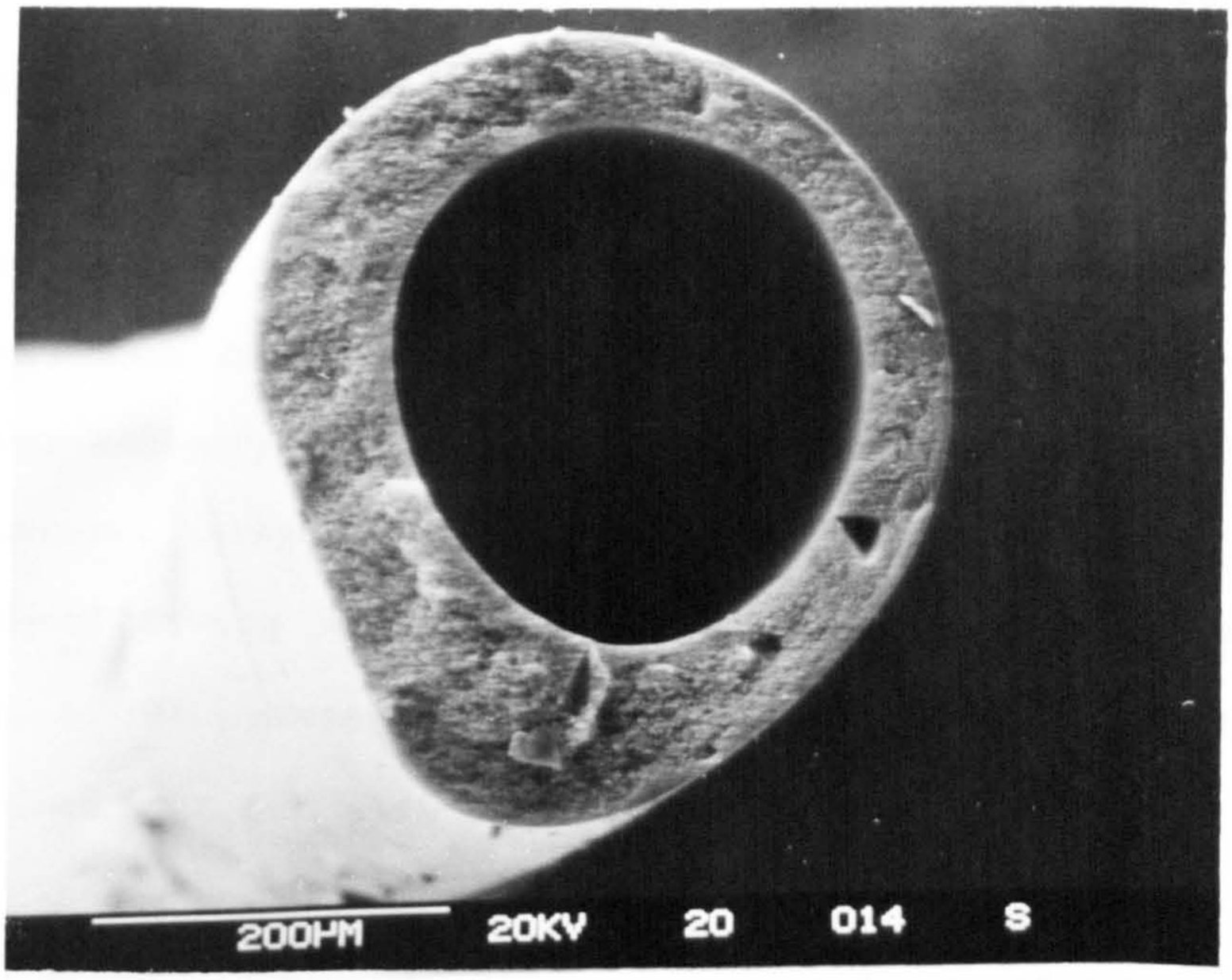

Plate 3.7 DMF type fibre (30%).

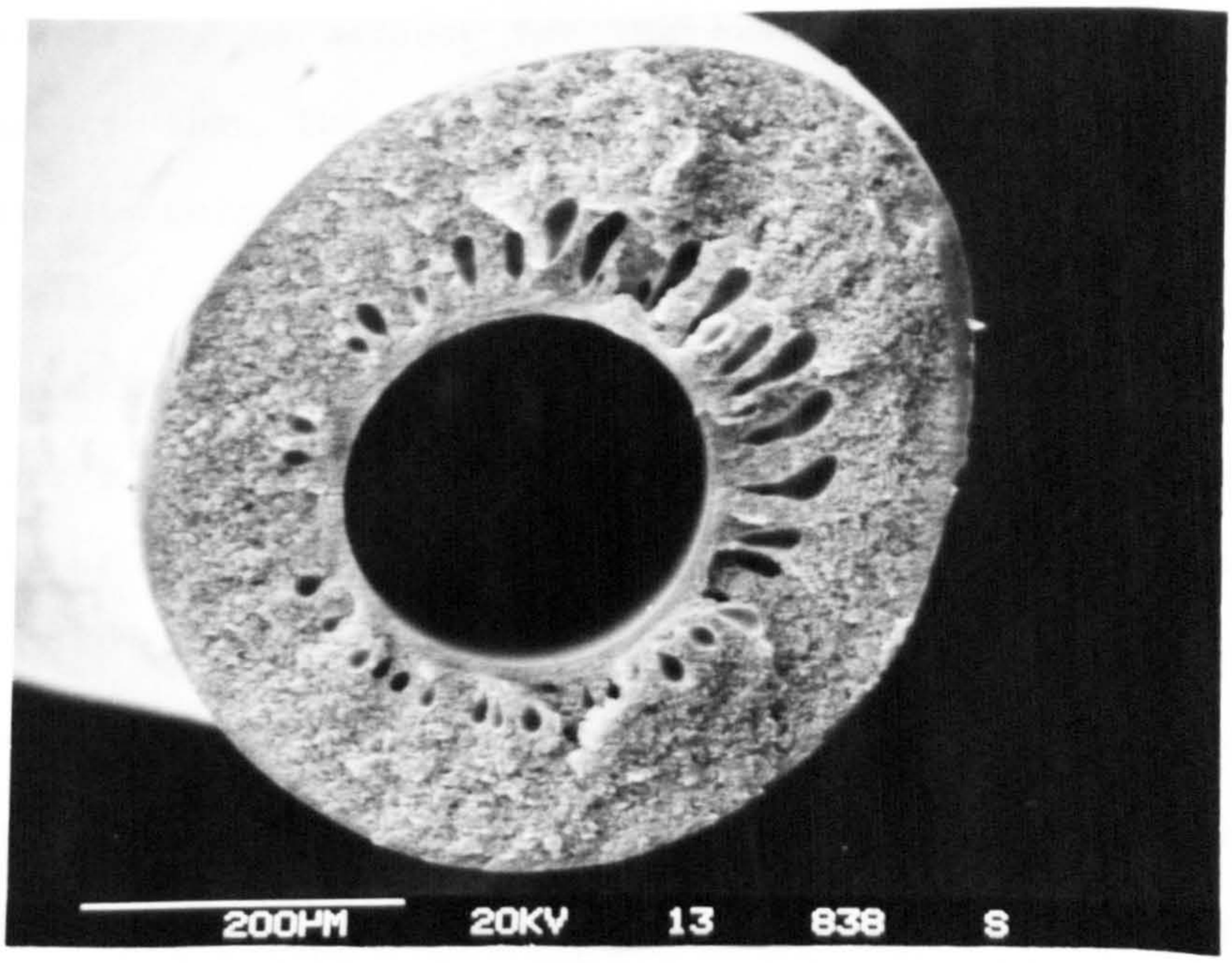

Plate 3.8 l-Fp type fibre (30%).

It was noted that Monsanto [56] incorporated the nonsolvent formamide into their 1-Fp dope formulations. The reasons for this were not exactly clear from their patent literature and so trial formulations containing the formamide were made. A 30% P3500 dope was made using a liquid carrier consisting of 95% 1-Fp and 5% formamide. This produced fibres having a morphology with fewer macrovoids (see Plate 3.9) than the fibres spun from 1-Fp alone. From these results it was argued that a higher concentration of formamide might produce fibres with still fewer structural irregularities and this was found to be the case as fibres produced from a 30% dope made from a liquid mixture consisting of 90% 1-Fp : 10% formamide showed a complete absence of macrovoids when examined by S.E.M. (see Plate 3.10).

These results showed that there was a definite advantage in incorporating formamide into the casting dopes and poses the question of how the formamide alters the phase inversion process such that these sponge-like structures are obtained. There are two possible explanations to account for the behaviour. The simplest explanation suggests that the dopes containing the formamide are of a higher viscosity which according to Frommer and Lancet [48] reduces the rates of diffusion of the nonsolvent and solvent. Table 3.3 shows the viscosities of the various types of spinning dope. The data represent values estimated at zero shear rate at 30^{o}C (See appendix 2). On the basis of the data in Table 3.3 a prediction could be made to suggest that the 9:1 1-Fp:Fa dopes would have the best morphology (i.e. least macrovoid content) followed by the 1-Fp type dopes. The DMAc and DMF dopes would be expected to have similar (and poorer) morphologies. The observations made from examination of the various fibres produced do not totally agree with the prediction, and so a more involved relationship probably exists.

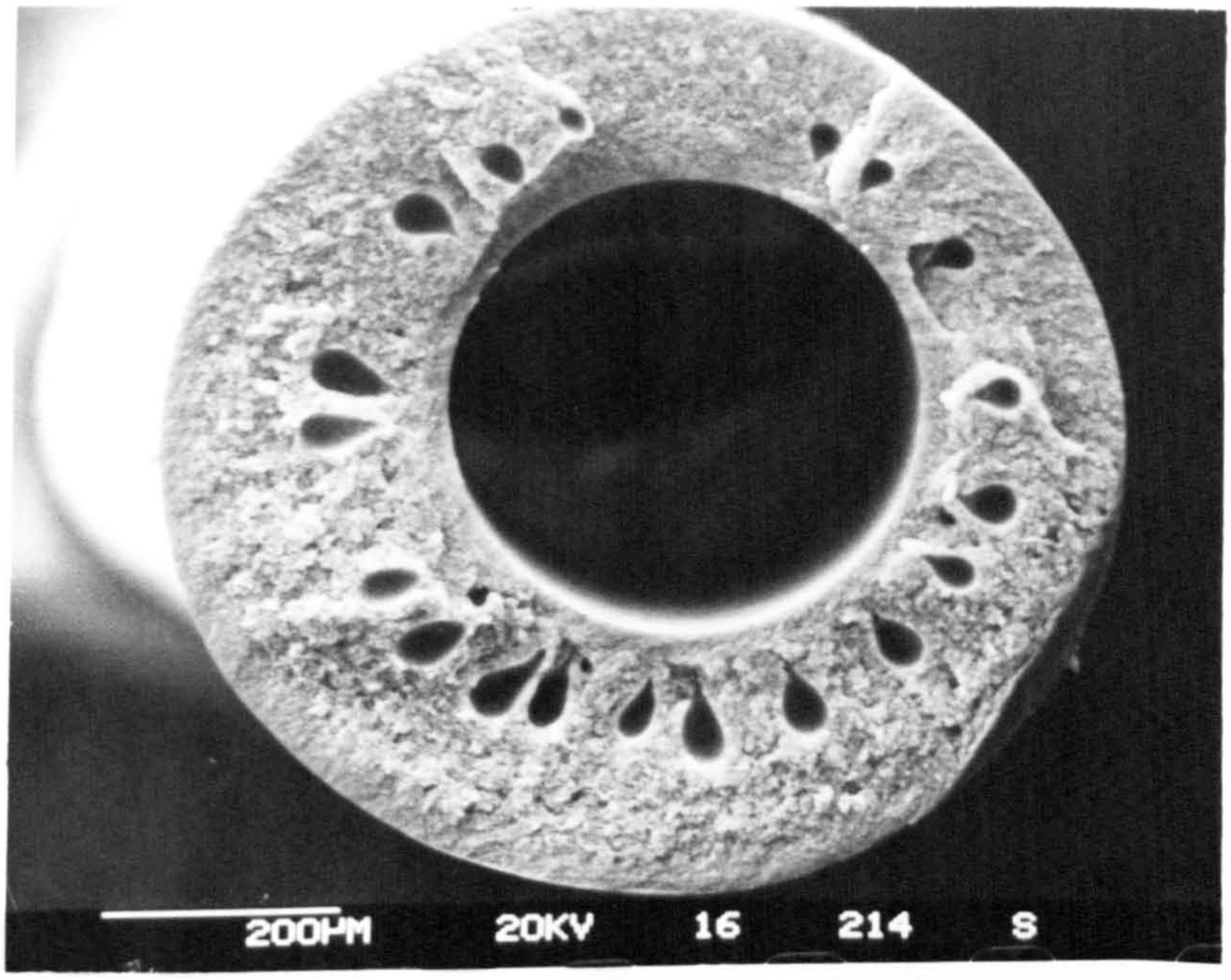

Plate 3.9 95:5 1-FP:FA type fibre (30%)

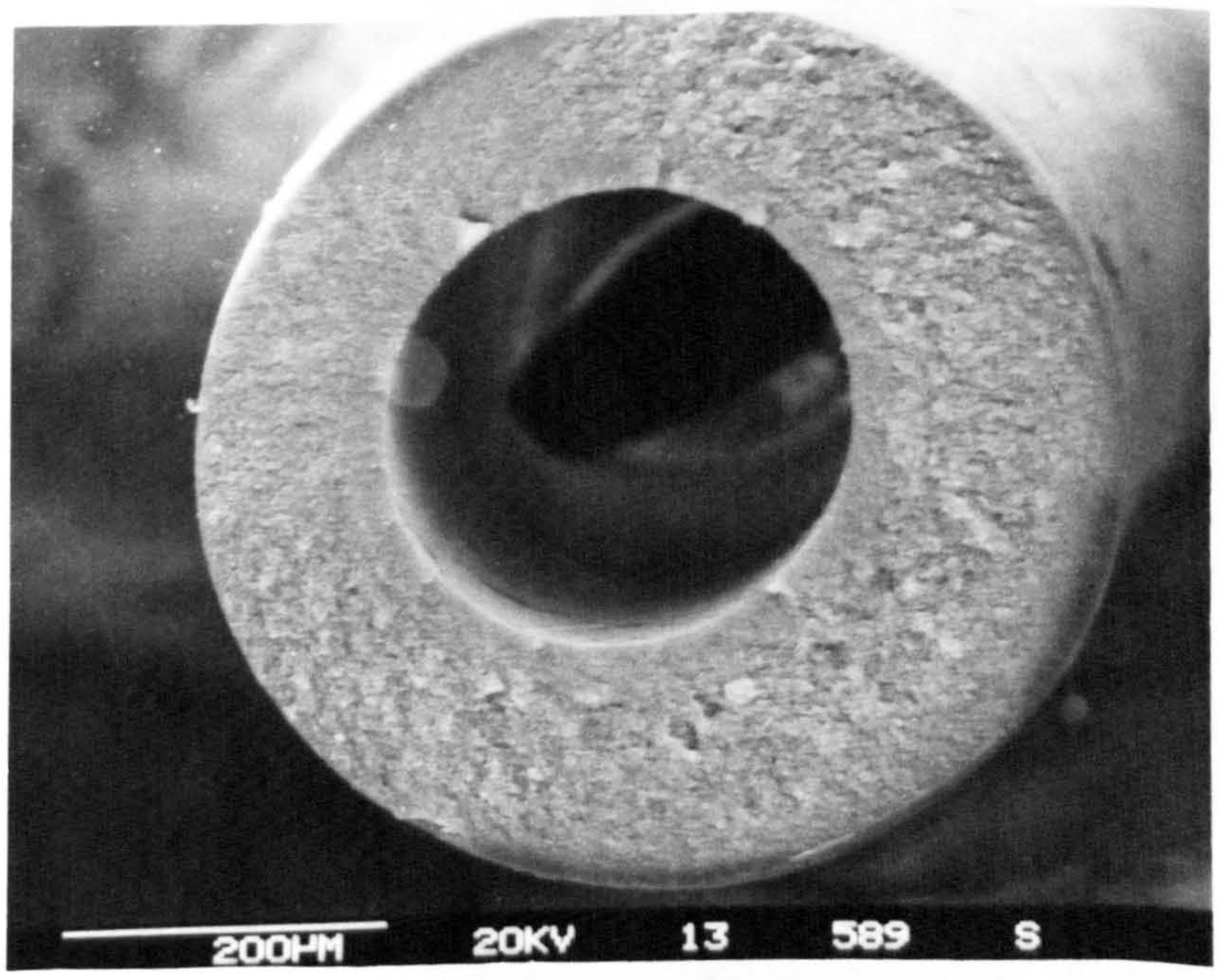

Plate 3.10 9:1 1-Fp:FA type fibre (30%).

Table 3.3 Viscosities of 30% Polymer Spinning Solutions.
(30^{o}C. zero shear rate).

Liquid Carrier	Viscosity (Pa s)
DMAc	10
DMF	12
1-Fp	110
9:1 1-Fp:Fa	267

Kesting [40] suggests a second more complicated explanation. Kesting noted that the rates of precipitation of solutions of cellulose acetate containing specifically formamide were slower than solutions without the formamide addition. This he accounted for in the following way. Formamide can associate with water (the main precipitant) by hydrogen bonding. This association thus lowers the activity of the water as a nonsolvent and consequently reduces the rate of precipitation.

In an attempt to understand the mechanism by which the liquid carriers, and especially formamide affected the rate of precipitation several experiments were carried out. The first of these was designed to examine the heat of mixing of the mobile components of the phase inversion process (see Section 2.4.8). Initially the change in temperature on mixing a 10 ml volume of water with 10 ml of liquid carrier component was measured. The results (Table 3.4) showed that the most exothermic process occurred with the mixing of DMAc and water, correlating with the high rate of precipitation and extensive macrovoid formation observed in the formation of membranes from these components.

Table 3.4 Temperature changes associated with liquid mixing.

Liquid Carrier Component	Component Mixed In	Change in Temperature (^{o}C)
DMAc	Water	+18.1
DMF	Water	+15.9
1-Fp	Water	+7.6
Formamide	Water	-3.3
1-Fp	Formamide	+7.0

Table 3.5 Effect of formamide on heat of mixing 1-Fp with water.

% 1-Fp :	% Fa	Change in Temperature (^{o}C).
100	0	+7.6
90	10	+3.6
80	20	+2.6
70	30	-0.7
40	60	-1.8
0	100	-3.3

Each solvent used to dissolve the polymer will readily mix with water. The fact that DMAc evolves the most heat on mixing suggests that its interaction with water is greater than that of 1-Fp. As a polymer molecule only remains in solution so long as it is surrounded by solvent molecules, then if the solvent molecules readily migrate away from the polymer, attracted by the precipitant, then rapid coagulation will occur. Thus precipitation of DMAc type dopes is more rapid than 1-Fp types.

There was further evidence of the reluctance of the 1-Fp to migrate out of the precipitating membrane. It was observed during spinning that fibres spun from dopes containing 1-Fp sometimes redissolved after coagulation if they had not been subjected to the soaking stage. Fig 3.3 and Table 3.6 show the retention of 1-Fp, in comparison to DMAc, in the hollow fibres after spinning and demonstrates that soaking times in excess of 200 hours are necessary to remove solvent to acceptable levels.

Table 3.6 Retention of solvent after spinning.

(a) 1-Fp.

Washing Time / hours.	1	24	48	216	336
% Solvent Retained.	15.2	3.6	2.8	2.0	0.8

(b) DMAc.

Washing Time / hours.	0	2.5	115
% Solvent Retained.	6.5	5.0	2.0

The most interesting feature of the experiment was the mixing of formamide with water. This proved to be an endothermic process. When formamide mixes with water, the new hydrogen bonds formed are weaker than the intermolecular forces in the two separate liquids so that, on balance, the process is endothermic. How these changes in intermolecular forces affect the morphology of the membranes can be understood by reference to the rate of precipitation of the polymer.

Formamide is a nonsolvent for polysulphone. Addition of formamide in sufficient quantities to a polymer solution will initiate precipitation. However, the formamide can be incorporated in small concentrations into the 1-Fp dopes (up to around 15% in the liquid

Fig 3.3 Retention of solvent after spinning.

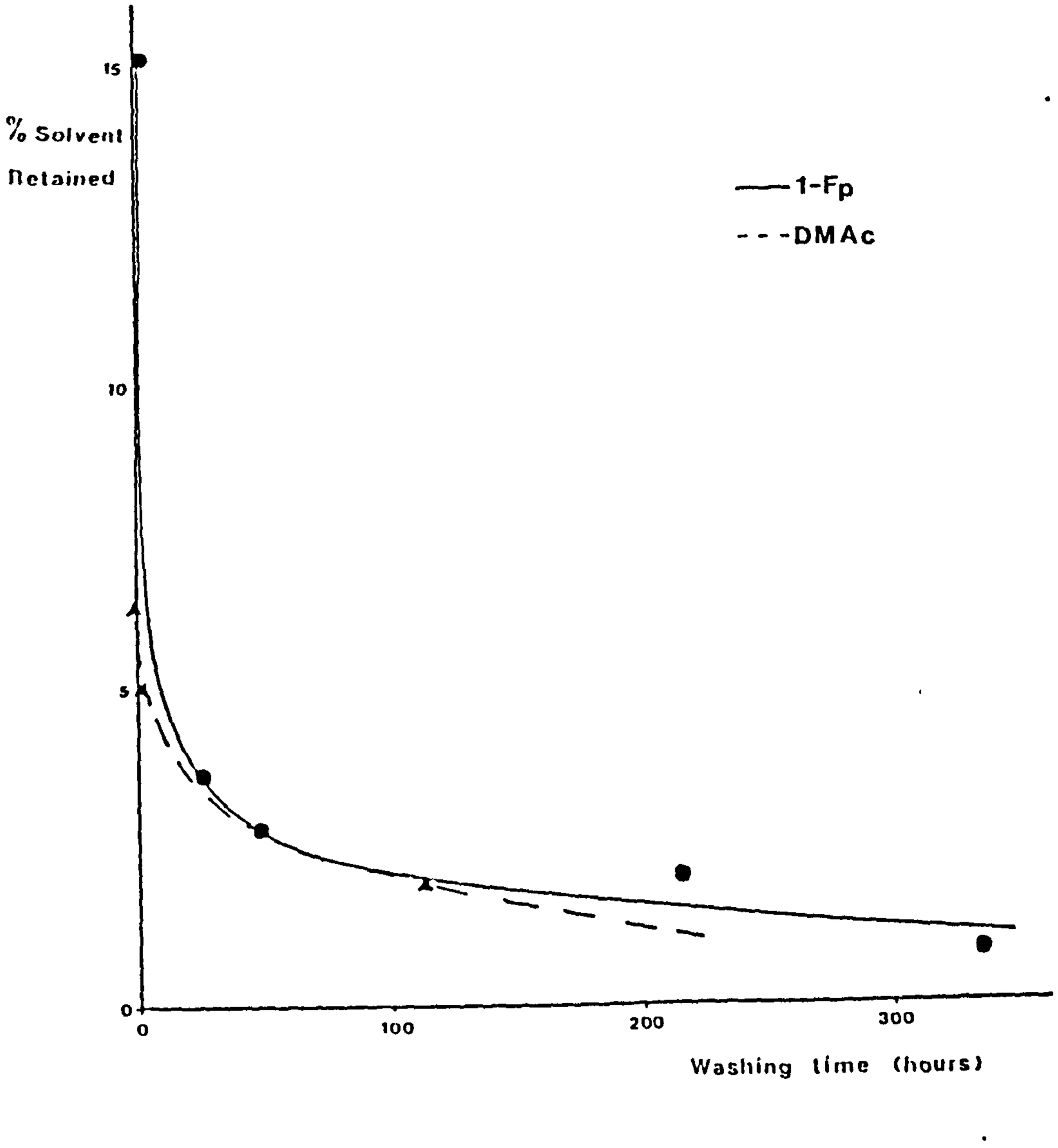

carrier). The presence of the formamide alters the affinity of the liquid carrier for the nonsolvent water. Table 3.4 shows how increasing quantities of formamide in the liquid carrier reduce the amount of heat liberated on mixing with water. Thus the water acts in competition with the formamide (incorporated in the dope) during the precipitation process resulting in a decrease in the rate of precipitation. The tenacity of the formamide for the solvent l-Fp is the likely cause of the peculiarity observed in the Schlieren detection experiments. In all the experiments carried out on the various types of dope coagulated in water, solvent was always observed to diffuse out of the precipitating membrane, except in the case of the 9:1 l-Fp:Fa dopes where no solvent was observed diffusing out of the forming membrane even after a considerable period of time (greater than five minutes). Thus, in the case of the l-Fp:Fa system, coagulation occurs by the mechanism of nonsolvent diffusion into the polymer solution, whereas the other types coagulate by nonsolvent - solvent exchange or solvent diffusion out of the precipitating membrane (indistinguishable in Schlieren detection experiments).

(b) Precipitant selection.

Apart from the effect of different dope compositions the composition of the coagulation bath is also, of course, of importance in the phase inversion process. Four precipitants were briefly examined, in film studies, in order to observe their effect on the membrane morphology. The coagulants chosen were water, ethanol, acetone and formamide. In an industrial process it would be advantageous to use water as the coagulant as it would be economically the cheapest both in terms of its own cost and in waste disposal and/or recovery.

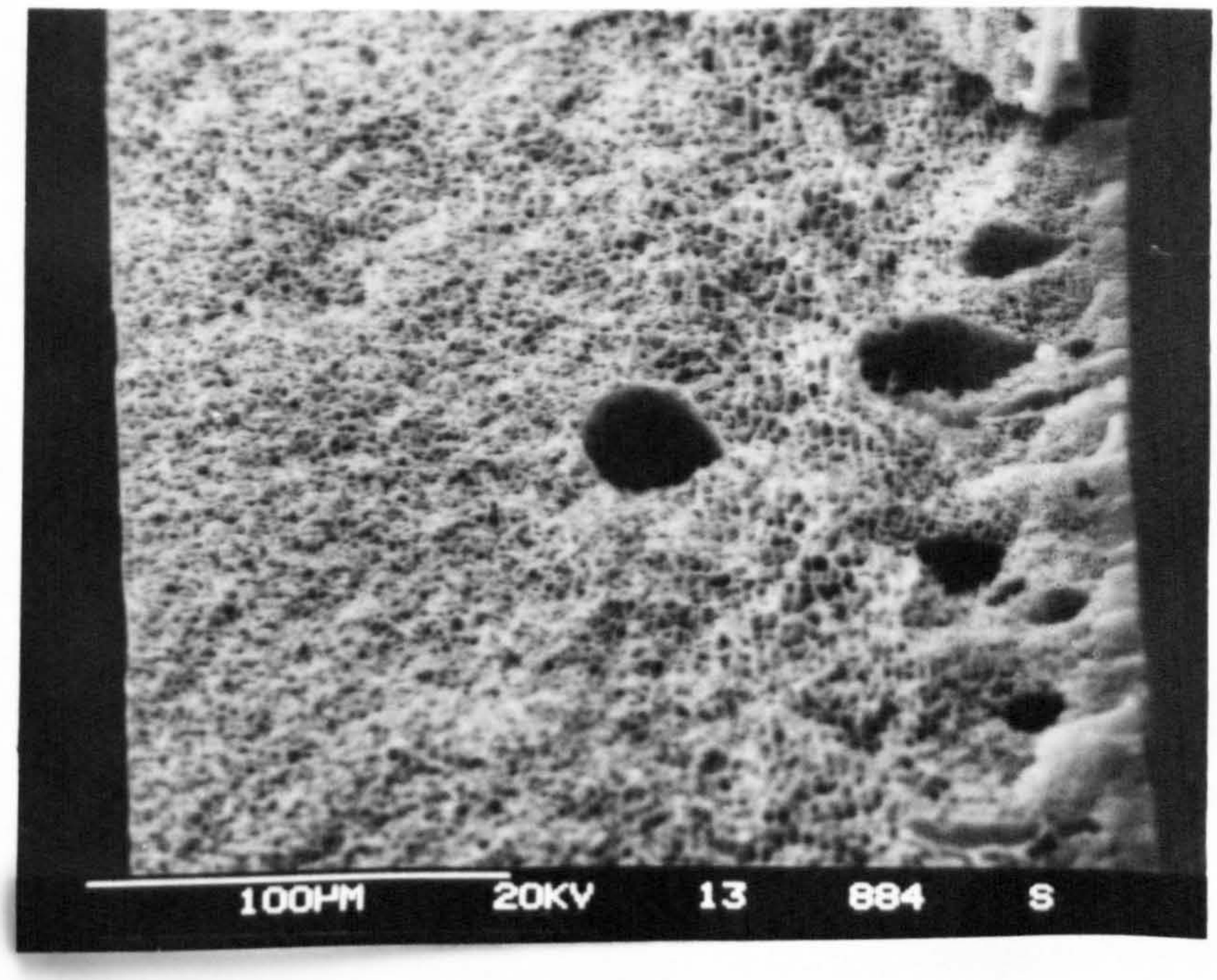

Plate 3.11 1-Fp type film (30%) coagulated in ethanol.

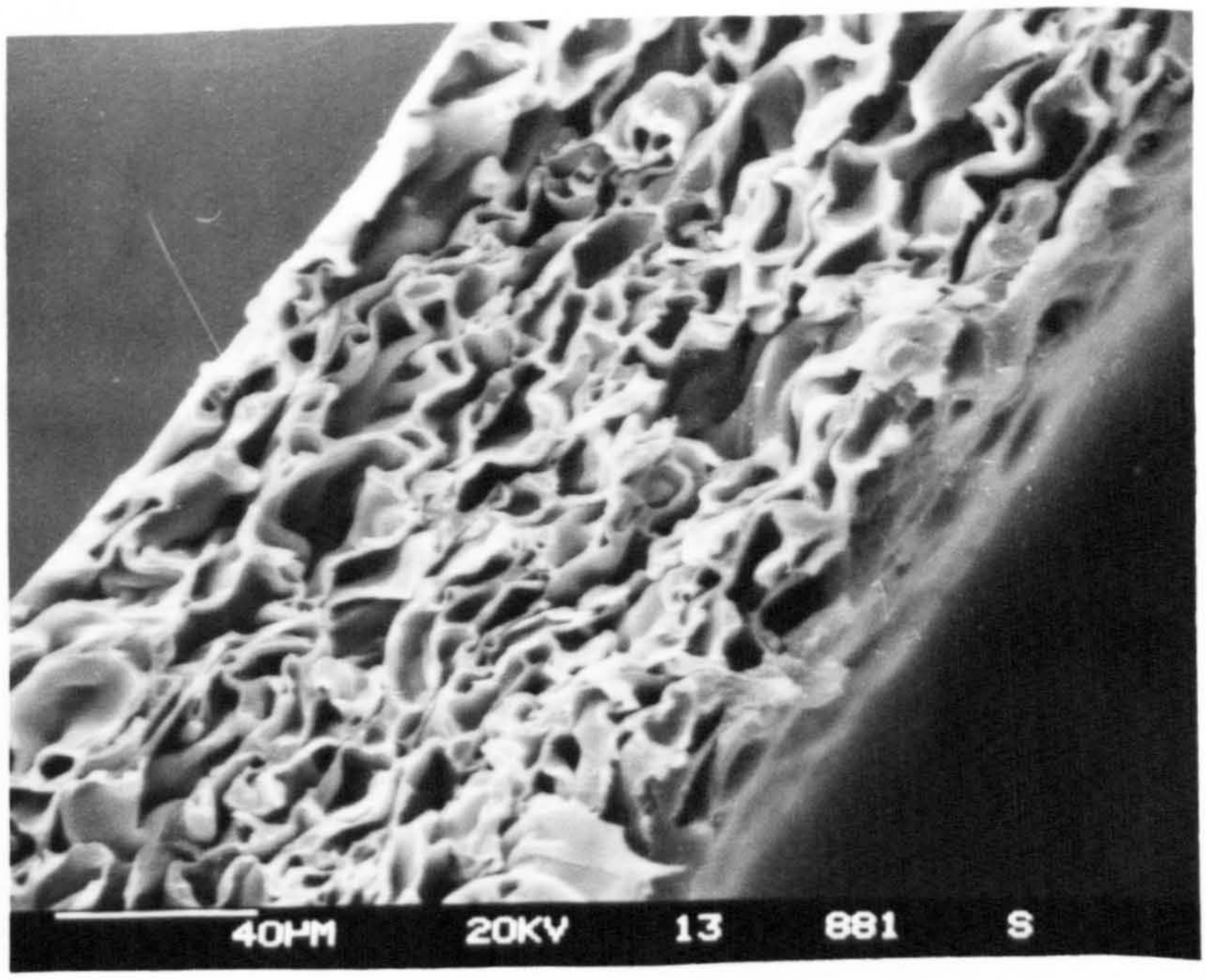

Plate 3.12 1-Fp type film (30%) coagulated in acetone.

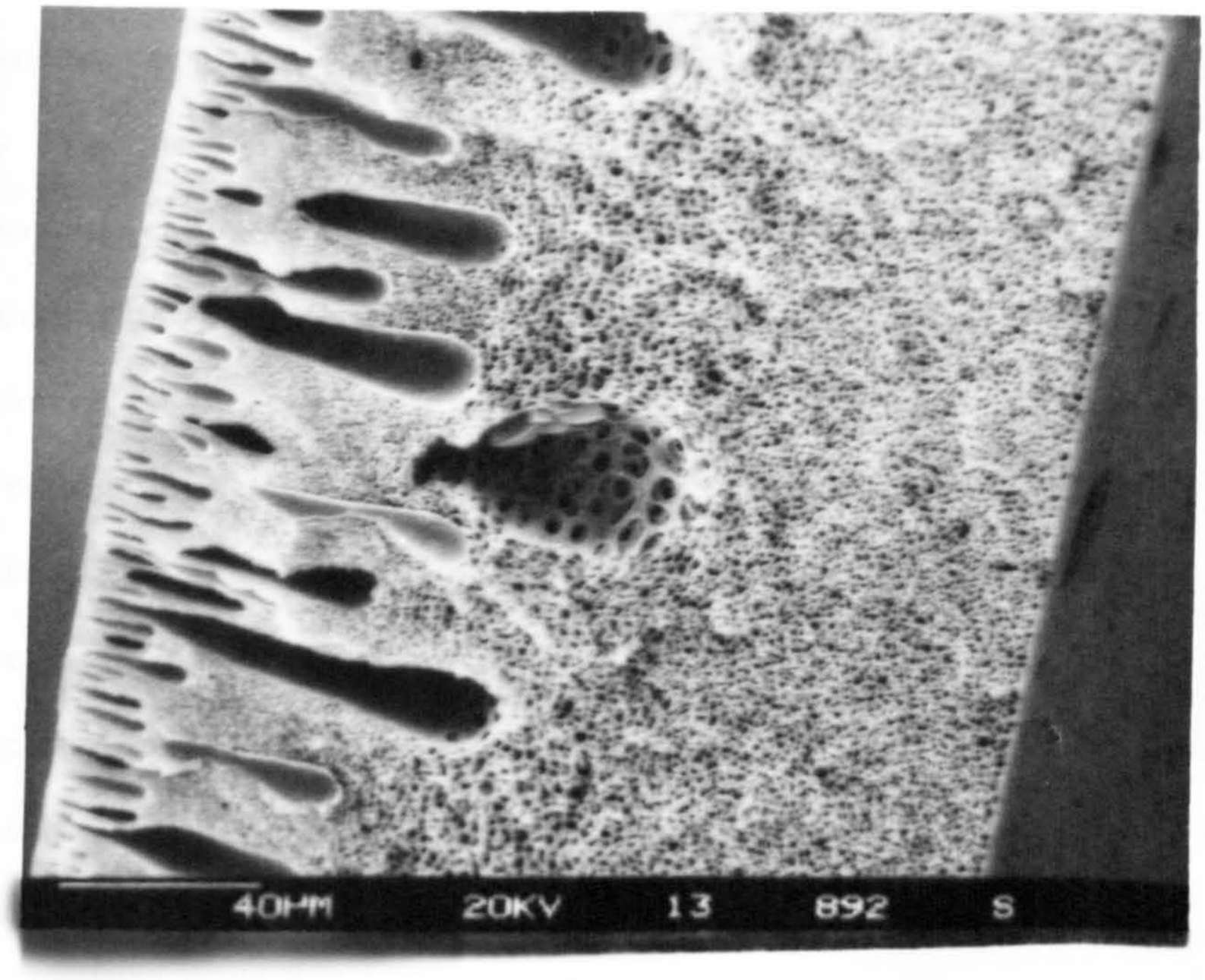

Plate 3.13 1-Fp type film (30%) coagulated in formamide.

Plate 3.14 Non-circular lumen brought about by too low a WIR.

Plates 3.6, 3.11, 3.12 & 3.13 show the results for a 30% polymer 1-Fp dope coagulated in the four precipitants. The film coagulated in acetone produced a membrane with a morphology of a completely different nature to any other membrane produced. The membrane structure appeared to be made up of a series of skin layers spaced out with non-interconnecting pores. It was thought that such a structure would exhibit a very low permeability to penetrating gases as the effective thickness of the membrane would be too great. The other three films produced had a similar morphology to each other. The film coagulated in ethanol looked to be a promising candidate for further study as it had a very uniform pore structure with only a few macrovoids. However, it was decided not to spin fibres into ethanol or any other alcohol due to the flammability hazards associated with containing such a large volume of alcohol in the coagulation bath.

3.1.4 Summary.

The reduction of macrovoids was succesfully achieved. Total elimination of these structural imperfections was achieved for the polysulphone system by the incorporation of formamide into the dope. What precise mechanism of interaction acted to prevent macrovoid formation is still not perfectly clear. It is possible that the formamide acts simply to raise the viscosity of the dope and retard solvent - nonsolvent exchange within the coagulating membrane. However, the findings of the heat of mixing experiments suggest that the interaction of the formamide is more complicated involving the formation of moderately strong hydrogen bonds which interfere with the kinetics of phase inversion. Does formamide only work within the environment of N-acylated heterocyclic solvents or will formamide act to prevent

structural irregularities forming in other solvent systems? This may be an important piece of work for the future.

The other methods used to eliminate macrovoids also met with some success. Increasing the polymer content definitely reduced the number of macrovoids found in the DMAc type membranes, and switching to DMF dopes as a result of small scale work using cast films proved the worth of this experimental procedure. The effect of concentration also acted to decrease the macrovoid content, as predicted, however, the limits imposed by viscosity showed the weakness of this method.

The effectiveness of removing macrovoids on the improvement in collapse pressure was apparent as the fibres spun from the 1-Fp:Fa type dopes commonly had collapse pressures in excess of the test measurement limit of 5.86 MPa (850 psi). However, the fibres spun from DMAc at the 40% polymer level, although having a virtually macrovoid free structure, had a collapse pressure of only 2.41 MPa (350 psi). This low level of fibre collapse was of the same order of that obtained from the lower polymer concentration dopes. Further details concerning the nature of fibre collapse are given in appendix 3.

So far only improvements in the fibre morphology and collapse pressure have been examined. What effect these changes had on the gas transport characteristics is discussed in section 3.3.

3.2 Examination of spinning parameters.

3.2.1 Introduction.

Certain major spinning parameters were examined during the course of the research with the aim of developing a model which could predict the fibre dimensions from a set of spinning parameters. This was considered to be a task which would at best meet with only limited success due to the number of interacting parameters associated with hollow fibre formation. In addition to this objective it was hoped that correlations might be found between spinning parameters and/or fibre morphology and gas transport characteristics of the membranes. Fig 3.4 shows the pathways of understanding sought in order to be able to develop membranes with specific permselectivity.

Fig 3.4 Correlation pathways sought in membrane development.

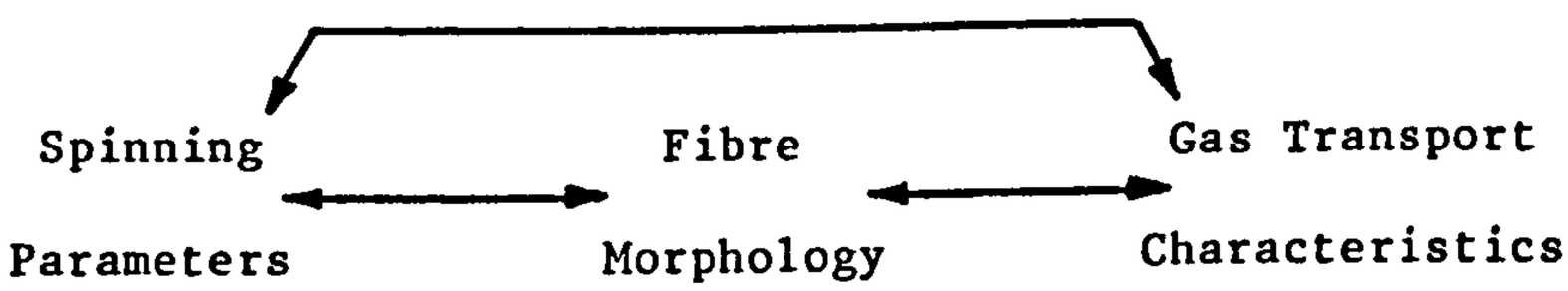

Initially this section examines each spinning parameter studied in a qualitative manner, discussing the effect of each on the fibre structure. Hollow fibre spinning is a complicated process and it is hoped that this first subsection will show some of the problems encountered and act as an aid to trouble shooting for future hollow fibre spinners. The remainder of this section deals with the development and testing of the model whose function was to predict the fibre dimensions.

3.2.2 Some generalisations on the effect of spinning parameters on fibre formation.

(a) Polymer extrusion rate (PER).

This term describes the rate at which dope is extruded by the metering pump and is measured in $cm^3\ min^{-1}$. The main effect of altering the PER is to vary the fibre diameter and wall thickness. Altering the PER has little effect on the diameter of the fibre lumen. If the PER is allowed to fall below a certain level, the reduction in wall thickness becomes such that the pressure from the internal coagulant causes the wall to rupture intermittently producing a fibre which has a rough surface. This surface roughness may be easily detected during spinning by allowing the coagulated fibre to run through the spinner's hands. If the PER is reduced further, then the cast filament will tend to break at the spinneret making spinning impossible. When the PER is increased above a certain level the fibre will run slack in the coagulation bath as the linear extrusion rate of dope through the spinneret will far exceed the wind up speed.

(b) Spinneret dimensions and assembly.

The dimensions of the spinneret are important as they act to affect the linear extrusion rate. The smaller the annulus the greater the linear speed at which the fibre is extruded for a given PER. The alignment of the capillary tube in the centre of the orifice was found to be important as this determines the concentricity of the lumen within the fibre. Monsanto [75] have designed adjustment screws for their spinnerets to this purpose. Mounting of the spinneret was also found to be of importance. The spinneret should be mounted such that the face of the spinneret is parallel to the surface of the coagulant and also the spinneret should be positioned vertically above the first guide roller so

that the extruded filament is not dragged out of the spinneret at an angle. It is of prime importance that the spinneret be clean and completely free of encrusted polymer before spinning is commenced, otherwise striations may appear along the length of the fibre. Such striations may affect the morphology of the thin skin layer. The striations are thought [40] to arise due to premature precipitation brought about by a seeding effect of the encrusted polymer, in a somewhat similar fashion to initiation of crystal growth in saturated solutions.

(c) Water injection rate (WIR).

The rate at which the internal coagulant is injected through the capillary of the spinneret will determine the size of the fibre lumen. As a consequence of controlling the size of the lumen the WIR also affects the total fibre diameter. The wall thickness tends to be fairly insensitive to the WIR at the upper range of injection rates examined. At lower levels the wall thickness increases with reduction in the WIR. When the WIR falls below a certain level fibres are formed with lumens which do not have a circular cross-section (see Plate 3.14). Increasing the WIR has little deleterious effect on the fibre structure except where the internal pressure is insufficient to cause rupture of the fibre wall when a low PER is used.

(d) Jet gap.

The length of the jet gap has little influence on the fibre structure. This may cease to be the case where volatile components are incorporated in the polymer dope. The jet gap acts as the region in which spin stretch (or jet stretch) primarily occurs. So long as the jet gap is sufficiently large to incorporate the full jet stretch the jet gap is a relatively insensitive parameter. Further details of the role of the jet gap are given in Section 1.3.

(e) Wind up speed (WUS).

The wind up speed controls the final dimensions of the fibre. Whereas the PER and WIR can be used to vary the total fibre diameter and fibre lumen with respect to each other, the WUS can be used to enlarge or reduce the fibre dimensions whilst maintaing the same total diameter : lumen diameter ratio. Too high a WUS will simply cause the filament to break at the spinneret and too low a WUS causes the filament to run slack in the coagulation bath.

(f) Jet stretch ratio (or spin stretch).

The jet stretch ratio is the ratio of the WUS to LER and is a measure of how much the membrane is drawn during the spinning process. The effects of the two extremes have already been discussed above and so generally the jet stretch ratio should lie between 0.5 and 5.0.

3.2.3 Prediction of fibre dimensions from spinning parameters.

This subsection deals with the development of a model to predict the dimensions of a hollow fibre membrane from a few of the more important spinning parameters. The data used to test the validity of the model were obtained from spinning runs in which all parameters were kept constant except for the one under examination. Full details of the spinning runs (or batches) are given in Appendix 4. Batches with identification codes starting with numbers less than 21/2 were spun solely by the previous researcher and have been incorporated into this section merely to add further data.

(a) Simplified case - Spinning a solid, non-porous fibre.

In this scenario the complications of the fibre lumen and voids within the annulus have been removed and so the model is concerned with nothing more than the dry-jet wet-spinning of a textile fibre. Unfortunately, the diameter of a textile fibre is rarely calculated from spinning parameters, it being more usual to calculate linear density. However, it was possible to derive the following model by logically considering conservation of mass of the polymer.

The main parameters considered in this simplified case were:-

V = rate of extrusion of dope, or PER ($cm^3\ min^{-1}$).

ρ_d = density of the dope ($g\ cm^{-3}$).

X = fraction of polymer in dope by weight (dimensionless).

S = rate at which fibre was wound up on the collection drum ($cm\ min^{-1}$).

ρ_f = density of the fibre ($g\ cm^{-3}$).

d_f = fibre diameter (cm).

The rate at which polymer is extruded through the spinneret

$$= V \rho_d X \qquad (g\ min^{-1}). \tag{3.1}$$

If the length of the fibre wound up in one minute is S cm, then one minutes spinning will produce S cm of fibre weighing:

$$V \rho_d X \qquad (g). \tag{3.2}$$

The volume of circular cross-section fibre produced in one minute will be:

$$\frac{\pi d_f^2 S}{4} \qquad (cm^3). \tag{3.3}$$

If the density of the fibre is known to be ρ_f then the weight produced per minute is:

$$\frac{\pi d_f^2 \, S \, \rho_f}{4} \quad (g). \tag{3.4}$$

Thus combining equations 3.2 & 3.4 a solution for determining the fibre diameter, d_f, in terms of spinning parameters can be made.

$$\frac{\pi \, d_f^2 \, S \, \rho_f}{4} = V \, \rho_d \, X \tag{3.5}$$

$$d_f^2 = \frac{4 \, V \, \rho_d \, X}{\pi \, S \, \rho_f} \tag{3.6}$$

$$d_f = \sqrt{\frac{4 \, V \, \rho_d \, X}{\pi \, S \, \rho_f}} \tag{3.7}$$

Thus an expression for the diameter of a solid dry-jet wet-spun fibre is relatively easily derived.

(b) Prediction of the dimensions of a hollow fibre membrane.

This case is more complicated as models for the fibre lumen and porous annular region must be defined. However, the lumen and annulus can be considered separately.

(i) Prediction of the diameter of the fibre lumen.

If it is assumed that the internal cogulant injected into the extruding polymer produces a circular bore of volume equal to the volume of coagulant injected per minute,

$$\text{i.e.} \quad a = \frac{\pi d_i^2 S}{4} \quad (cm^3\ min^{-1}). \tag{3.8}$$

where a = the water injection rate ($cm^3\ min^{-1}$).

d_i = the internal diameter, i.e. the diameter of the lumen (cm).

S = the wind up speed ($cm\ min^{-1}$).

then rearrangement of equation 3.8 gives an expression for the internal diameter:

$$d_i^2 = \frac{4\ a}{\pi\ S} \tag{3.9}$$

This equation was tested against data obtained from several spinning runs. The results shown in Table 3.7 and in graphical form in Figs. 3.5, 3.6, 3.7 & 3.8 show a very good correlation with the predicted values calculated using equation 3.9. The deviations observed in batches 25/1 and 37/1 were thought to have occurred from a combination of two factors. The deviation shows that a smaller bore was produced than predicted, most likely due to the injection of less coagulant than predicted. The reason for the low WIR lies in the performance characteristics of the peristaltic pump which was used to deliver the internal coagulant to the spinneret. Under certain circumstances a high pressure of internal coagulant at the output side of the pump can cause problems where back slippage of coagulant can occur through the peristaltic 'nip'. This results in a lower rate of coagulant injection compared with the pump setting. The kind of circumstances which could cause this high output pressure were thought to be associated with the dope viscosity. Both batches 25/1 and 37/1 were made from the 9:1 mixture of 1-formylpiperidine : formamide. These dopes had the highest viscosity of all the dopes prepared. The high viscosity of the dope was thought to hinder the expansion of the internal coagulant on extrusion

Fig 3.5 Effect of WIR on d_i^2 (Batch 11/4).

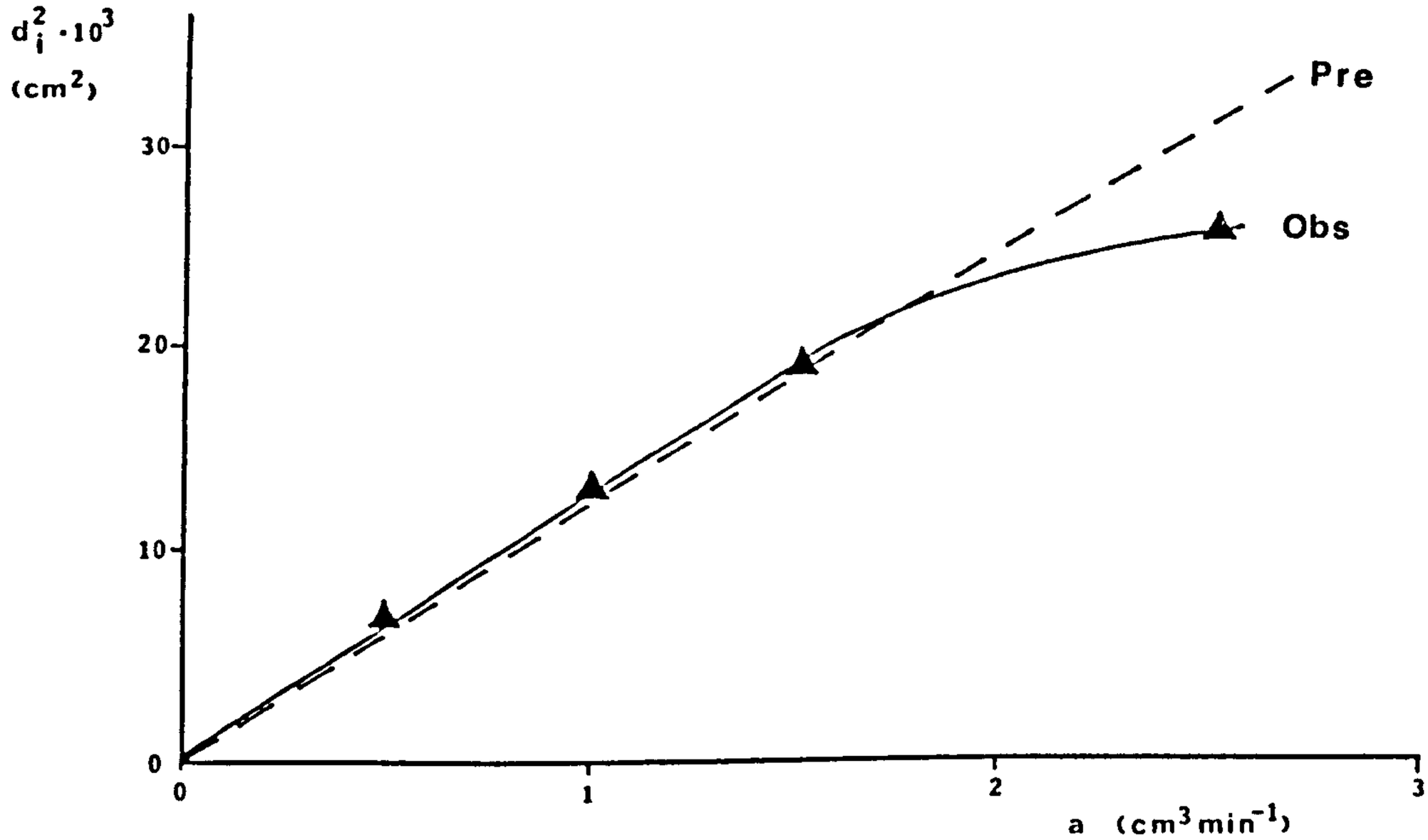

Fig 3.6 Effect of WIR on d_i^2 (Batch 44/3).

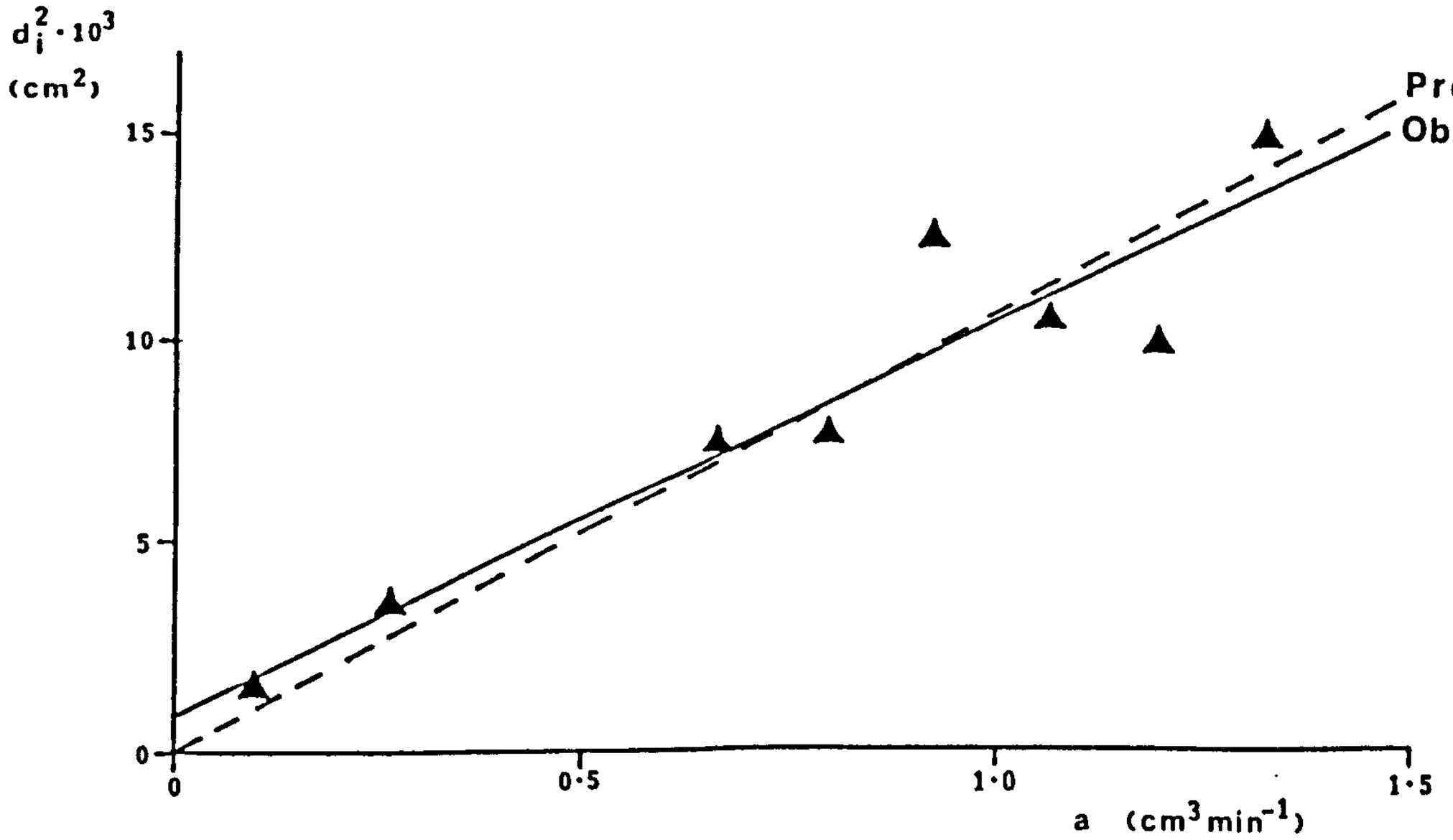

Fig 3.7 Effect of WIR on d_i^2 (Batch 25/1).

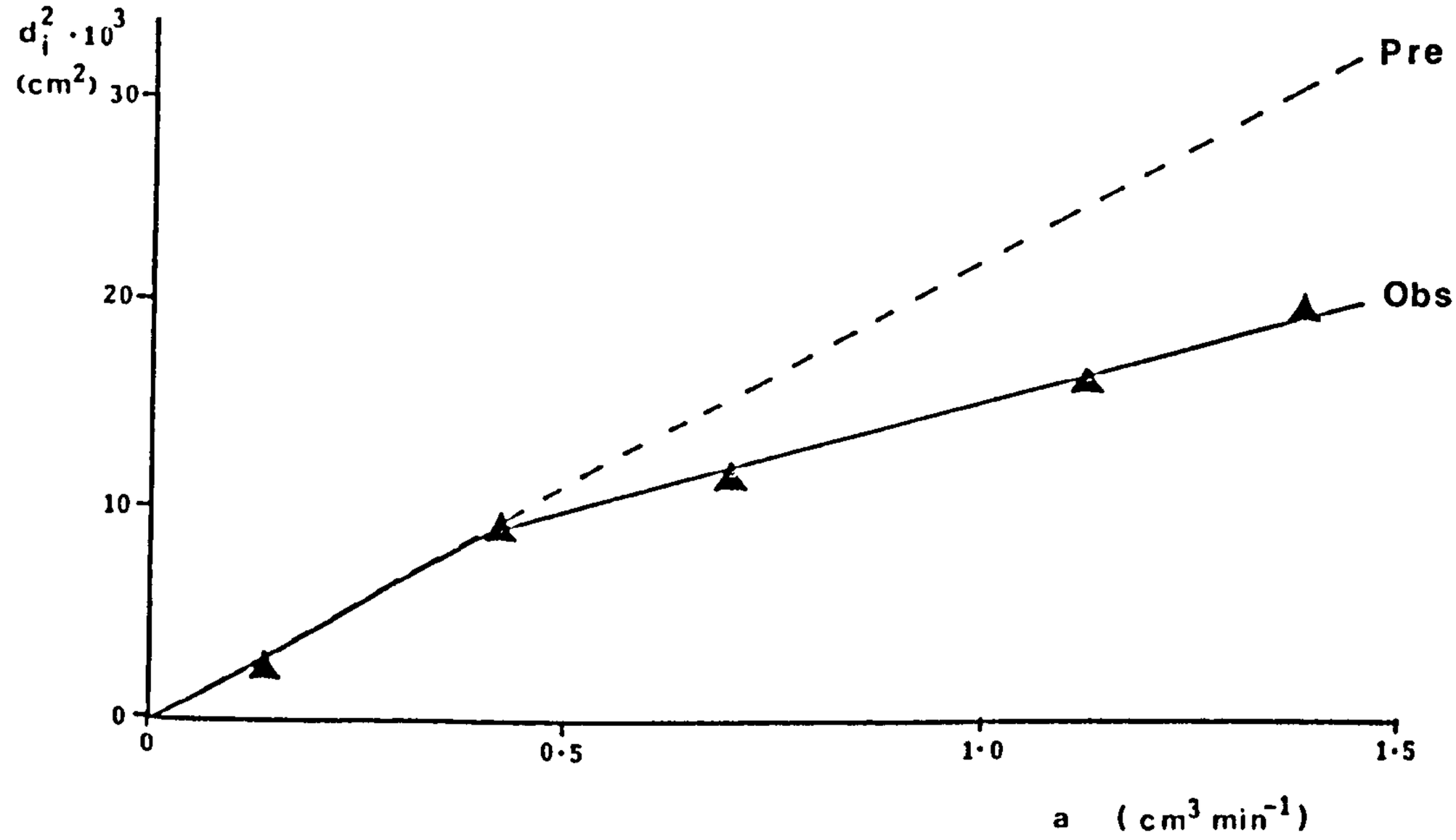

Fig 3.8 Effect of WIR on d_i^2 (Batch 37/1).

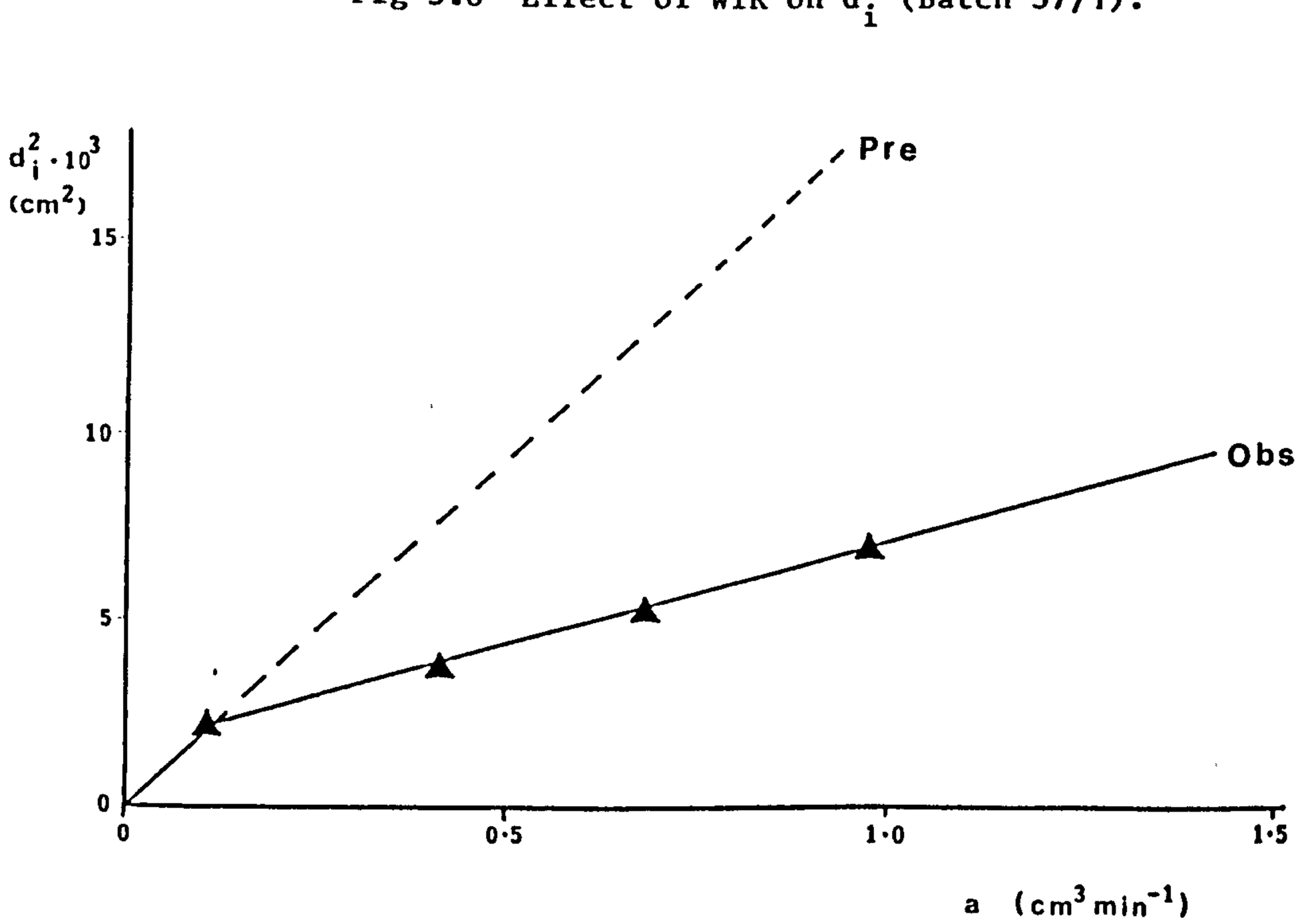

from the spinneret capillary causing a build up of pressure in the silicone tubing of the peristaltic pump.

Table 3.7 Effect of W.I.R. on fibre dimensions.

Batch	a	d_i obs	d_i^2 obs	d_i^2 pre	d_f obs	d_f^2 obs
	$cm^3\ min^{-1}$	μm	$10^{-3}\ cm^2$	$10^{-3}\ cm^2$	μm	$10^{-3}\ cm^2$
11/4a	0.5	265	0.70	0.63	558	3.11
11/4g	0.75	310	0.96	0.94	575	3.31
11/4b	1.0	365	1.33	1.25	621	3.86
11/4c	1.5	440	1.94	1.88	651	4.24
11/4d	2.5	510	2.60	3.13	719	5.17
25/1k	0.14	160	0.26	0.31	530	2.81
25/1l	0.42	300	0.90	0.94	570	3.25
25/1j	0.69	340	1.16	1.54	600	3.60
25/1i	1.12	400	1.60	2.50	620	3.84
25/1h	1.38	450	2.03	3.08	620	3.84
37/1d	0.14	157	0.25	0.26	525	2.76
37/1c	0.42	191	0.37	0.76	562	3.16
37/1e	0.69	227	0.52	1.25	495	2.45
37/1f	0.98	261	0.68	1.78	514	2.64
44/3j	0.10	125	0.16	0.11	366	1.34
44/3i	0.26	189	0.36	0.28	335	1.12
44/3h	0.52	240	0.58	0.56	412	1.70
44/3b	0.66	275	0.76	0.71	406	1.65
44/3c	0.79	279	0.78	0.85	412	1.70
44/3d	0.92	353	1.25	0.98	493	2.43
44/3e	1.06	323	1.04	1.13	455	2.07
44/3f	1.19	316	1.00	1.27	445	1.98
44/3g	1.32	385	1.48	1.41	508	2.58

The excellent correlations observed from batches 11/4 and 44/3 imply that equation 3.9 is a realistic interpretation of the lumen formation and if the peristaltic pump was replaced by a pump of better performance it was thought that the model would hold true for even the most viscous dopes.

(ii) Prediction of the dimensions of the fibre annulus.

Having successfully determined a model of the fibre lumen the next step was to calculate that portion of the fibre containing polymer and voids.

i.e. Total annular volume = volume of polymer + volume of voids. (3.10)

From the model of the formation of a solid non-porous fibre the weight of polymer produced per minute was:

$$V \rho_d X \qquad (g). \tag{3.11}$$

Knowing the density of the polymer to be ρ_p then equation 3.11 is equivalent to a volume produced per minute of:

$$\frac{V \rho_d X}{\rho_p} \qquad (cm^3) \tag{3.12}$$

From elementary geometry it can be calculated that the total annular volume produced per minute must be:

$$\frac{\pi S}{4} (d_f^2 - d_i^2) \qquad (cm^3) \tag{3.13}$$

Thus if:

Total annular volume (produced per minute) = Volume of polymer (produced per minute) + volume of voids (produced per minute) (3.14)

then:

$$\frac{\pi S}{4} (d_f^2 - d_i^2) = \frac{V \rho_d X}{\rho_p} + q \tag{3.15}$$

where q is the volume of voids produced per minute ($cm^3\ min^{-1}$)

Equation 3.15 can be rearranged to reveal the fibre dimensions:

$$(d_f^2 - d_i^2) = \frac{4\,(V\,\rho_d\,X + q\,\rho_p)}{\pi\,\rho_p\,S} \qquad (3.16)$$

or

$$(d_f^2 - d_i^2) = \frac{4\,V\,\rho_d\,X}{\pi\,\rho_p\,S} + \frac{4\,q}{\pi\,S} \qquad (3.17)$$

Unfortunately this equation cannot be readily utilised for the prediction of fibre dimensions as the value of q cannot be predicted (yet) prior to spinning. Also the value of ρ_d can only be estimated due to difficulties in accurately measuring a volume of viscous dope. However, the validity of the equation may be tested graphically. Figs 3.9, 3.10 & 3.11, produced from the data in table 3.8, show the effect of dope extrusion rate on the function $(d_f^2 - d_i^2)$. According to equation 3.17 a linear relationship should be obtained with the gradient of the slope being $(4\,\rho_d\,X)/(\pi\,\rho_p\,S)$ and an intercept on the 'y' axis with a value of $4\,q\,/\,\pi S$. Indeed the graphs do show a good correlation between $(d_f^2 - d_i^2)$ and V. Calculation of q from the intercept for batch 43/1 produced a negative value of -0.29 cm^3 (and this applied to batches 11/3 & 22/1 as well). This clearly does not make sense. For a porous fibre the value of q must be positive. This discrepancy was thought to result from the definitions of the fibre dimensions. In this model it was assumed that once the fibres had been wound up on the collection drum then the fibre dimensions are fixed. However, in the early days of the research when the fibres were collected on cones it was noted from the wrapping patterns embossed on to the cone package that the fibres shrink during the prolonged soaking stage. All the fibre dimensions were measured after the soaking and drying stages whilst the model predicts the fibre dimensions prior to the removal of residual solvent by soaking. It would, in the future, be worth measuring the dimensions prior to soaking to ensure that this explanation is correct and then, perhaps, an

appropriate shrinkage factor could be devised to correct the model. From the data obtained on the fibre lumen it would suggest that the lumen does not change during the soaking stage of the process.

Table 3.8 Effect of polymer extrusion rate on fibre dimensions.

Batch	V	d_f	d_i	$(d_f^2 - d_i^2)$
	$cm^3\ min^{-1}$	μm	μm	$10^{-3}\ cm^2$
43/1n	1.25	360	285	0.48
43/1m	1.65	400	308	0.65
43/1o	1.81	409	295	0.80
43/1p	2.37	447	295	1.13
43/1q	2.92	474	289	1.42
11/3d	1.5	448	295	1.14
11/3c	2.2	512	310	1.66
11/4g	3.1	575	310	2.35
11/3a	4.0	674	335	3.42
11/3b	5.0	724	350	4.02
21/2c	2.02	460	330	1.03
21/2b	2.21	485	330	1.26
21/2a	2.65	520	330	1.62
21/2d	3.10	540	330	1.83

Table 3.9 Effect of wind up speed on d_f.

Batch	S	S^{-1}	d_f	d_f^2
	$m\ min^{-1}$	$min\ m^{-1}$	μm	$10^{-3}\ cm^2$
43/1d	6.9	0.145	580	3.36
43/1c	11.5	0.087	465	2.16
43/1b	14.4	0.069	395	1.56
43/1f	16.8	0.060	365	1.33
43/1e	20.0	0.050	357	1.27
44/3	7.7	0.130	541	2.93
44/3	11.3	0.088	425	1.81
44/3	11.9	0.084	455	2.07
44/3	14.4	0.069	412	1.70

Fig 3.9 Effect of FER on fibre dimensions (Batch 11/3).

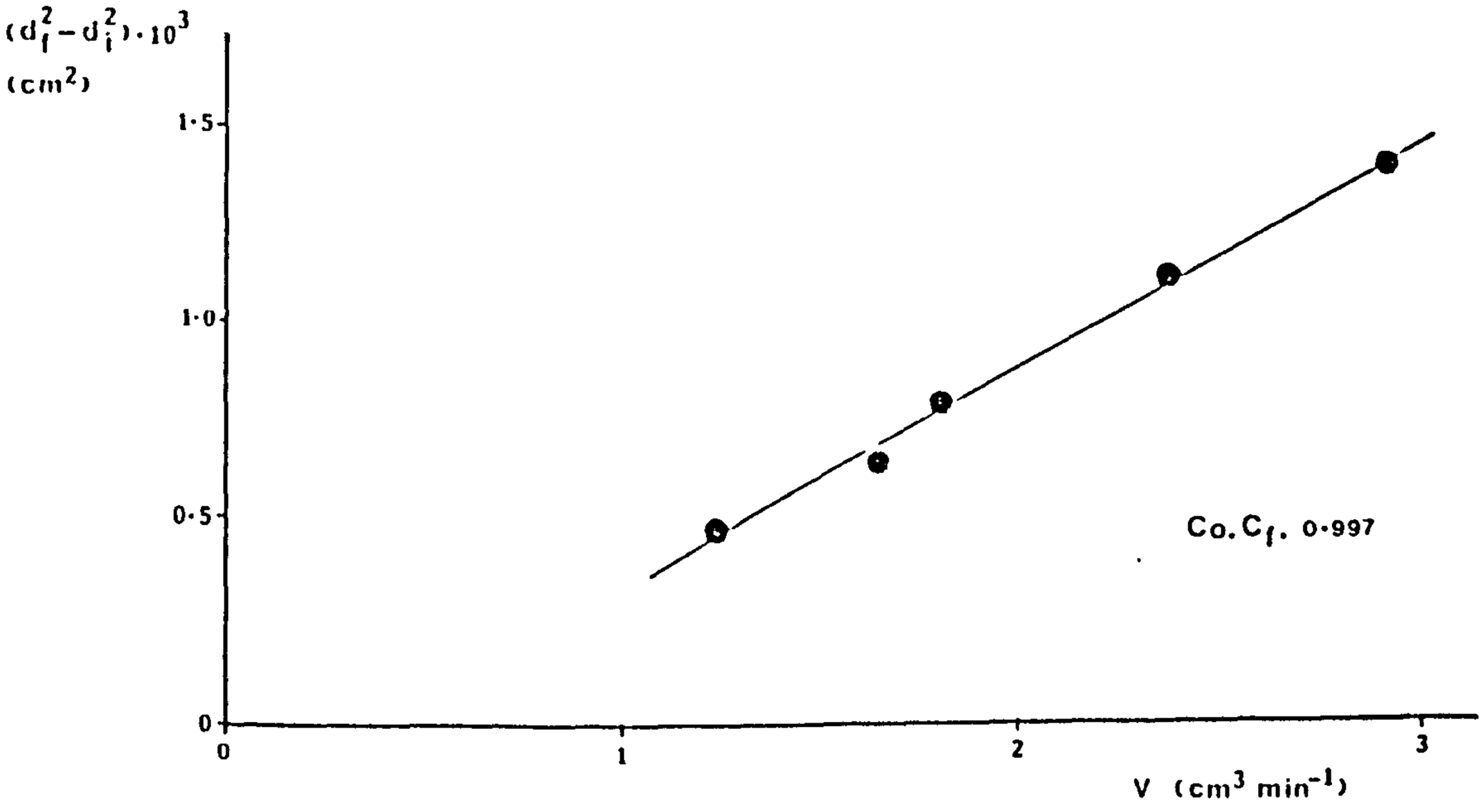

Fig 3.10 Effect of FER on fibre dimensions (Batch 43/1).

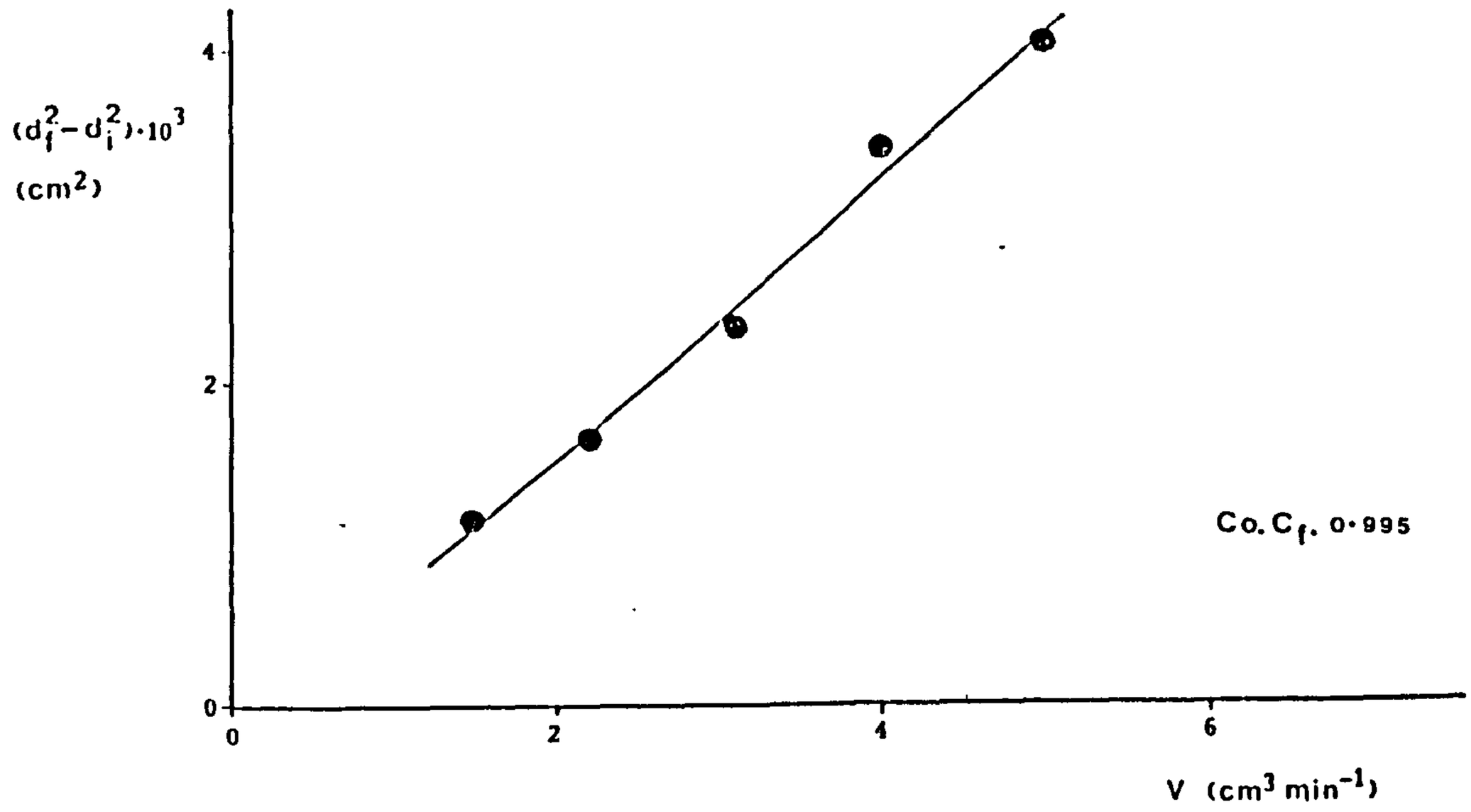

Fig 3.11 Effect of PER on fibre dimensions (Batch 21/2).

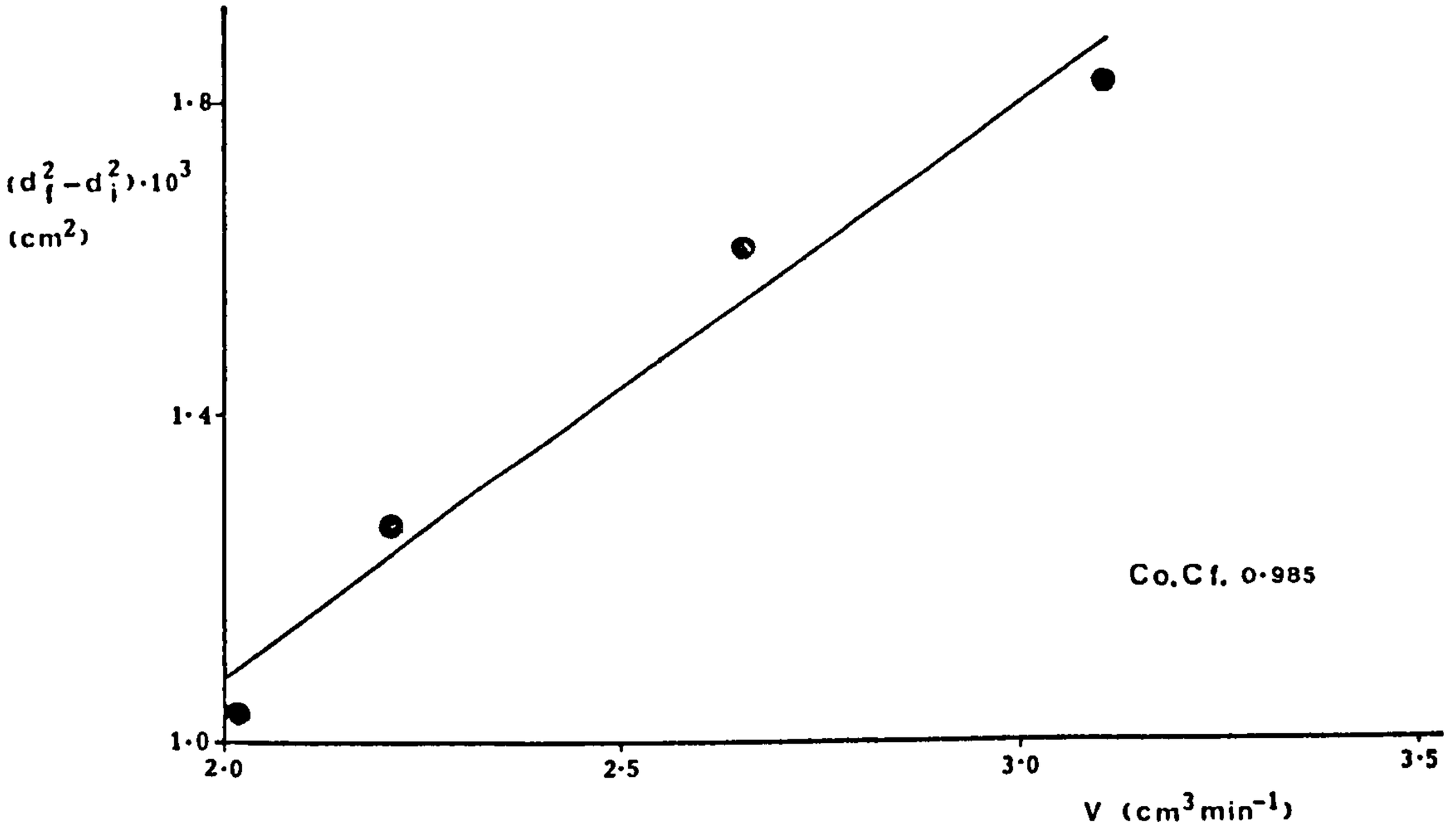

Equation 3.17 can further be tested against data from the spinning runs by examining the relationship between wind up speed (S) and fibre diameter (d_f). According to the model, the square of the fibre diameter should be inversely proportional to S. Thus a graph of d_f^2 against 1/S should produce a straight line. Table 3.9 shows the two batches (43/1 & 44/3) which were spun with varying wind up speeds to test this relationship. Fig 3.12 & 3.13 show the results. Both batch 43/1 and 44/3 showed good correlations (coefficients of 0.99 & 0.96 respectively) indicating that the relationship was as predicted.

In addition to those relationships tested, the rearrangement of equation 3.16 and substitution of equation 3.9 for d_i reveals an expression which allows the relationship between fibre diameter (d_f) and water injection rate (a) to be tested.

$$d_f^2 = \frac{4\,(V\,\rho_d\,X + q\,\rho_p)}{\rho_p\,S} + \frac{4\,a}{\pi\,S} \qquad (3.18)$$

Figs 3.14 & 3.15 show graphically the data taken from batches 11/4 and 44/3 (shown in Table 3.7) which demonstrate the relationship. As predicted by the model the square of the fibre diameter is directly proportional to the water injection rate; the fairly good correlations (0.990 & 0.874) lend evidence to this. Batch 25/1 (not shown graphically) also had a good correlation (0.943) but batch 37/1 produced a correlation coefficient of -0.453 suggesting that in this case the data was unrelated. Why the fibres of batch 37/1 failed to show a direct relationship was not fully understood, but it was thought that the very viscous dope used to produce batch 37/1 could have in some way affected the die swell of the extruded filaments.

Fig 3.12 Effect of WUS on d_f^2 (Batch 43/1).

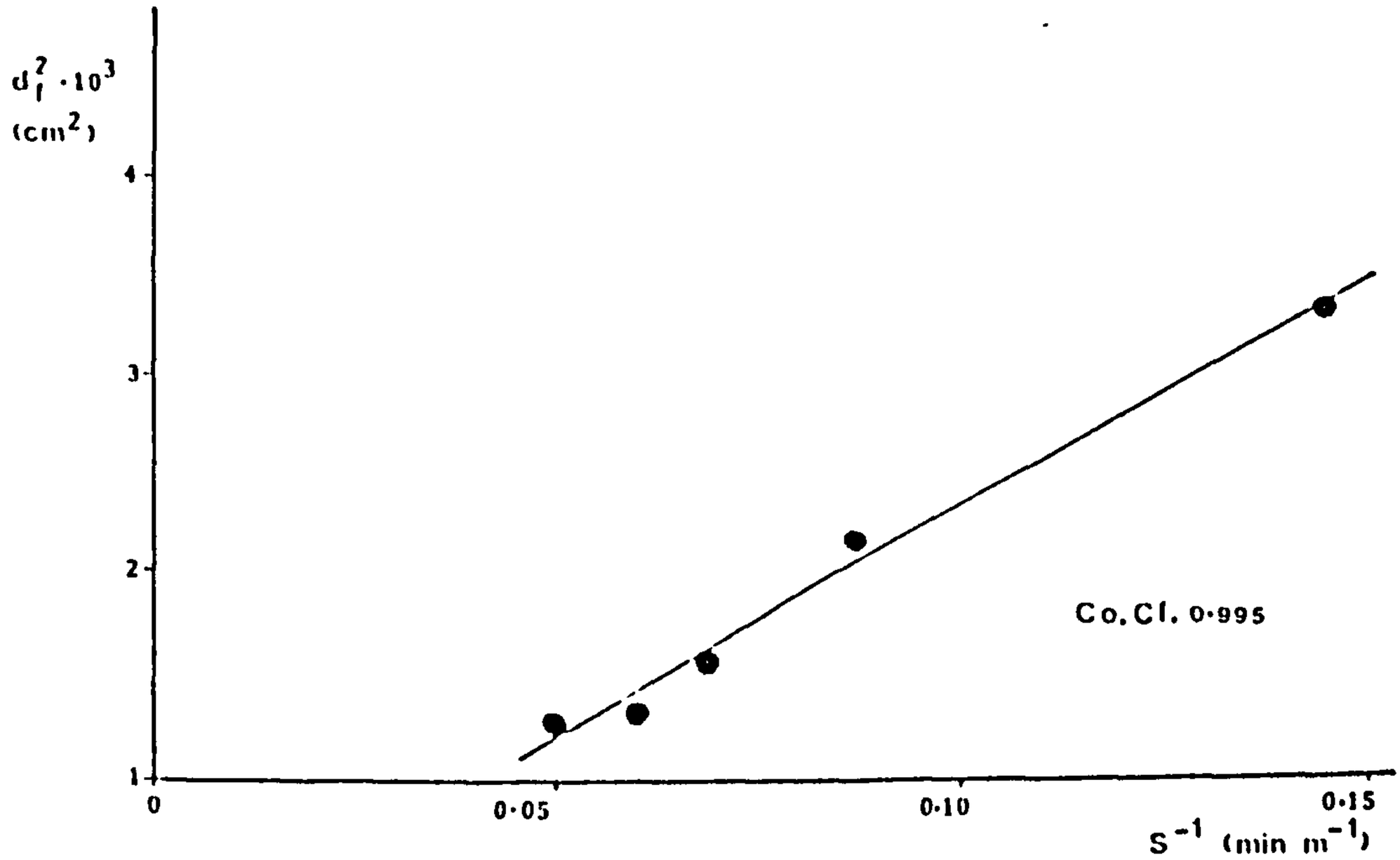

Fig 3.13 Effect of WUS on d_f^2 (Batch 44/3).

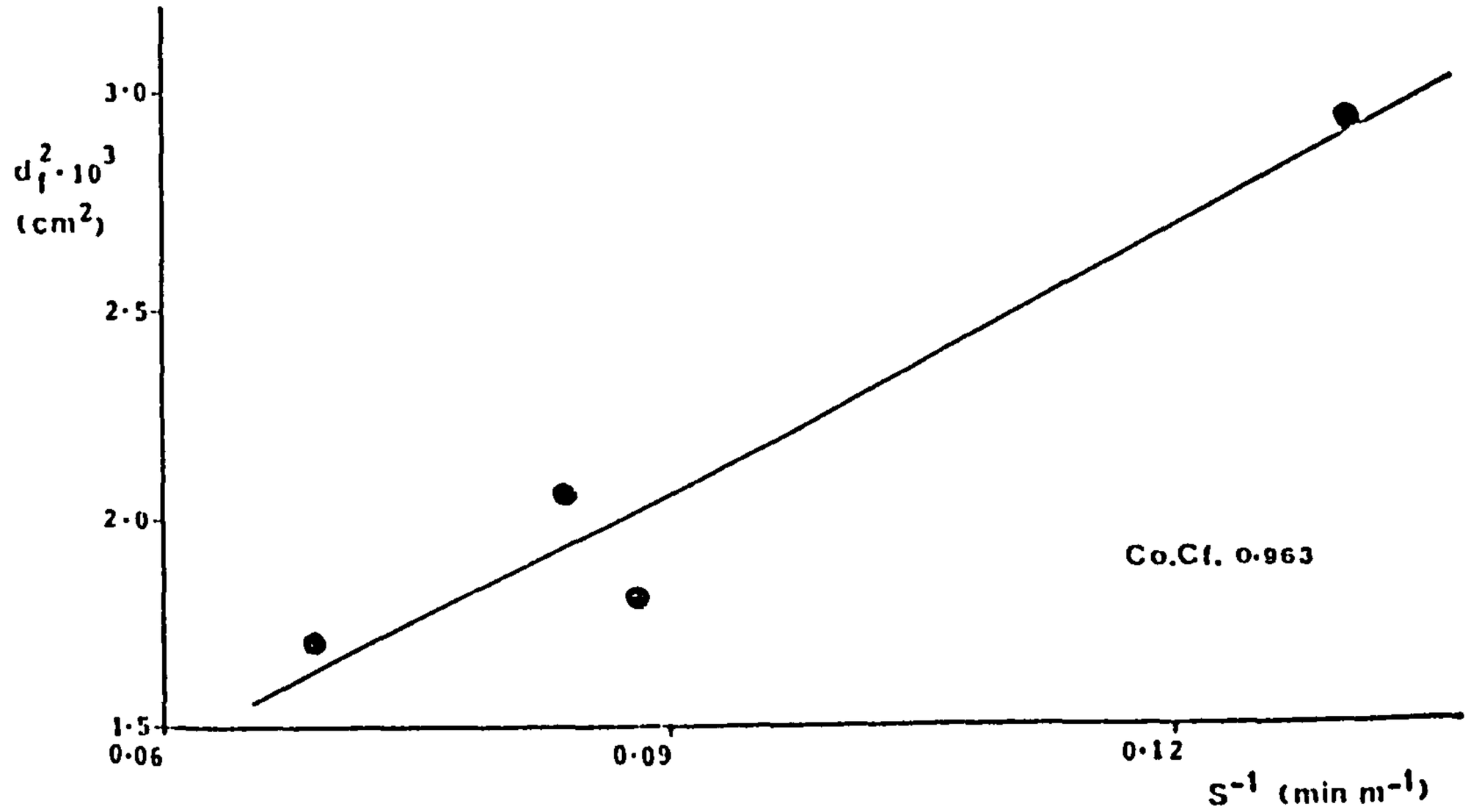

Fig 3.14 Effect of WIR on d_f^2 (Batch 11/4).

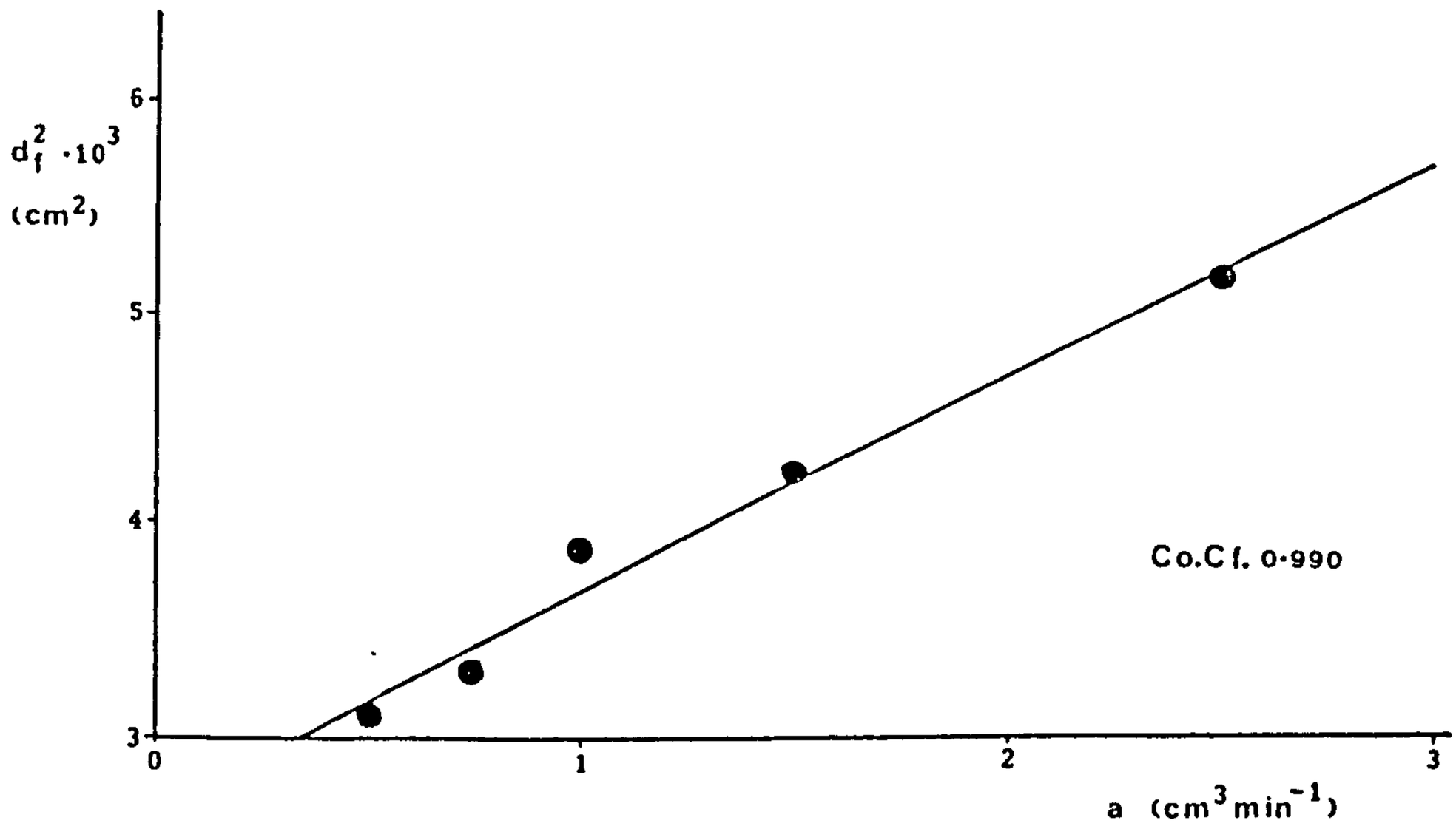

Fig 3.15 Effect of WIR on d_f^2 (Batch 44/3).

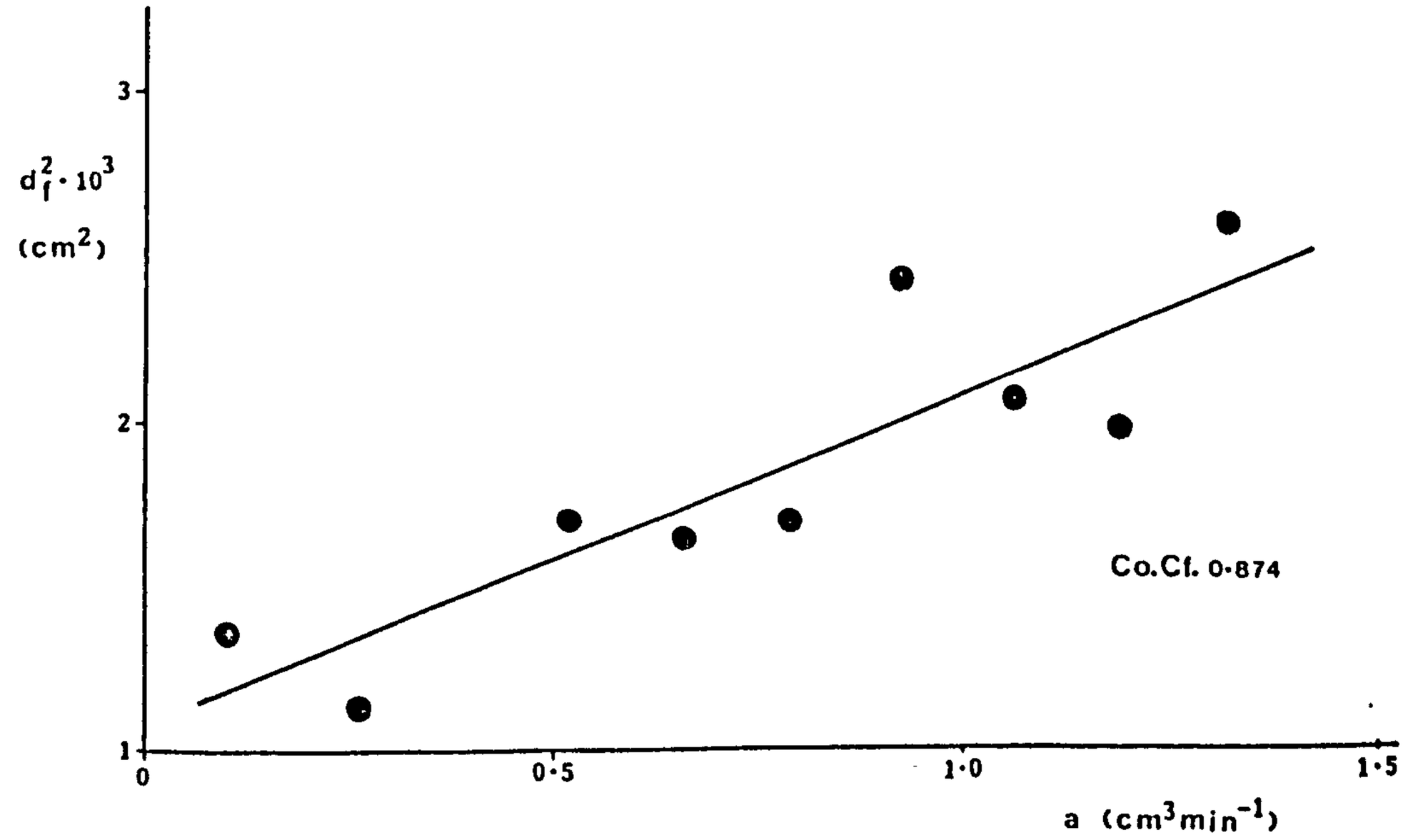

3.2.4 Observations on morphology and pore structure.

Qualitative observation by examining fibre cross-sections by S.E.M. is very difficult as each image may be subject to several interpretations. Quantitative examination is nearly impossible without the aid of sophisticated image analysis equipment. However, with the aid of photographs taken during the course of the research and measurements made of % void volume the following observations were made concerning the fibre morphology and its formation during the phase inversion process.

(a) Effect of concentration.

V. Rogers observed [78] a decrease in the % void volume content of fibres spun from solutions of increasing polymer content. No further studies were made except on a qualitative basis from the micrographs taken of DMAc type fibres (see plates 3.1, 3.3 & 3.4). Apart from the decrease in macrovoid content (possibly resulting in the decrease in % void volume), it was noted that in the fibres spun from solutions of higher polymer concentration there were fewer inter-connecting pores. At 40% polymer concentration (see plate 3.15) the voids were observed to be more or less discrete from their neighbours. The likely consequence of this would be an increase in the tortuosity of the fibre to diffusing species causing a drop in the permeability due to the increase in the effective thickness of the membrane.

(b) Effect of spinning parameters.

Polymer extrusion rate:- Table 3.10 lists the % void volume content of batches 43/1 and 11/3. Both batches were spun to examine the effect of PER on various parameters. The table indicates that an increase in PER generally results in an increase in the % void volume, although no further deductions can be made from this small amount of data.

Water injection rate:- Table 3.11 shows that W.I.R. appeared to have no bearing on the fibre's % void volume.

Wind up speed:- Similarly, the effect of the W.U.S. on the % void volume appeared to have an indiscriminate effect as the data in table 3.12 shows.

Table 3.10 Effect of P.E.R. on % Void Volume.

Batch	Polymer Extrusion Rate $cm^3\ min^{-1}$	% Void Volume
11/3d	1.5	30.7
11/3c	2.2	41.3
11/3a	4.0	41.5
11/3b	5.0	48.2
43/1n	1.2	30
43/1m	1.7	37
43/1o	1.8	37
43/1p	2.4	40
43/1q	2.9	40

Table 3.11 Effect of W.I.R. on % Void Volume

Batch	Water Injection Rate $cm^3\ min^{-1}$	% Void Volume
44/3j	0.10	59.3
44/3i	0.26	36.1
44/3h	0.52	57.5
44/3b	0.66	47.9
44/3c	0.79	49.9
44/3d	0.92	61.2
44/3e	1.06	54.9
44/3f	1.19	51.9
44/3g	1.32	57.7
25/1k	0.14	53
25/1l	0.42	49
25/1j	0.69	53
25/1i	1.12	51
25/1h	1.38	34

Table 3.12 Effect of W.U.S. on % Void Volume.

Batch	Wind Up Speed $m\ min^{-1}$	% Void Volume
43/1d	6.9	35
43/1c	11.5	44
43/1b	14.4	32
43/1f	16.8	37
43/1e	20.0	54
44/3k	7.7	71.9
44/31	11.3	45.8
44/3e	11.9	54.9
44/3m	14.4	53.1

(c) Effect of different solvent systems.

The effect of different liquid carriers has already been discussed in relation to the elimination of macrovoids but what other morphological features are affected by the different spinning systems? Comparison of the annular regions produced by the different liquid carriers shows that the porous substructure depends on the solvent system used. Plate 3.16 suggests that the microvoids present in the 1-Fp:Fa system are of a larger size than those of the DMAc system (Plate 3.17). This observation could be attributed to the difference in the rate of coagulation.

Plate 3.18 shows the outer skin layer (zones A_o, B_o) of a 9:1 1-Fp:Fa type hollow fibre. As can be seen the nodules making up the skin layer appear to be of a fairly coarse structure compared with those making up the skin layers of DMAc and 1-Fp type membranes (Plates 3.19 & 3.20). In the DMAc and to a lesser extent the 1-Fp types the skin layer appears to consist of an aggregation of finer and finer nodules proceeding to the outer edge. The coarse nature of the 9:1 1-Fp:Fa skin could account for the much higher permeability associated with this type

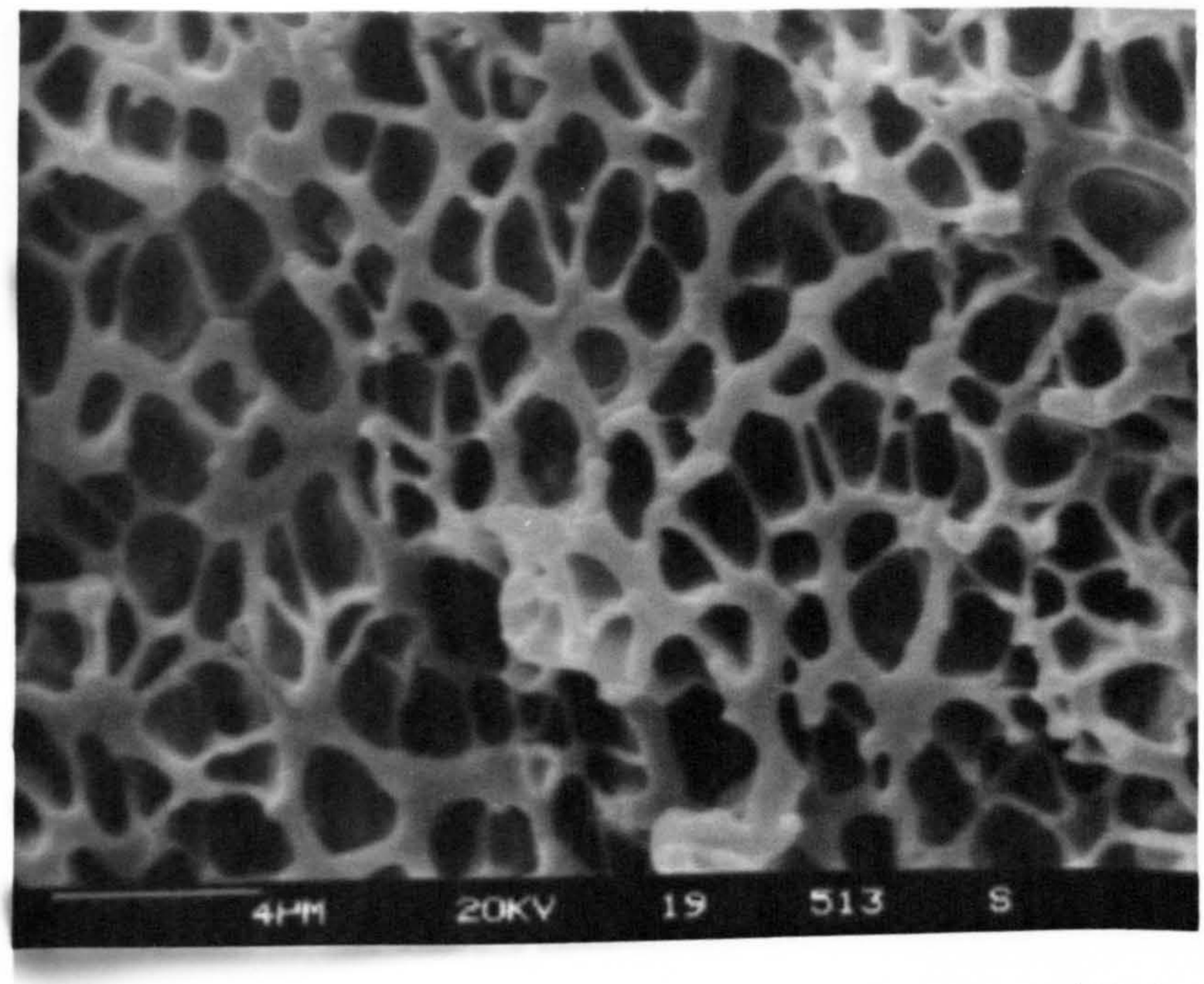

Plate 3.15 Pore structure of DMAc type fibre (40%).

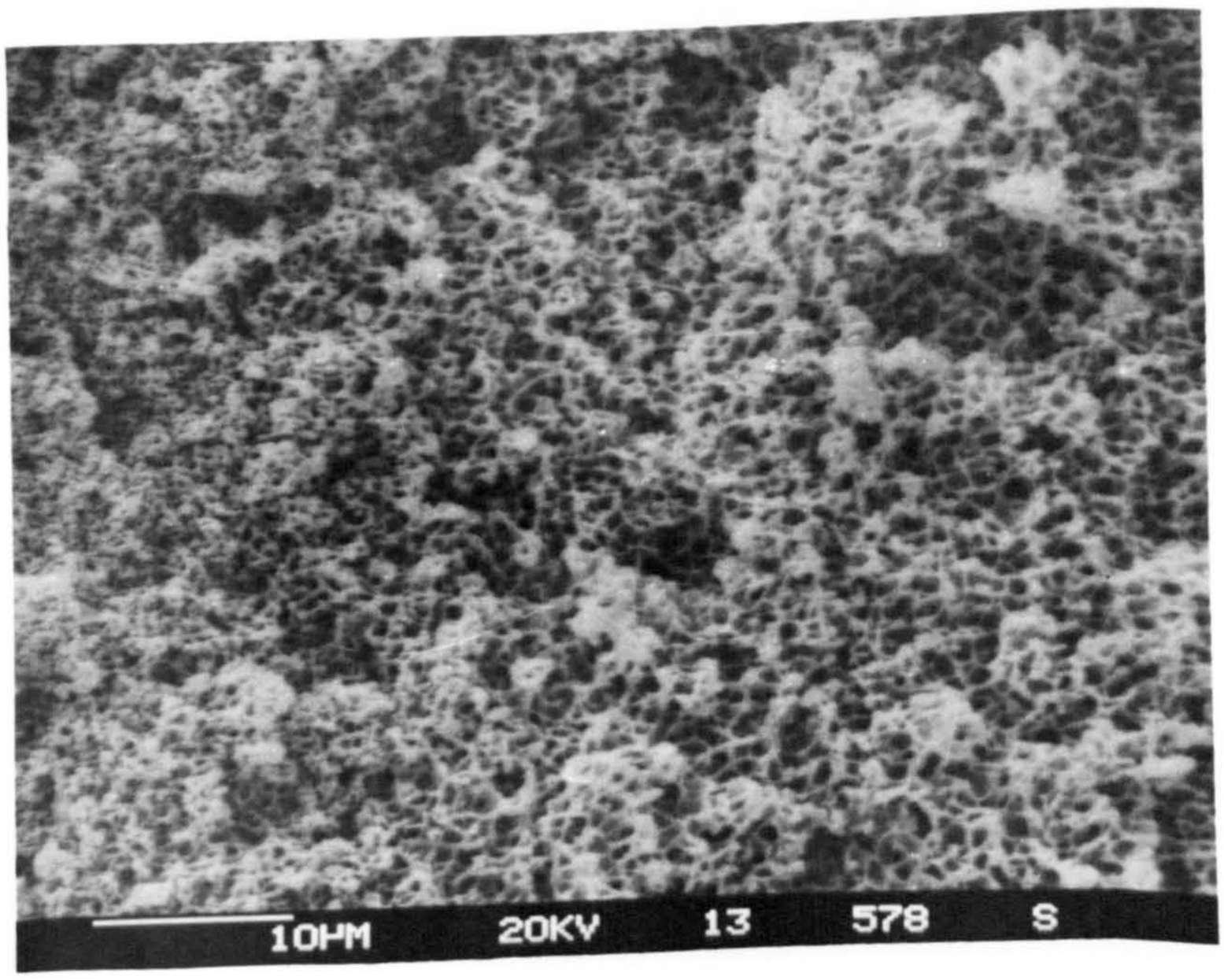

Plate 3.16 Pore structure of 9:1 1-Fp:Fa type fibre (30%).

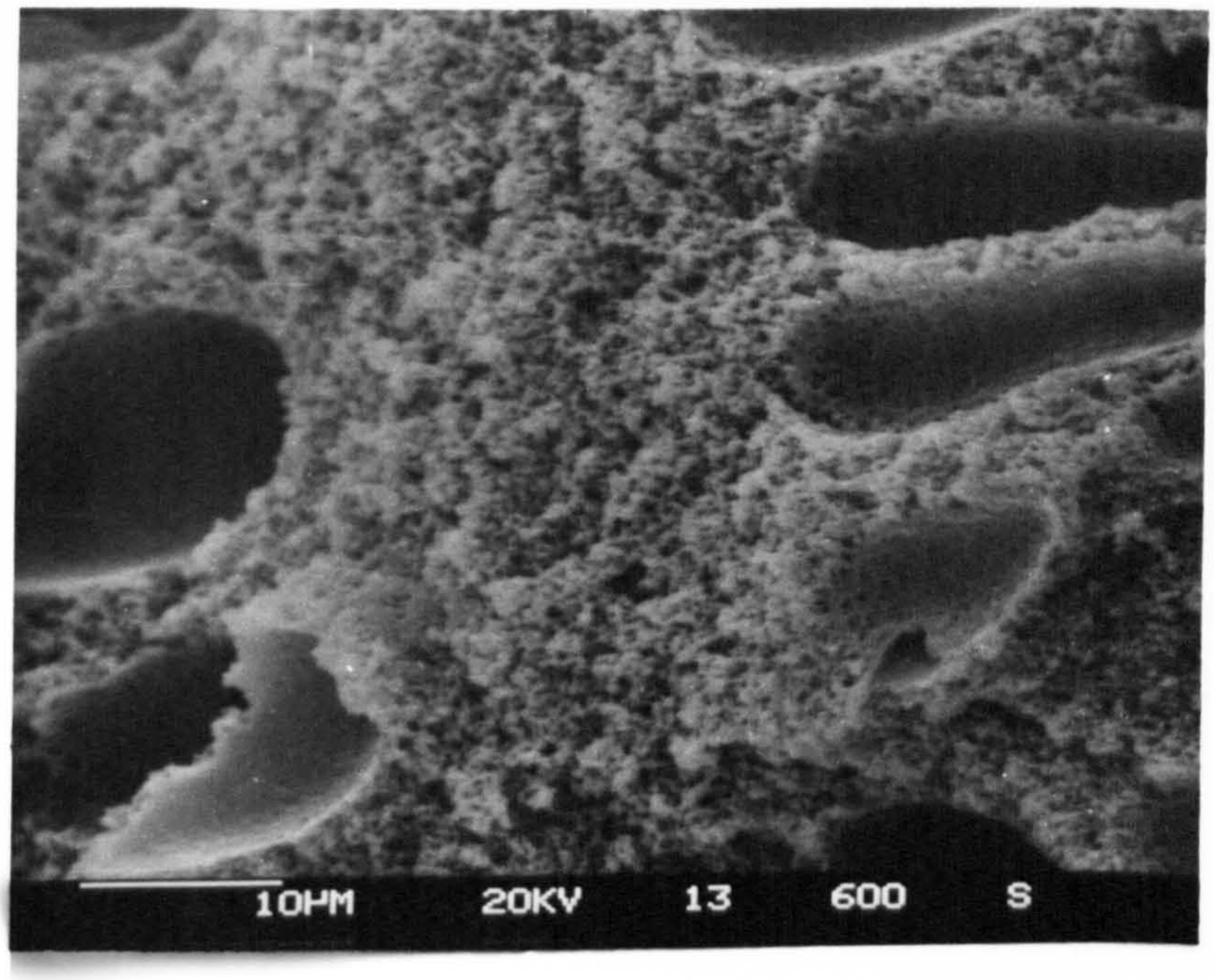

Plate 3.17 Pore structure of DMAc type fibre (30%).

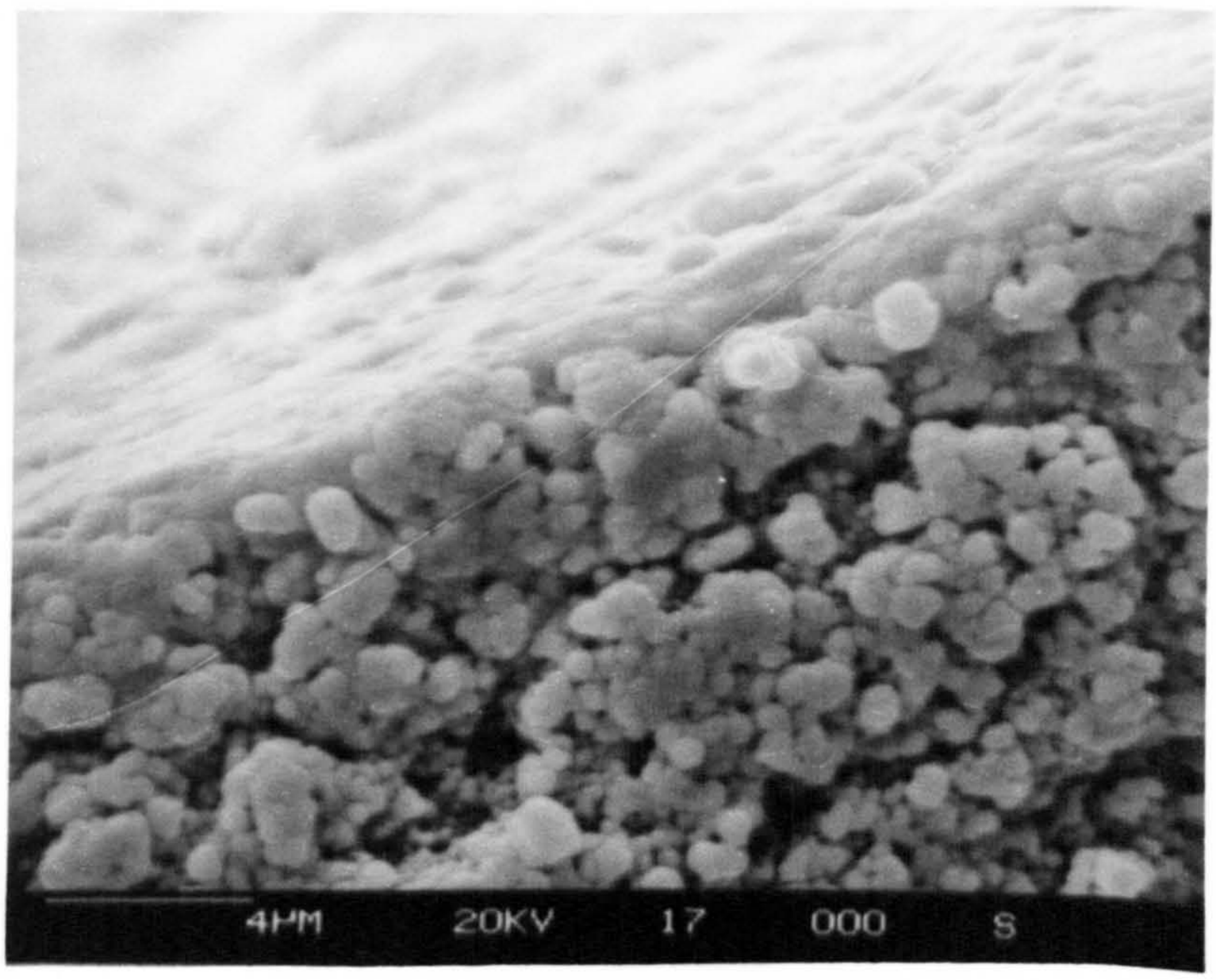

Plate 3.18 Outer skin layer 9:1 1-FP:FA type fibre (30%).

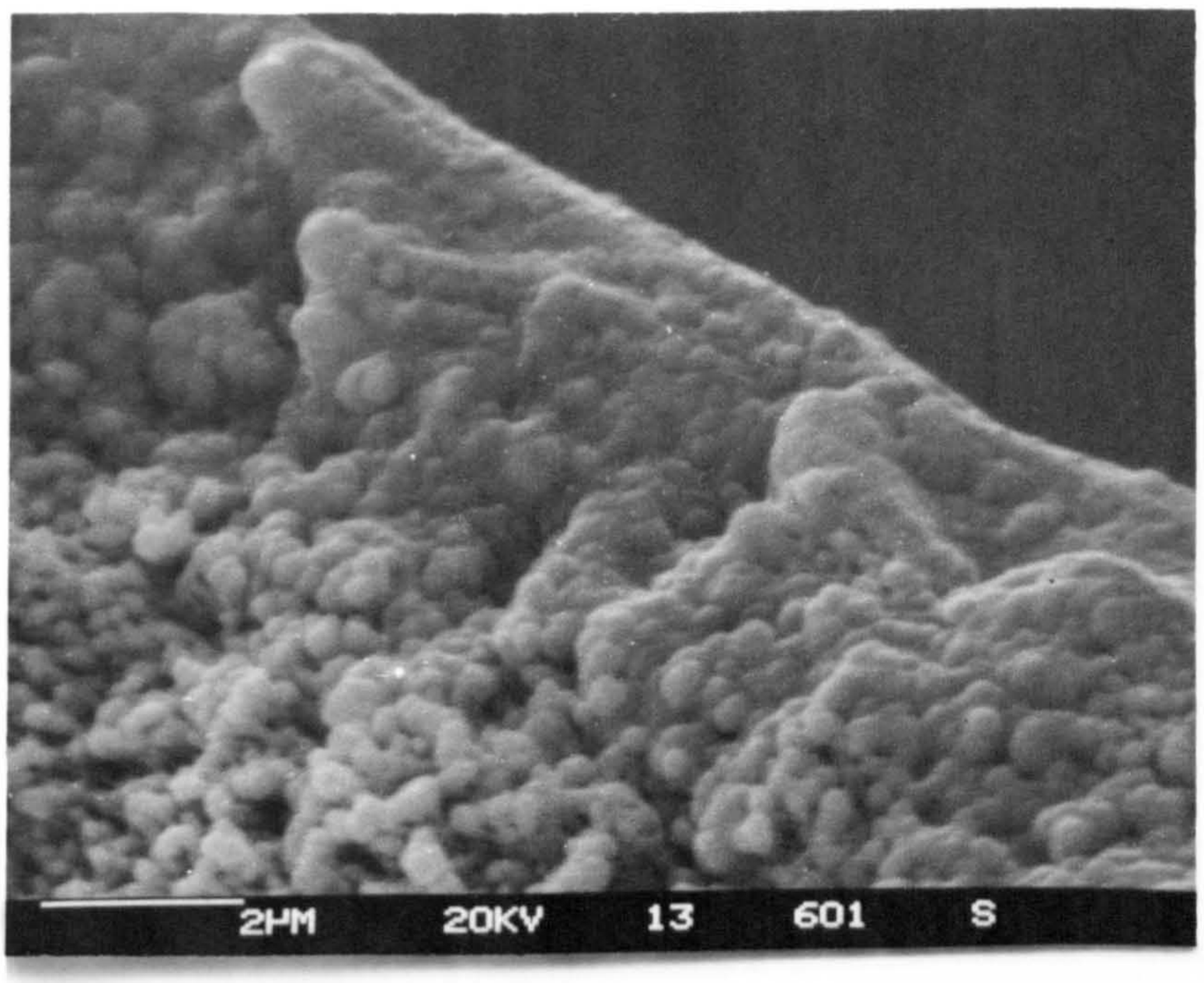

Plate 3.19 Outer skin layer DMAc type fibre (30%).

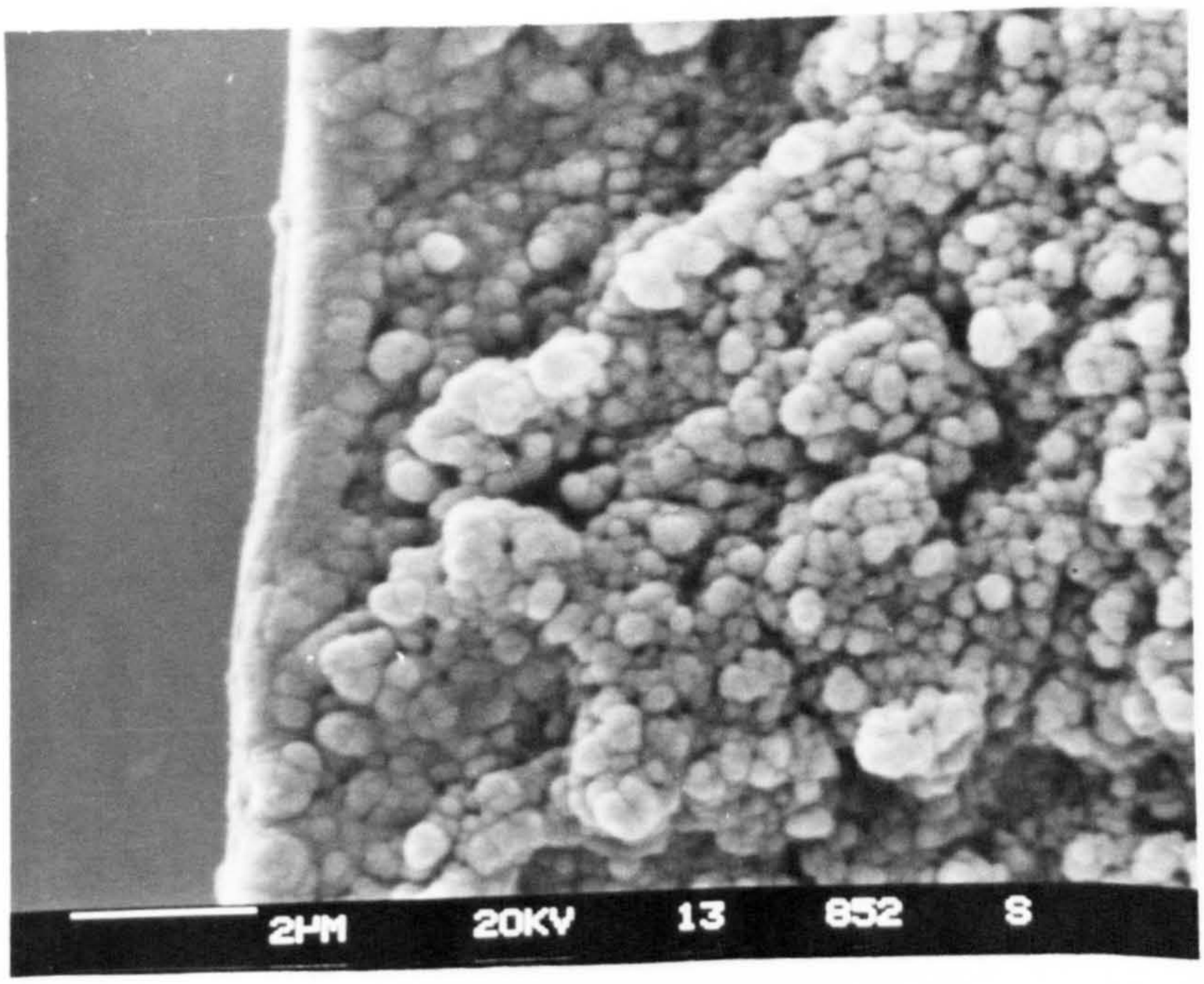

Plate 3.20 Outer skin layer 1-Fp type fibre (30%).

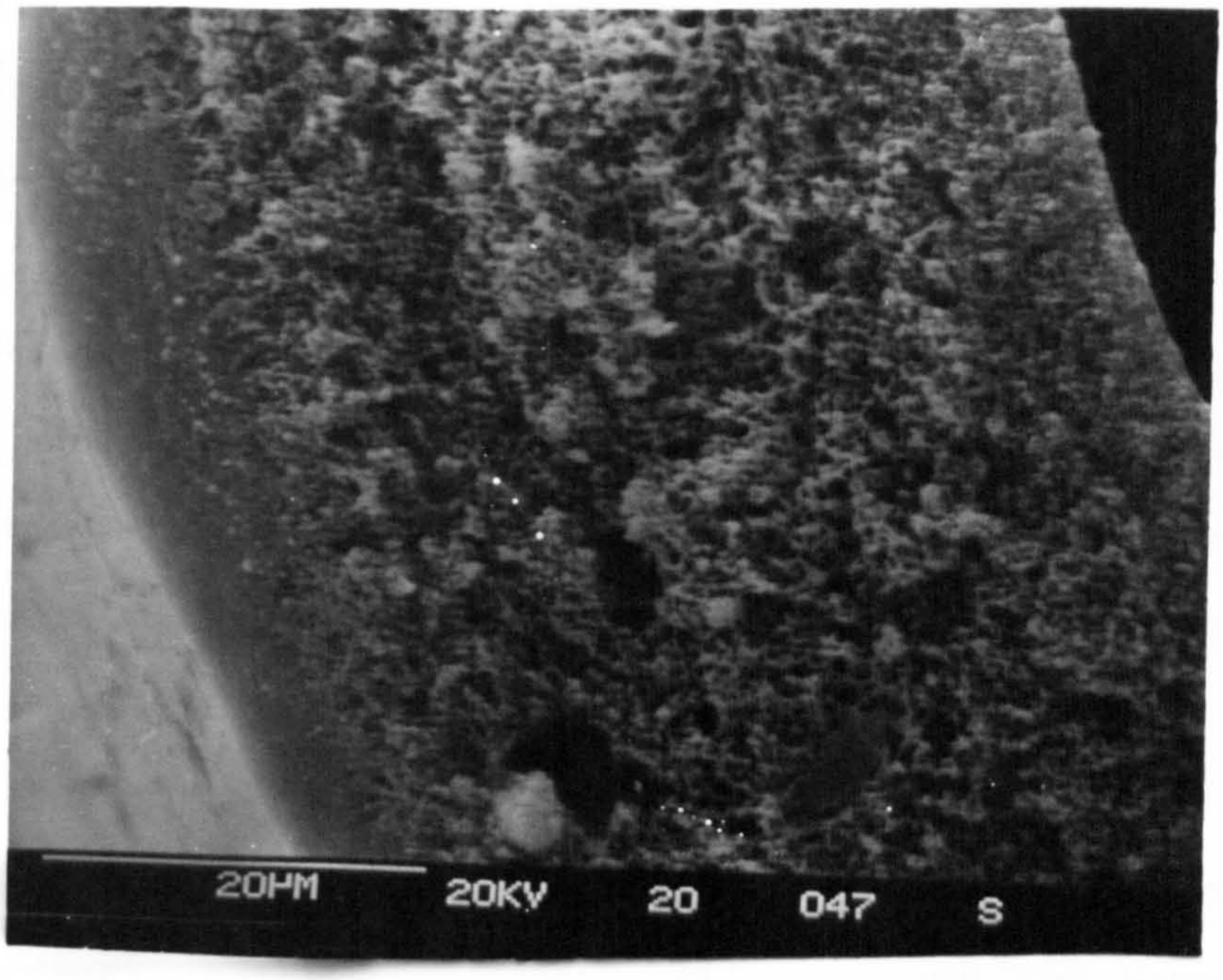

Plate 3.21 Pore structure of DMF type fibre (30%).

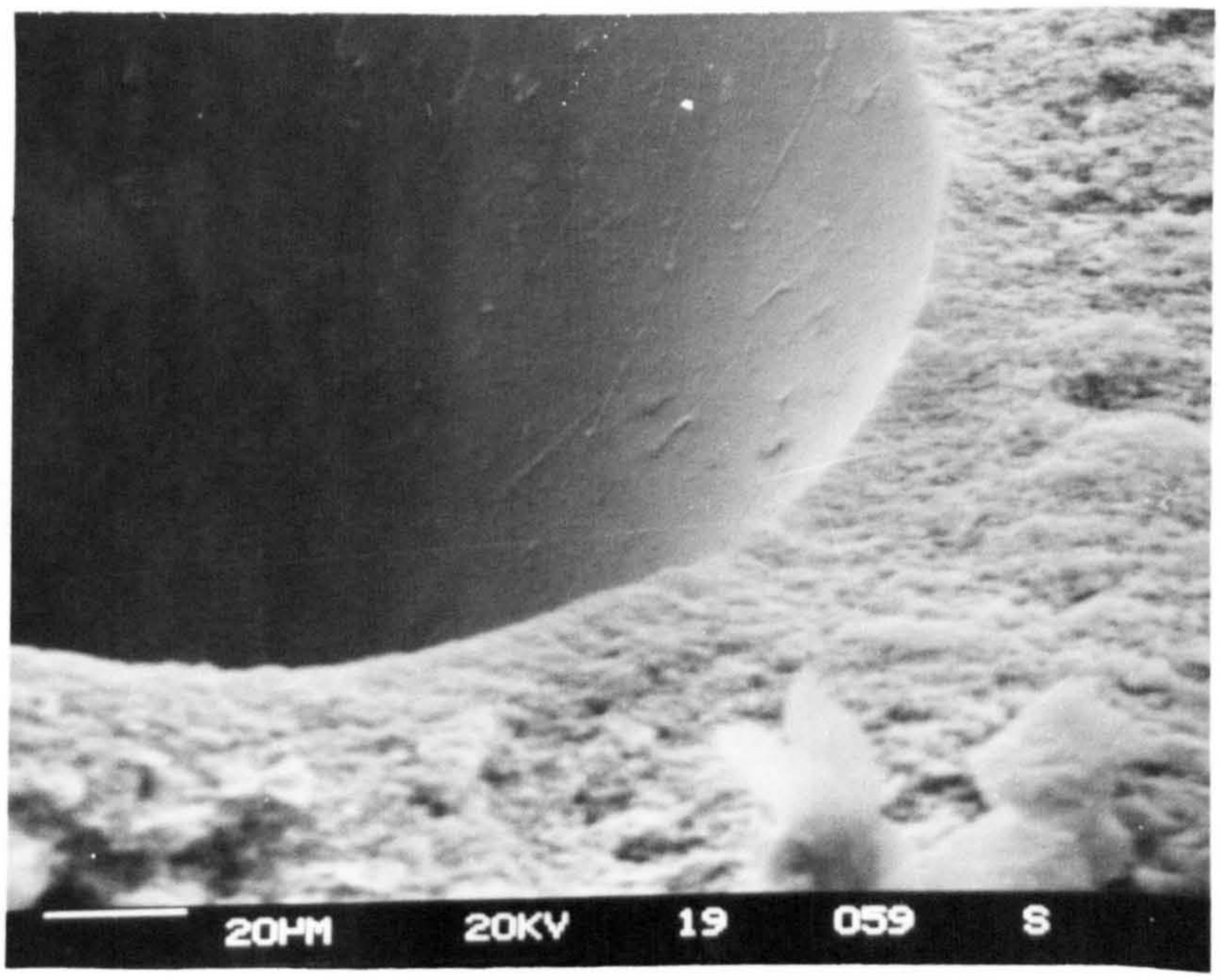

Plate 3.22 Inner skin layer of 95:5 1-Fp:Fa (30%).

of membrane (see section 3.3.5) due to the much greater volume of interstitial space between nodules. With the coarse nodule structure there is a much higher probability of surface defects or holes being present in the skin layer. This is another possible explanation for the high permeability observed in the uncoated 1-Fp:Fa type fibres.

Plate 3.21 shows the porous substructure of the DMF type fibres. Although the fibres show more or less complete elimination of macrovoids the fibres appear to have a very large dense A_o zone. Where the thickness of the skin becomes too great the rate of permeation decreases and is thus disadvantageous. In effect the fibre's properties approach those of a dense membrane, i.e. high selectivity but poor permeability.

Little has been said about the inner skin layer (zone A_i). What part does this morphological feature play in the permeation process? The disadvantages associated with a thick skin layer have been mentioned above. Where a suitable thickness of skin has formed on the outer surface of the membrane, the inner skin only acts disadvantageously as an extra barrier to permeation, increasing the effective thickness of the membrane. However, the internal skin layer does not benefit from the jet gap or coating procedures which control the morphology of the outer skin. Where the internal coagulant comes into immediate contact with the inner part of the cast filament, the formation of skin occurs, but with the likelihood of a higher proportion of defects in the skin. The die-swell stresses relieved in the jet gap for the outer skin cannot be relieved in the inner skin - thus defects often result. This can be seen to occur as elimination of macrovoids from zone B_i is far harder to achieve than it is from B_o, indicating the tendency of the inner skin to form with defects (allowing macrovoid formation). The consequence of the presence of the defects is that the holes through the surface layer allow the permeating gases a path of lower resistance thus raising the

overall permeability of the membrane. Plate 3.22 shows a typical fibre lumen with defects in the surface clearly visible.

3.2.5 Summary.

The aim of the work in this section was to analyse the hollow fibre spinning process, specifically to model spinning parameters in terms of fibre dimensions, membrane morphology, and porosity. To this end the research carried out was moderately successful. Correlations between spinning parameters and fibre dimensions were found although the model derived was not suitable to meet the objective of producing hollow fibre membranes of pre-specified dimensions. The main problem in understanding the membrane fabrication process lies in the lack of knowledge of the formation of the voids. In order to make further progress a detailed study of voids, their type, formation and quantity needs to be made, i.e. What conditions favour the formation of interconnecting voids? What range of void sizes exist in a particular type of hollow fibre membrane?

The void volume content of the fibre should be calculated in a manner which does not require measurements of fibre dimensions to be made. Void volume data could provide a useful insight into the term 'q' used in the model. The precise porous substructure within a hollow fibre may well be determined by other spinning parameters not studied in sufficient detail during this period of research. For example, extrusion and coagulating temperature may well influence the mechanism of precipitation thus controlling the formation of voids.

3.3 Gas transport properties of hollow fibre membranes.

3.3.1 Introduction.

In the previous section an attempt was made to quantify the effects of spinning parameters on fibre structure. In this section the relationship between spinning parameters / fibre structure and the gas transport properties of the membranes is discussed. In the majority of fibres examined two permselective properties were measured, namely the permeation rate constant and the separation factor.

This section also examines some of the gas transport properties not related to the spinning parameters. Examination of the coating procedure and effectiveness of the coatings is discussed. The validity of quoting separation factors based on the ratio of permeation rate constants measured using pure gases is tested by comparison with data obtained from measurements made using binary gas mixtures.

Note:- The data used in this section were mainly obtained from gas transport measurements made during the course of the research. However, further data were obtained from the unpublished work of R. Fielding who made measurements on fibre batches spun by V. Rogers. A permeation rig of similar design was used by R. Fielding and comparisons were made between the rigs to ensure that the two data sets were compatible. The extra data were of particular use in the creation of the scatter diagrams showing membrane performance.

3.3.2 Experimental error in gas transport measurements.

The main problem in trying to determine any relationship involving gas transport properties of the hollow fibres was the high level of experimental variability in the results. The problem arises from the fact that all the experimental errors of the entire process from spinning, measurement of fibre dimensions, etc. all become incorporated into the determination of the permeation rate constant. The biggest single source of variability arises in the preparation of the fibre modules. The problems arise as each module holds only a relatively small area of membrane surface (approximately 30 cm^2) and its assembly involves considerable handling of the delicate surface layer. The result of this was that often damage occurred to the permselective layer causing the permeability of the module to increase. Holes and scratches in the surface layer change the rate determining permeation mechanism from solution-diffusion to Knudsen flow. Other sources of inconsistency encountered during the measurement of permeation rate constants were variability in room temperature, and variability in packing in the permeator chamber brought about by the measurement of hollow fibres of differing fibre diameter. These consequences mean that large amounts of data are needed in order that reliable relationships can be concluded. However, due to the length of time required to make permeation rate measurements (one module per day) the number of modules examined was less than that which would be desirable to produce clear correlations.

In conclusion, it was estimated that any permeation rate constant measurement made on an uncoated module could be subject to an experimental variability of 20%. Coated modules although subject to an extra physical process tended to show slightly less variability due to the removal of the error associated with physical damage to the permselective skin layer.

3.3.3 Membrane performance.

Permeation rate constants were measured over a large range. Modules were tested, during the course of the research, which had permeation rate constants either side of the measurable range of the laboratory rig (i.e. above 4000 GPU and below 0.03 GPU). This five orders of magnitude difference in permeability is not uncommon in the field of membrane research and so data which fell within this range were commonly plotted as the logarithmic function. Separation factors, however, tended to range at most over two orders of magnitude, commonly falling within the range 0.7 to 50. Where membranes were extremely permeable to all gases (as in the case of a damaged or ruptured membrane) the separation factor rarely seemed to fall below that which was attributable to Knudsen flow separation (see section 1.2.2 - Permeation through microporous media).

In order for the hollow fibre membranes to be of practical use for separating gas mixtures, they must exhibit both high permeability and high selectivity. These two requirements commonly act in conflict. Either a membrane will exhibit high permeability and low selectivity or else a low permeability and a favourable selectivity. In order to characterise a particular hollow fibre's performance against other hollow fibres a graph was constructed depicting the logarithmic function of the permeation rate constant against the separation factor. Such graphs show both properties of importance, with the membranes having the best performance being situated farthest away from the origin. Without technical details of the plant to be used, the gas mixture to be separated, the level of purity required and the acceptable slippage it is impossible to make a finer analysis of the relative performance of each

membrane. If such process information was available then weighting factors could be applied to the graphs of $'P_i$ against α^i_j to give a more realistic interpretation of membrane performance.

3.3.4 The effect of coating.

The majority of fibre modules examined had separation factors of the order associated with Knudsen flow separation, suggesting that the skin layer, where separation of gases by solution-diffusion is said to occur, was damaged. The modules used in this state would be useless both for industrial separation applications and in terms of research for elucidating the effect of spinning parameters on gas transport parameters. The performance of the modules was improved by utilising the coating technique developed by Monsanto [64]. By sealing the defects in the surface layer with a highly permeable polymer the diffusion pathways of permeating species can be diverted to include passage through the thin dense regions of the skin layer. The coating material used by Monsanto was used to a great extent on the modules produced during the research. This silicone elastomer was chosen for its high permeability to penetrating gases. Monsanto quote [56] a concentration of 1% for their coating solutions and an application time of 10 min for the majority of their examples (see appendix 5). However, it was decided to examine a range of coating concentrations and application times to examine whether or not an optimum application existed. Experiments carried out on the 1-Fp:Fa type fibres (batch 35/1) over a range of concentrations and times are shown in Fig 3.16a-j and in Table 3.13. From the graphs it can be seen that the main changes occur between the uncoated and the first test values (i.e. 0.5% and 0.5 min). At concentrations and times above the minimum test values little

variation in permeability was observed. However, the separation factors observed showed some further dependence on the coating procedure. Due to the inherent experimental variability, no further deductions can be safely made. From the results of these coating trials it was decided that all further experiments would be conducted on fibres which had been coated with a 5% solution and immersed for a period of time above 15 minutes to ensure that the sensitivity of the permeability measurement to the coating method was minimised. The level of coating used by Monsanto could cause problems with regard to data interpretation, as Fig 3.16 shows that these levels are fairly sensitive, and small inaccuracies in the coating procedure could cause large variations in the permeation rate constant of the composite membrane.

Table 3.13 Effect of coating procedure on gas transport properties.

(a) Effect of concentration of coating solution (15 min immersion).

% Sylgard 184	Permeation Rate Constants (GPU)			Separation Factors	
$^{w}/_{w}$	H_2	CO_2	CH_4	H_2/CH_4	CO_2/CH_4
0	3840	1050	1460	2.64	0.72
1	109	78.7	12.2	8.91	6.44
2	88.8	75.1	7.32	12.1	10.3
5	58.4	68.0	6.70	8.72	10.2
7	60.1	62.5	5.04	11.9	12.4

(b) Effect of immersion time in coating solution (5% Sylgard).

Time	Permeation Rate Constants (GPU)			Separation Factors	
(min)	H_2	CO_2	CH_4	H_2/CH_4	CO_2/CH_4
0	3840	1050	1460	2.64	0.72
2	97.2	89.3	9.60	10.1	9.30
8	74.2	78.0	6.70	11.1	11.6
15	58.4	68.1	6.70	8.72	10.2
20	59.0	53.6	4.29	13.8	12.5
26	47.6	45.8	3.99	11.9	11.5

Fig 3.16 Effect of coating procedure on gas transport properties.

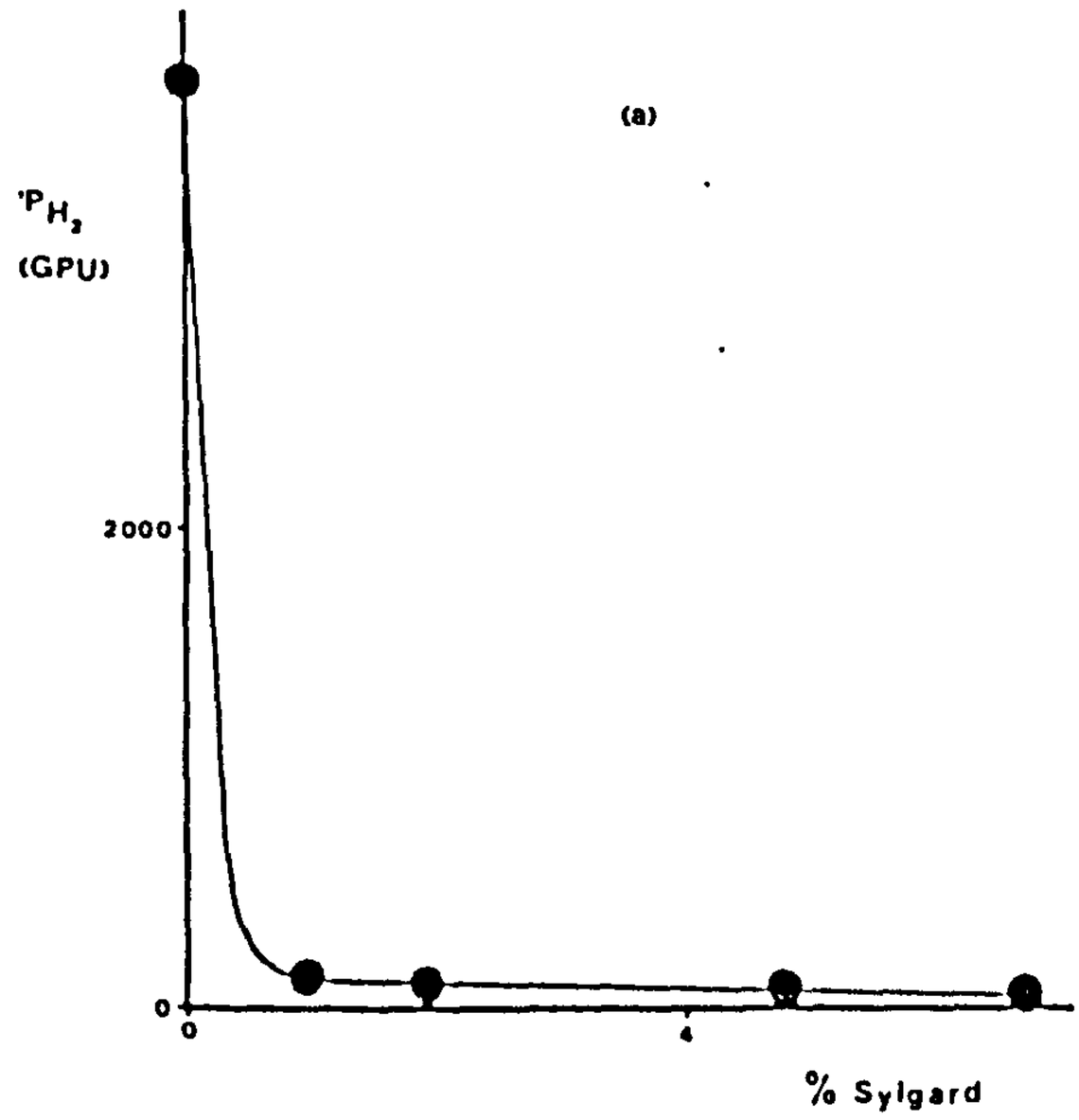

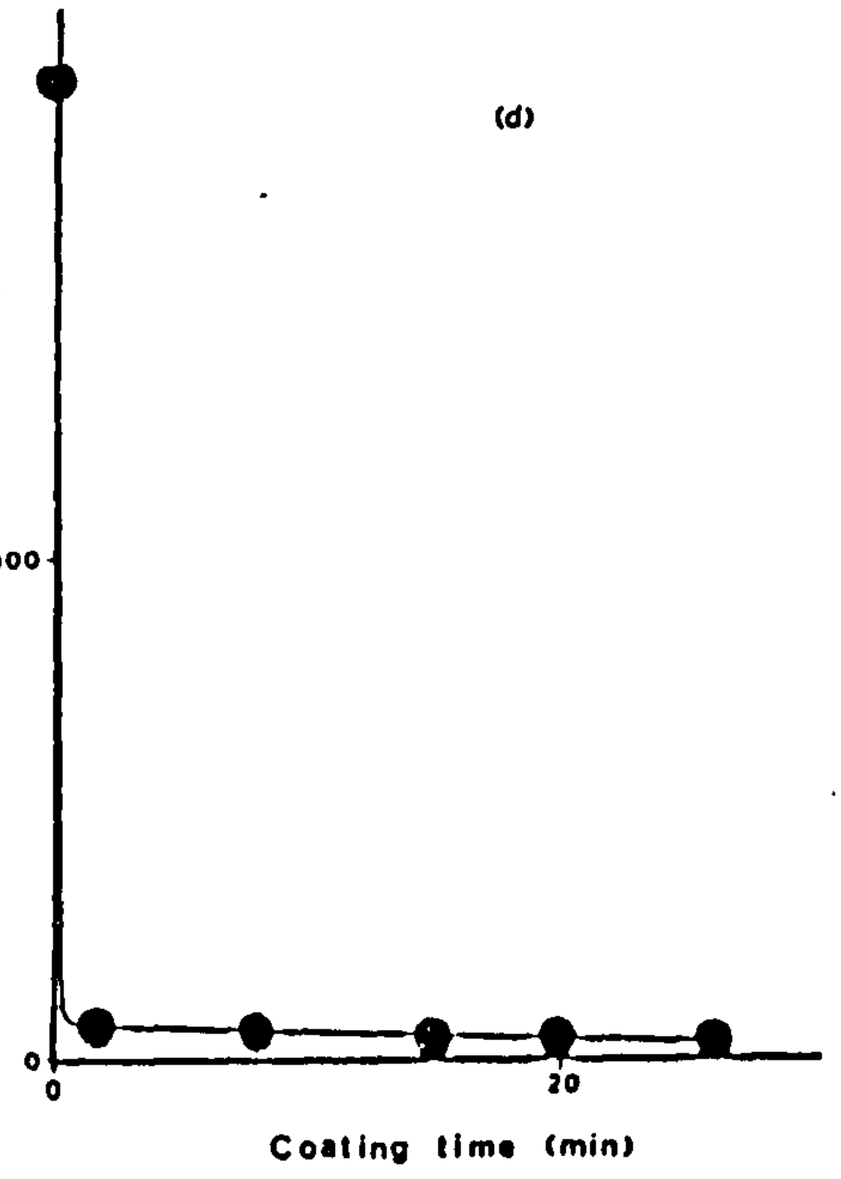

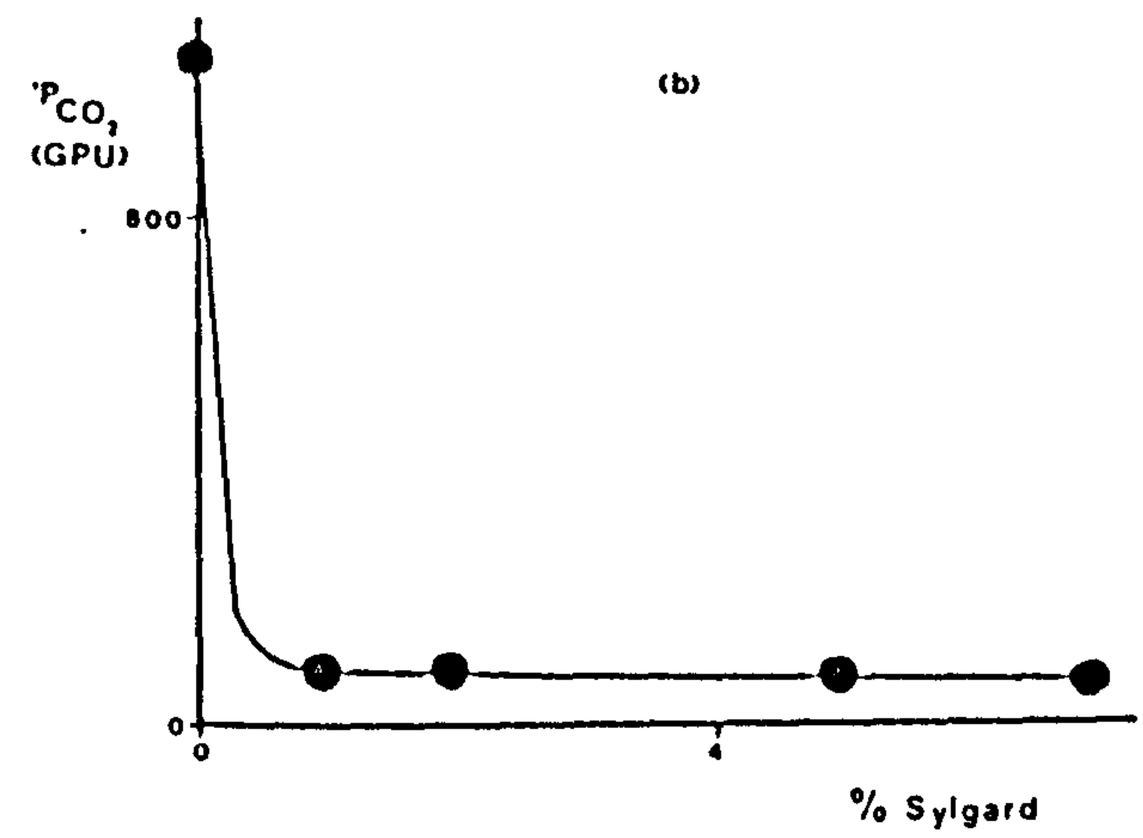

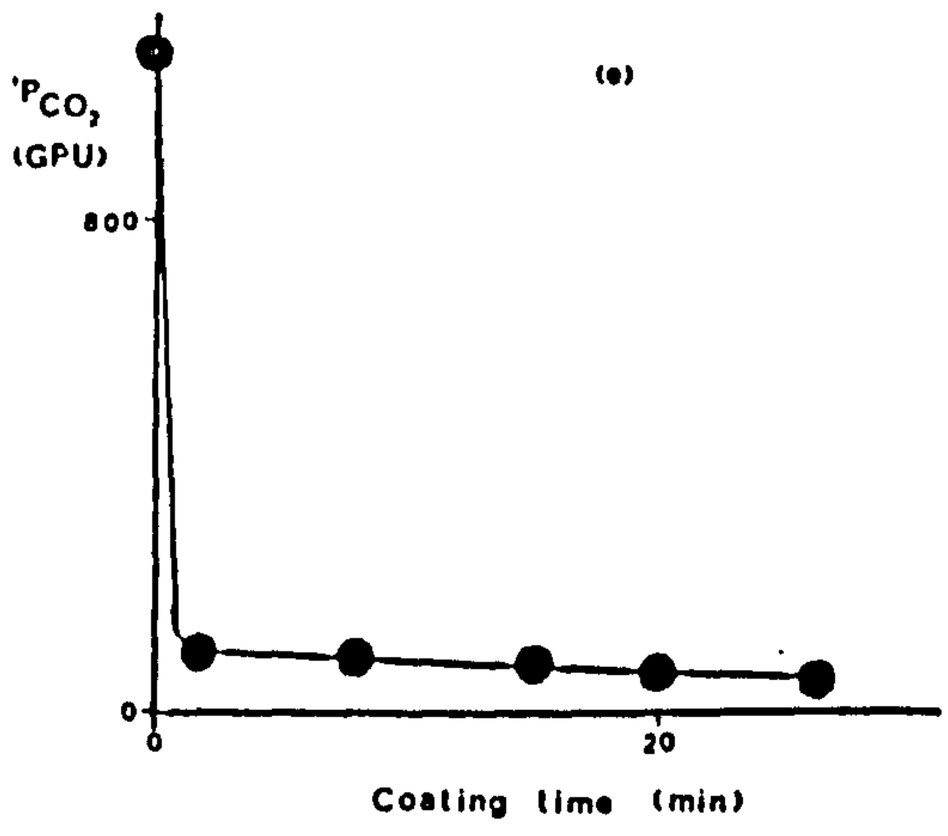

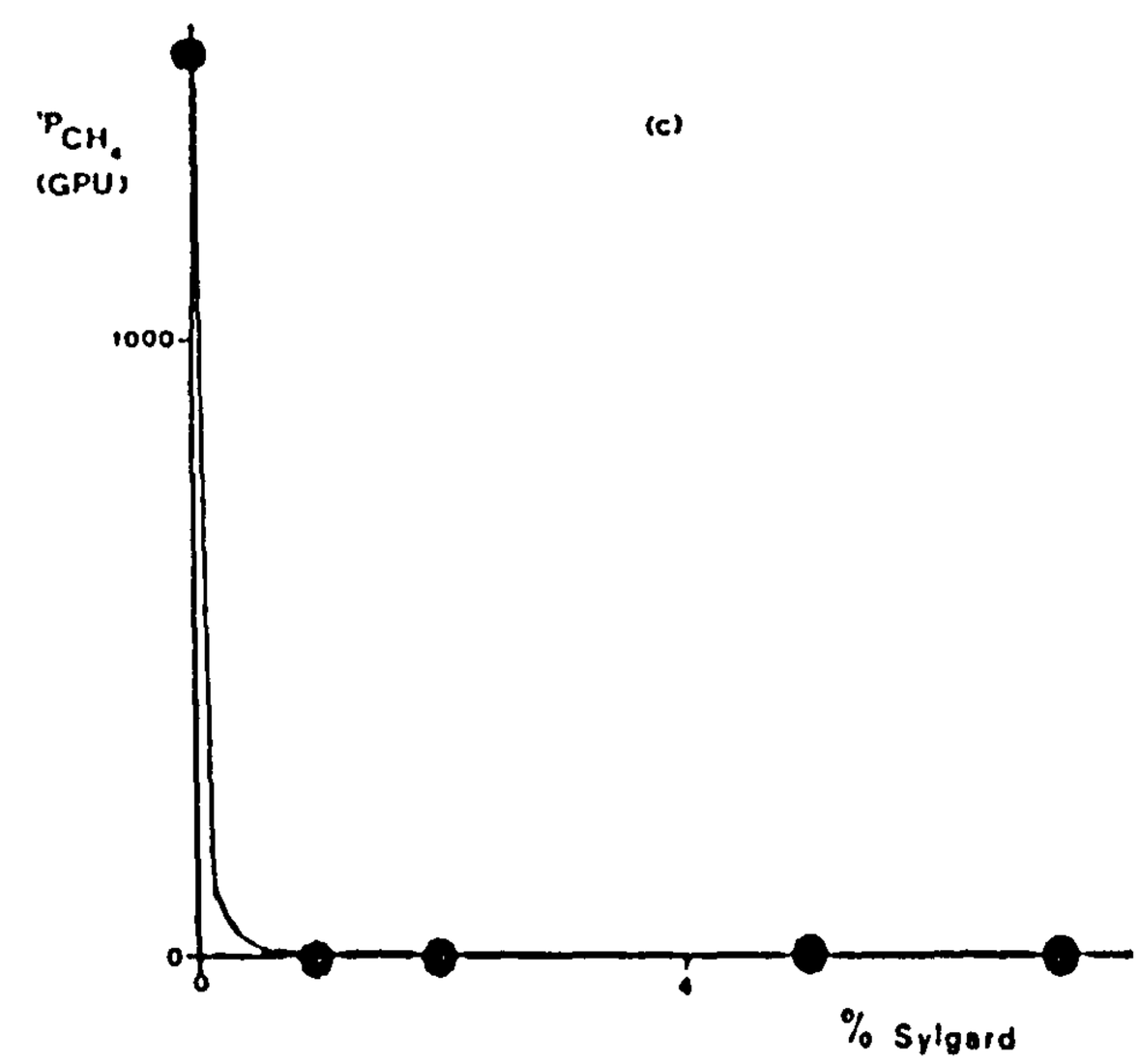

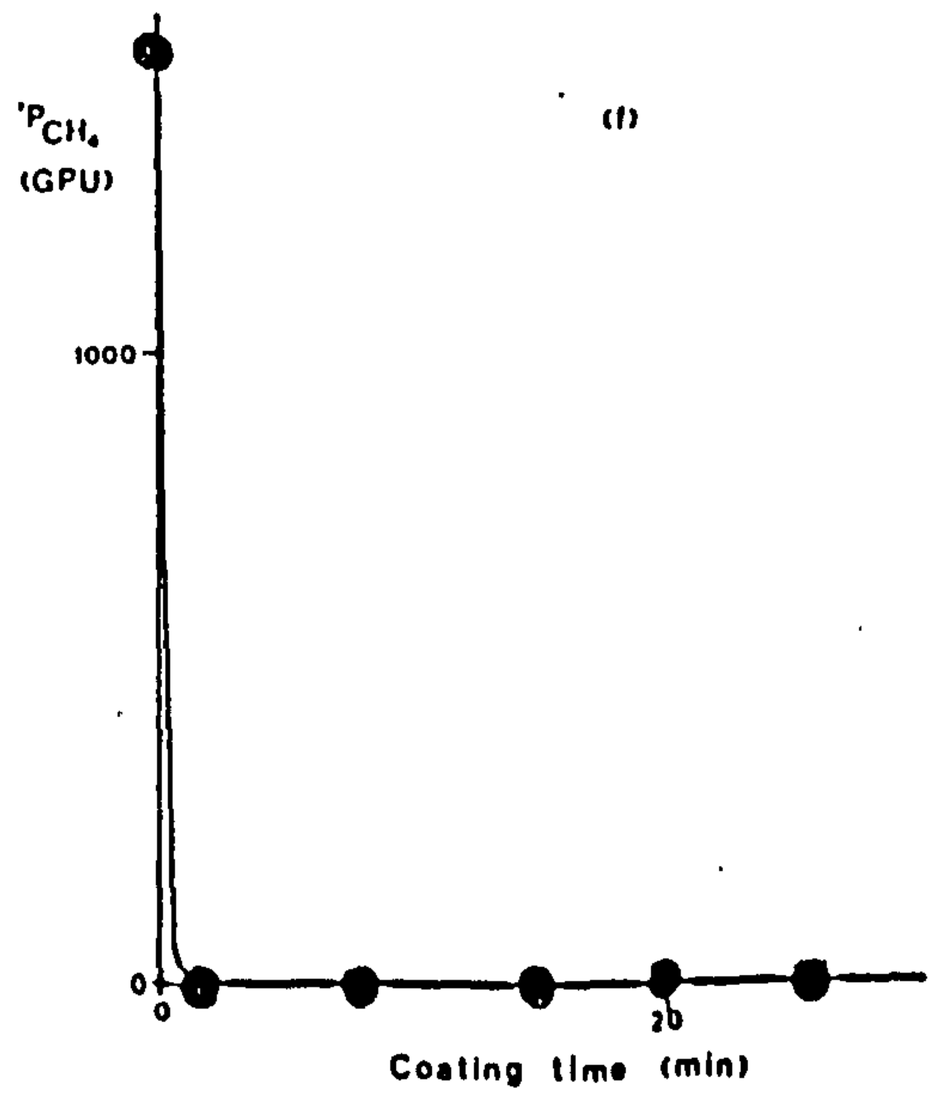

Fig 3.16 Effect of coating procedure on gas transport properties.

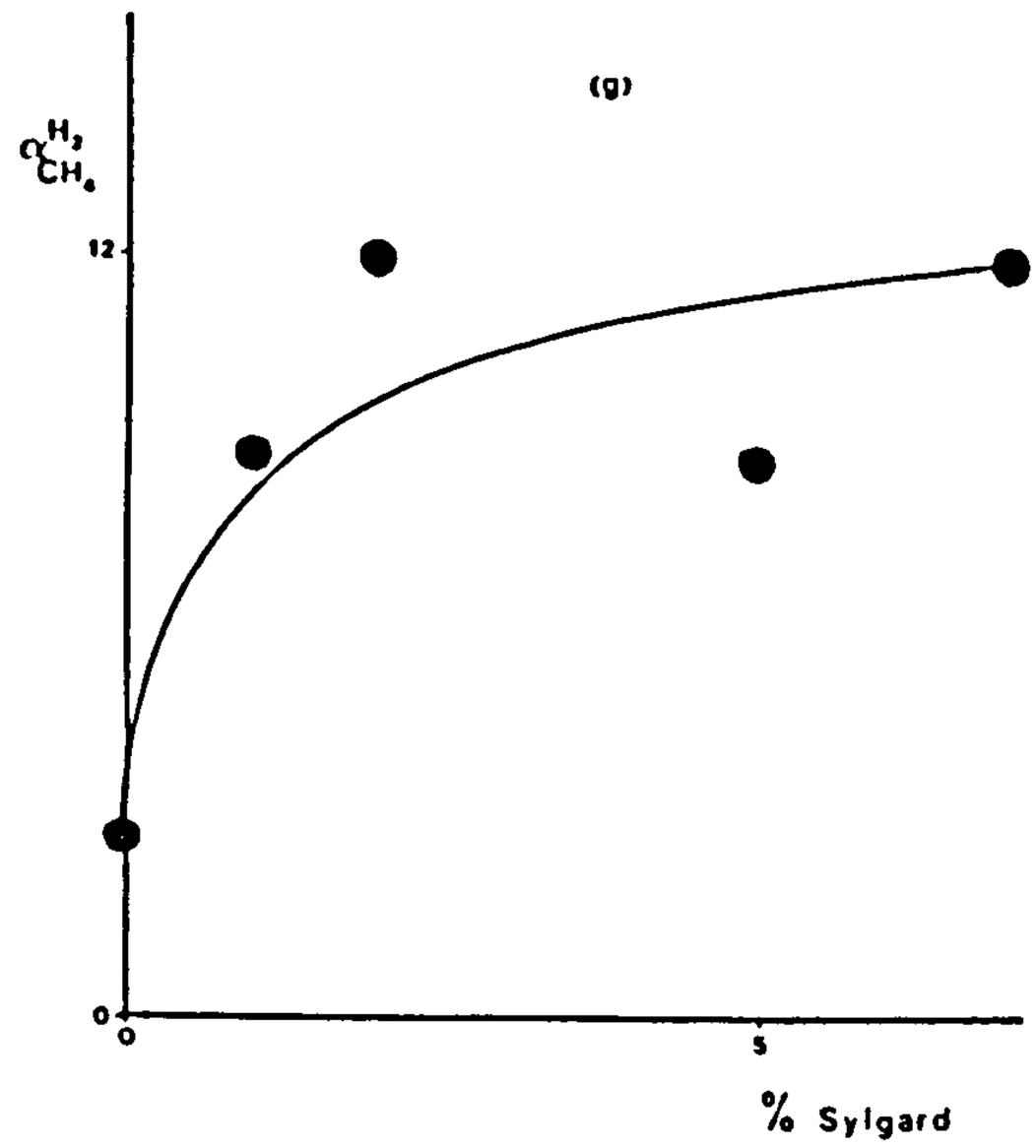

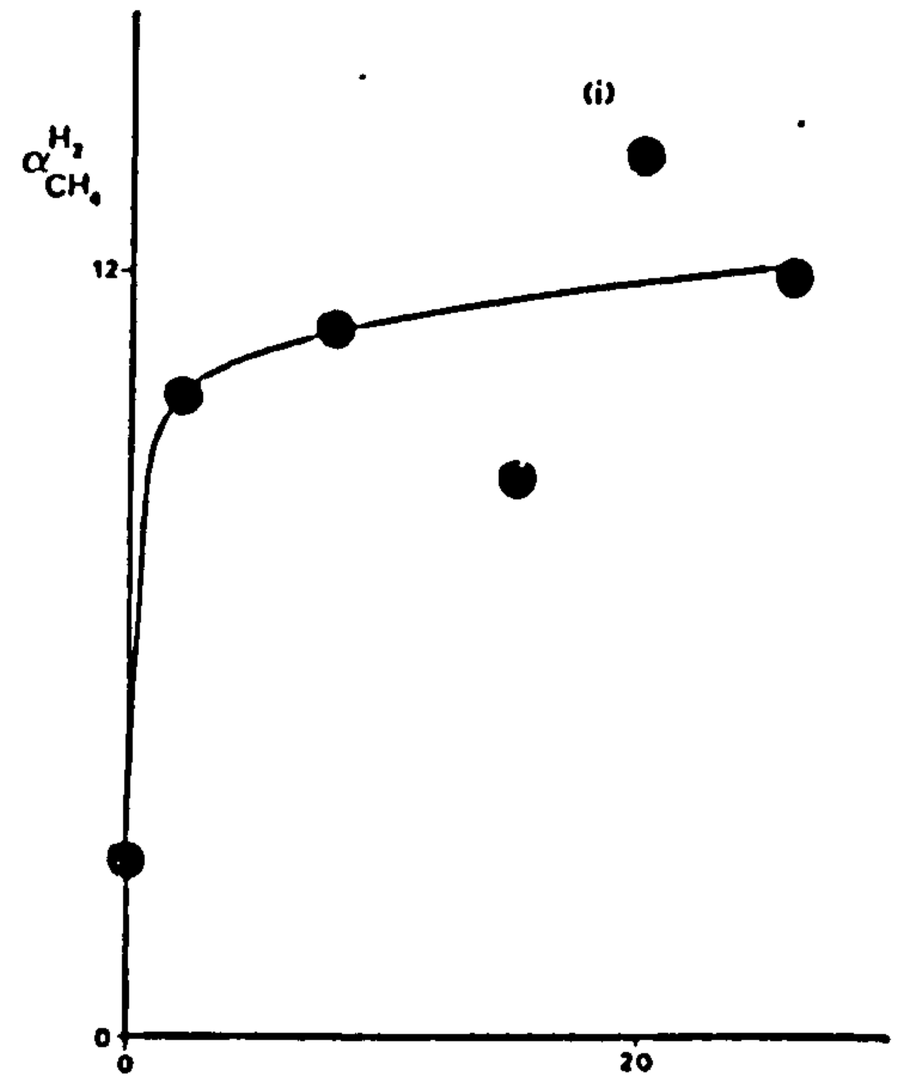

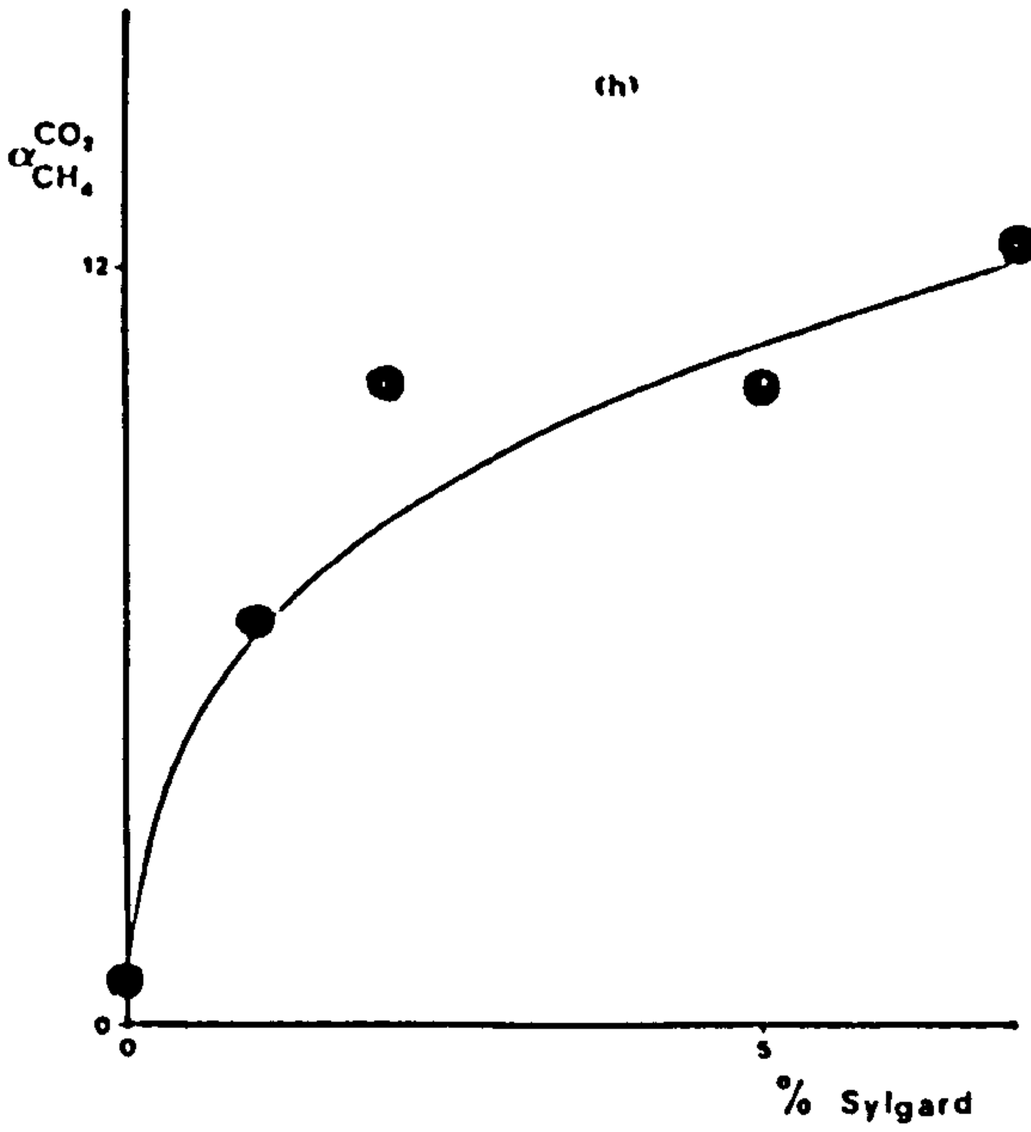

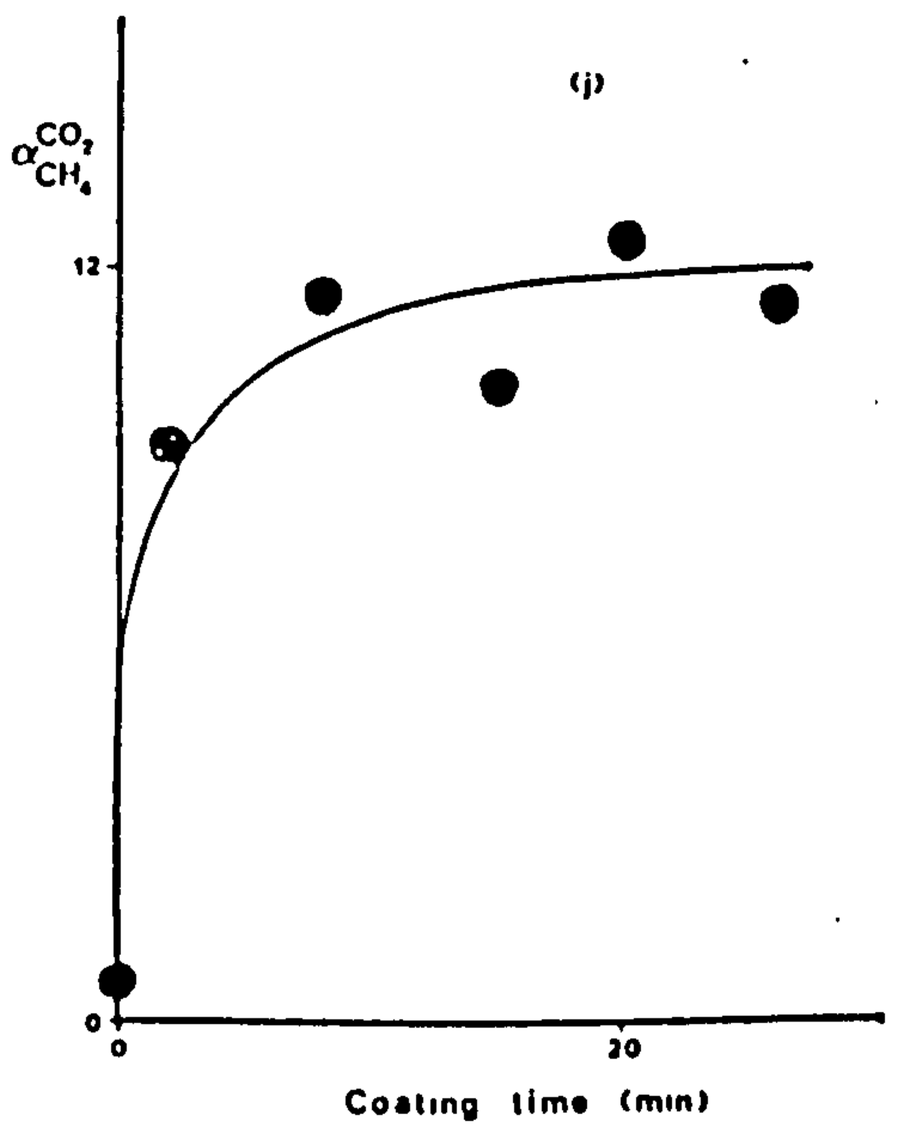

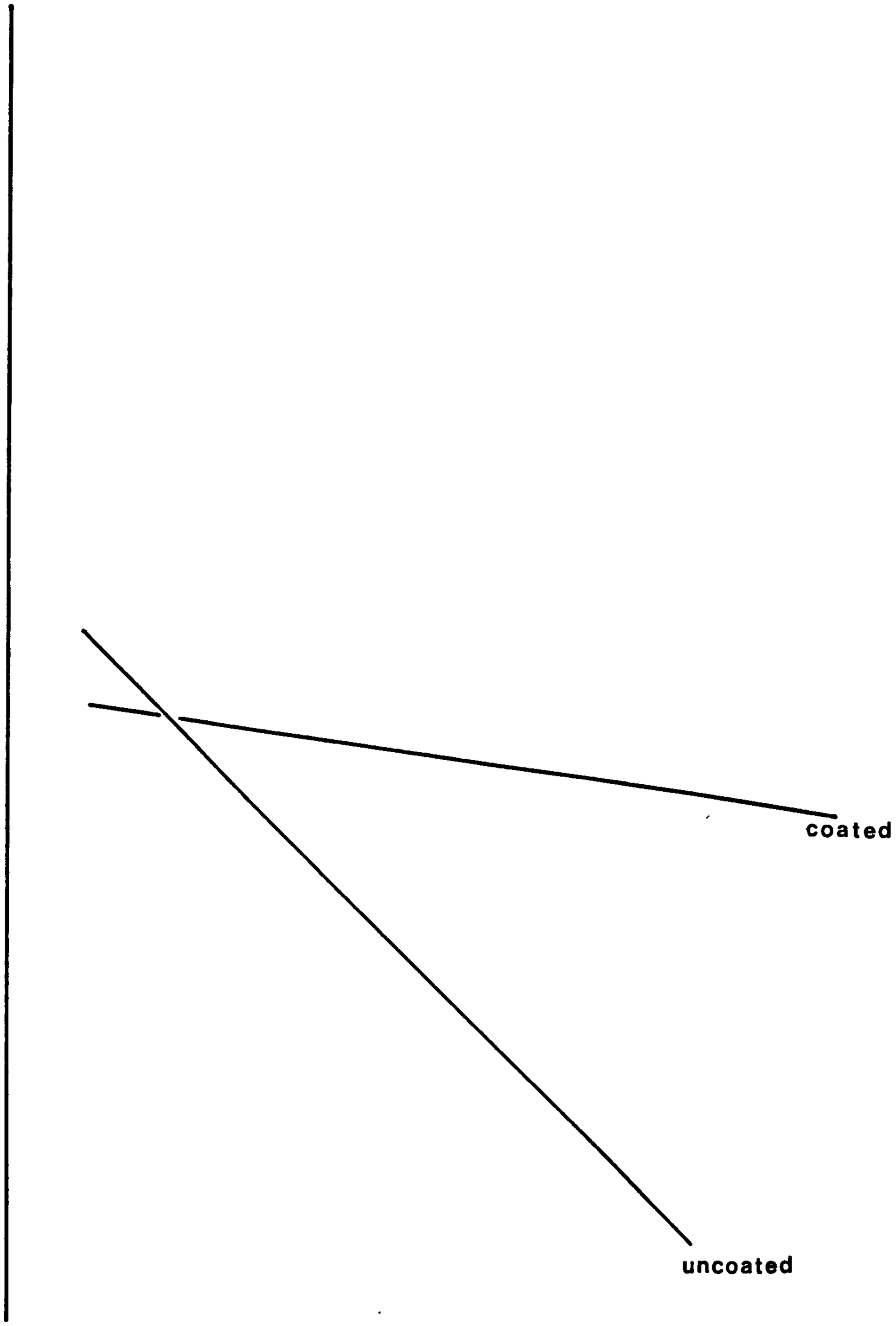
coated
uncoated

Fig 3.17 Effect of coating on H_2 / CH_4 performance.

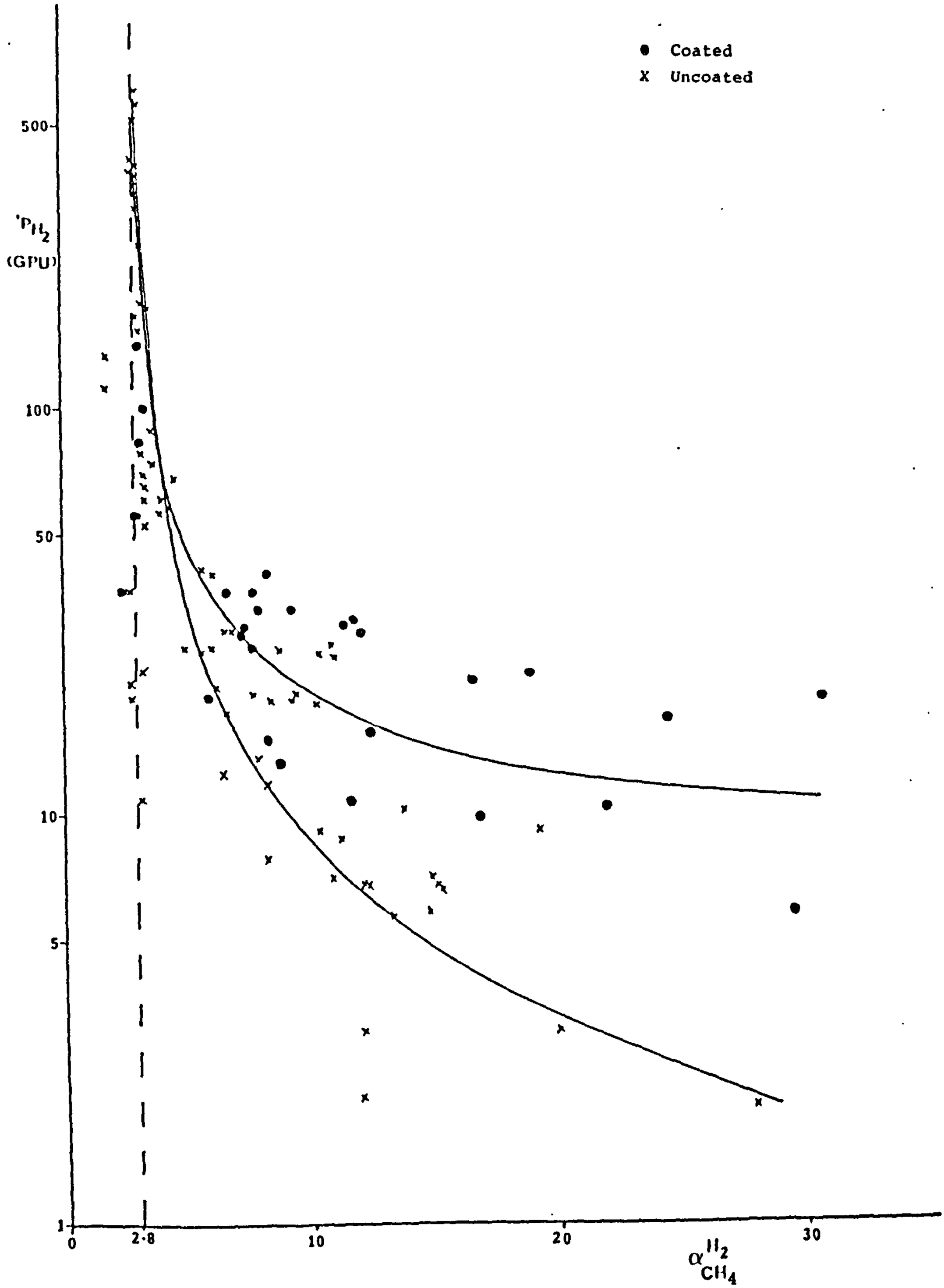

Fig 3.17 Effect of coating on H_2 / CH_4 performance.

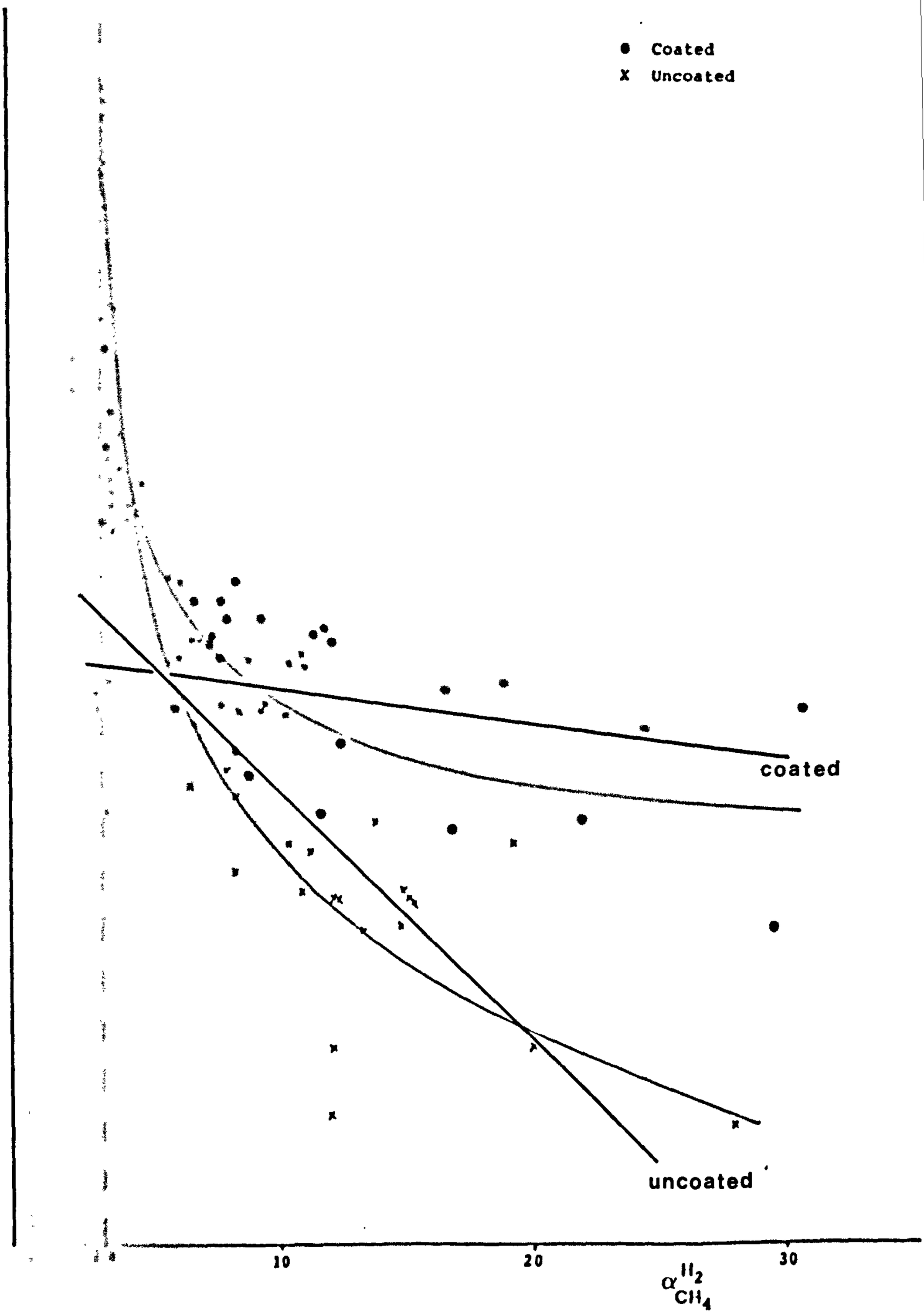

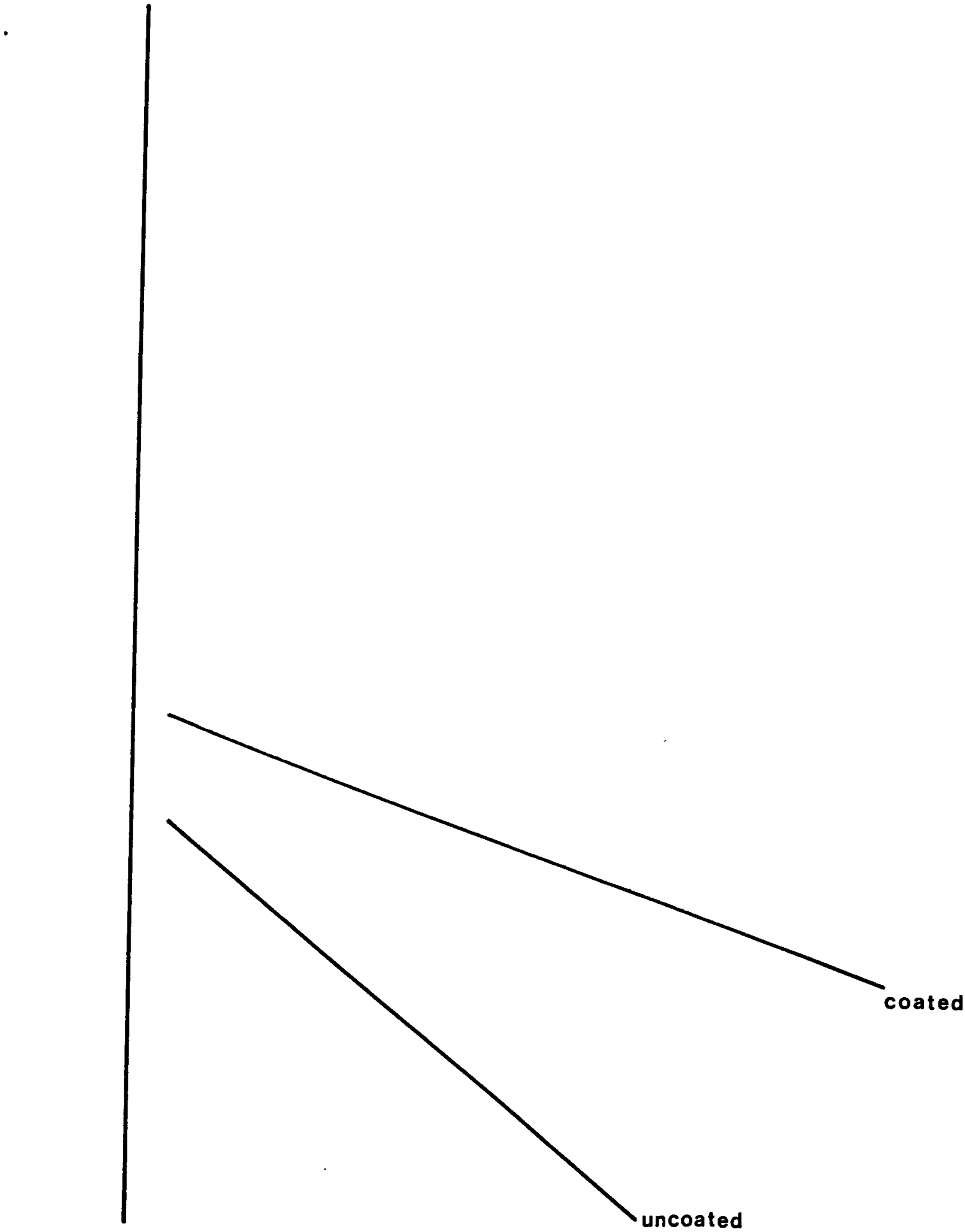
coated
uncoated

Fig 3.18 Effect of coating on CO_2 / CH_4 performance.

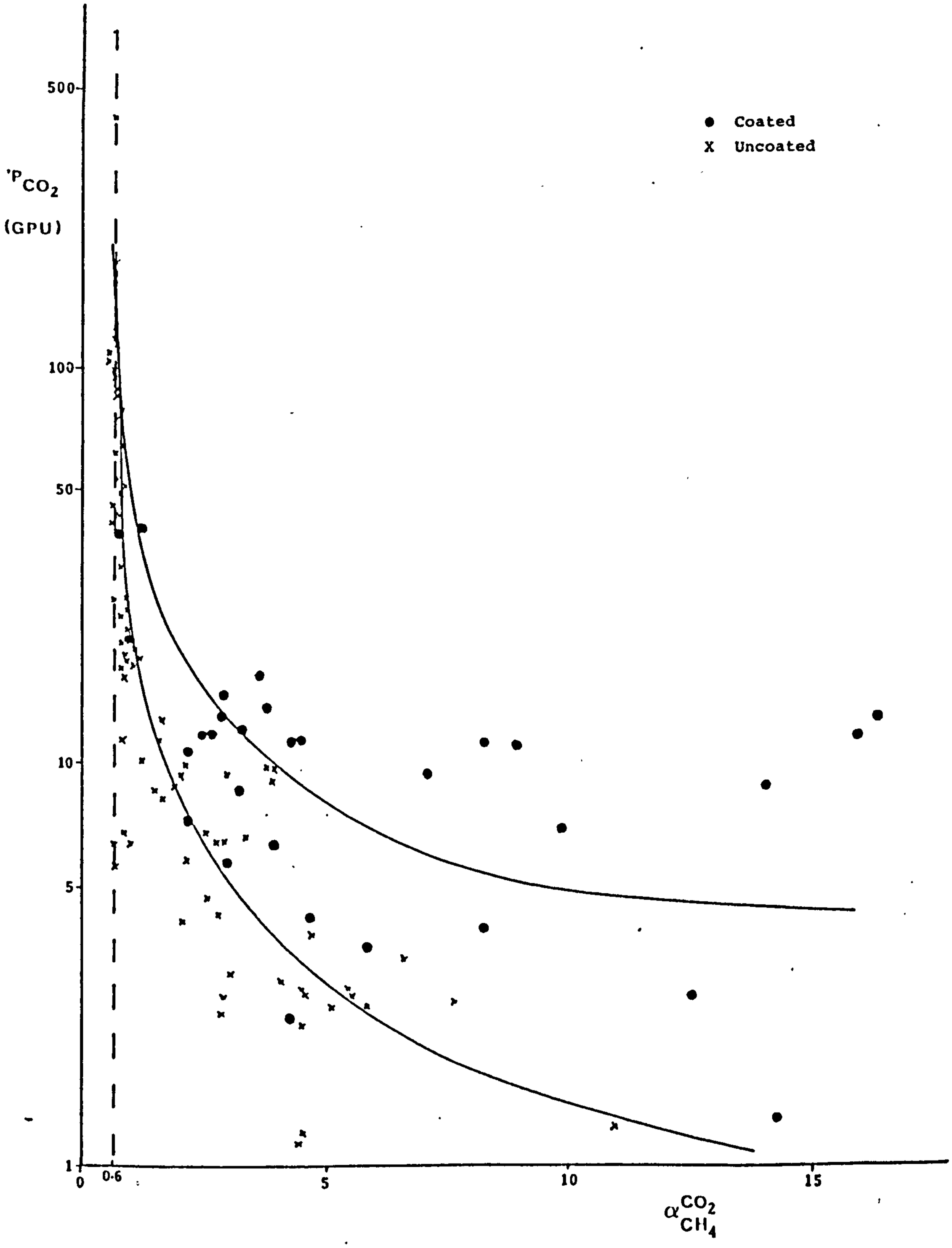

Fig 3.18 Effect of coating on CO_2 / CH_4 performance.

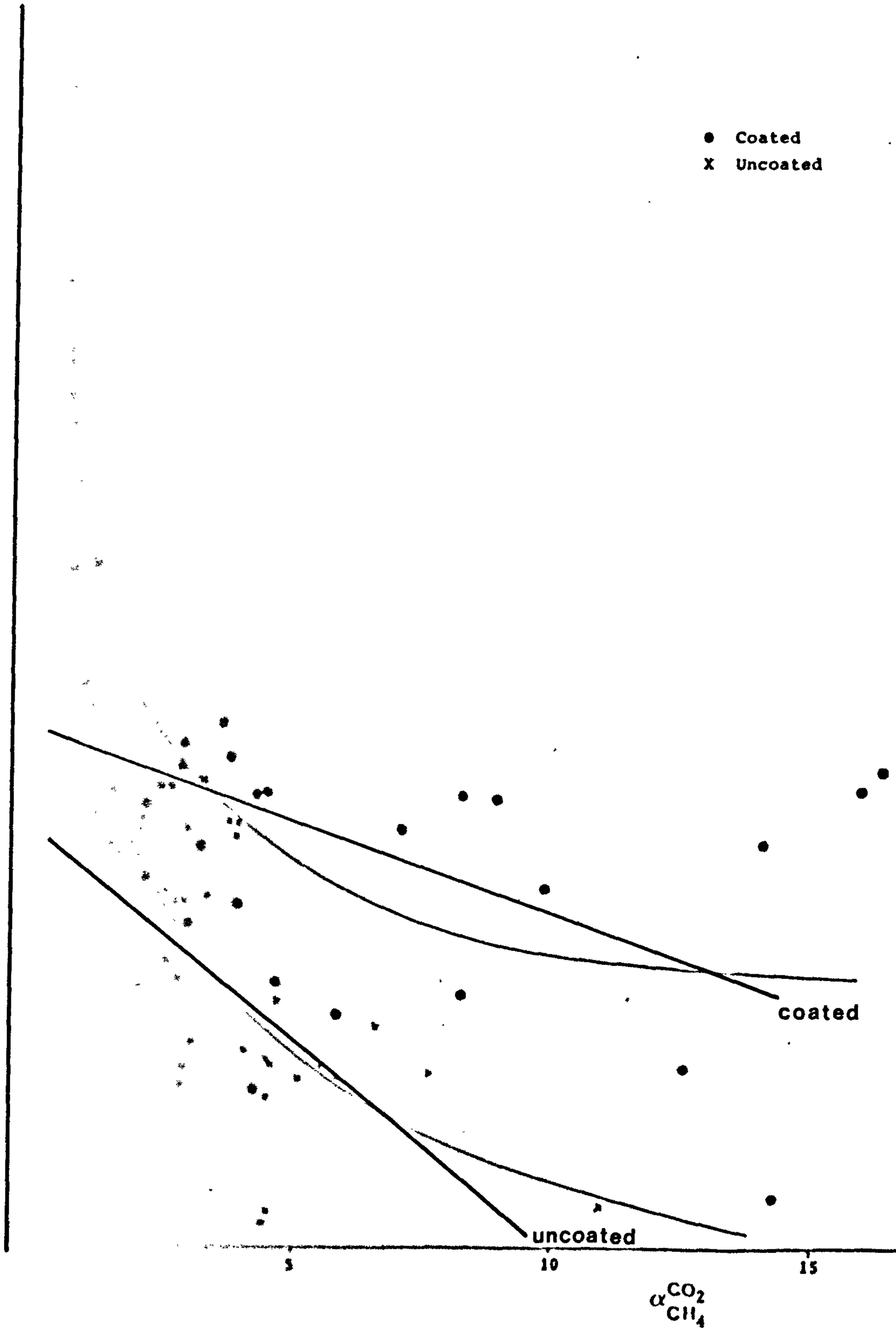

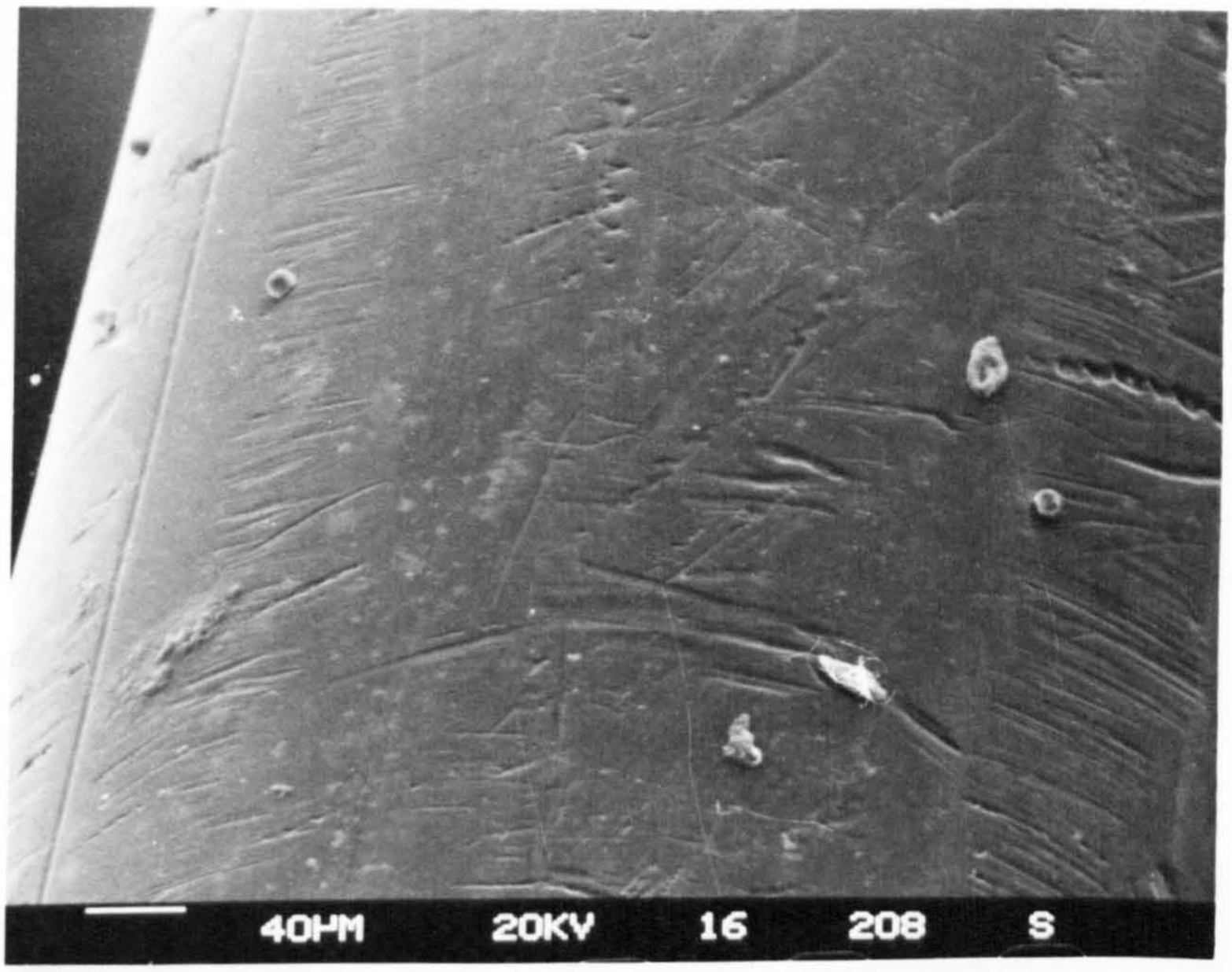

Plate 3.23 Typical hollow fibre outer surface before coating.

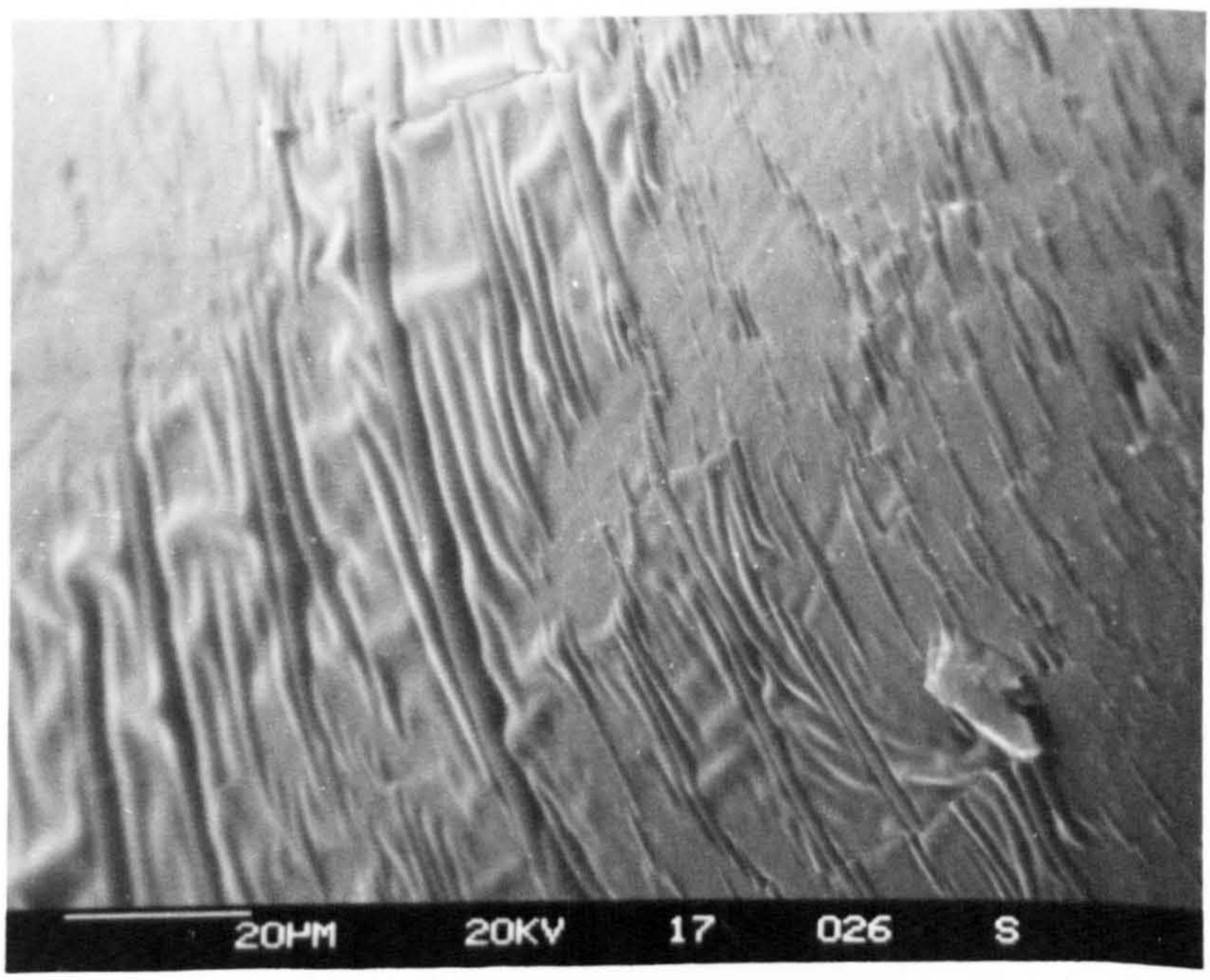

Plate 3.24 Typical hollow fibre outer surface after coating.

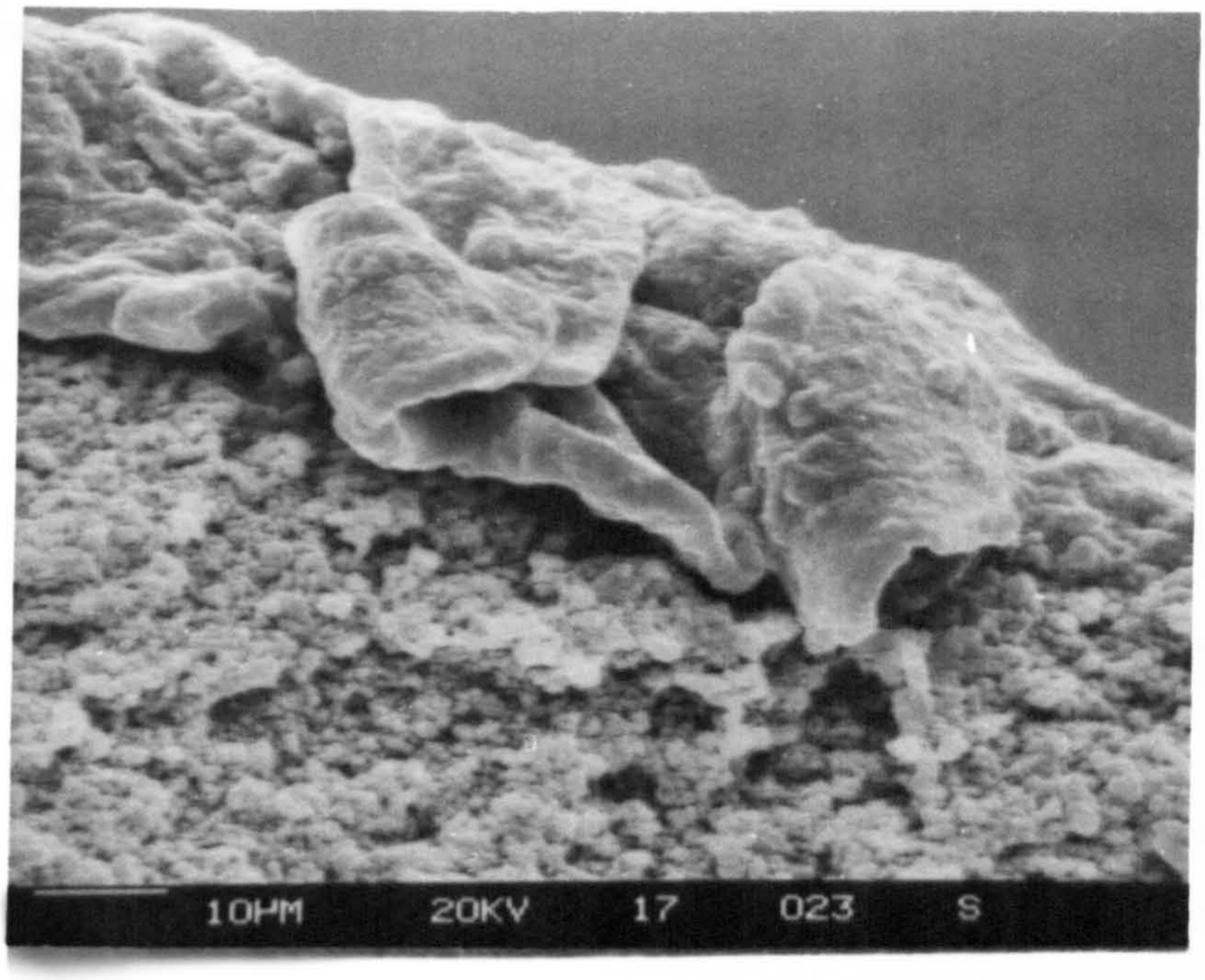

Plate 3.25 Cross-section of coated hollow fibre.

Figs 3.17 & 3.18 show the overall performance of the hollow fibre membranes spun from the DMAc type dopes. Both graphs show that the permeation rate constant increases with decreasing separation factor, until the limiting separation factor, attributed to separation by Knudsen diffusion, is reached. Additional best fit straight lines have been supplemented for the portion of the graphs where the points fall above the Knudsen value to demonstrate the improvement in performance of coated fibres over uncoated fibres. Although the correlation coefficients are not high the method does show that a considerable improvement in performance can be achieved by coating the modules which justifies the use of this dubious graphical procedure.

Plates 3.23 & 3.24 show the difference in appearance of the outer surface of a hollow fibre membrane before and after coating with 5% Sylgard 184 silicone elastomer. The presence of the silicone elastomer is easily observable. The elastomeric nature of the coating material can be seen to be important as the coating appears to be complete and no crazing or cracks were observed. The thickness of the coating cannot easily be determined. When the fibres are sectioned for examination under S.E.M. the elastic coating tends to shrink away from the fracture face. Plate 3.25, however, shows a section of fibre where a portion of the silicone film is lying across the fracture face. From this image it was estimated that the coating on a typical fibre would be less than 3 μm in thickness, except where the coating fills the surface defects.

A second coating material was investigated. The material chosen was a vinyl pyridine - styrene - butadiene copolymer latex. This material was chosen for its elastomeric nature, compatibility of application and most importantly, to incorporate the slightly basic vinyl pyridine. It was hoped that the basic character would influence the permeability of the membrane to carbon dioxide (an acidic gas).

However, as Table 3.14 shows, the application of the latex appeared to reduce the permeation rate constant of all permeating species by approximately 93.5%. No benefit was observed in the separation factors which remained at the level of Knudsen separation. It was assumed that the latex coating material merely built up on the surface of the fibres without filling and sealing the pores in the skin layer. This inability of the material to penetrate into the pores was attributed either to the poor wettability of the polysulphone to aqueous systems or to difficulties associated with the large size of the copolymer molecules in penetrating the surface pores. The advantage of the Sylgard 184 system is that it is post-cured.

Table 3.14 Effect of coating with vinylpyridine - styrene - butadiene latex.

Gas Transport Property.		Before Coating.	After Coating.
Permeation rate constant (GPU) :	Hydrogen	3840	257
	Methane	1460	95.2
	Carbon dioxide	1050	79.3
Separation factor :	Hydrogen / Methane	2.64	2.60
	Carbon dioxide / Methane	0.72	0.83

3.3.5 Effect of solvent system on gas transport properties.

From the observations on the morphology of 1-Fp:Fa type fibres it was predicted that due to the make-up of the outer skin layer the membranes would be highly permeable to penetrating gases. This was immediately evident when examining uncoated fibres of this type (Plates 3.18 and in comparison 3.19 & 3.20). Most modules exhibited permeation rate constants too high to record. Even after coating the fibres showed much higher permeation rate constants compared with DMAc type fibres. Figs. 3.19 & 3.20 show comparisons in performance between the 1-Fp:Fa and DMAc types of fibre. For both separations the overall performance of the 1-Fp:Fa type was considerably better than that of the DMAc type. The lower permeability of the DMAc type most likely results from the much thicker skins which form during the rapid precipitation in the phase inversion process. Another explanation for the lower permeability could lie in the general morphology of the membranes. Cabasso [47] states that macrovoids represent 'dead space' in permeation processes. The abundance of macrovoids in the DMAc system would tend to verify this statement. However, it seems likely that only macrovoids which are skinned (i.e. integrally sealed by polymer with no inter-connecting pores) act as dead space and that macrovoids with pores in their surface would decrease the tortuosity of the permeation pathways. The vast majority of macrovoids encountered in the DMAc type fibres had many pores in their boundary walls. Where macrovoids are non-interconnecting a decrease in the permeation rate might be expected. As the mean pore size of the DMAc type microvoids was observed to be less than that of the 1-Fp:Fa, it may be that the DMAc type fibres contain a larger proportion of non-interconnecting pores.

The separation factors of the two types of fibre mainly fall within the same range. However, a few of the DMAc type fibres exhibited much

higher separation factors (coupled with much lower permeation rate constants). These membranes having high separation factors were thought to have a much greater effective thickness either in terms of thick skin layers or in terms of non-interconnecting pores. Modules which produced these high values had almost no permeability to methane. At these low levels of permeation the possibility of error in the method of measurement increases (bubbles driven along the 1 ml flow meter may be subject to gas diffusion through its thickness resulting in lower values of the permeation rate constant being recorded). Further examination of Figs 3.19 & 3.20 suggests that in the case of the 1-Fp:Fa type fibres the traditional trade off between permeability and separation factor does not occur. Both graphs suggest a slight increase in the separation factor with increasing permeation rate constant. The reasons for this are unclear although conclusions should not be made hastily from scatter diagrams such as these, as the data represented often carry hidden trends (i.e. the results of batch 37/1, spun with varying W.I.R., manifest themselves very strongly in the scatter diagram). This may cause misleading interpretations to be made. One other consideration which might be of importance concerns the improvement in the ability of the spinner to produce a better quality hollow fibre membrane as experience is gained. As the majority of DMAc type fibres were spun before the 1-Fp:Fa type it is possible (although in the opinion of the author unlikely) that the 1-Fp:Fa fibres show better gas transport characteristics at least partially due to the improvement in spinning techniques.

The permeation rate constants of the fibres spun from the other solvent systems were not examined during the course of the research.

Fig 3.19 Effect of solvent on H_2 / CH_4 performance.

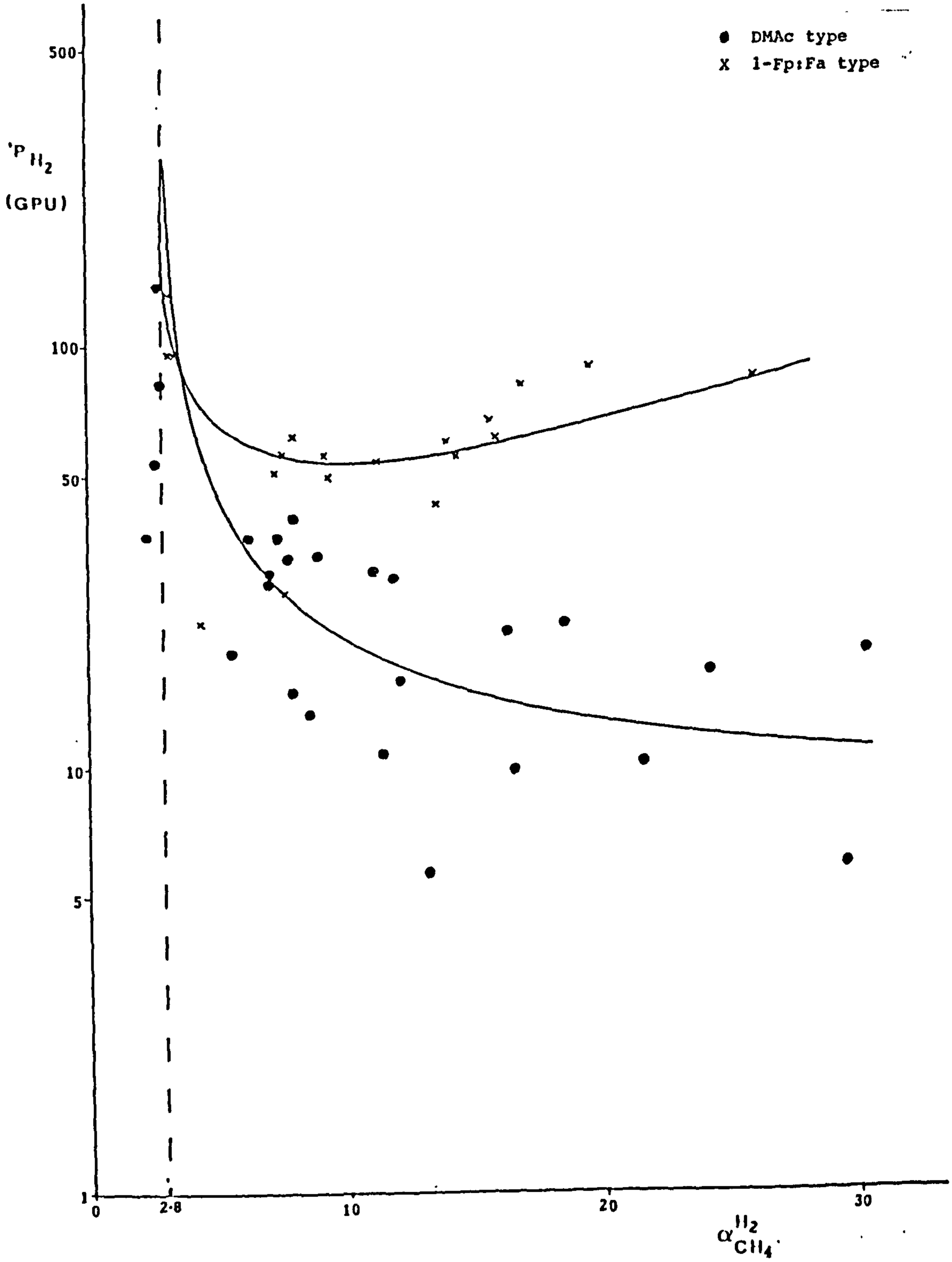

Fig 3.20 Effect of solvent on CO_2 / CH_4 performance.

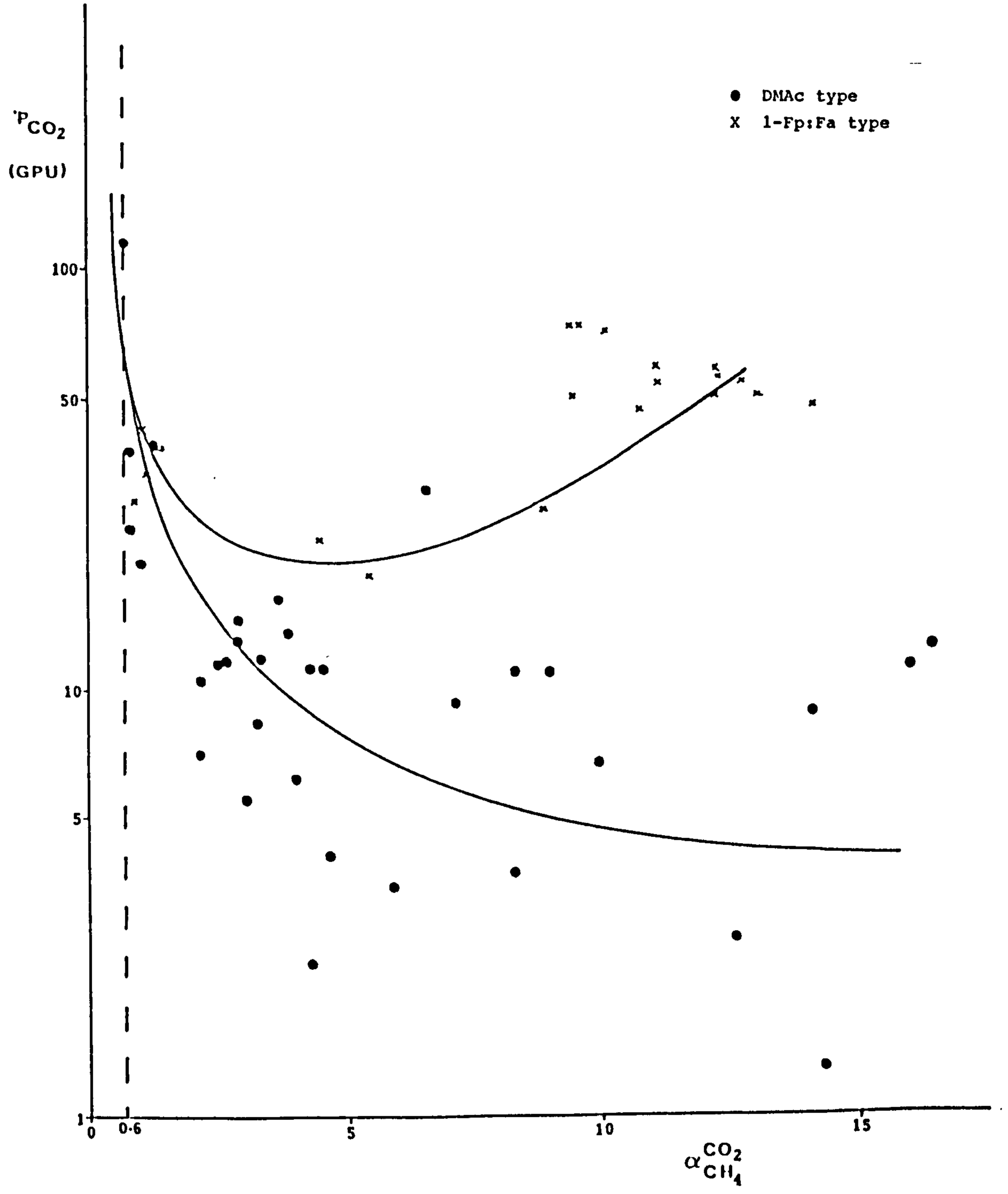

3.3.6 The effect of fibre dimensions on gas transport properties.

In the previous section the relationship between spinning parameters and fibre dimensions, in part, was established. The next logical step was to link up the relationships between the fibre dimensions and the gas transport properties. In the previous section the fibre dimensions were described in terms of the overall diameter and the diameter of the fibre lumen. It was thought likely that the wall thickness would be the principal fibre dimension of interest in this section as it represents, to some extent, the effective thickness of the membrane.

(a) Wall thickness (d_w).

With the levels of understanding established at the time of the experiments it was difficult to spin fibres having constant lumen dimensions whilst having a varying wall thickness. Two batches were produced toward this aim and they are shown, together with their gas transport behaviour in Table 3.15. Note that batch 43/1 was coated before testing whilst batch 21/2 was uncoated and shows typical separation values associated with a damaged surface skin layer.

Table 3.15 Effect of wall thickness on gas transport properties of hollow fibres.

Batch	d_w	d_i	$'P_i$ (GPU)			Separation Factor	
	μm	μm	H_2	CO_2	CH_4	H_2/CH_4	CO_2/CH_4
43/1n*	37	285	19.0	8.80	0.622	30.5	14.2
43/1m*	46	308	26.7	12.7	0.775	38.3	16.3
43/1p*	76	295	4.53	1.27	0.089	50.9	14.3
43/1q*	93	289	3.56	1.57	0.034	106	46.9
21/2c	65	330	59.1	17.5	15.2	3.9	1.15
21/2b	75	330	69.9	19.2	21.8	3.2	0.88
21/2a	95	330	53.0	16.5	17.7	3.0	0.93
21/2d	105	330	40.7	11.6	7.27	5.6	1.59

Table 3.16 Effect of wall thickness and lumen diameter on gas transport properties of hollow fibres.

Batch	d_f (μm)	d_i (μm)	d_w (μm)	$'P_i$ (GPU) H_2	CO_2	CH_4	Separation Factor H_2/CH_4	CO_2/CH_4
11/4a	558	265	147	25.6	7.87	4.92	5.2	1.6
11/4g	575	310	133	26.1	8.33	5.55	4.7	1.5
11/4b	621	365	128	28.4	9.04	4.30	6.6	2.1
11/4c	651	440	106	56.3	17.7	16.1	3.5	1.1
11/4d	719	510	105	155	44.3	55.4	2.8	0.8
37/1d*	525	157	184	22.7	23.5	5.19	4.38	4.53
37/1c*	562	191	186	34.8	23.5	3.30	10.7	7.21
37/1e*	495	227	134	87.2	55.7	4.77	18.3	11.7
37/1f*	514	261	127	85.6	48.4	3.42	25.0	14.1

* denotes coated module.

Figs 3.21 and 3.22 show the relationship between wall thickness (d_w) and the permeation rate constant ($'P_i$) for two of the gases permeating through fibres of batch 43/1. The graphs show there is a general trend of a decrease in the permeation rate constants with increasing wall thickness. This was to be expected as the wall thickness is related to the amount of polymer through which the permeating gases must penetrate. However, the relationship is not of a straightforward inverse nature. The precise relationship is difficult to establish with the variable data collected. Fig 3.23 suggests that the relationship might be an inverse proportionality between wall thickness and the logarithmic function of the permeation rate constant, although the reasons for this correlation are as yet not understood.

Fig 3.21 Effect of wall thickness on $'P_{H_2}$ (constant d_i).

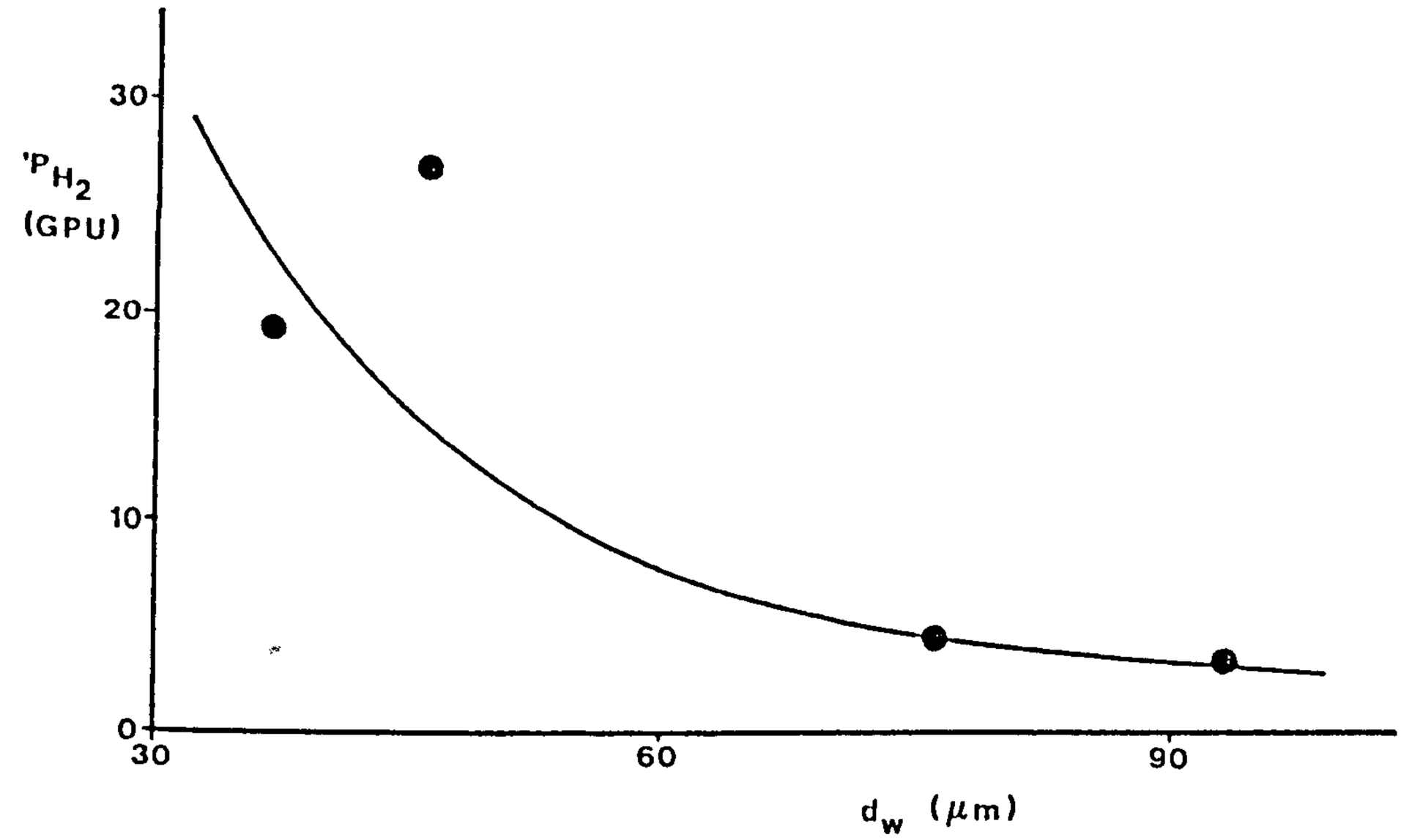

Fig 3.22 Effect of wall thickness on $'P_{CH_4}$ (constant d_i).

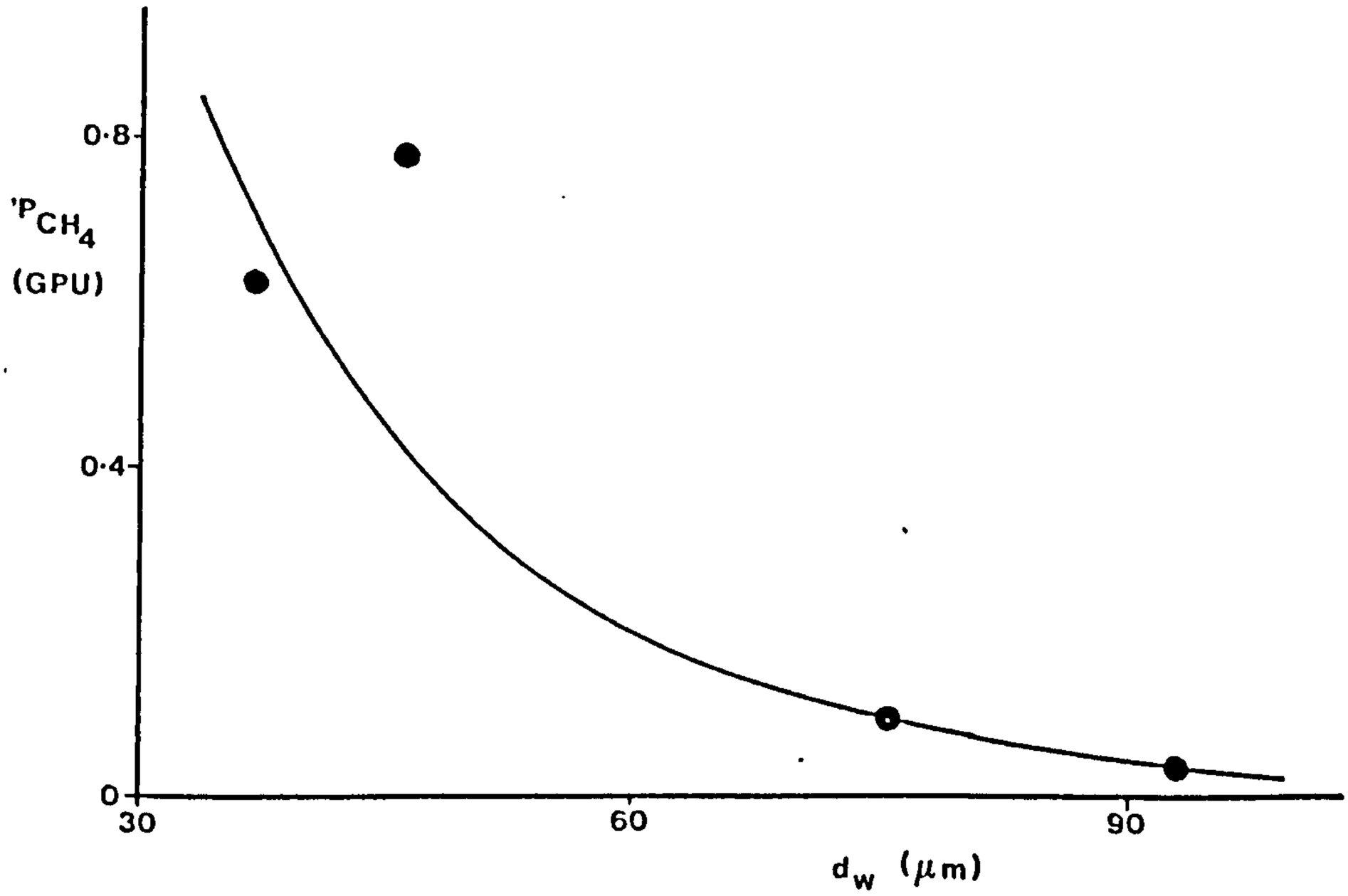

Fig 3.23 Correlation of wall thickness to $'P_{H_2}$.

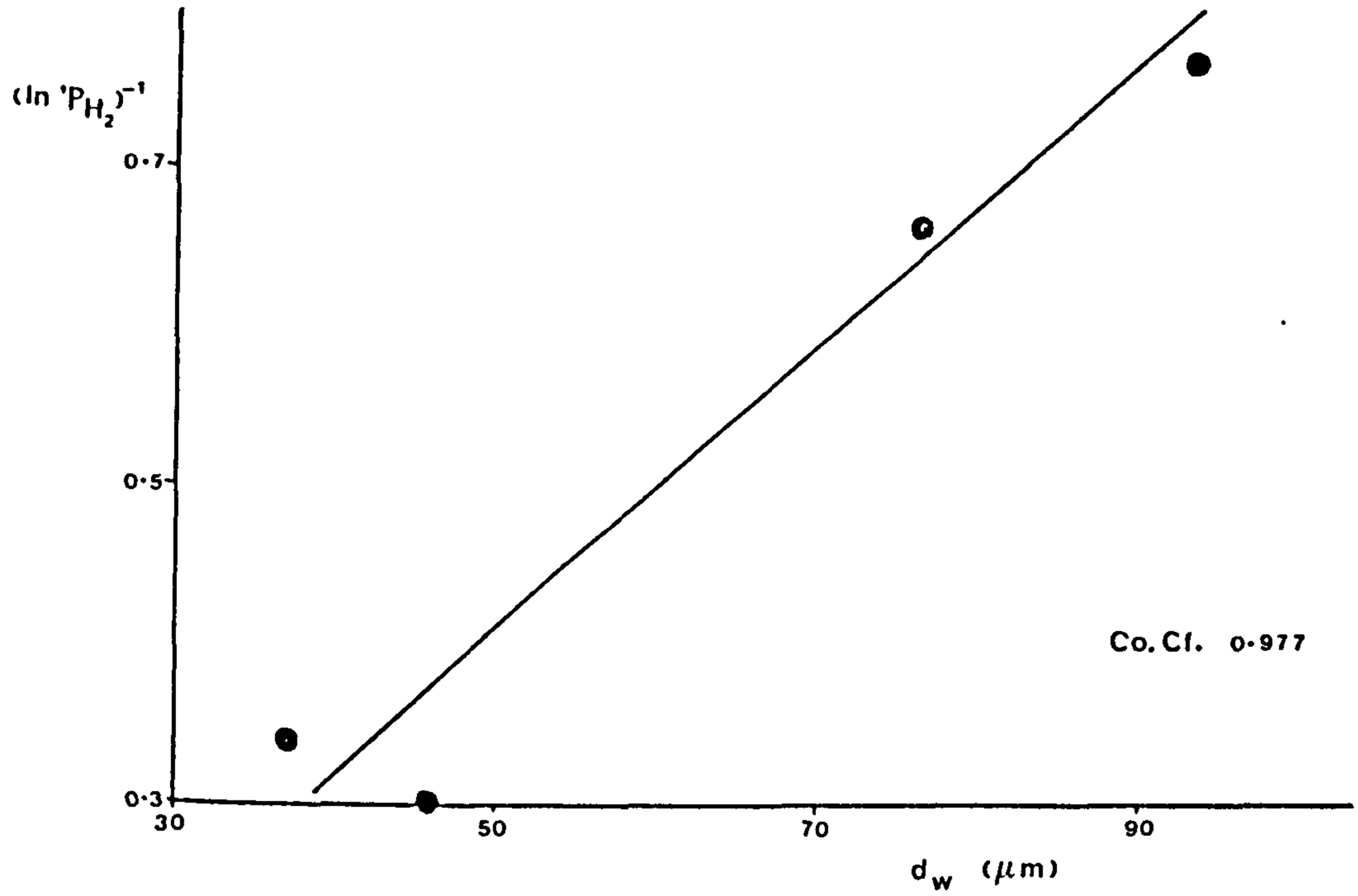

Fig 3.24 Effect of wall thickness on the separation factor.

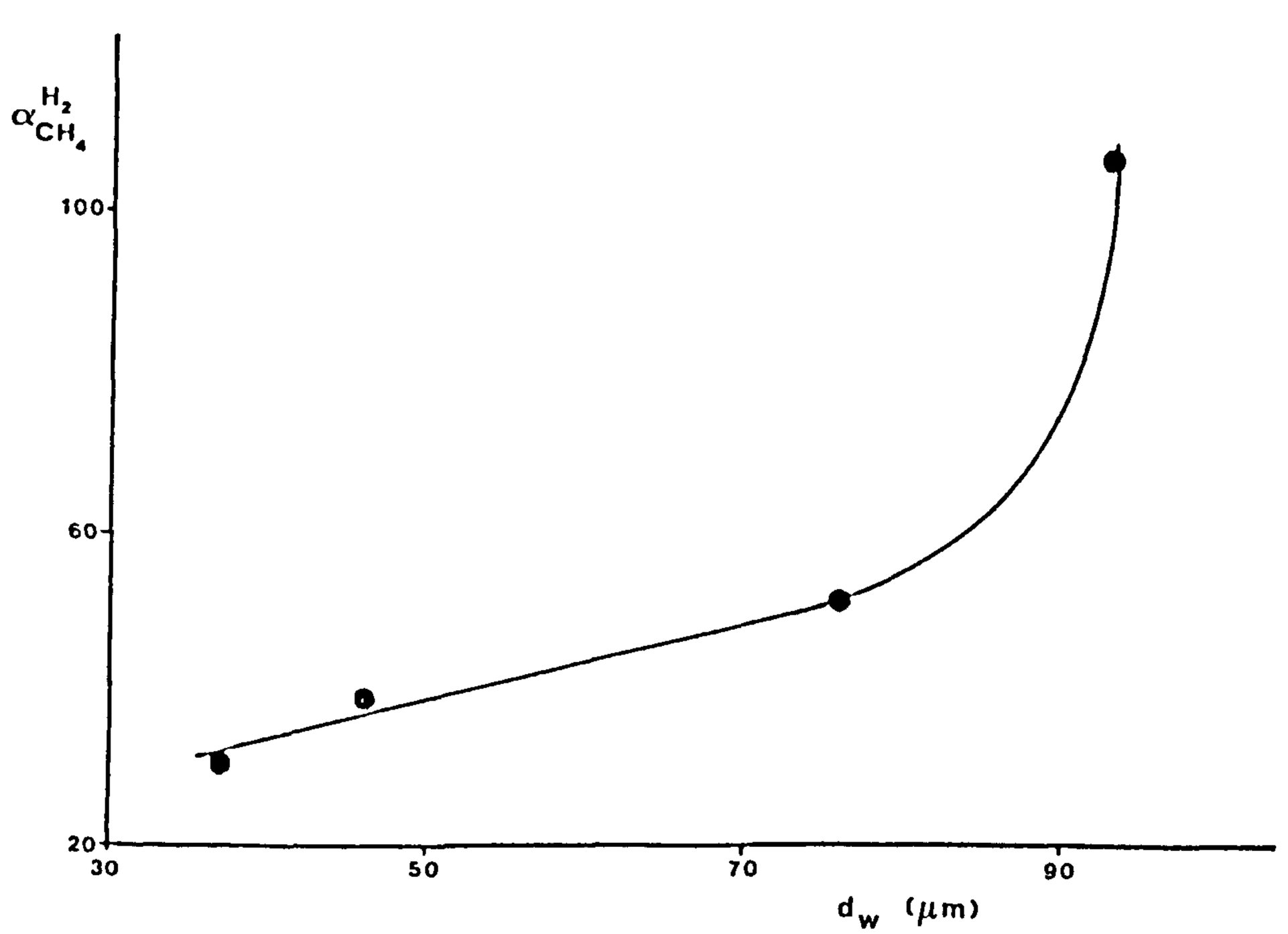

Fig 3.25 Effect of wall thickness on $'P_{H_2}$ (varying d_i).

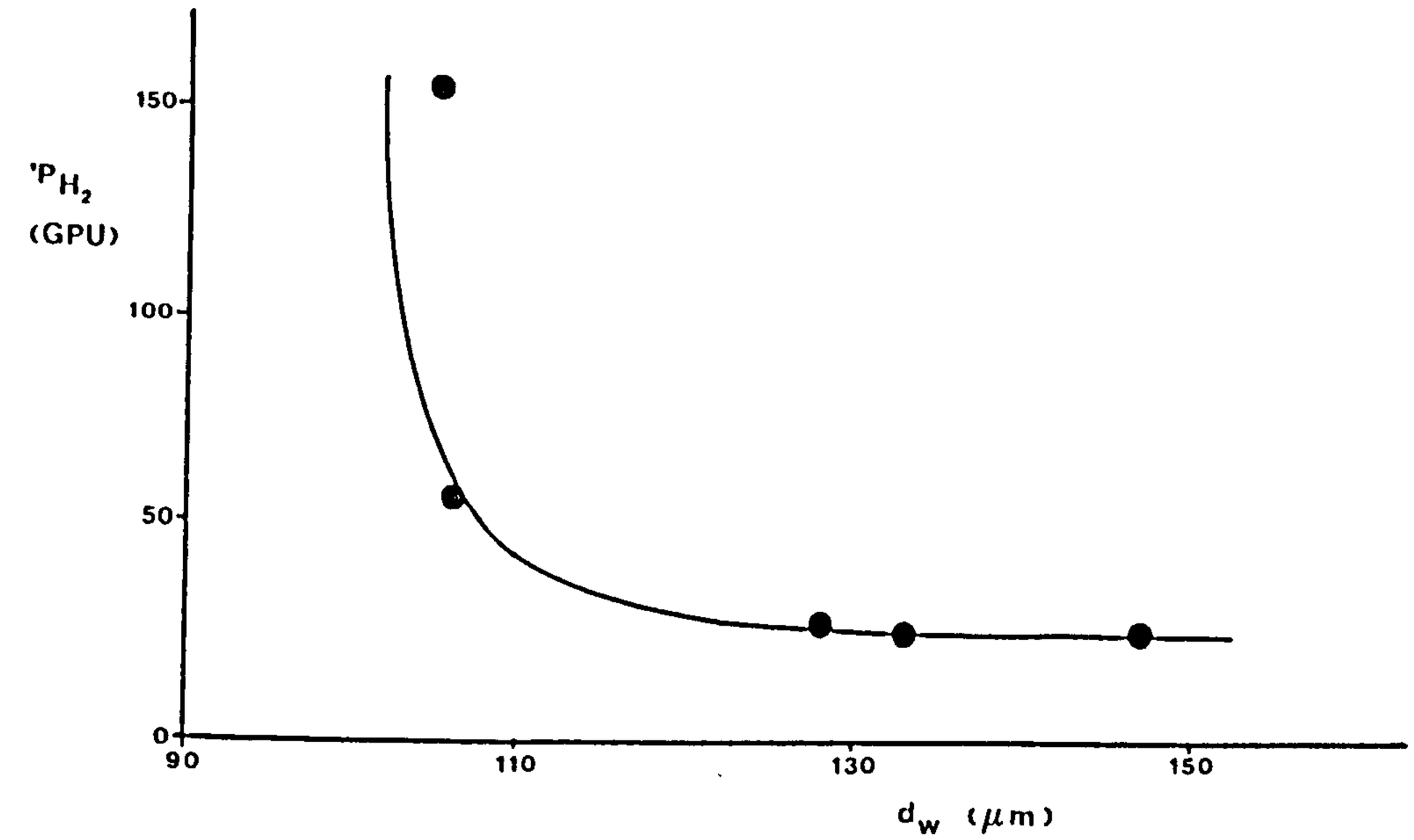

Fig 3.26 Effect of wall thickness on $(\ln'P_{H_2})^{-1}$ (varying d_i).

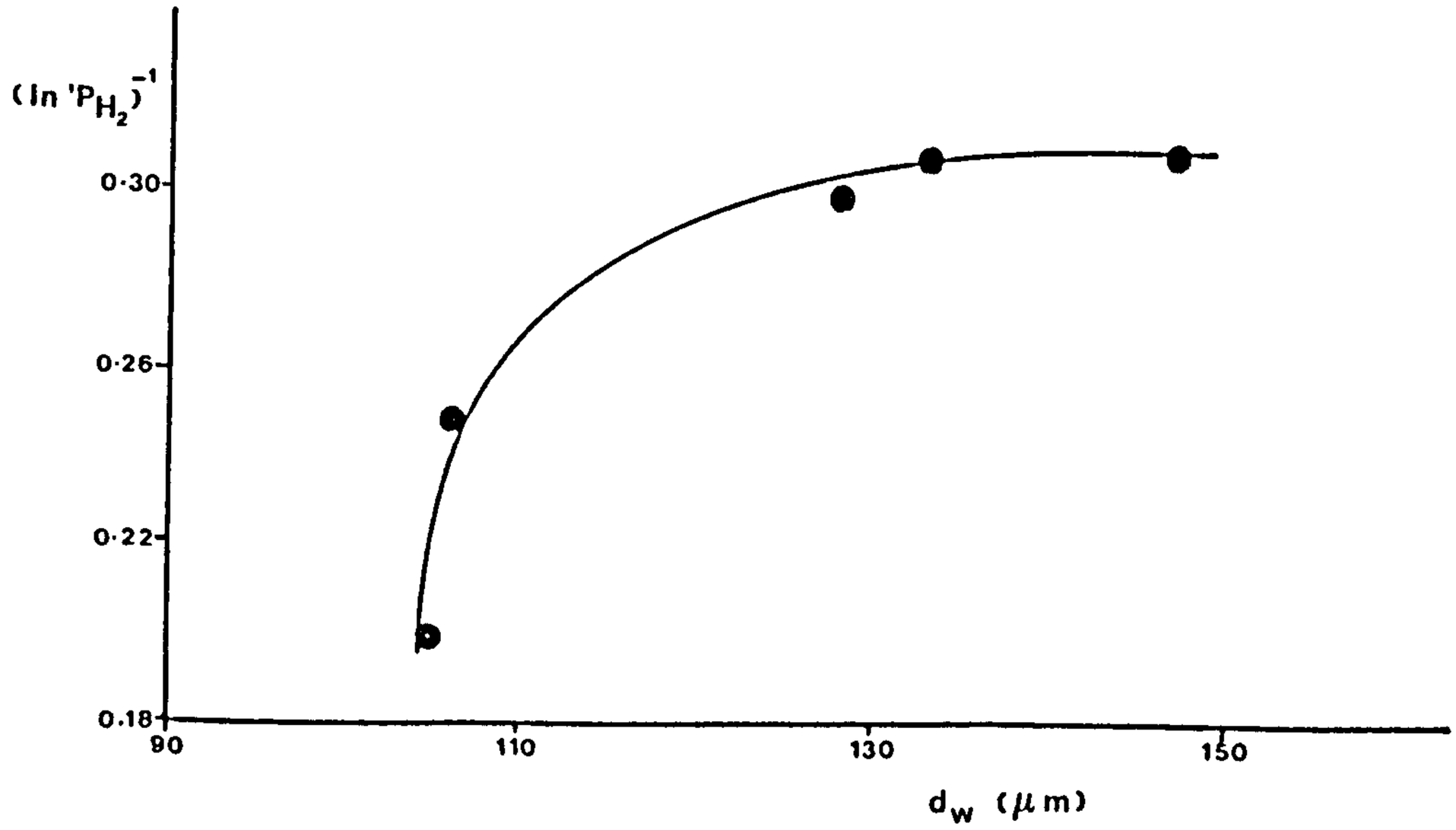

Table 3.15 also shows how the separation factors have been affected by an increase in the wall thickness. Increasing the wall thickness should lead to an improvement in the separation factors as the more polymer the permeating gas has to penetrate the more enhanced the effects of the solubility and diffusion coefficients become as the permeation process becomes more dependent on the solution diffusion mechanism. This was indeed found to be the case for batch 43/1 where a factor of three improvement in the separation factor was recorded. Fig 3.24 shows the relationship for batch 43/1. At first the rate of increase in separation factor appears to be linear followed by a large increase in the separation factor. This high value recorded must be treated with some caution, however, as the permeation rate of methane from which the it was derived was at a very low level, close to the minimum limit of measurement. In batch 21/2, however, the difference in separation factor was disappointing. The defects in the skin layer were such that pathways of low resistance were present in the membrane allowing the penetrating gases to bypass the areas of higher resistance.

(b) Diameter of fibre lumen (d_i).

No fibre batches were spun with constant wall thickness and varying lumen diameter. In order to achieve this two spinning parameters (P.E.R. and W.I.R.) would have to be adjusted such that as the lumen diameter increased the wall thickness was not allowed to decrease which occurs when only the W.I.R. is manipulated. At the time that the spinning runs were carried out, insufficient knowledge prevented a suitable batch of fibres from being spun. It is, however, possible to detect whether or not the lumen diameter has any effect by examining the relationship of wall thickness with the permeation rate constants for batches of fibres where the lumen diameter was not constant. If a graph was produced with a similar shaped slope to that obtained when examining

the effect of wall thickness at constant lumen diameter (i.e. Figs 3.21 & 3.23) then it would be fairly safe to assume that the lumen diameter had little effect (compared to wall thickness) on the permeation rate constants. Table 3.16 and Figs 3.25 and 3.26 examine this possibility for batch 11/4 (uncoated) and 37/1 (coated). Unfortunately batch 37/1 does not have a sufficient spread of values to allow determination of the relationship, but 11/4 shows clearly the decline in the permeation rate constant with increasing wall thickness. The shape of the graph in Figs 3.25 and especially 3.26 shows that the relationship is different from that shown in Figs 3.21 & 3.23. Therefore it is safe to assume that the lumen diameter does play an important role in determining a hollow fibre's gas permeability. It was thought that the internal diameter could perhaps affect the permeation rate constants where the lumen bore was sufficiently small to cause a build up of pressure within the lumen which would act against the feed pressure. Such internal pressure ought to be taken into account during the calculation of the permeation parameters; however, in the laboratory rig, the downstream pressure was measured a good distance from the fibre module, so that no accurate assessment of the internal pressure could be made. This would tend to cause a higher value of pressure difference to be recorded, resulting in a lower value of permeation rate constant to be calculated for the fibres of small bore dimensions.

It is interesting to note that the separation factors of the coated batch 37/1 increase with increasing lumen diameter (decreasing d_w) whilst the uncoated batch 11/4 shows the opposite trend. It is difficult to suggest a reason for this in terms of the internal diameter. In terms of wall thickness, it would be expected that the separation factor would increase with increasing wall thickness, especially for the coated fibres. However, this does not appear to be the case. Although the reason for this trend observed in 37/1 was not understood, it must be

assumed that within the fibres of spinning run 37/1 other factors besides the lumen diameter and wall thickness vary from batch to batch.

(c) Fibre dimeter (d_f).

Table 3.17 shows the gas transport properties of the fibre batches from three spinning runs. Also indicated is the fibre diameter of these fibres. In the majority of cases the permeation rate constants can be seen to fall with increasing fibre diameter. Fig 3.27 shows a typical variation of $'P_i$ with d_f.

Table 3.17 Effect of fibre diameter on gas transport properties of hollow fibres.

Batch	d_f	d_w	$'P_i$ (GPU)			Separation Factor	
	μm	μm	H_2	CO_2	CH_4	H_2/CH_4	CO_2/CH_4
43/1n*	360	37	19.0	8.80	0.622	30.5	14.2
43/1m*	400	46	26.7	12.7	0.775	38.3	16.3
43/1p*	447	76	4.53	1.27	0.089	50.9	14.3
43/1q*	474	93	3.56	1.57	0.034	106	46.9
21/2c	460	65	59.1	17.5	15.2	3.9	1.15
21/2b	485	75	69.9	19.2	21.8	3.2	0.88
21/2a	520	95	53.0	16.5	17.7	3.0	0.93
21/2d	540	105	40.7	11.6	7.27	5.6	1.59
11/3d	448	70	116	31.0	37.4	3.1	0.8
11/3c	512	90	41.5	12.3	7.69	5.4	1.6
11/4g	575	133	26.1	8.33	5.55	4.7	1.5
11/3a	674	150	13.7	4.58	1.76	7.8	2.6
11/3b	724	180	12.1	4.23	1.46	8.3	2.9

* denotes coated modules.

Close examination of the table shows that the differences in fibre diameter are largely due to differences in wall thickness and so it is hardly suprising that the permeation rate falls with increasing d_f as that trend was established earlier in connection with the effect of the

wall thickness. What is interesting, however, is that the permeation rate constant appears to be inversely proportional to the fibre diameter. Figs 3.28, 3.29 and 3.30 show that this is the case for all the gases tested on batch 11/3 and Figs 3.31 and 3.32 show that the relationship holds for the other batches as well. This appears to hold for both coated and uncoated fibres. This inverse relationship can be better interpreted if the inverse permeability function $('P_i)^{-1}$ is considered in terms of resistance to flow. Hence, the resistance to flow of permeating species is directly proportional to the fibre diameter. Why the fibre diameter shows this proportionality and the wall thickness shows the relationship through the logarithmic function is not clear since when d_i is constant the wall thickness is directly proportional to the fibre diameter, as:-

$$d_f = 2\,d_w + d_i \qquad (3.19)$$

Examination of the data from Table 3.16 shows that the fibres of batch 11/4 do not show the same relationship as those examined above. Fig 3.33 shows that a direct relationship was still observed, but the resistance to flow increased as the fibre diameter decreased. This observation was not understood. Batch 37/1 shows too much variability to draw any further conclusions.

The effect of d_f on the separation factors of the batches 11/3, 43/1 and 21/2 is also shown in Table 3.17. Although the data shows considerable variability there can be seen to be an a general increase in the separation factor with increasing fibre diameter. This, no doubt, correlates to the increase in wall thickness.

Fig 3.27 Effect of fibre diameter on $'P_{H_2}$.

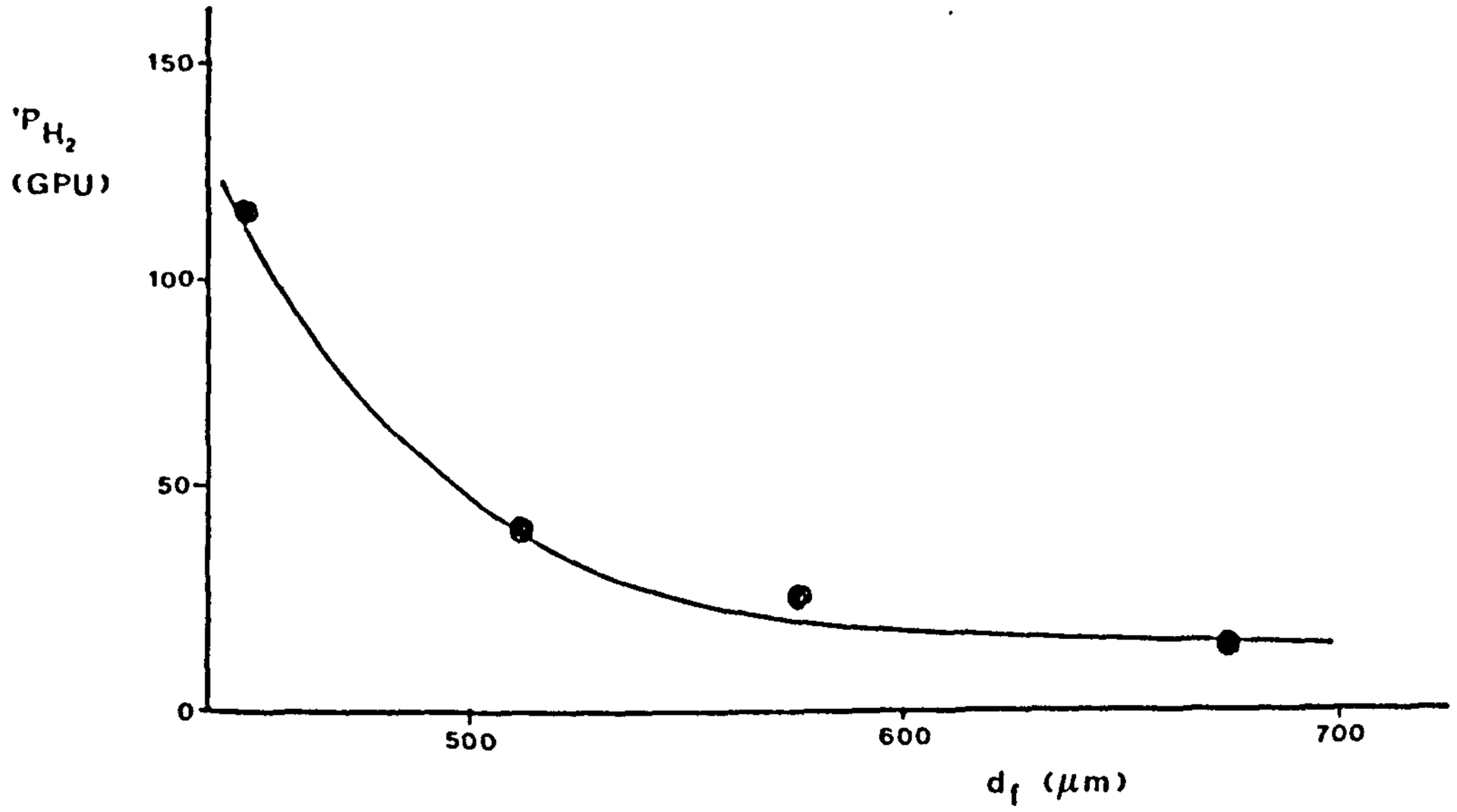

Fig 3.28 Effect of d_f on the resistance to flow of H_2 (Batch 11/3).

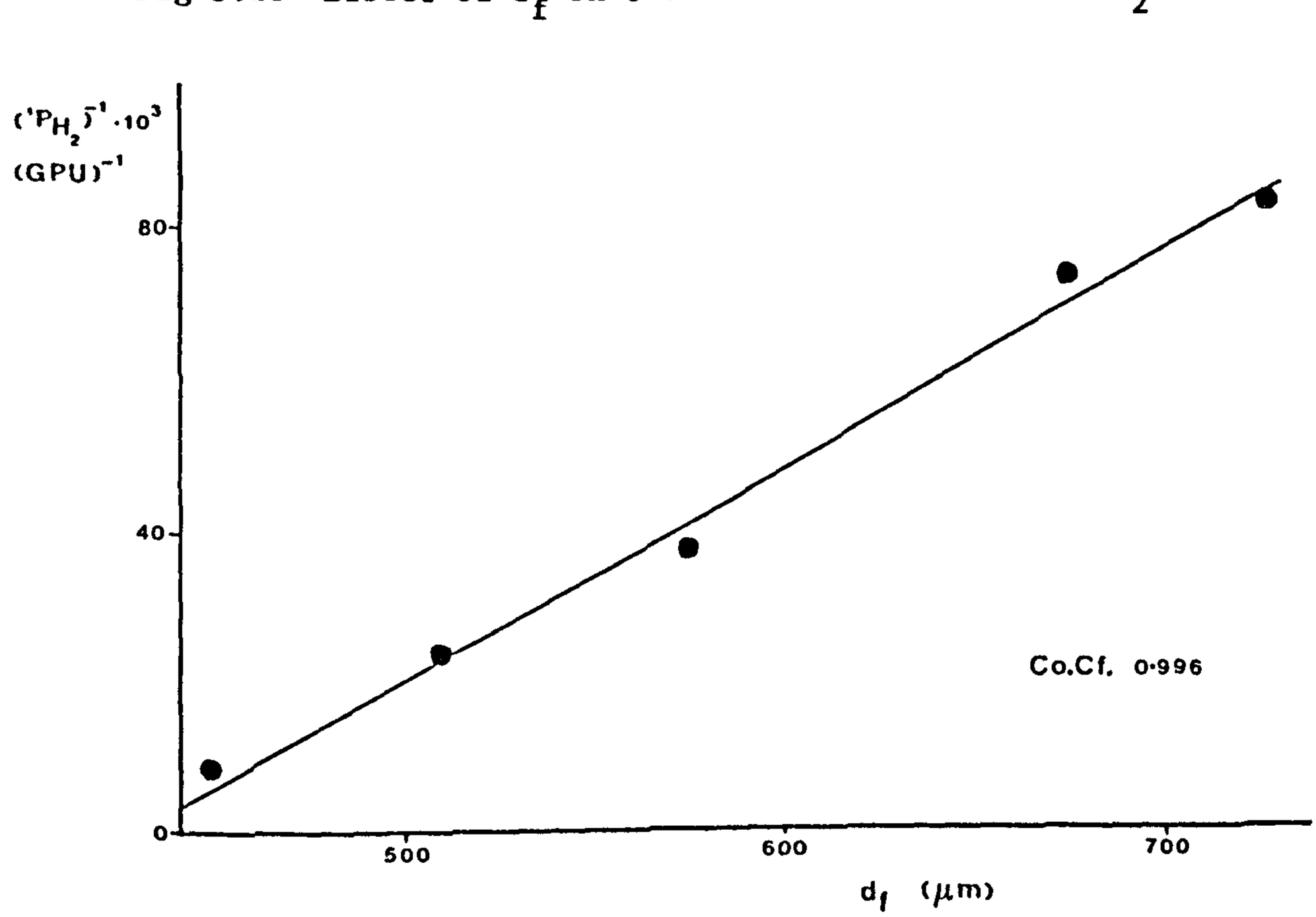

Fig 3.29 Effect of d_f on the resistance to flow of CO_2 (Batch 11/3).

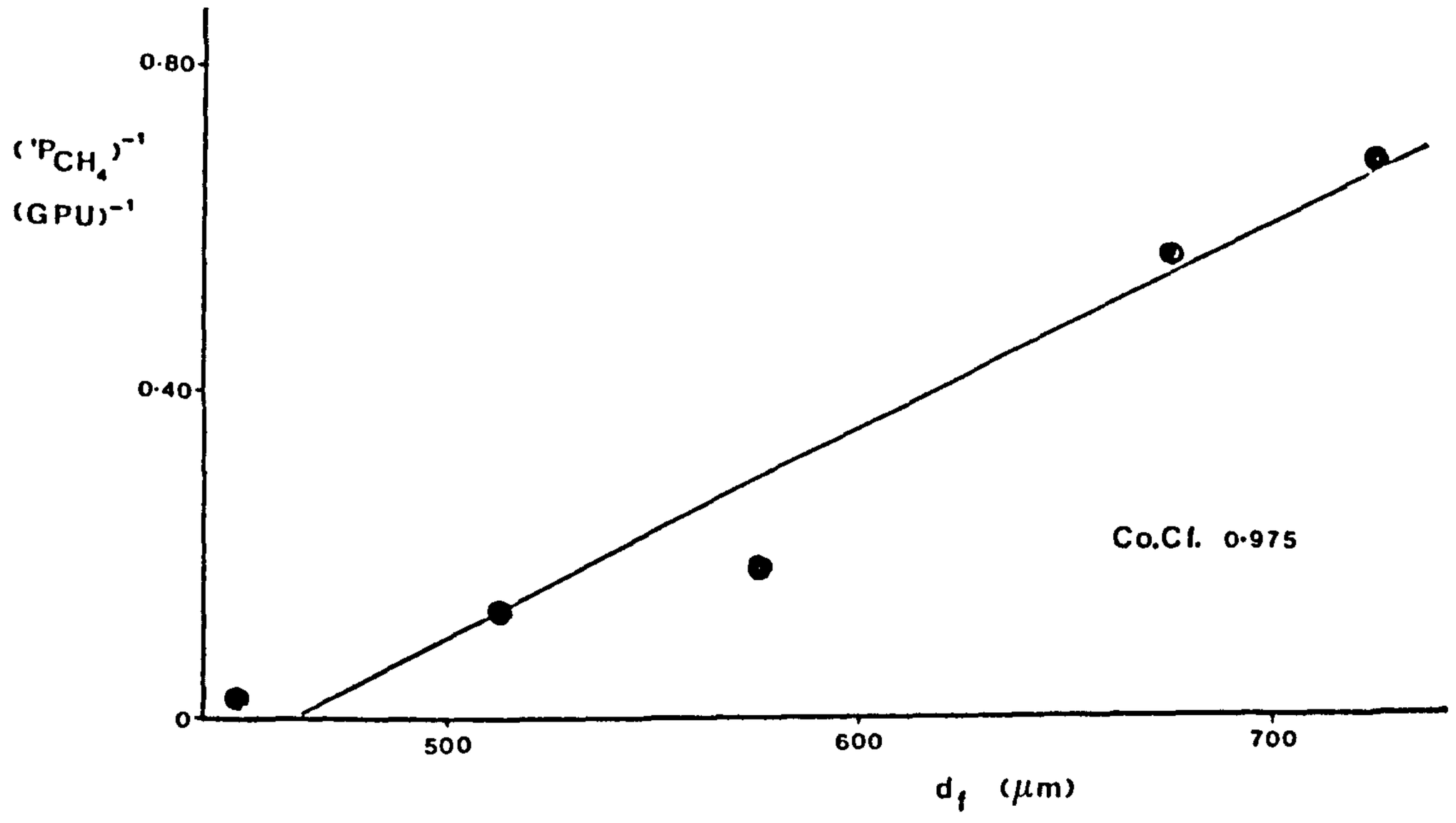

Fig 3.30 Effect of d_f on the resistance to flow of CH_4 (Batch 11/3).

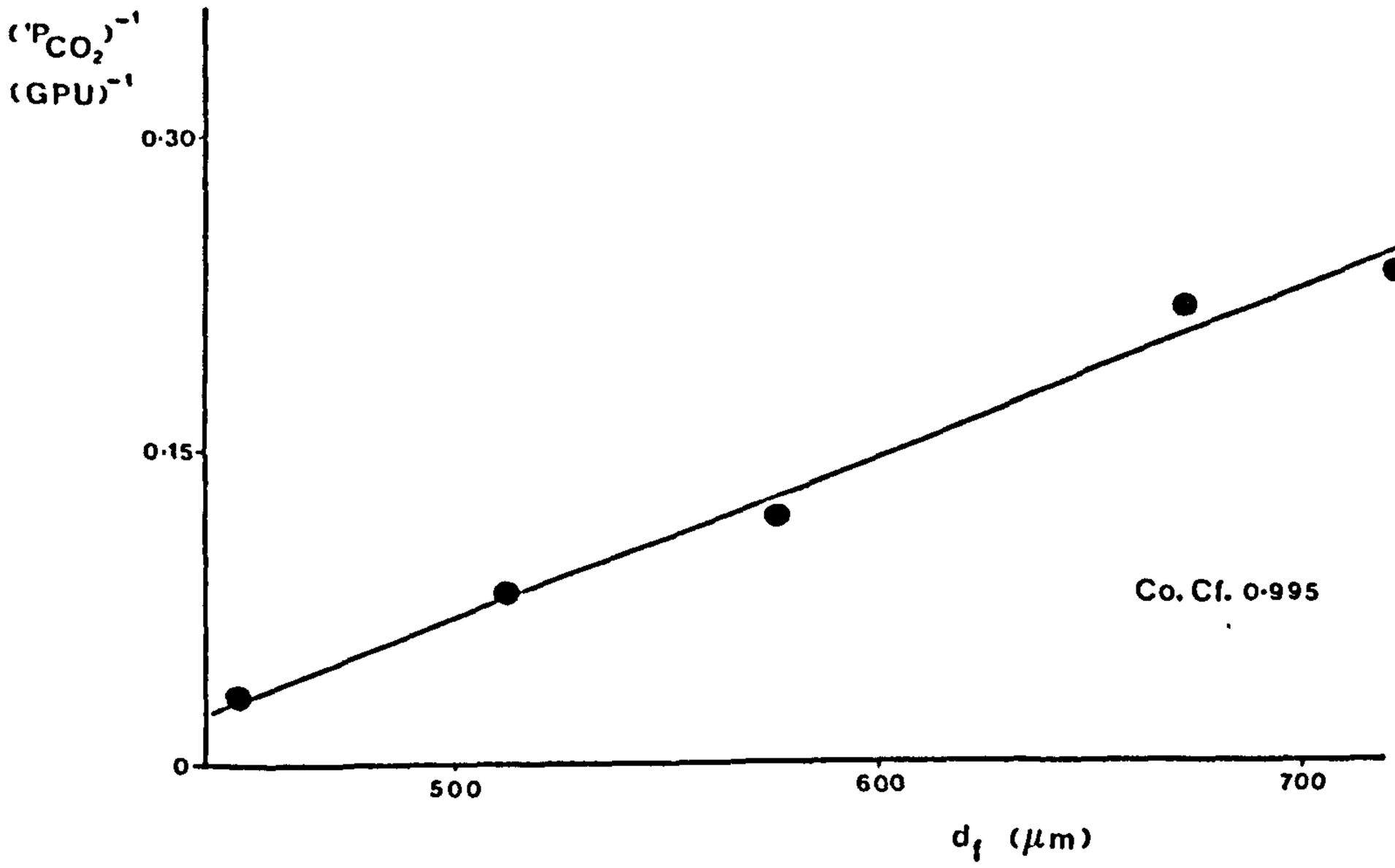

Fig 3.31 Effect of d_f on the resistance to flow of H_2 (Batch 43/1).

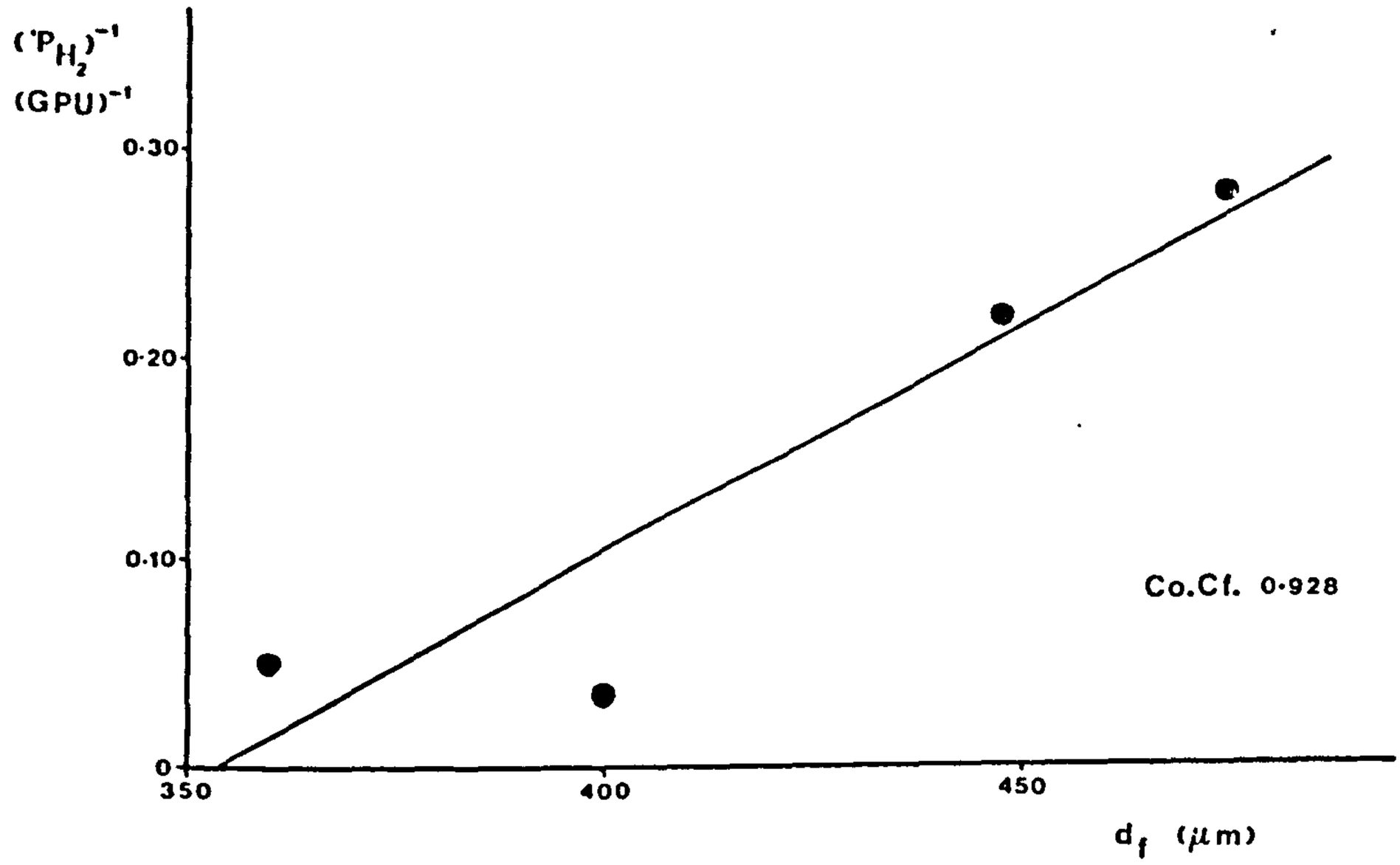

Fig 3.32 Effect of d_f on the resistance to flow of H_2 (Batch 21/2).

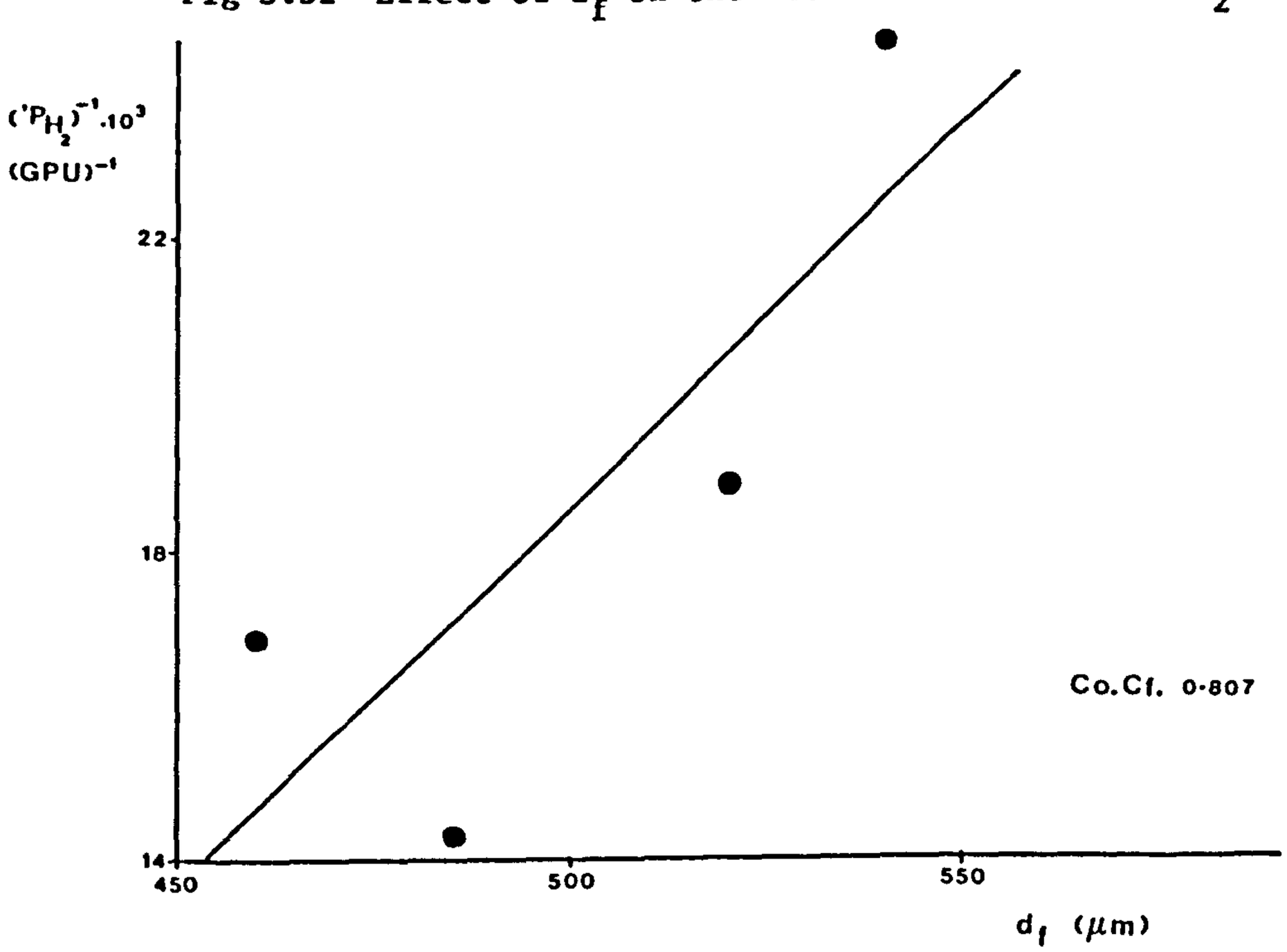

(d) Summary.

Only slight progress was made in linking the gas transport properties of membranes to their geometric dimensions. The inverse relationships between the permeation rate constants and the fibre diameter (and wall thickness) were the only real link in this direction. In future, however, with the knowledge developed in section 3.2, it should be possible to spin fibres suitable for this kind of analysis.

As the fibres produced in this research were designed to discover the influence of spinning parameters on various hollow fibre properties, the next subsection discusses the final link specified in Fig 3.4, i.e. the relationships between the spinning parameters and the gas transport properties of membranes spun using these parameters.

3.3.7 The effect of spinning parameters on gas transport properties.

The fibres produced in the spinning runs were for the most part constructed to produce data to enable analysis to be made of the effect of each spinning parameter individually. Thus this section attempts to correlate the spinning parameters to the gas transport properties.

(a) Polymer extrusion rate.

Fig 3.34 produced from Table 3.18 shows clearly that the permeation rate constants of gases rise with decreasing polymer extrusion rate (at constant WUS). This was, of course, expected as the decrease in the extrusion rate represents a decrease in the amount of polymer per unit length of fibre. Thus a fibre is formed with either thinner walls and/or greater void volume. In either case the resistance to flow will decrease (permeation rate constant will increase) with decreasing extrusion rate. From the previous analyses of behaviour (Sections 3.2.3

Fig 3.33 Effect of d_f on the resistance to flow of H_2 (Batch 11/4).

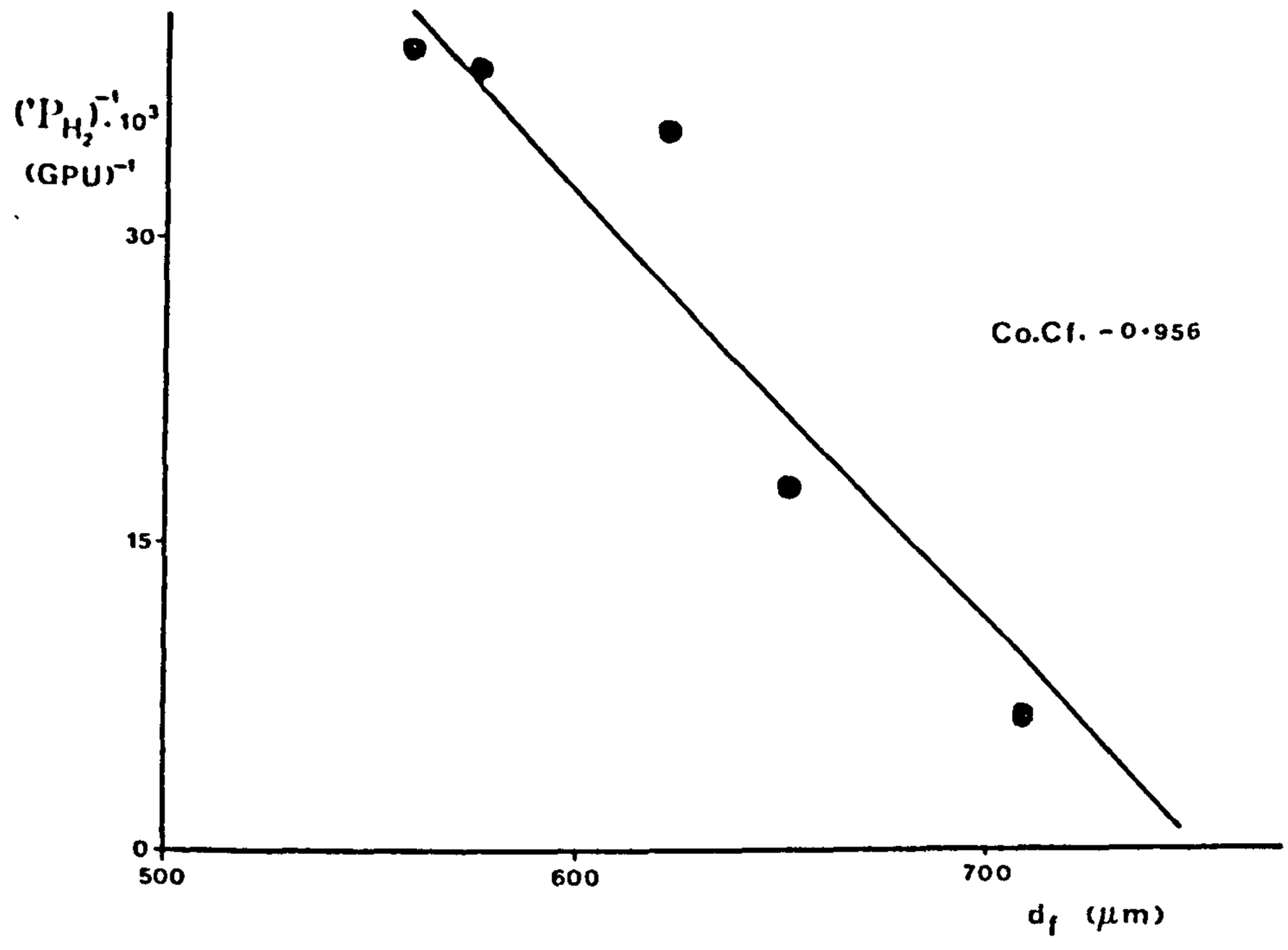

Fig 3.34 Effect of PER on $'P_{H_2}$ (Batch 11/3).

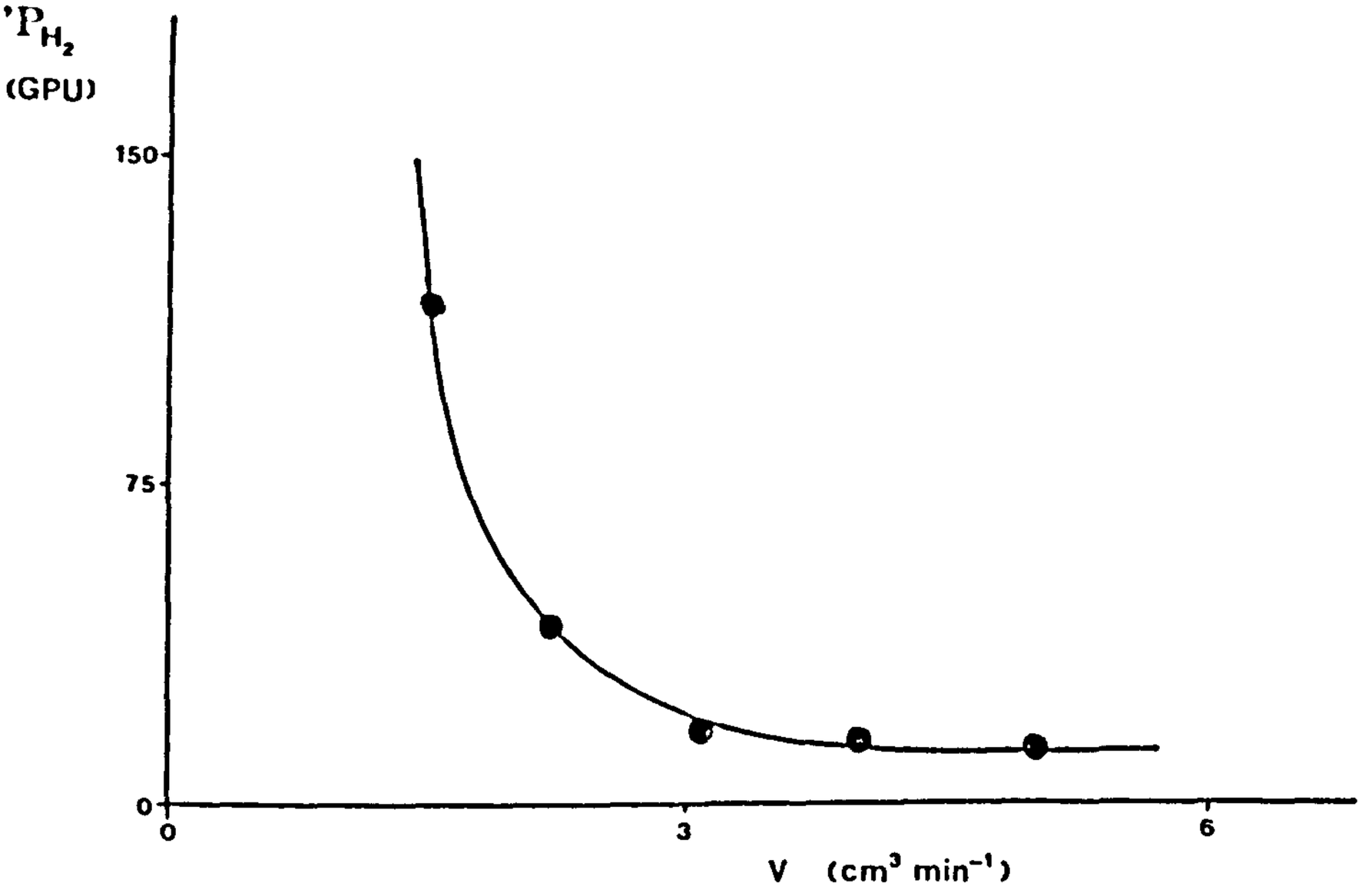

& 3.3.6) it was deduced that the square of the fibre diameter is directly proportional to P.E.R. and that the permeation rate constant is inversely proportional to the fibre diameter. Thus it was expected that:-

$$V \propto ('P_i)^{-2} \qquad (3.20)$$

However, it was generally found that as good a correlation existed between P.E.R. and $'P_i$ by a simple inverse proportionality. Figs 3.35 - 3.40 show comparative graphs for the various batches listed in Table 3.18. The reasons behind this discovery were not understood, but it remains an important step forward in the eventual development of tailoring fibres for specific gas transport requirements.

Table 3.18 Effect of P.E.R. on gas transport properties.

Batch	P.E.R.	Permeation Rate Constant (GPU)			Separation Factor	
	$cm^3\ min^{-1}$	H_2	CO_2	CH_4	H_2/CH_4	CO_2/CH_4
43/1n*	1.25	19.0	8.80	0.622	30.5	14.2
43/1m*	1.65	29.7	12.7	0.775	38.3	16.3
43/1p*	2.37	4.53	1.27	0.089	50.9	14.3
43/1q*	2.92	3.56	1.57	0.034	106	46.9
21/2c	2.02	59.1	17.4	15.2	3.9	1.15
21/2b	2.21	69.9	19.2	21.8	3.2	0.88
21/2a	2.65	53.0	16.4	17.7	3.0	0.93
21/2d	3.10	40.7	11.6	7.27	5.6	1.59
11/3d	1.5	116	31.0	37.4	3.1	0.83
11/3c	2.2	41.5	12.3	7.69	5.4	1.6
11/4g	3.1	26.1	8.33	5.55	4.7	1.5
11/3a	4.0	13.7	4.58	1.76	7.8	2.6
11/3b	5.0	12.1	4.23	1.46	8.3	2.9

* denotes coated modules.

Fig 3.35 Effect of PER on $('P_{H_2})^{-1}$ (Batch 11/3).

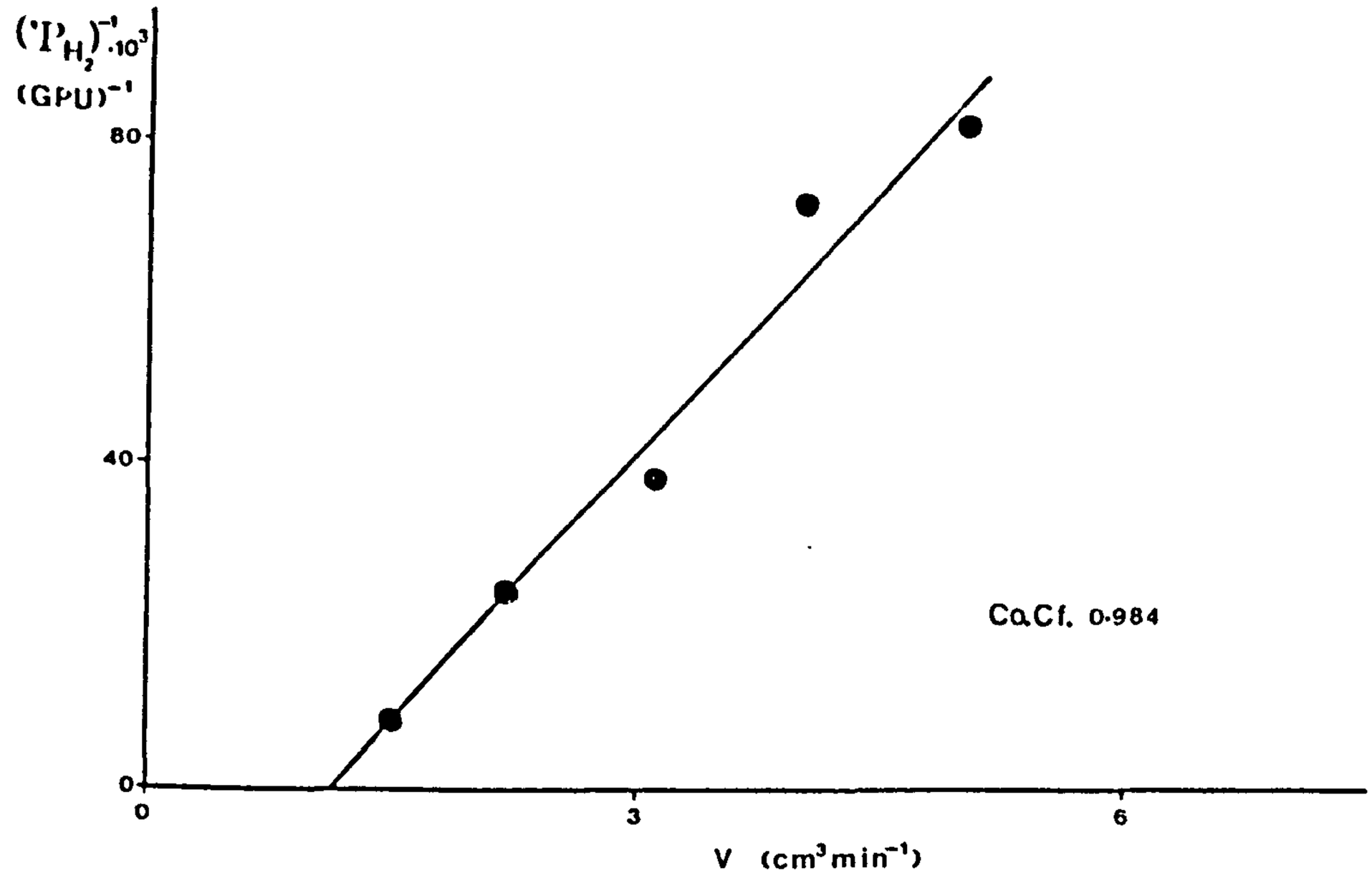

Fig 3.36 Effect of PER on $('P_{H_2})^{-2}$ (Batch 11/3).

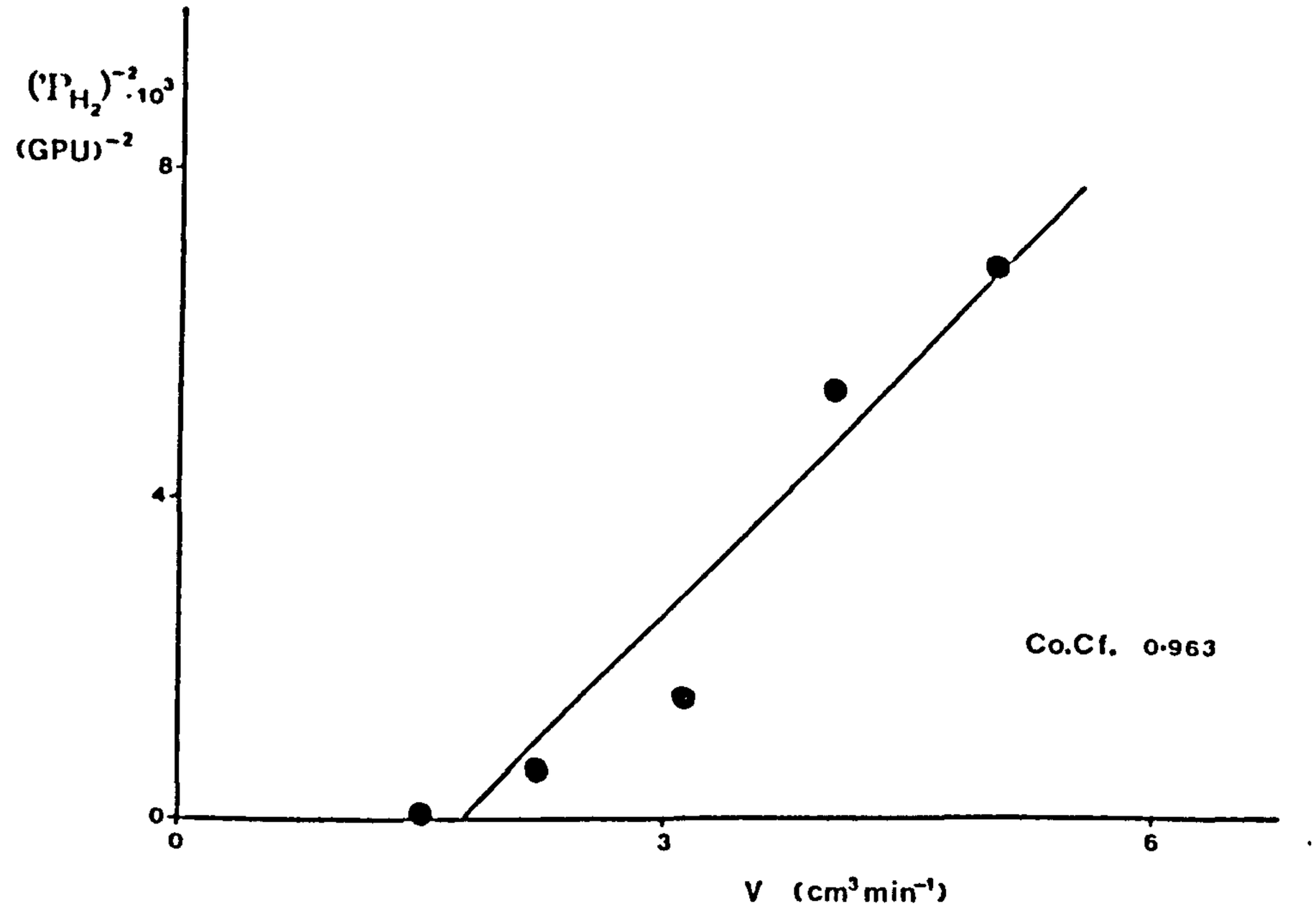

Fig 3.37 Effect of PER on $('P_{H_2})^{-1}$ (Batch 43/1).

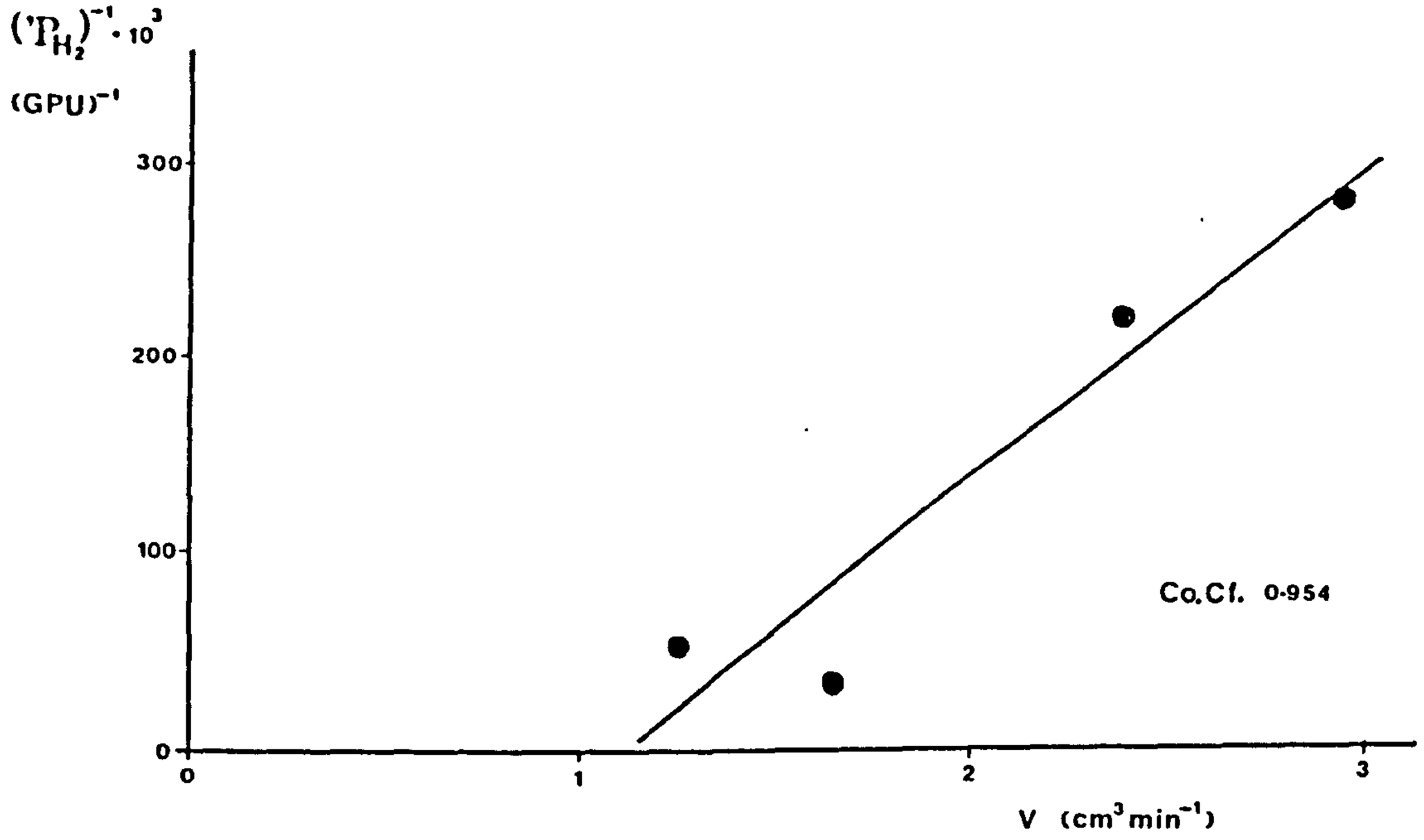

Fig 3.38 Effect of PER on $('P_{H_2})^{-2}$ (Batch 43/1).

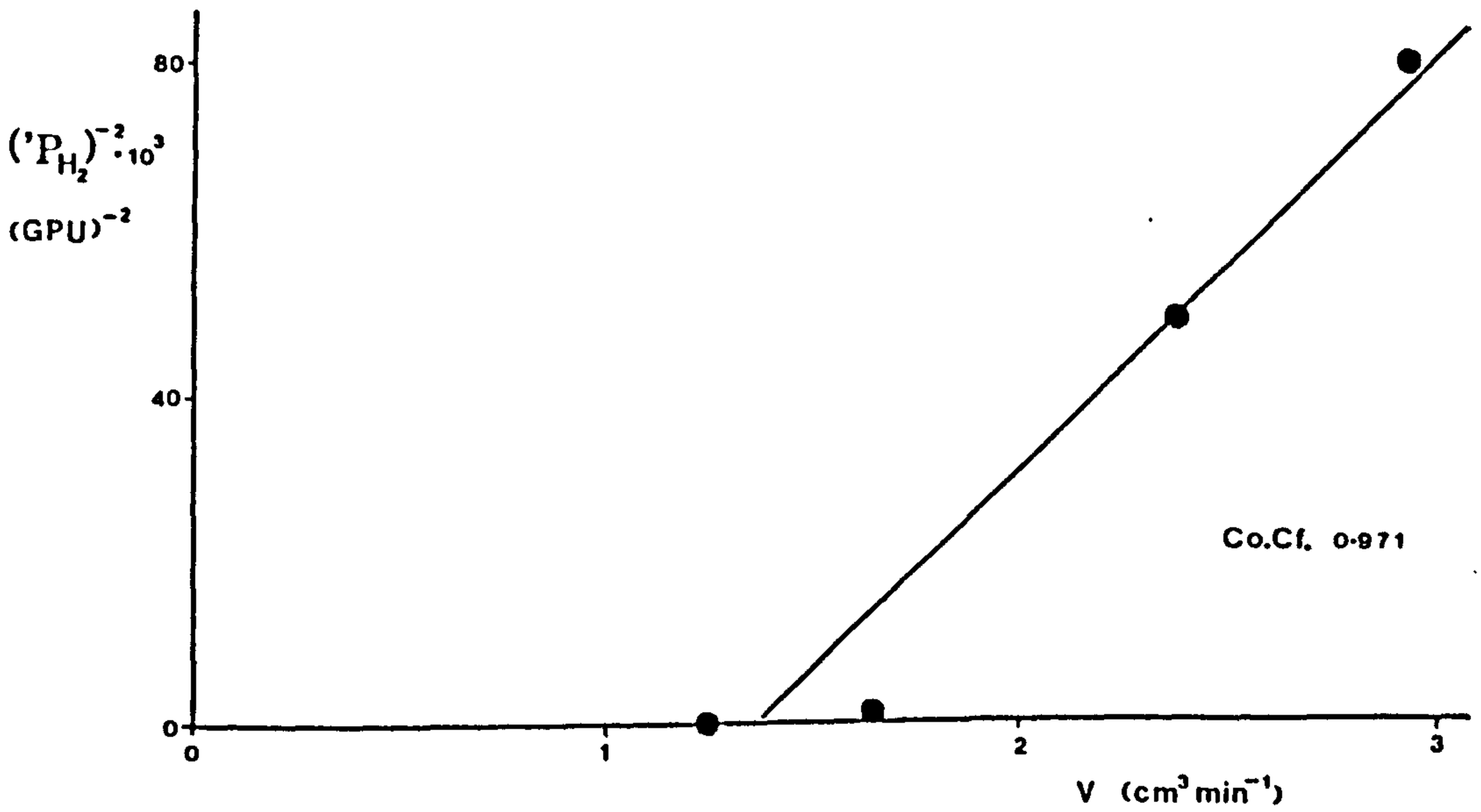

Fig 3.39 Effect of PER on $('P_{H_2})^{-1}$ (Batch 21/2).

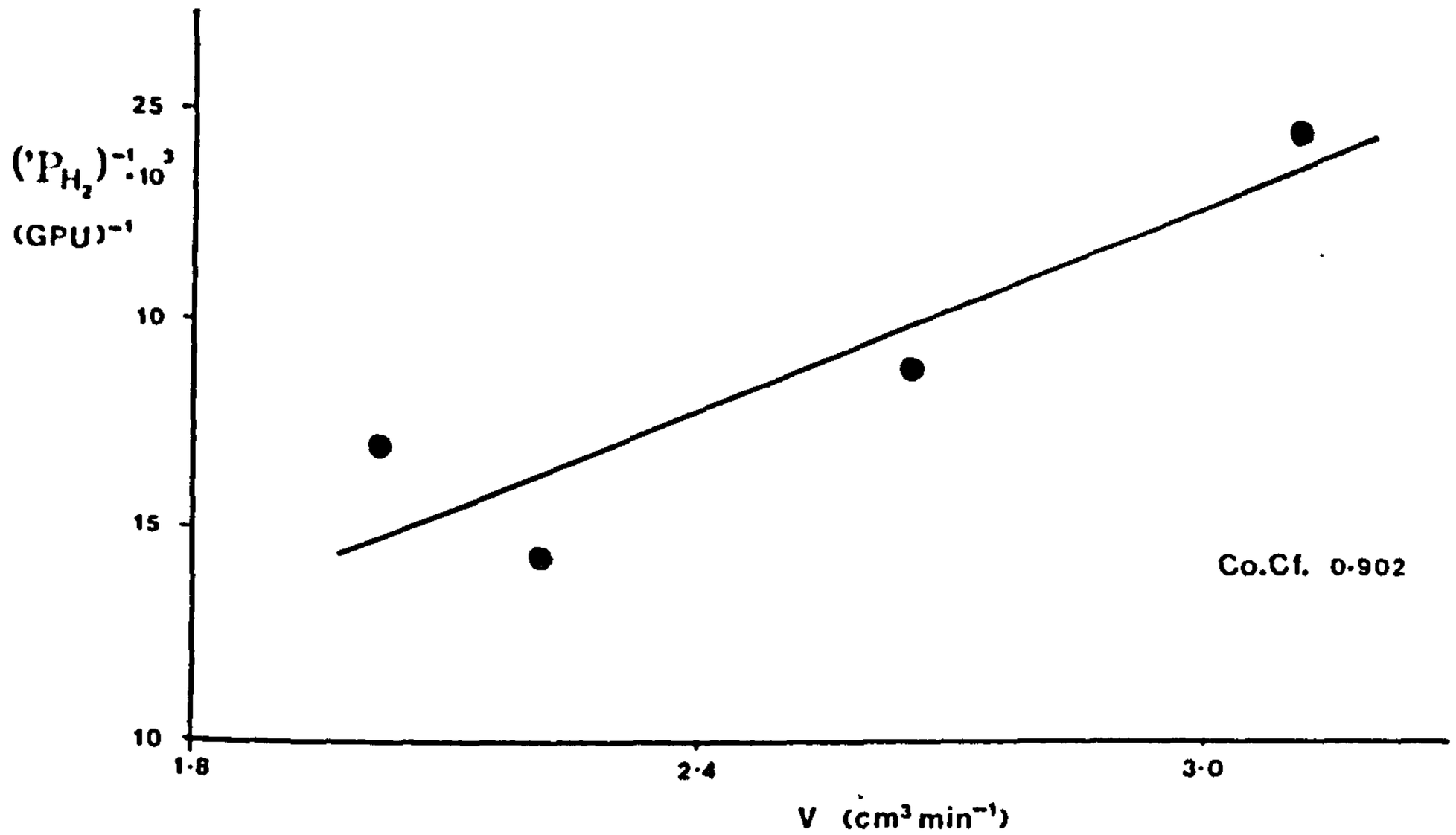

Fig 3.40 Effect of PER on $('P_{H_2})^{-2}$ (Batch 21/2).

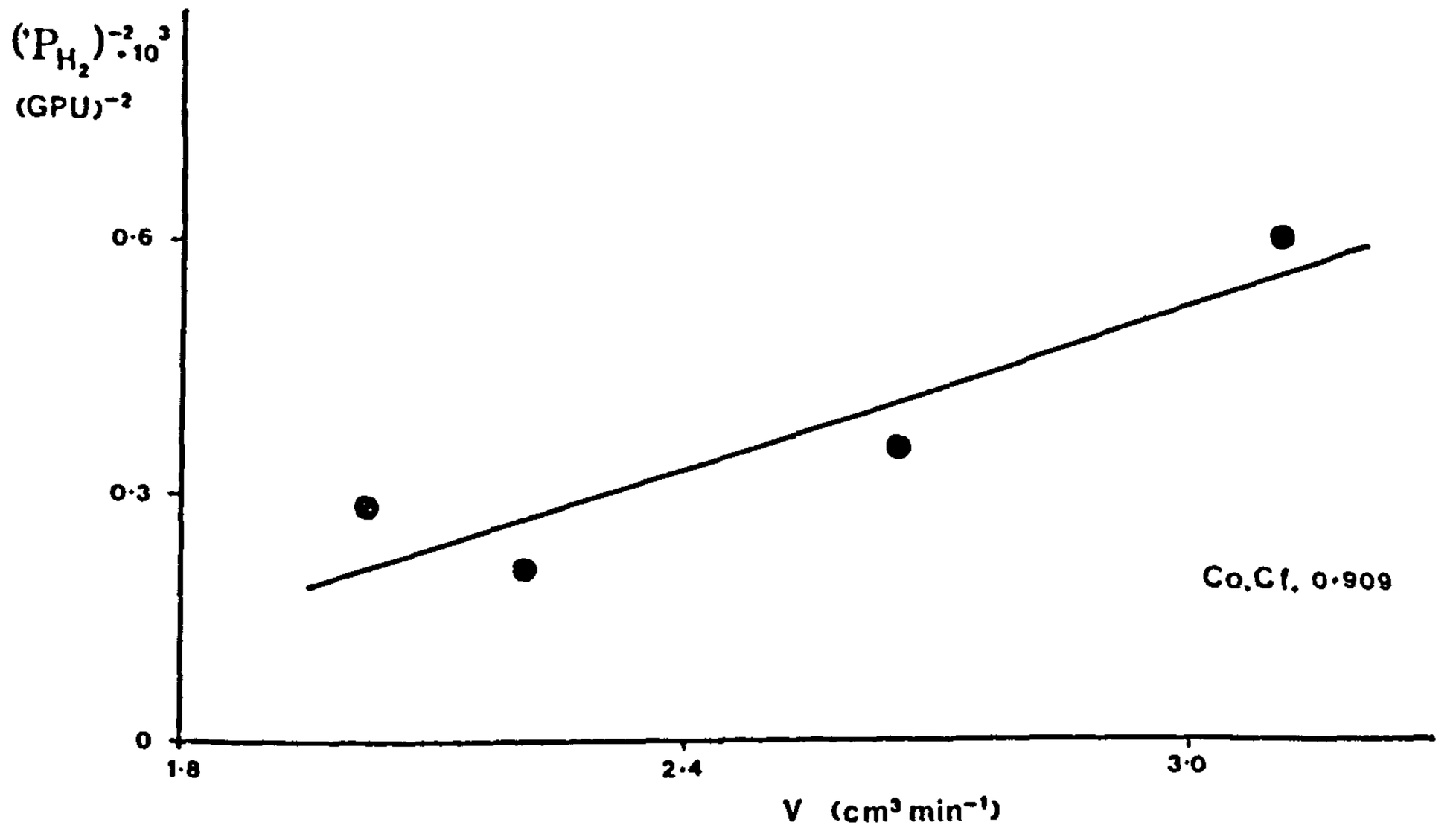

Fig 3.41 Effect of PER on the separation factor (Batch 11/3).

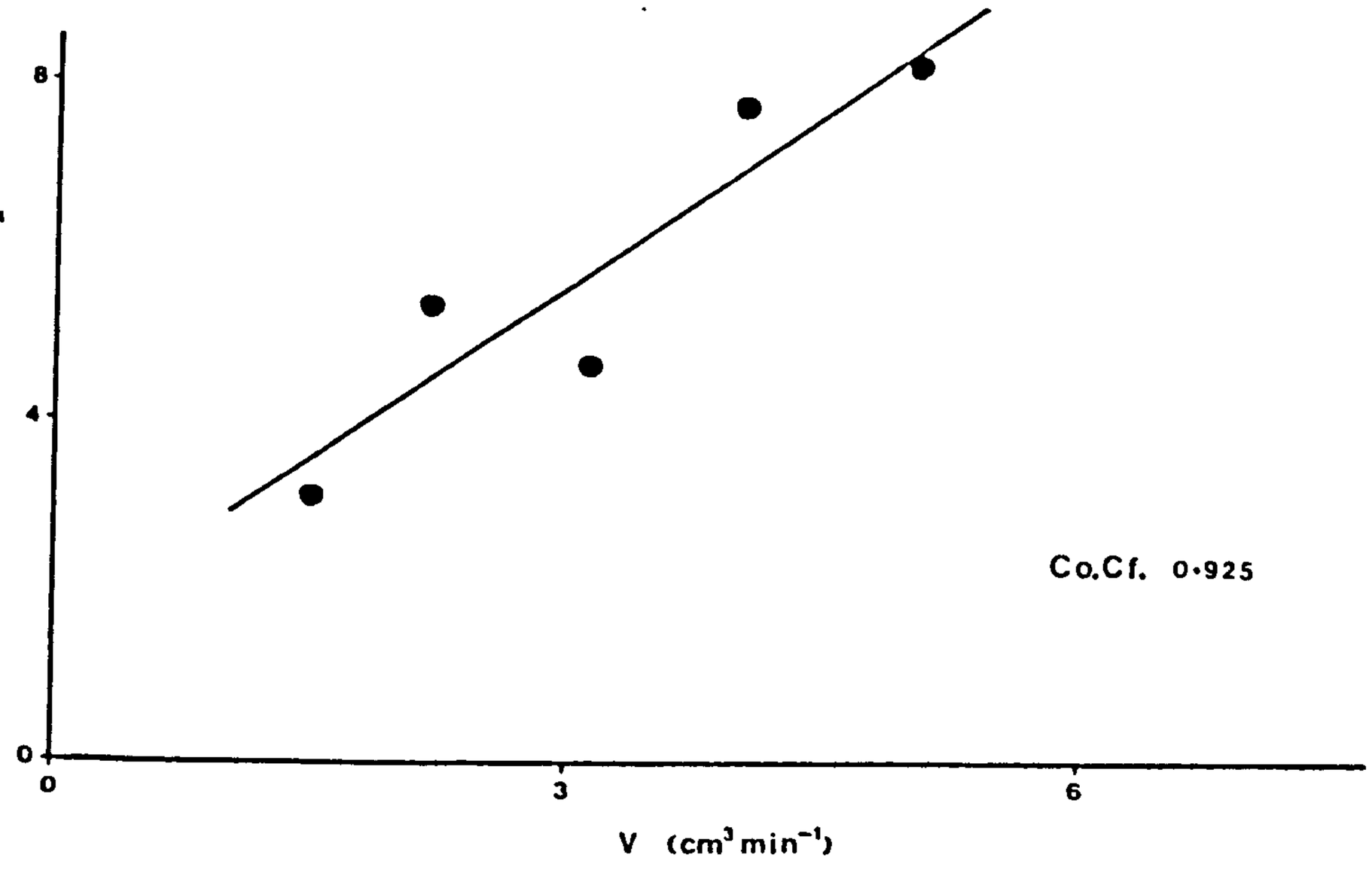

Fig 3.42 Effect of PER on the separation factor (Batch 43/1).

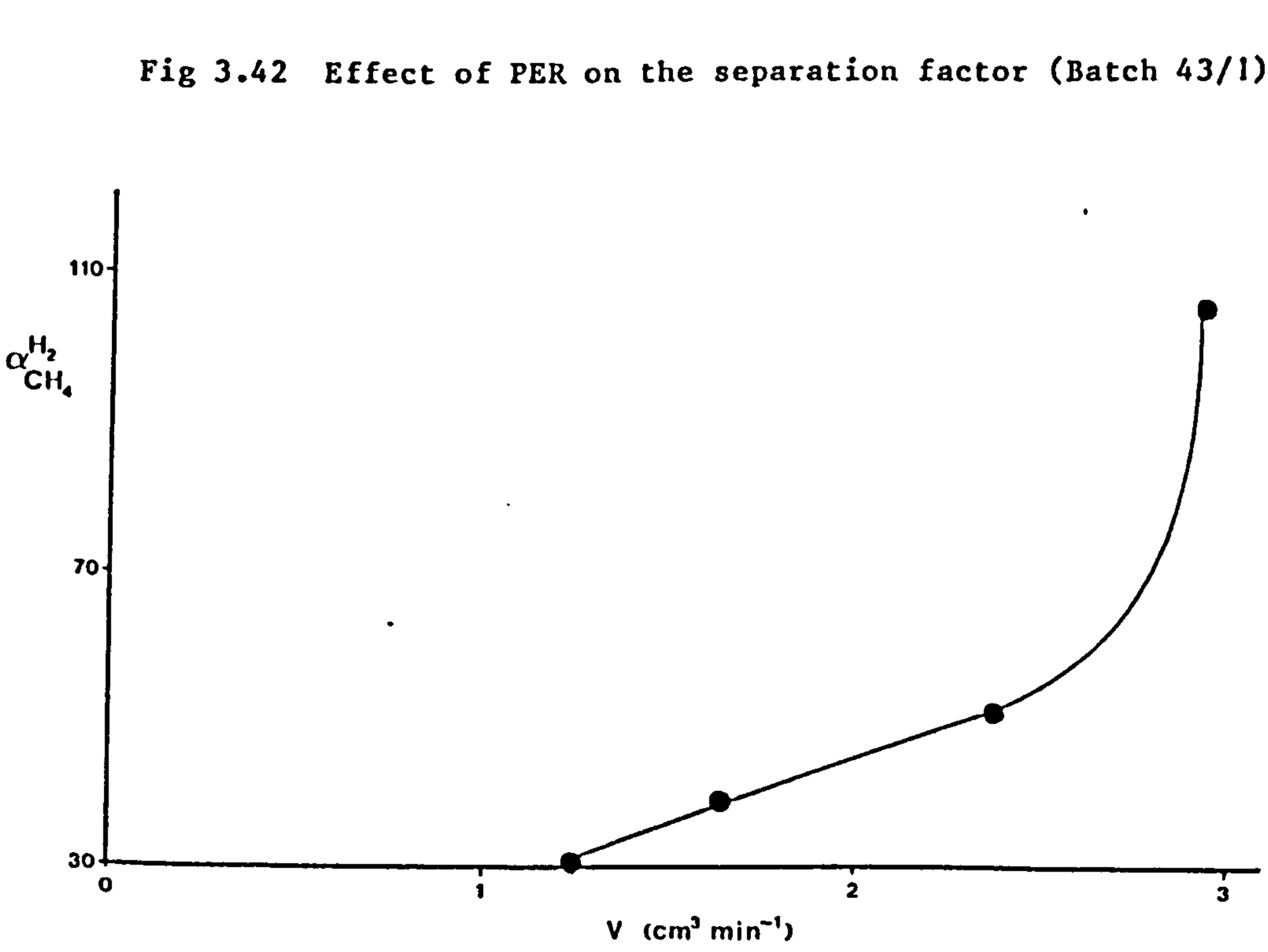

Table 3.19 Effect of W.I.R. on gas transport properties.

Batch	W.I.R.	Permeation Rate Constant (GPU)			Separation Factor	
	$cm^3\ min^{-1}$	H_2	CO_2	CH_4	H_2/CH_4	CO_2/CH_4
37/1d*	0.14	22.7	23.5	5.19	4.38	4.53
37/1c*	0.42	34.8	28.5	3.30	10.7	7.21
37/1e*	0.69	87.2	55.7	4.77	18.3	11.7
37/1f*	0.98	85.6	48.4	3.42	25.0	14.1
11/4a	0.5	25.6	7.87	4.92	5.2	1.6
11/4g	0.75	26.1	8.33	5.55	4.7	1.5
11/4b	1.0	28.4	9.04	4.30	6.6	2.1
11/4c	1.5	56.3	17.7	16.1	3.5	1.1
11/4d	2.5	155	44.3	55.4	2.8	0.8

* denotes coated modules.

Table 3.20 Effect of W.U.S. on gas transport properties.

Batch	W.U.S.	Permeation Rate Constant (GPU)			Separation Factor	
	$m\ min^{-1}$	H_2	CO_2	CH_4	H_2/CH_4	CO_2/CH_4
43/1d*	6.9	6.04	2.59	0.205	29.5	12.6
43/1c*	11.5	6.42	2.56	0.117	54.9	21.9
43/1b*	14.4	17.0	6.88	0.703	24.2	9.78
43/1e*	20.0	26.2	11.4	0.711	36.9	16.0

* denotes coated modules.

Examination of Table 3.18 also shows that the separation factors generally improve with increasing polymer extrusion rate. Again this was expected to be the case as the increase in polymer per unit length of fibre produces a more effective barrier to permeating gases, enhancing the effect of the solution-diffusion mechanism. This applies to both coated and uncoated fibres, though the effect was quite dramatic for the fibres of 43/1. Due to the variability of the data and other problems associated with measurement (mentioned previously) it was difficult to draw further conclusions concerning fibres in general. However, examination of two of the batches (Figs 3.41 & 3.42) suggests the

possibility of a linear correlation between the separation factor and the extrusion rate, though further study would be necessary to confirm this.

(b) Water injection rate.

The data in Table 3.19 shows that permeation rate constants increase with increasing water injection rate. Fig 3.43 shows an example of the interaction. The precise nature of the relationship is not yet fully understood and it might well be complex. What is especially interesting is the different ways in which the separation factor changes as a result of increased W.I.R (see Figs 3.45 & 3.46). Batch 11/4 (uncoated) shows a gradual decrease in the separation factor, whilst Batch 37/1 (coated) shows a marked rise in the separation factor. It is uncertain whether this results from the effect of coating, the effect of spinning solvent, the effect of lumen diameter and flow restrictions associated therewith, or some other unknown factor. One would predict a decrease in the separation factor, on the grounds that inflation of the fibre lumen at constant P.E.R. should result in a decrease in the wall thickness which, if the porosity of the membrane remained constant, would result in a reduction in the resistance to permeate flow (hence the observed rise in the permeation rate constants). One would then expect a decrease in the separation factors as the mode of permeation changes in favour of Knudsen flow. In Batch 37/1, the methane permeation rate constants have, if anything, decreased with rising W.I.R., resulting in a substantial increase in performance, as both permeation rate and separation factor have increased.

Future work to ascertain the reason for the rise in separation factor could be of enormous value because, as yet, the full extent to which the separation factors and permeabilities could be made to rise is unknown. It should not be forgotten that for membranes to become economically viable in gas separation processes, their performance must

be maximised by both increased permeability and separation factor.

(c) Wind up speed.

Fig 3.44 produced from Table 3.20 shows that as the wind up speed increases the permeation rate constant also increases. This was not a surprising result as the wind up speed can be thought of as a control on the amount of polymer per unit length of membrane. The wind up speed controls the amount the fibre was drawn (or stretched) during the spinning process. Thus increasing the W.U.S. results in thinner walls (also smaller lumen diameters) and this results in less resistance to flow to permeating species, hence the increased permeation rate constants. Due to the change in the fibre lumen, as well as the fibre diameter, it is difficult to predict the shape of the relationship. The data in Table 3.20 shows no obvious correlation; whether this is due to the complexity of the relationship governing the interaction or due to the inherent error in the results cannot be ascertained from the small amount of data collected.

The values of separation factor calculated from the permeation rate constants of Batch 43/1 show no trend, most likely due to the poor quality of the permeation rate constant data. It would be expected that the separation factor should fall with increasing wind up speed due to the thinner walls produced by the increased stretching of the extruded filament. The results of Batch 43/1 neither confirm nor disagree with this prediction.

Fig 3.43 Effect of WIR on $'P_{H_2}$.

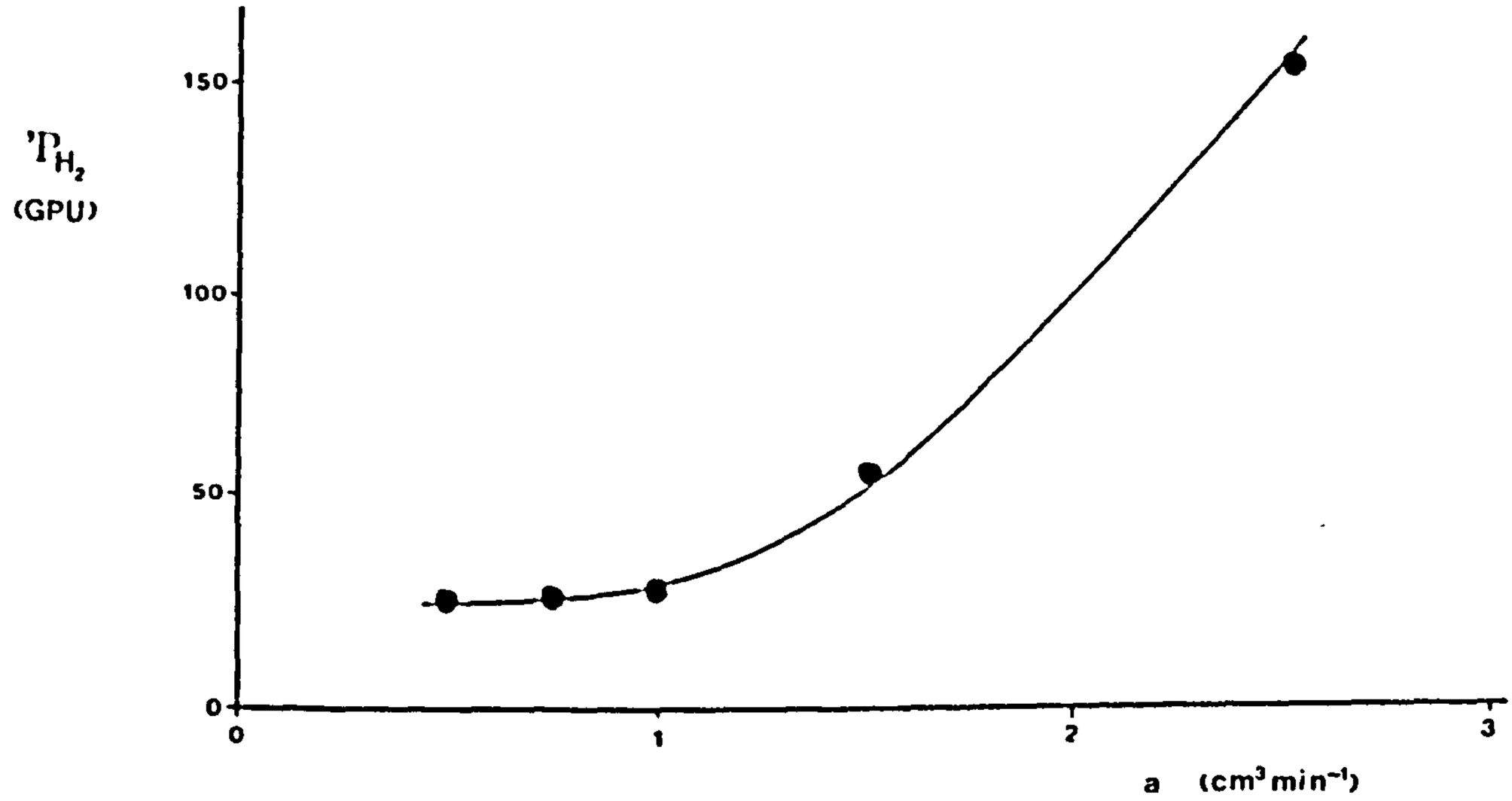

Fig 3.44 Effect of WUS on $'P_{H_2}$.

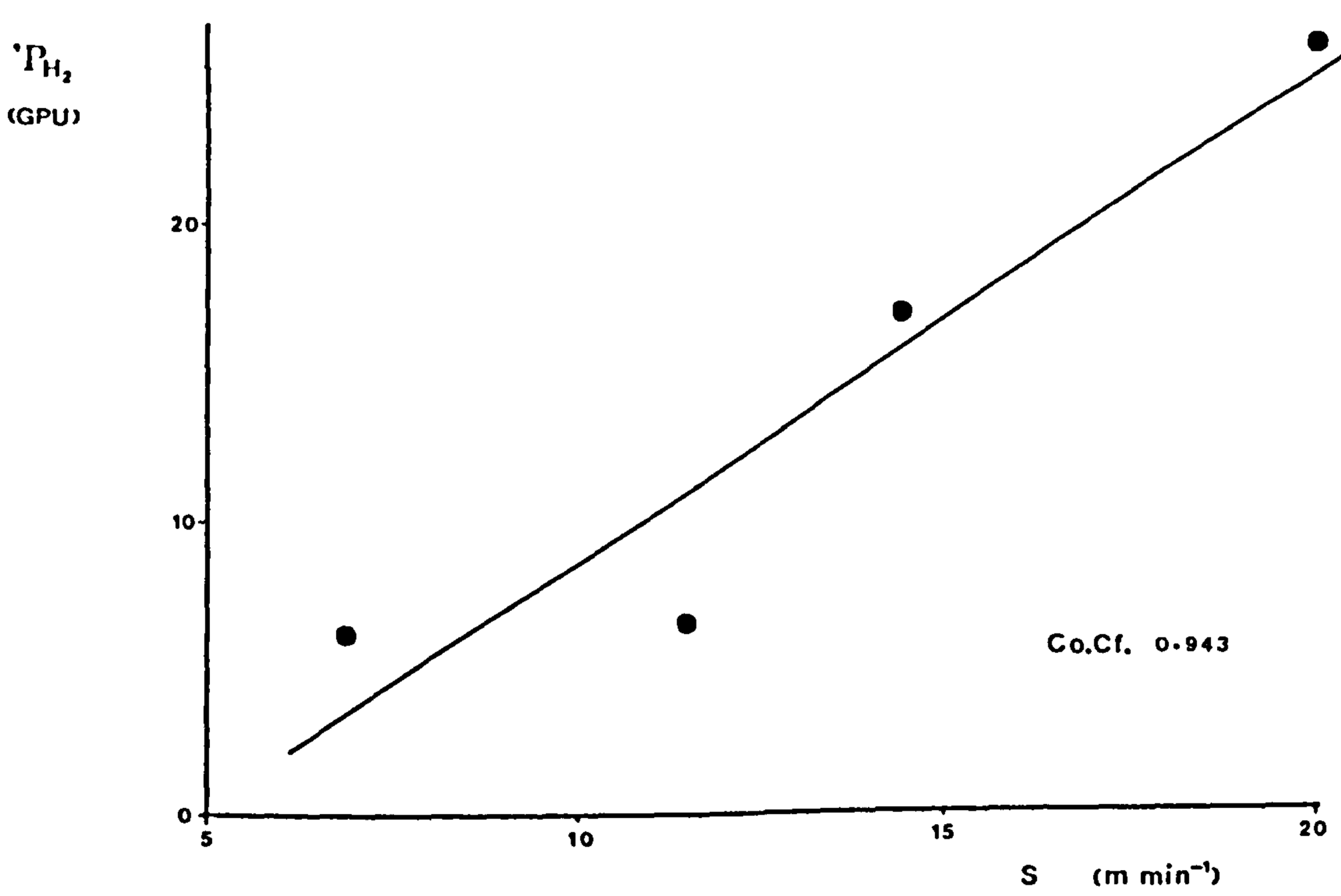

Fig 3.45 Effect of WIR on the separation factor (Batch 37/1).

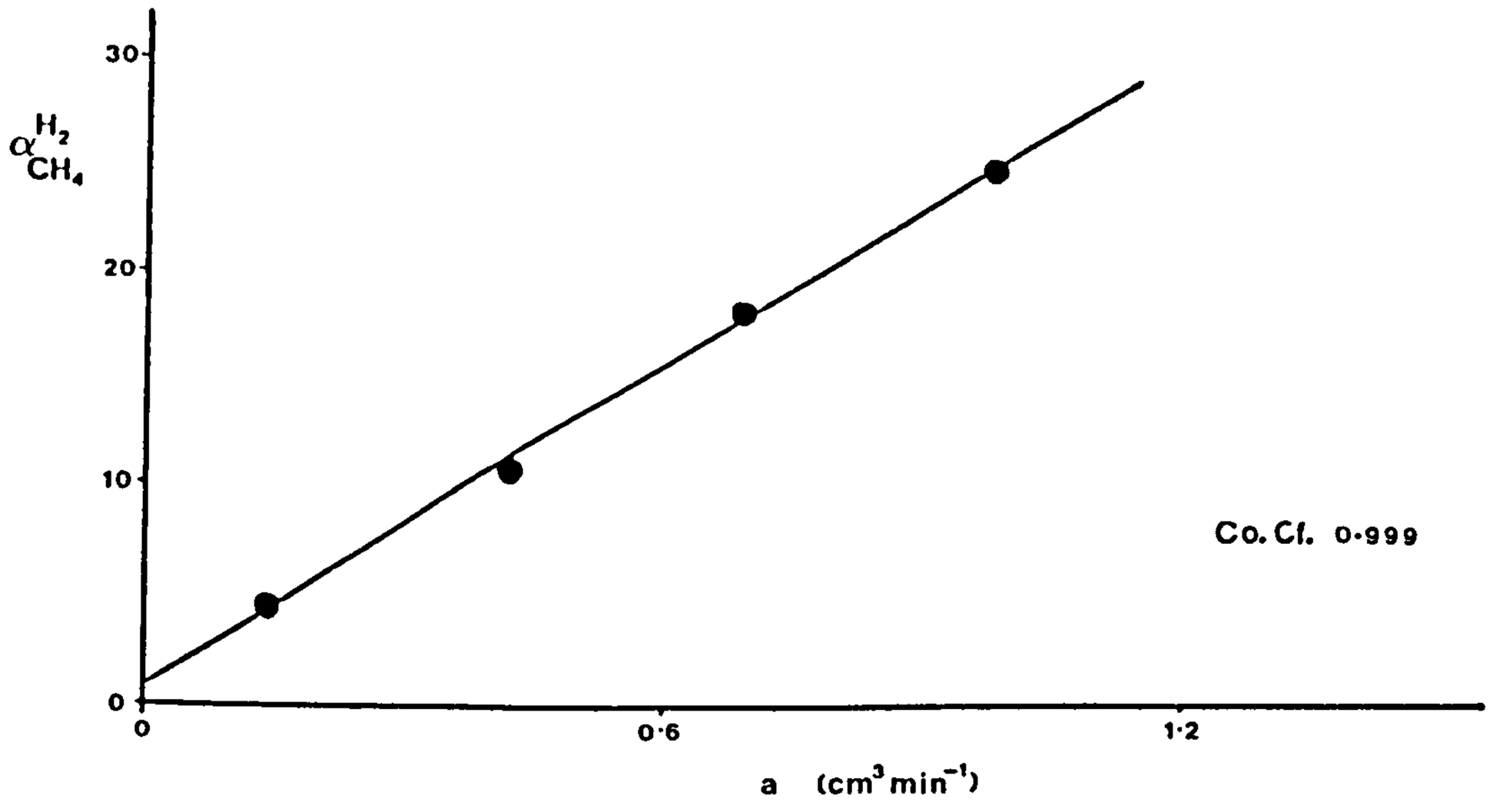

Fig 3.46 Effect of WIR on the separation factor (Batch 11/4).

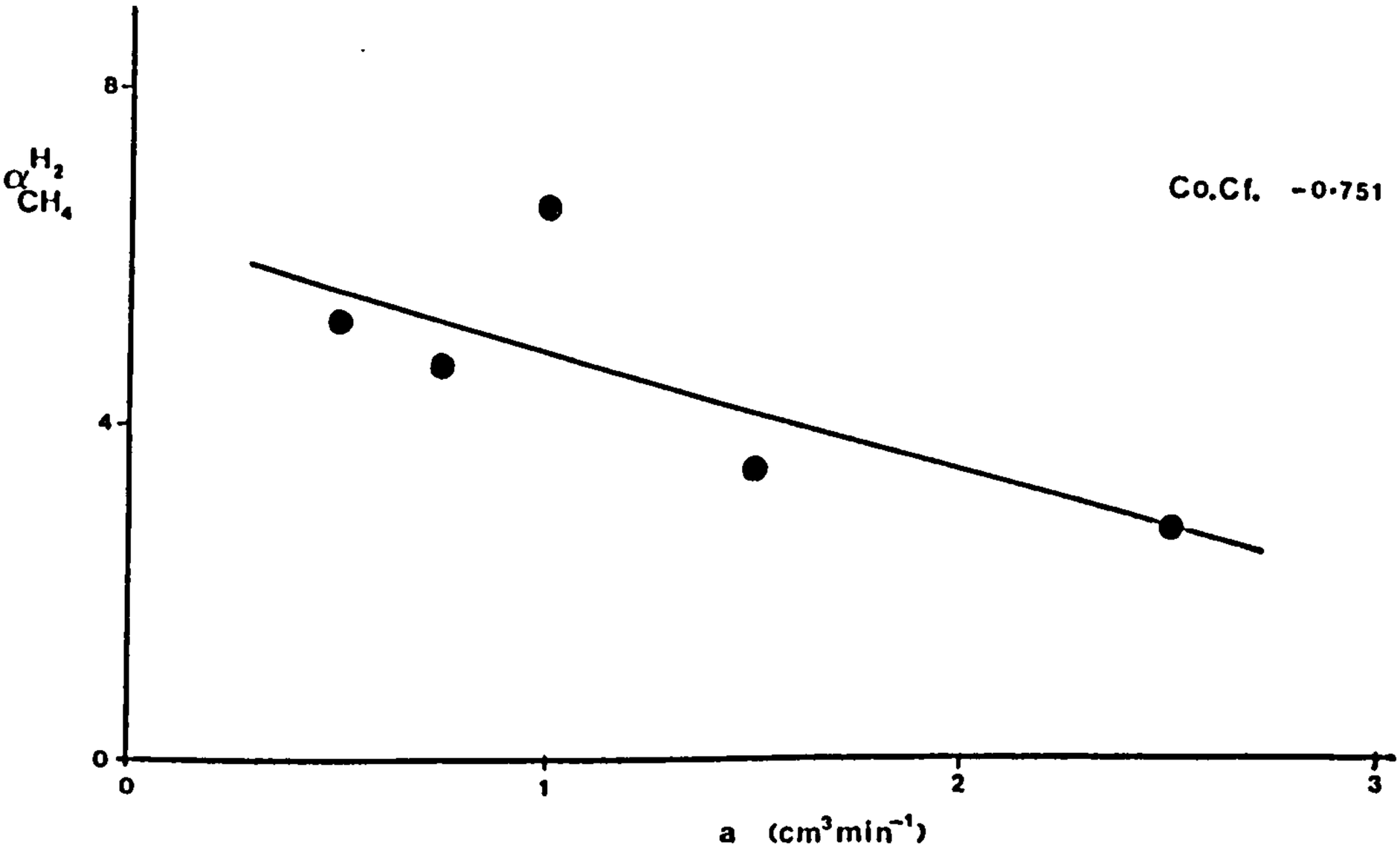

(d) Summary.

Again, unfortunately only a small amount of knowledge was gained from this study of the inter-relationships, as was the case in the previous sub-section. The main problem was, of course, the levels of error in the original measurements. In retrospect, it seems likely that a lot more data would be required to allow a successful evaluation of the role of spinning parameters on gas transport properties.

3.3.8 Separation of binary gas mixtures.

This subsection describes the work done to examine the performance of the membranes in a real separation situation. Two gas mixtures were obtained, one being a 50:50 mixture of hydrogen and methane and the other a 50:50 mixture of carbon dioxide and methane. From these experiments, important comparisons could be made between these binary gas separations and the single gas measurements made in the majority of the investigations in the study. Thus the validity of the separation factors based on single gas measurements could be tested.

Batch 37/1 was chosen for this study as the fibres were of the 9:1 1-Fp:Fa variety (and, although the information is not especially relevant to this section, had varying internal diameters and wall thicknesses as a consequence of being spun over a range of water injection rates). The enrichment factors (Φ) of the modules were calculated from the mole fractions of one species in the permeate and feed as described in section 2.4.7, using the formula reproduced below:-

$$\Phi_j^i = \frac{x_j^l \, (1 - x_j^h)}{x_j^h \, (1 - x_j^l)} \qquad (3.21)$$

where X_j^h = mol. fraction of j in the feed.

X_j^l = mol. fraction of j in the permeate.

Pseudo permeation rate constants were also calculated from the results of the permeation experiments. Table 3.21 lists the fibres from batch 37/1 tested and shows the values calculated from both the binary mixture experiments and from single gas experiments.

Table 3.21 Gas transport properties of batch 37/1 (coated).

Batch		37/1d	37/1c	37/1e	37/1f
d_i (μm)		157	191	227	261
d_w^i (μm)		184	186	134	127
'P hydrogen	(GPU)	22.7	34.8	87.2	85.6
'P carbon dioxide	(GPU)	23.5	23.5	55.7	48.4
'P methane	(GPU)	5.19	3.30	4.77	3.42
Π hydrogen	(GPU)	12.6	32.8[a]	59.4	58.4
Π carbon dioxide	(GPU)	15.9	19.6	33.8	30.1
Π methane	(GPU)	2.80	3.30	3.97	2.89
$\alpha H_2, CH_4$		4.38	10.7	18.3	25.0
$\Phi H_2^2, CH_4^4$		3.72	7.41	11.1	14.8
$\alpha CO_2, CH_4$		4.53	7.21	11.7	14.1
$\Phi CO_2^2, CH_4^4$		3.55	4.84	6.41	8.14

[a] Extraordinarily high variability between modules (error +/- 24%).

It is immediately evident that the 'true' values of separation are considerably lower (approx. 33% lower) than the levels suggested by the ratio of permeation rate constants. The enrichment factors are consistently lower by a more or less constant 33% (within experimental variability), suggesting that the simple measurements made using single pure gases might well be an alternative to more complicated measurements

made with gas mixtures.

The pseudo permeation rate constants (Π_i) are consistently lower than their corresponding permeation rate constants, measured during single gas permeation experiments. These lower values were thought to arise from competition between the two different molecular species in the mixture for sorption sites in the membrane. Meares [76] states that fluxes of the components of a gas mixture are lower than one would expect from the single gas permeability measurements.

The mechanism which caused these lower values to be obtained was not understood. It was initially thought that pseudo permeation rate constants ought to be the same as the single gas permeation rate constants. In order to try and understand why the values for the mixture experiments were lower, a simple model was constructed to map out the diffusion jumps of two molecular species in a hypothetical membrane. In the model it was assumed that diffusion could only proceed in one direction, from the high pressure side of the membrane to the low pressure side. The membrane itself consisted of five layers of sorption sites within which a diffusing molecule could only jump from the site in which it was sorbed to the site directly beneath it, and only if this site was vacant. After jumping from the fifth row the molecule was collected and categorised according to its species.

In the first experiment, the two permeating species were allowed to compete equally for the sorption sites on the membrane surface. However, species 1 was able to complete a diffusion jump twice as quickly as species 2. Fig 3.47 shows a section of the membrane. Each turn represents the minimum time necessary for species 1 to complete a jump, i.e. species 2 can only jump once every two turns. The molecules arrive randomly at the surface and are replenished at the end of each turn. At each turn any species designated 2 changes its notation to 3 to indicate that it has remained in the sorption site for one turn and will be

eligable to jump the following turn. Thus it is not until the sixth turn that species 1 appears at the low pressure side of the membrane and species 2/3 is not collected until turn 11. The model takes several turns to equilibrate, thus Fig 3.47 also shows turns 144 - 146. Notice that the membrane shows a considerable number of vacant sites (designated 0). On average the membrane contains 37 vacant sites at any one time after equilibrium. These vacant sites do not appear in a membrane in which two species pemeate at the same rate as shown in Fig 3.48. Similarly if the simulation is carried out with separate gases then no vacant sites appear. This suggests that the membrane does not operate as effectively with gas mixtures as with separate gases. The presence of these sites could account for the lower rate constants observed for the gas mixtures. In the model, these vacancies arise due to the lower jump rate of the slower diffusing species. The other consequence of the lower jump rate is that the faster moving species is held up. In Fig 3.47, turn 3, the highlighted site becomes occupied by species 1. This species would move to the site beneath it the following turn. However, this site does not become vacant in turn 4 as it is filled by the slower diffusing species 2/3. This situation cannot occur, in this model, for species 2/3 as 2/3 diffuses at the same rate as the offending molecule in the lower site (which is also a 2/3 specie). This implies that the ratio of the pseudo permeation rate constant to the permeation rate constant (single gas) of the potentially faster permeating species should be lower than that of the slower permeating species. This prediction appears to be true as Table 3.22 confirms this from the data collected from batch 37/1.

Fig 3.47 Mixture permeation model : Diffusion controlled separation.

Turn 1

```
1 2 1 2 1 2 2 2 1 1 1 1 1 2 2 2
-------------------------------
0 0 0 0 0 0 0 0 0 0 0 0 0 0 0 0
0 0 0 0 0 0 0 0 0 0 0 0 0 0 0 0
0 0 0 0 0 0 0 0 0 0 0 0 0 0 0 0
0 0 0 0 0 0 0 0 0 0 0 0 0 0 0 0
-------------------------------
0 0 0 0 0 0 0 0 0 0 0 0 0 0 0 0
```

Turn 2

```
1 3 2 3 2 3 3 3 2 2 1 1 2 3 3 3
-------------------------------
1 0 1 0 1 0 0 0 1 1 1 1 1 0 0 0
0 0 0 0 0 0 0 0 0 0 0 0 0 0 0 0
0 0 0 0 0 0 0 0 0 0 0 0 0 0 0 0
0 0 0 0 0 0 0 0 0 0 0 0 0 0 0 0
-------------------------------
0 0 0 0 0 0 0 0 0 0 0 0 0 0 0 0
```

Turn 3

```
2 1 3 1 3 2 1 2 3 3 1 2 3 1 1 2
-------------------------------
1 2 0 2 0 2 2 2 0 0 1 1 0 2 2 2
1 0 1 0 1 0 0 0 1 1 1 1 1 0 0 0
0 0 0 0 0 0 0 0 0 0 0 0 0 0 0 0
0 0 0 0 0 0 0 0 0 0 0 0 0 0 0 0
-------------------------------
0 0 0 0 0 0 0 0 0 0 0 0 0 0 0 0
```

Turn 4

```
3 1 1 1 2 3 1 3 2 1 2 3 1 1 1 3
-------------------------------
0 3 2 3 2 3 3 3 2 2 1 0 2 3 3 3
1 0 1 0 1 0 0 0 1 1 1 1 1 0 0 0
0 0 0 0 0 0 0 0 0 0 0 0 0 0 0 0
0 0 0 0 0 0 0 0 0 0 0 0 0 0 0 0
-------------------------------
0 0 0 0 0 0 0 0 0 0 0 0 0 0 0 0
```

Turn 5

```
1 1 1 1 3 1 2 2 3 1 3 2 1 2 2 2
-------------------------------
2 1 3 1 3 2 1 2 3 3 0 2 3 1 1 2
0 2 0 2 0 2 2 2 0 0 1 0 0 2 2 2
1 0 0 0 0 0 0 0 0 0 1 1 0 0 0 0
1 0 1 0 1 0 0 0 1 1 1 1 1 0 0 0
-------------------------------
0 0 0 0 0 0 0 0 0 0 0 0 0 0 0 0
```

Turn 6

```
1 1 1 1 1 1 3 3 1 2 1 3 1 3 3 3
-------------------------------
3 1 1 1 2 3 1 3 2 1 2 3 1 1 1 3
0 3 2 3 2 3 3 3 2 2 0 0 2 3 3 3
0 0 0 0 0 0 0 0 0 0 1 0 0 0 0 0
1 0 0 0 0 0 0 0 0 0 1 1 0 0 0 0
-------------------------------
1 0 1 0 1 0 0 0 1 1 1 1 1 0 0 0
```

% Permeate Composition 1=100 : 2=0

Turn 144

```
1 2 1 2 3 3 1 1 1 1 1 2 2 2 3 1
-------------------------------
3 1 3 1 3 3 1 1 2 2 1 2 2 2 1 1
3 1 0 2 3 3 1 2 2 1 1 1 1 2 1 3
1 1 0 2 3 3 2 1 2 2 1 2 1 1 3 3
3 1 1 2 3 3 1 1 2 2 2 2 2 2 3 3
-------------------------------
0 1 1 2 0 0 2 2 2 0 2 2 0 0 0 0
```

% Permeate Composition 1=45 : 2=55

Turn 145

```
2 3 1 3 2 2 1 1 1 1 1 3 3 3 2 2
-------------------------------
1 0 1 1 2 2 1 1 3 3 1 3 3 3 2 1
2 1 2 3 2 2 1 3 3 1 1 1 1 3 1 1
2 1 0 3 2 2 3 0 3 3 1 3 1 1 1 2
1 1 0 3 2 2 0 1 3 3 3 3 3 3 2 2
-------------------------------
2 1 1 0 2 2 1 1 0 0 0 0 0 0 2 2
```

% Permeate Composition 1=45 : 2=55

Turn 146

```
3 2 1 1 3 3 2 2 2 1 1 2 1 1 3 3
-------------------------------
1 2 1 2 3 3 1 1 1 1 1 2 2 2 3 1
3 0 3 1 3 3 1 1 2 2 1 2 2 2 1 1
3 1 0 2 3 3 1 2 2 1 1 1 1 2 1 3
0 1 0 2 3 3 2 0 2 2 1 2 1 1 3 3
-------------------------------
1 1 0 2 0 0 0 1 2 2 2 2 2 2 0 0
```

% Permeate Composition 1=45 : 2=55

Fig 3.48 Mixture permeation model : Weighted sorption.

Turn 117

```
1 1 1 1 1 1 2 1 1 1 1 1 1 1 1 1
-------------------------------
1 1 1 1 1 1 2 1 1 2 1 1 1 1 1 1
1 1 1 1 1 1 1 1 2 1 1 1 2 1 1 2
1 1 1 1 1 1 1 1 1 1 1 1 1 2 1 1
1 1 1 1 2 1 1 1 1 1 1 1 1 1 1 1
-------------------------------
1 1 1 1 1 1 1 1 1 1 1 2 2 1 1 1
```

% Permeate Composition 1=88 : 2=12

Turn 118

```
1 1 1 1 2 1 2 1 1 1 1 2 1 1 1 1
-------------------------------
1 1 1 1 1 1 2 1 1 1 1 1 1 1 1 1
1 1 1 1 1 1 2 1 1 2 1 1 1 1 1 1
1 1 1 1 1 1 1 1 2 1 1 1 2 1 1 2
1 1 1 1 1 1 1 1 1 1 1 1 1 2 1 1
-------------------------------
1 1 1 1 2 1 1 1 1 1 1 1 1 1 1 1
```

% Permeate Composition 1=85 : 2=15

Fig 3.49 Mixture permeation model : Combined control of separation.

Turn 223

```
1 1 1 1 1 2 1 1 1 1 1 1 1 1 1 1
-------------------------------
3 1 1 1 1 1 3 3 1 1 1 2 1 1 1 1
0 3 1 1 1 1 3 3 1 1 3 0 3 2 1 3
0 1 3 1 1 1 0 0 1 3 0 1 0 0 1 0
1 3 3 2 1 1 0 1 1 0 0 1 0 0 1 0
-------------------------------
1 0 0 0 2 2 0 1 1 0 0 1 0 1 1 0
```

% Permeate Composition 1=83 : 2=17

Turn 224

```
1 1 2 1 1 3 1 1 1 2 1 1 1 1 1 1
-------------------------------
1 1 1 1 1 0 1 1 1 1 1 3 1 1 1 1
2 1 1 1 1 1 2 2 1 1 1 0 1 3 1 1
0 2 1 1 1 1 2 2 1 1 2 0 2 0 1 2
0 1 2 3 1 1 0 0 1 2 0 1 0 0 1 0
-------------------------------
1 2 2 0 1 1 0 1 1 0 0 1 0 0 1 0
```

% Permeate Composition 1=78 : 2=22

Table 3.22 Difference in rate constant ratios for batch 37/1 (coated).

	37/1d	37/1c	37/1e	37/1f	Mean
Π / 'P (hydrogen)	0.56	0.89	0.68	0.68	0.70
Π / 'P (methane)	0.62	0.99	0.85	0.85	0.83

If the faster moving species is restricted more than the slower then this causes a detrimental effect on the separation factor. For the situation detailed in Fig 3.47 then, assuming a 50:50 feed composition, the enrichment factor is reduced to unity. Fig 3.48 & 3.49 show models where species 1 is preferentially sorbed onto the surface of the membrane (7 times more likely to be sorbed). In Fig 3.48 the two species diffuse at the same rate, whilst in Fig 3.49 species 2/3 diffuses at half the speed of that of species 1. In Fig 3.48, where no vacant sites develop and where the faster permeating species is not inhibited, the enrichment factor obtained is 5.85, whilst in Fig 3.49 where the rate of permeation of species 2/3 is halved the enrichment factor decreases to 4.56. How much this very simple model represents reality is difficult to gauge; the restrictions incorporated in the model, such as unidirectional diffusion and rigid control of the jump rate tend to over-emphasise the situations which can occur as a result of competition. However, over-emphasis is not at issue here; the fact that such simple model enables an interpretation of experimental results to be made is encouraging.

Meares [76] discusses the ability of certain gases (such as carbon dioxide) to plasticize polymers above T_g causing an increase in permeability of the membrane. The significance of this is that if a gas mixture containing such a gas permeates through the membrane then the membrane will exhibit enhanced permeability to all the gases in the mixture thus lowering the enrichment factor. This cannot be easily

tested from the enrichment factors measured as the plasticizing effect was masked by the effect of competition on the enrichment factor. However, the pseudo permeation rate constant for methane determined from the carbon dioxide / methane mixture would be expected to be greater than that determined from the hydrogen / methane mixture. Table 3.21 shows that there is little conclusive evidence to suggest that plasticization has occurred in the polysulphone membranes (T_g = 195 ^{o}C.). It was, however, noted during the single gas measurements that the permeation rate of CO_2 increased with time until equilibrium was reached (i.e. after approx. 60 min.) and that the membrane showed greater permeability to other gases immediately after being subjected to CO_2 (This behaviour was absent with the other gases). It was, therefore, concluded that plasticization of the polymer did occur in the membrane even though the polymer was significantly below its T_g.

Table 3.23 Difference in methane pseudo permeation rate constants.

	37/1d	37/1c	37/1e	37/1f
ΠCH_4 (from H_2/CH_4 mixture)	2.80	3.30	3.97	2.89
ΠCH_4 (from CO_2/CH_4 mixture)	3.70	3.15	4.07	2.77

Analysis of the data produced using the gas mixtures revealed the practical effectiveness of the membrane modules. This is best illustrated in terms of the increase in purity of the source gas as a result of one pass through the 30 cm^2 of membrane contained in the permeation chamber. Table 3.24 expresses the effectiveness of batch 37/1.

Table 3.24 Effectiveness of batch 37/1 (coated).

(a) Hydrogen / Methane

	Feed		Raffinate		Permeate		% increase
	% H_2	% CH_4	% H_2	% CH_4	% H_2	% CH_4	in purity
37/1d	46.2	53.8	46.0	54.0	76.2	23.8	0.2
37/1c	46.2	53.8	45.6	54.4	85.0	15.0	0.6
37/1e	46.2	53.8	45.0	55.0	90.5	9.5	1.2
37/1f	46.2	53.8	45.1	54.9	92.7	7.3	1.1

(a) Carbon dioxide / Methane

	Feed		Raffinate		Permeate		% increase
	% H_2	% CH_4	% H_2	% CH_4	% H_2	% CH_4	in purity
37/1d	44.4	55.6	44.2	55.8	73.8	26.1	0.2
37/1c	44.4	55.6	44.0	56.0	78.6	21.4	0.4
37/1e	44.4	55.6	44.0	56.0	84.0	16.0	0.4
37/1f	44.4	55.6	43.1	56.9	86.5	13.5	1.3

The change in composition between the feed and raffinate is a measure of the increase in purity of the stream, and the concentration of methane in the permeate is related to the slippage. Therefore the data in Table 3.24 shows that the overall effectiveness of this specific separation process was poor. Too much methane was lost as slippage for such a poor increase in purity. However, these levels of purity and slippage apply only to the set of operating conditions used. A reduction in the flow rate across the membrane surface, i.e. through the permeator chamber, could be expected to increase the effectiveness of the process, as discussed later.

3.3.9 The effect of linear feed flow along the membrane surface.

The increase in purity of methane in the raffinate should be very much dependent upon the flow rate of gas over the membranes (controlled by the reject flow control valve). A slower rate of flow through the permeation chamber should yield an increase in purity of the raffinate whilst a higher rate of flow would probably produce a raffinate of composition very similar to that of the feed. Two experiments were conducted to examine the importance of varying the flow through the permeation chamber. The first experiment was simply to examine the effect of different flow rates and the second was designed to observe the change in performance of the membrane.

(a) The effect of linear feed flow rate through the permeator chamber.

The flow rate of gas travelling from feed to raffinate was varied whilst measurements of the enrichment factors were made. The method by which these measurements were made was as follows:- Initially the module under test was subjected to a high flow rate (> 2000 cm^3 min^{-1}) for ten minutes. The reject flow control valve was then adjusted to the desired flow rate. After twelve minutes the composition of the feed was measured. The procedure was then twice repeated in order to measure the raffinate and permeate compositions. Table 3.25 shows how the effectiveness of the process varied over the four flow rates investigated.

Fig 3.50 shows graphically the change in enrichment factor with increasing reject flow rate. The graph shows that above 600 cm^3 min^{-1} there is very little effect. However, below 600 cm^3 min^{-1} the module tested was extremely sensitive to flow rate. The significance of this is that in the interest of producing data for batches which are to be

compared to other batches then it is essential that the reject flow rate be set above the sensitive region indicated in Fig 3.50. Assuming the % CH_4 in the permeate is related to the slippage then from examination of the figures for purity and % CH_4 in permeate it is clear that the two properties act against each other, in a smilar manner to other separation techniques (see section 1.1.2). Thus for processes where the level of slippage is economically important a high flow rate would be favourable, whereas for high purity (high value) products a slow flow rate would be chosen.

Table 3.25 Effect of linear feed flow rate on the effectiveness of batch 37/1f (coated).

Flow Rate $cm^3\ min^{-1}$	Enrichment Factor H_2/CH_4	% Increase in Purity	% CH_4 in Permeate
0[a]	3.56	20.3	24.6
46	6.56	13.3	15.1
577	12.0	2.3	8.84
1360	12.7	0.9	8.43

[a] At zero flow rate the rate at which feed gas arrives at the permeator is not zero, but is actually at a rate equal to the permeation rate of the gas mixture.

(b) The effect of restricted flow on permeate composition.

The experimental procedure for this investigation was similar to that of the previous experiment except that measurements were made at various times after the setting of the reject flow control valve. This enabled an examination to be made of the rate of reaction of the system to changes in the flow rate. In effect the experiment shows how quickly the faster permeating species is depleted from the permeation chamber. Table 3.26 shows the increase of hydrogen in the permeate with time, together with the change in purity of the raffinate and the loss of

methane to the permeate. This table shows the importance of maintaining constant flow control during processes run at low flow rates in order to avoid variations in purity and slippage.

Table 3.26 Effect of restricted flow on permeate composition.

Flow Rate $cm^3\ min^{-1}$	Time min	% Increase in Purity	% Hydrogen in Permeate	% CH_4 in Permeate
0	0	0.0	91.7	8.3
	3	7.3	83.0	17.0
	6	17.6	78.1	21.9
	9	19.9	76.0	24.0
	12	20.3	75.4	24.6
46	0	0.9	91.3	8.7
	3	10.5	85.9	14.1
	6	13.2	84.9	15.1
	9	13.3	84.9	15.1
	12	13.3	84.9	15.1
577	0	0.0	91.3	8.7
	3	2.3	91.1	8.9
	6	2.3	91.1	8.9
	9	2.3	91.1	8.9
	12	2.3	91.2	8.8
1364	0	0.9	91.7	8.3
	3	1.0	91.5	8.5
	6	0.9	91.5	8.5
	9	1.0	91.6	8.4
	12	1.0	91.6	8.4

[a] At zero flow rate the rate at which feed gas arrives at the permeator is not zero, but is actually at a rate equal to the permeation rate of the gas mixture; this is because the pressure difference across the membrane was maintained constant throughout the experiment.

Fig 3.51 shows the various levels of restriction imposed. Where the restriction was minimal the replenishment of the feed was sufficient to maintain a constant enrichment factor but where restriction was too great then problems associated with poor flow contol could arise as the permeate composition varies greatly with linear feed flow rate.

Fig 3.50 Effect of linear feed flow rate on the enrichment factor.

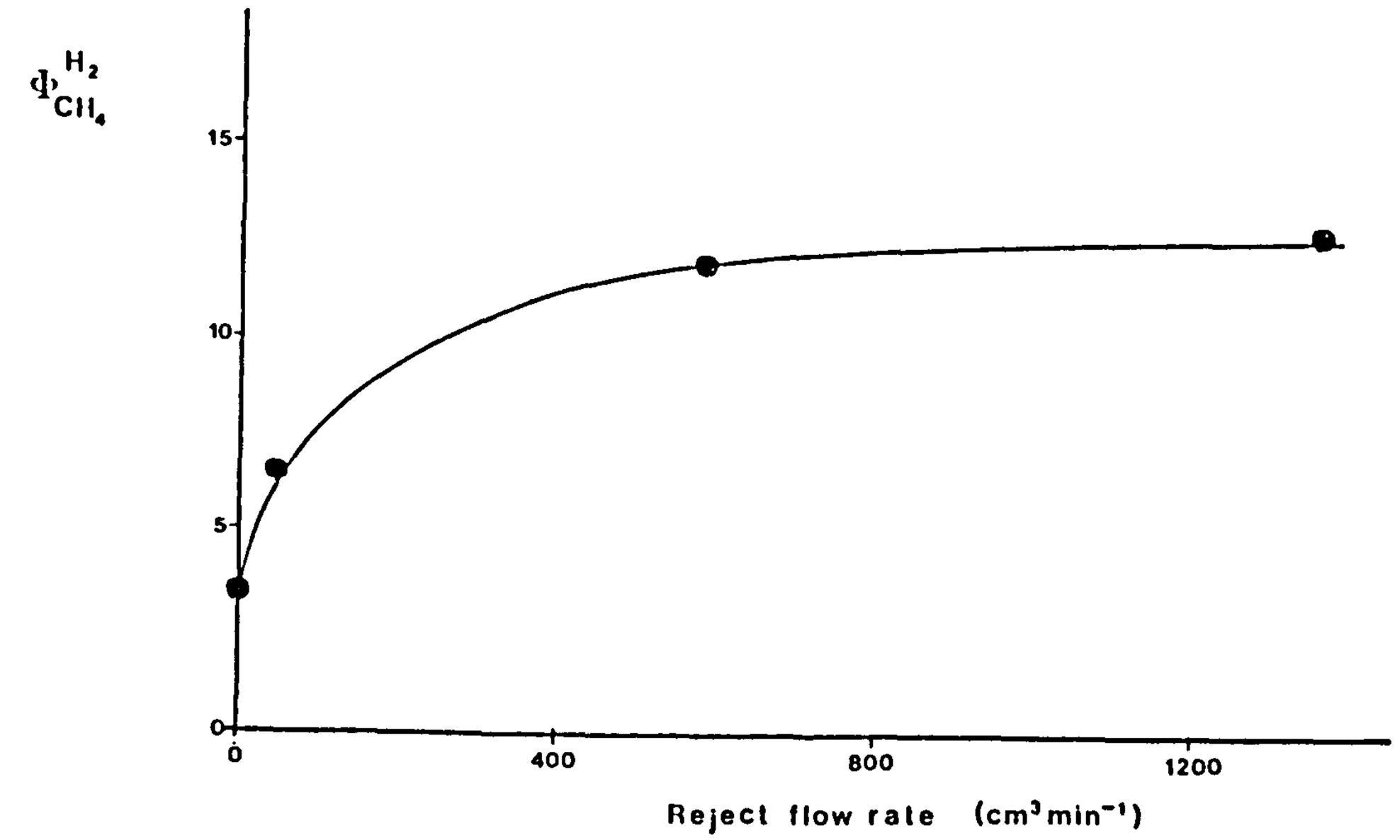

Fig 3.51 Effect of restricted feed on permeate composition.

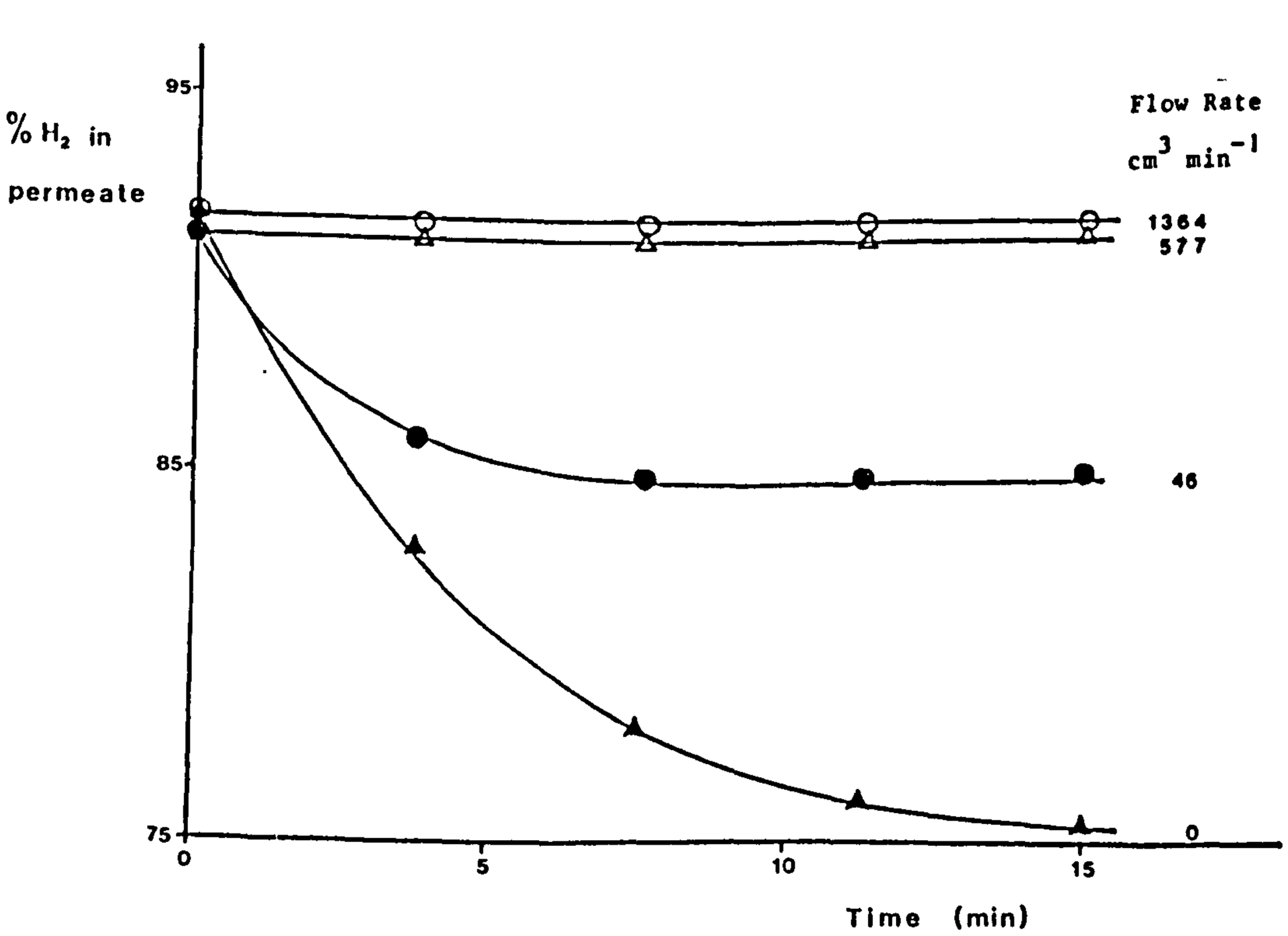

3.3.10 The effect of pressure on gas transport properties.

According to the permeation equation (3.22) the permeation rate constant ought to be independent of the differential pressure, as for any hollow fibre membrane the permeation rate (Q) should only be directly proportional to the pressure of the permeating species (dp).

i.e.

$$Q = {}'P\ A\ dp \qquad (3.22)$$

The dependence of the permeation rate constant on the differential pressure was examined using both single gases and binary gas mixtures. Tables 3.27 & 3.28 show measurements made using single gases on coated modules from batches 35/1g and 38/1a and Table 3.29 shows the results for a coated module of 38/1a when subjected to a binary gas mixture of hydrogen and methane.

Table 3.27 Effect of pressure on the nitrogen permeation rate constant of batch 35/1g (coated).

dp (psi)	$'P\ N_2$ (GPU)	dp (psi)	$'P\ N_2$ (GPU)
100	1.81	550	1.66
200	1.74	600	1.62
246	1.80	650	1.61
293	1.75	700	1.61
350	1.75	750	1.56
400	1.71	800	1.56
450	1.68	850	1.53
500	1.69		

Fig 3.52 Effect of differential pressure on $'P_{N_2}$ (Batch 35/1g).

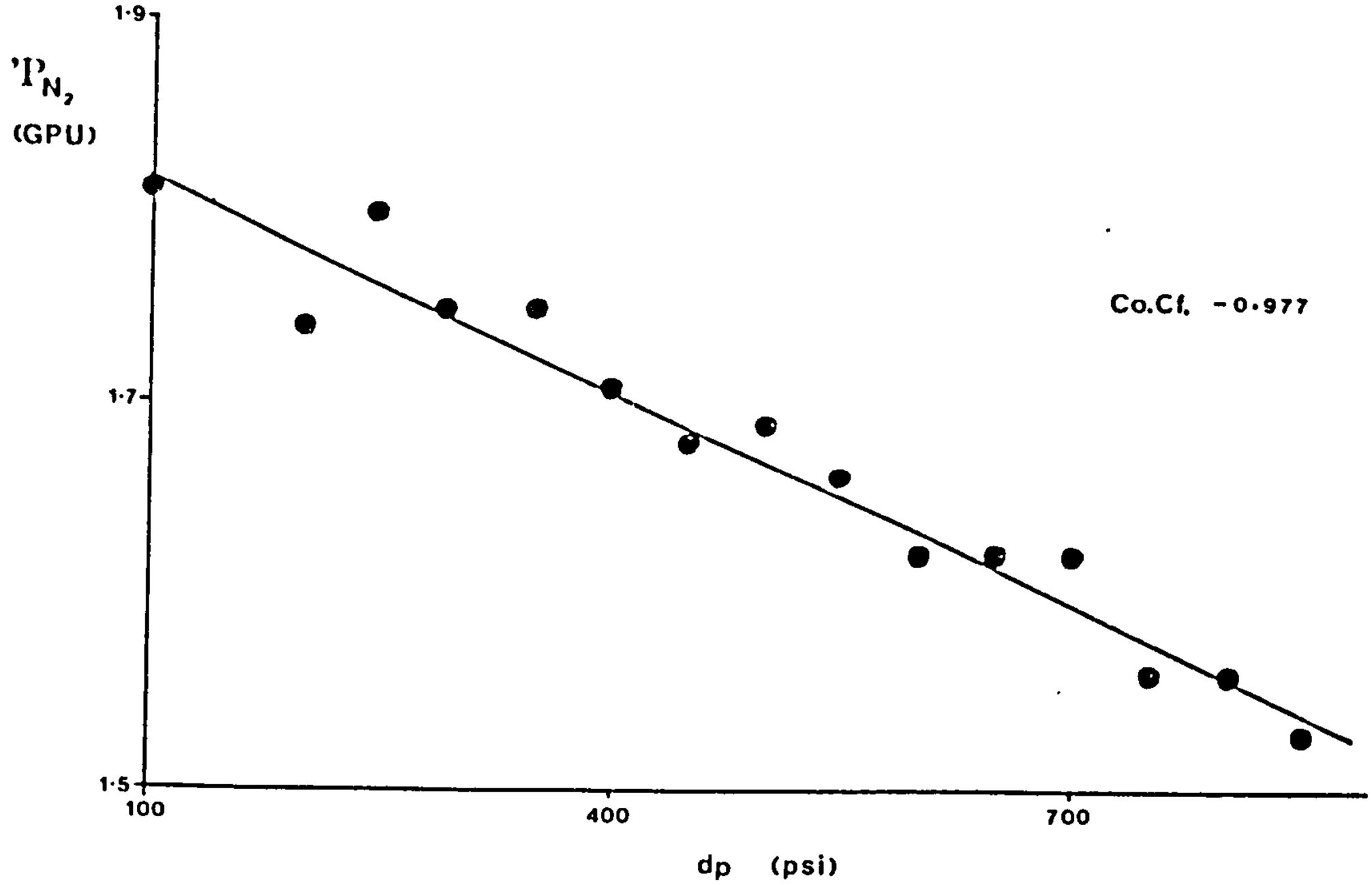

The linear drop in the nitrogen permeation rate constant with increasing differential pressure is shown in Fig 3.52. This drop in the permeation rate was attributed to an increase in the effective thickness of the membrane,

$$\frac{P_i}{z} = {}'P_i \qquad (3.23)$$

the permeation rate constant ($'P_i$) being the permeability (P_i) per unit thickness of membrane (z). This suggests that under conditions of high pressure the membrane is compressed. The force of compression would tend to close the interstitial space between the polymer nodules, discussed in section 3.2.4. This would lead to an increase in the effective thickness of the membrane, i.e. the amount of polymer the penetrant must pass through on its journey from the high pressure side of

the membrane to the low pressure side. If this is the case, then the fibres of batch 35/1g increase their effective thickness by 1.24 times when subjected to a seven times increase in differential pressure.

Table 3.28 Effect of pressure on the gas transport properties of batch 38/1a (coated).

dp (psi)	$'P\ H_2$ (GPU)	$'P\ CH_4$ (GPU)	α_{H_2,CH_4}
50	115	40.5	2.83
100	119	45.9	2.58
150	128	51.1	2.50
200	138	59.3	2.33
250	153	72.5	2.12
300	166	85.2	1.95
350	190	114	1.67
400	227	--	--

Table 3.29 Effect of pressure on the pseudo permeation rate constant & enrichment factor of batch 38/1a (coated).

dp (psi)	dw H_2 (psi)	dw CH_4 (psi)	Π_{H_2} (GPU)	Π_{CH_4} (GPU)	$\Phi^{H_2}_{CH_4}$
50	19	31	70.2	37.0	1.38
100	40	60	73.3	44.8	1.32
150	62	88	78.6	52.5	1.31
200	83	117	87.0	61.7	1.24
250	105	145	104	80.4	1.17
300	127	172	120	98.2	1.12
350	149	201	141	116	1.10
400	171	229	155	133	1.08
450	193	257	170	149	1.07
500	216	284	192	173	1.05

The results of batch 38/1a, however, show the opposite trend to those of batch 35/1g. A pronounced rise in the permeation rate constant was observed with increasing differential pressure. Lai et al. [77] suggest that this kind of pressure dependent permeability may arise due to the presence of pin-hole defects. This explanation certainly fits very well with the results of batch 38/1a. The levels of separation factor calculated for this batch are of the level associated with Knudsen

Fig 3.53 Effect of differential pressure on $'P_i$ (Batch 38/1a).

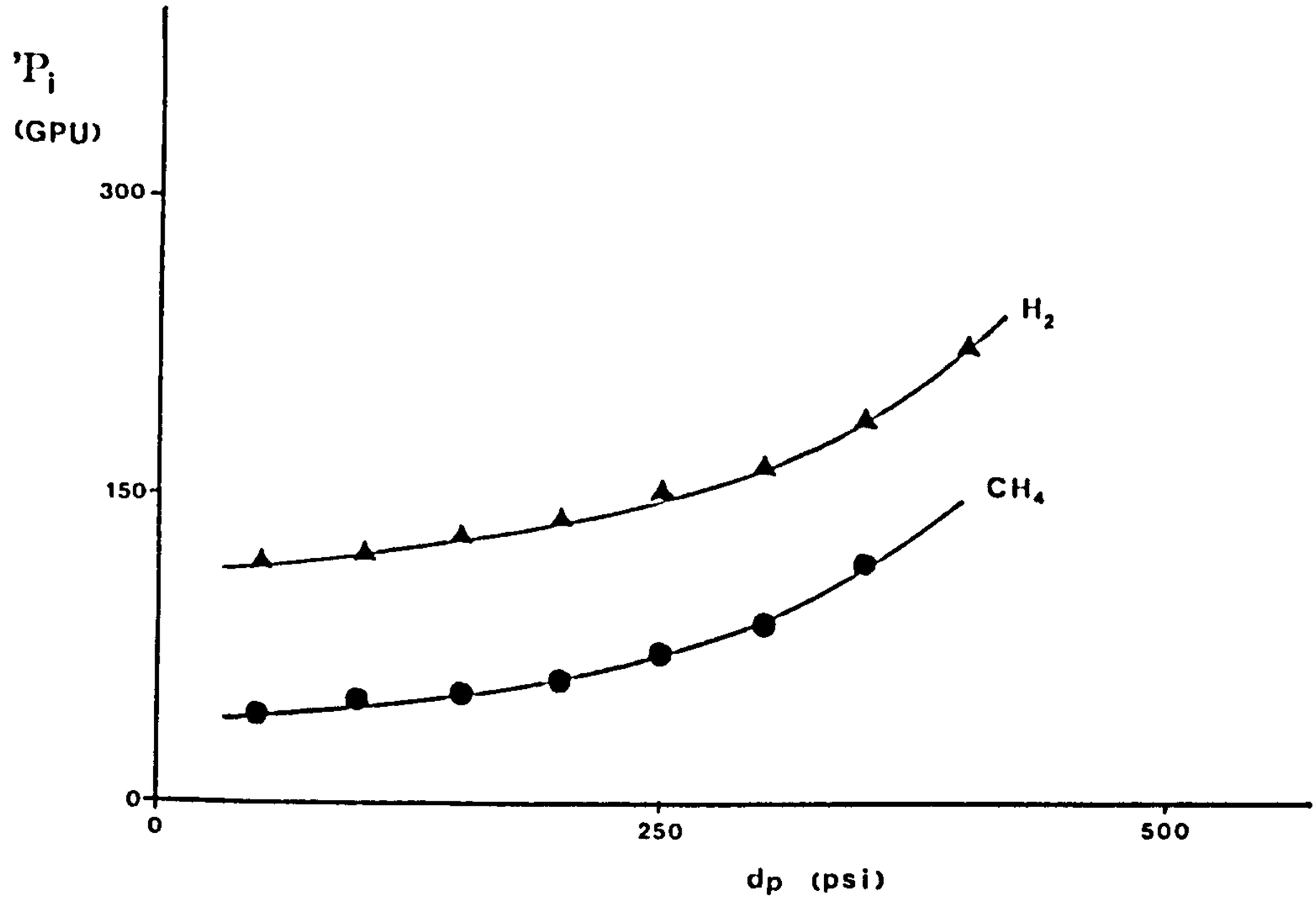

Fig 3.54 Effect of differential pressure on Π_i (Batch 35/1g).

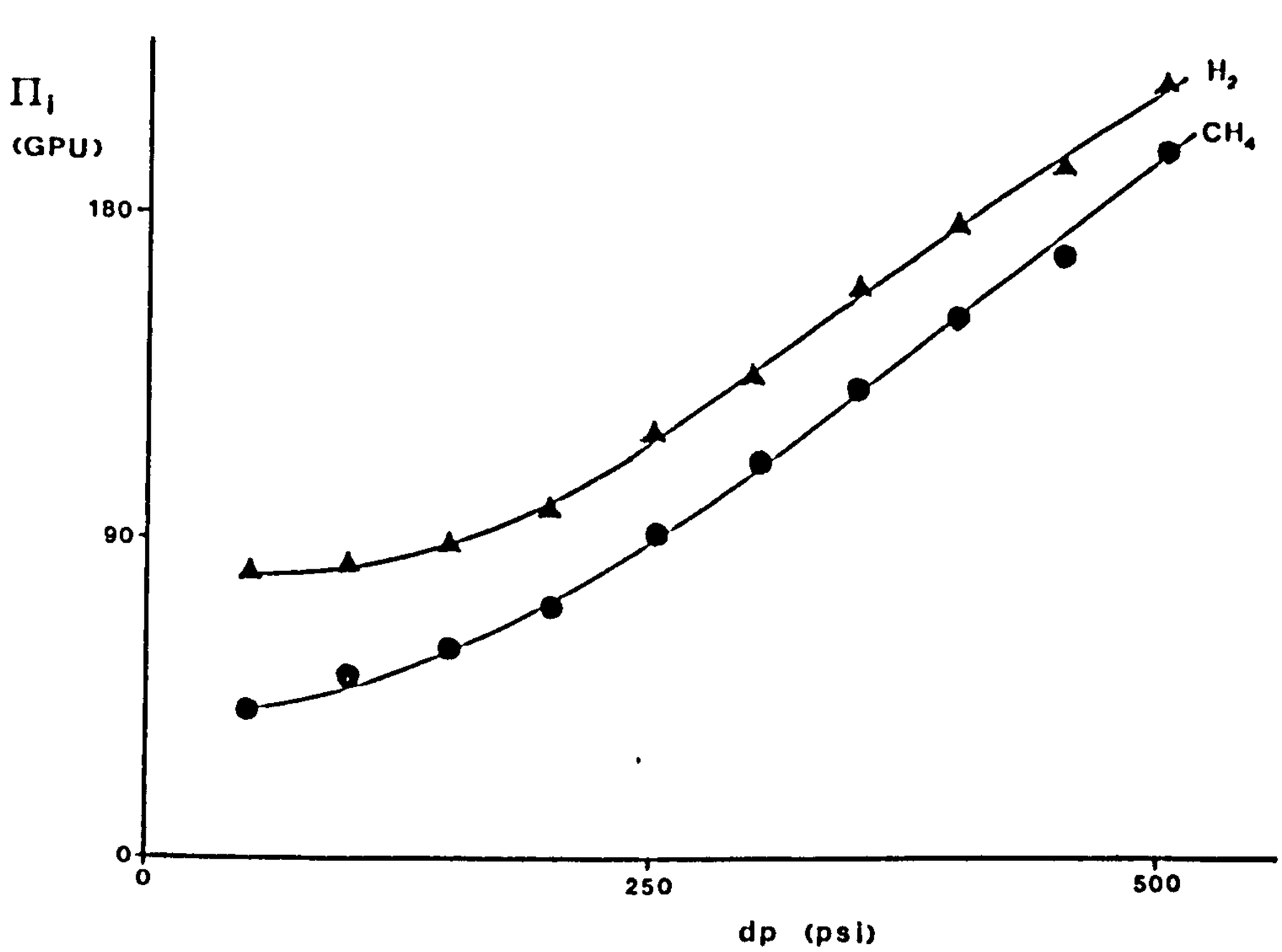

flow separation, suggesting that almost certainly defects are present in the permselective surface layer. In a region where a defect exists, a faster rate of permeate flow will occur compared to that of a defect free region. Thus the ratio of J_i : dp will be greater in a module containing surface defects than in an undamaged module. The significance of this is that the permeation rate constant (directly proportional to J_i/dp) will rise with increasing dp. Fig 3.53 shows this rise for batch 38/1a based on the single gas measurements.

Fig 3.54 shows the variation of pseudo permeation rate constant with differential pressure for batch 38/1a. Notice that above a differential pressure of 200 psi the pseudo permeation rate constant appears to increase linearly with increasing pressure difference. This suggets that above this level the proportion of the gas travelling through the defects increases in proportion to the pressure difference. It was also noted that the slopes of the two gases were converging indicating a drop in the separation factors. Fig 3.55 shows a linear drop in the separation factor (as calculated from single gas measurements), whilst Fig 3.56 shows the non linear decrease in enrichment factor (as calculated from the binary mixture studies).

It is interesting to note that separation factors below 2.8 were recorded for hydrogen/methane separation in both single gas and mixture studies. These were the first values recorded which were below the level associated with Knudsen flow separation. This decrease in separation factor to below 2.8 may possibly be attributable to the change in the mean free path of the penetrants as a result of the increased pressure difference. This would tend to cause a change from Knudsen separation values to viscous flow values. However, the separation values recorded were below that which could be attributed to viscous flow and so these low values remain unexplained.

Fig 3.55 Effect of differential pressure on the separation factor.

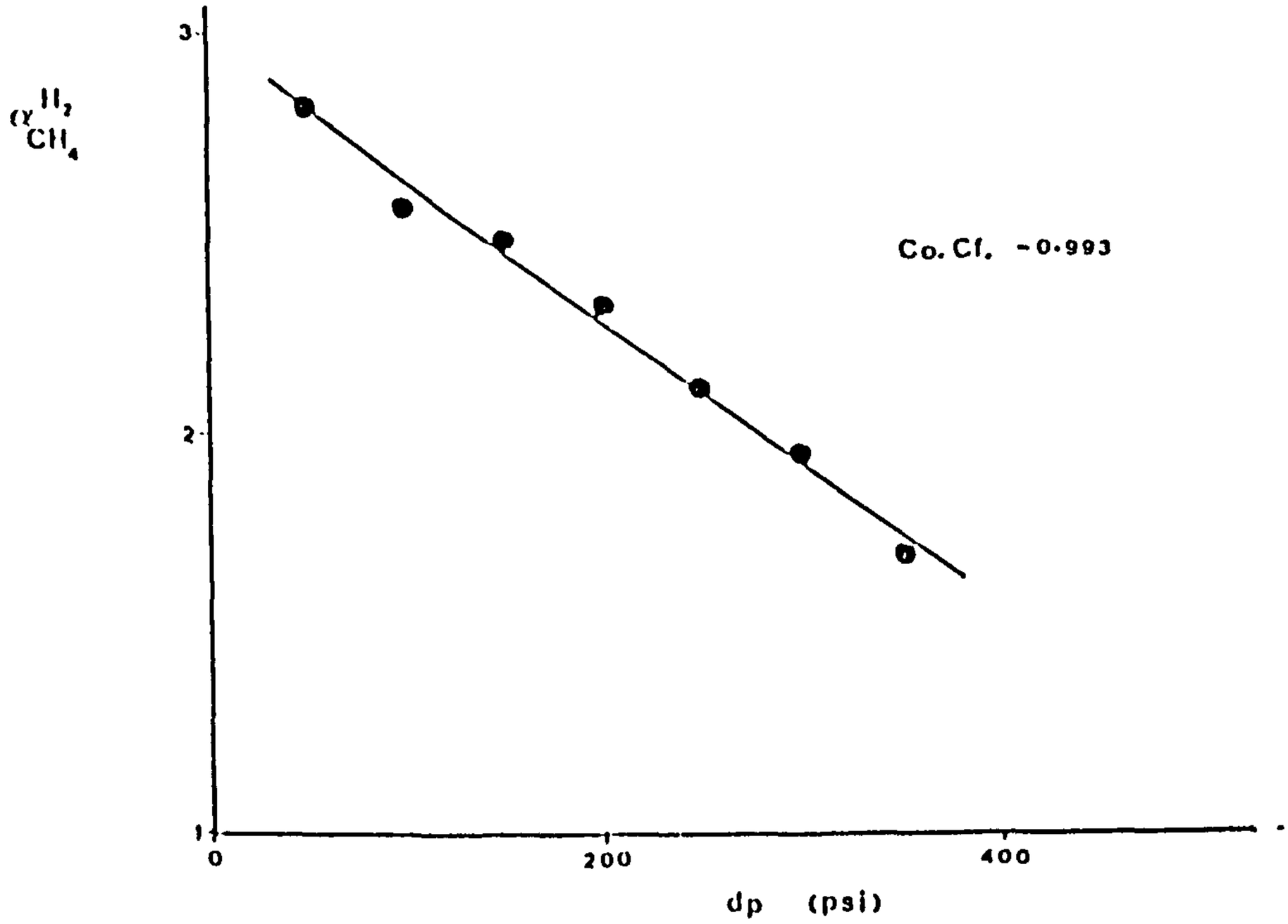

Fig 3.56 Effect of differential pressure on the enrichment factor.

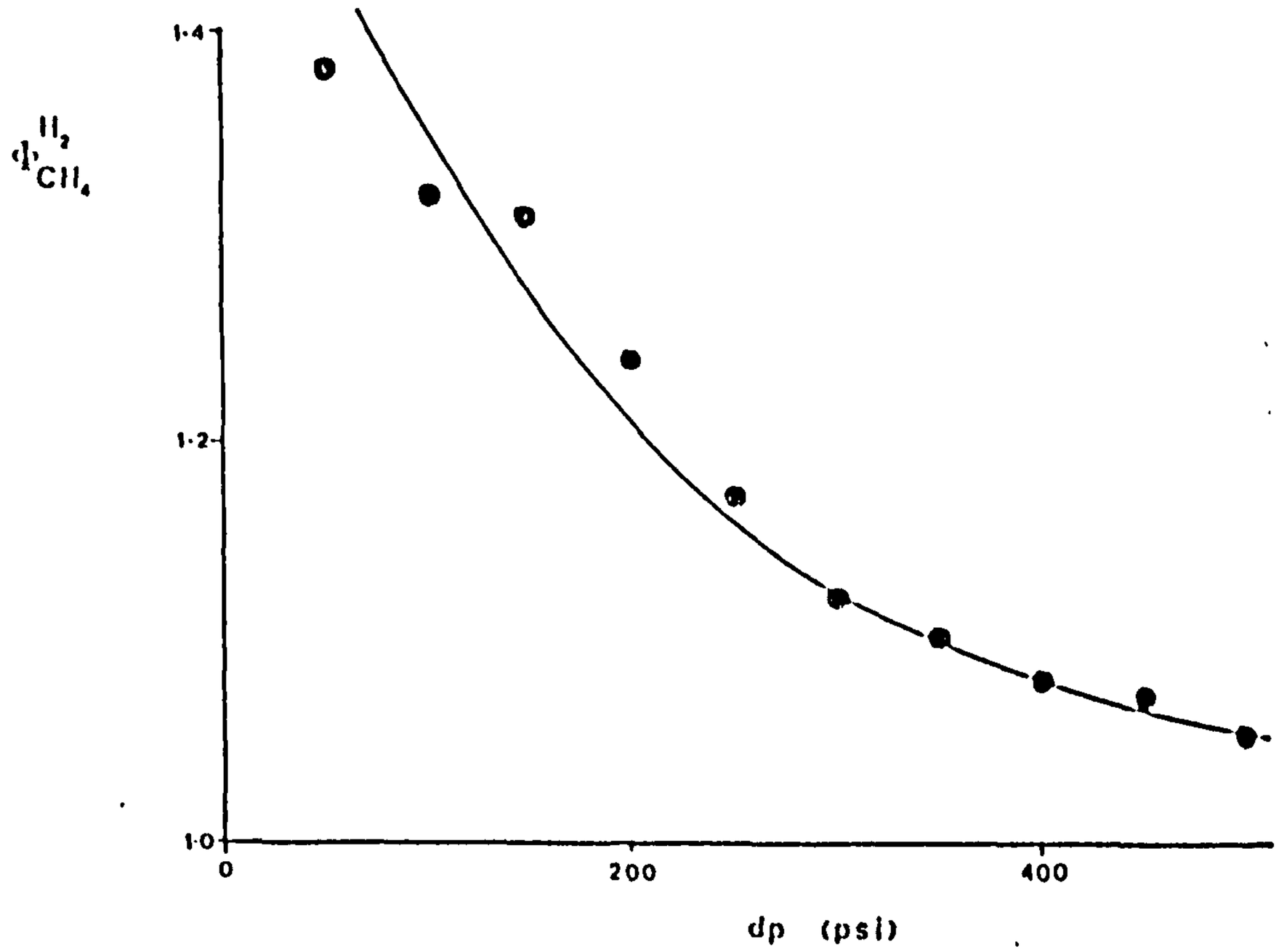

3.4 Routes to improved permeation performance.

3.4.1 Introduction.

The previous sections have shown that the hollow fibres made in the present study had adequate permeability but the selectivity was often poor, barely suitable for industrial usage. It was decided that one pathway to more selective membranes lay in changing the polymer. Noshay and Robeson [65] have reported (see Table 3.30) that superior gas transport properties can be attained using sulphonated polysulphones, in comparison with the unsulphonated polymer. Hollow fibre membranes were also produced from sulphonated poly(ethersulphones) by V. Rogers [78], using 32% zinc nitrate (aq) as coagulant and DMF as solvent, but the fibres produced exhibited permeation rates below the minimum measurement level. S.E.M. examination showed that the porosity of the membrane was too low (see plate 3.26).

Table 3.30 The effect of sulphonation on gas permeability [65].

Degree of sulphonation	Permeability,[a]			Separation Factor	
($-SO_3Na$/PSf)	H_2	CO_2	CH_4	H_2/CH_4	CO_2/CH_4
0.0	1650	920	20	83	46
0.1	1085	330	--	--	--
0.5	900	214	5	180	43
1.0	270	82	1	270	82
1.0 (acid form)	762	187	--	--	--

[a] Dry films cast from DMF solution. Permeability units: (cc mil/100in^2 24hr atm).

Another possibility leading to modified permeation behaviour was sought by blending of the polysulphone. In this experiment V. Rogers blended polysulphone with small amounts of poly(2-vinylpyridine). The

fibres produced had permeation rate constants approximately one tenth of that exhibited by the unblended polysulphone (see Table 3.31). The separation factors of these uncoated fibres remained at the same levels irrespective of the blending. However, coating of these fibres was not considered worthwhile as the permeation rate constants would drop by too excessive an amount.

Table 3.31 Effect of blending polysulphone with poly(2-vinylpyridine).

Batch	% Concentration of Poly(2-vinylpyridine)	$'P_H$ (GPU)	$\alpha^{H_2}_{CH_4}$	$\alpha^{CO_2}_{CH_4}$
32/1a	0	1350	2.34	0.67
30/1a	5	97.6	2.38	0.73
31/1a	10	105	2.80	0.80

Changing the polymer completely or blending of the polysulphone with other polymers proved to be a difficult approach. The problems associated with finding a new set of spinning parameters to control the phase inversion process would be very time consuming and perhaps even insoluble. These conclusions encouraged the use of the already developed polysulphone system so that modifications of the permselective behaviour would have to be achieved by alteration of the spun fibres. A brief study of coating was made using the butadiene-styrene-vinylpyridine copolymer latex (already discussed in section 3.3.4). This showed that adding this material to the outer surface was ineffective as the extra layer caused too great a drop in the permeation rate constants. Any modification would have to be such that the permeation rate constants remained relatively constant. One approach would be to chemically alter the dense permselective layer, whilst maintaining the underlying porous structure of the polysulphone membrane. Two techniques were considered

toward this aim. Firstly, the possible use of plasma polymerisation techniques was examined [79 - 81]. Plasma polymerisation could be the ideal method of modification. The process does not require the use of liquid solvents - all reactions taking place in the gaseous/plasma phase. An enormous variety of modifications could be made to the membrane surface using these techniques so long as the surface layer did not start to break down resulting in the loss of polymeric material. Plasma polymerisation techniques were not practised during the period of the research due to the complexities involved in starting an investigation of this nature. The second method considered was the surface sulphonation of the membrane. It was hoped that the favourable results of Noshay & Robeson would also be exhibited by a Loeb-Sourirajan asymmetric membrane where only the permselective surface layer was composed of sulphonated polysulphone.

3.4.2 Surface sulphonation of hollow fibre membranes.

Various sulphonating agents were considered for this study. Sulphur trioxide was chosen for its ability to be applied from the gas/vapour phase. The limitations of liquid solvents were established earlier during the coating experiments where it was realised that only a limited number of liquids could come in contact with the polysulphone hollow fibres without the risk of changing the underlying morphology of the membrane. The possibility of a gas phase reaction was, therefore, favoured.

Polysulphone was found to react readily with the sulphur trioxide vapour. Reaction was easily demonstrated by the ability of a reacted membrane to take up a stain from contact with an aqueous solution of a basic dye. The fact that a basic dye was taken up showed that acidic

groups were present on the membrane surface. Unreacted membranes showed no staining even after prolonged exposure to hot solutions of the dyestuff. Exposure times of less than 10 seconds to the SO_3 vapour were sufficient to produce immediate staining on contact with a cold solution of the dye.

After sulphonation the fibres of batch 35/1b were coated with the silicone elastomer in the normal manner. The gas transport properties of those modules tested are shown in Table 3.32.

Table 3.32 Gas transport properties of coated, sulphonated modules (Acid form).

Exposure Time (min)	Module N°.	Permeability (GPU)			Separation Factor	
		H_2	CH_4	CO_2	H_2/CH_4	CO_2/CH_4
0.0	1	52.2	7.18	72.6	7.27	10.1
	2	50.7	5.49	60.5	9.23	11.0
	3	63.2	3.95	51.4	16.0	13.0
	$\bar{x}$	55.4	5.54	61.5	10.0	11.1
1.0	4	66.1	4.51	48.8	14.7	10.8
	5	68.3	7.01	64.4	9.7	9.18
	6	50.6	3.10	37.7	16.3	12.1
	$\bar{x}$	61.7	4.87	50.3	12.7	10.3
1.5	7	16.8	0.31	3.84	54.0	13.3
	8	78.2	2.99	50.4	26.2	16.9
	9	18.2	0.70	4.39	26.1	6.30
	$\bar{x}$	78.2	2.99	50.4	26.2	16.9
2.0	10	70.5	4.73	65.0	14.9	13.7
	11	16.5	1.28	4.80	12.9	3.80
	$\bar{x}$	70.5	4.73	65.0	14.9	13.7

Interpretation of the results can be a little misleading as two changes appear to take place. In modules 7, 9 & 11 a big drop in the permeation rate constants was observed, whilst the other modules tended to show some increase in the hydrogen permeation rate constant and a slight decrease in the methane permeation rate constant. However, the variability of the results makes it difficult to confirm this trend. Although the levels of improvement experienced by Noshay and Robeson were not obtained, some improvement in the separation factor was achieved without the usual decrease in permeability.

Modules 7, 9 & 11 showed a much reduced level of permeation rate constant. The precise reasons for this are not clear. It may be that the SO_3 vapour has completely re-structured the surface layer of the membrane, producing a more dense structure, as observed in the fibres spun from sulphonated polyether sulphone (plate 3.26). Dense surface layers would naturally cause a decrease in the rate of permeation. However, this should be coupled with an appreciable increase in the separation factor. Modules 7 & 9 do show an increase in the hydrogen/methane separation factor, but poor results for carbon dioxide/methane separation.

Following exposure to the SO_3 vapour, the fibres were immersed in water to quench the reaction. In the following case, the modules were immersed in a dilute solution of sodium hydroxide in order that the sodium salt of the sulphonic acid might be produced. Noshay and Robeson used the Na^+ salt in the majority of their gas separation membranes. The results from modules prepared in this manner are shown in Table 3.33.

Table 3.33 Gas transport properties of coated, sulphonated modules (Na^+ salt).

Exposure Time (min)	Module N°.	Permeability (GPU)			Separation Factor	
		H_2	CH_4	CO_2	H_2/CH_4	CO_2/CH_4
0.0	1	52.2	7.18	72.6	7.27	10.1
	2	50.7	5.49	60.5	9.23	11.0
	3	63.2	3.95	51.4	16.0	13.0
1.0	12	129	31.5	62.5	4.10	1.99
	13	70.5	4.84	52.2	14.6	10.8
	14	38.3	4.02	48.9	9.52	12.2
2.0	15	1193	417	259	2.86	0.62
	16	permeation rate above measurable range				

Five modules were examined. All but one of the modules were adversely effected by the treatment. Exposure to the SO_3 vapour for two minutes followed by neutralisation in 1.5 g l^{-1} NaOH (aq) produced a membrane structure with surface defects of such magnitude that the silicone coating could not repair them. Evidence for this is apparent from the very high permeation rates and Knudsen separation values obtained. With the one minute treatment, enormous variability was recorded. All that can be said from analysis of the data is that no benefit was produced by neutralisation in the sodium hydroxide solution. It may be the case that the solution of NaOH used was of too high a concentration resulting in damage associated with high heats of neutralisation.

A single module was exposed to the SO_3 vapour for ten minutes and the fibres were then examined using S.E.M. The images produced are shown in plates 3.27 & 3.28 together with an unsulphonated fibre (plate 3.29) for comparison. What is immediately evident is that the SO_3 vapour has caused considerable change to the surface of the fibre. Certain areas appear to have been etched away. However, the changes in these regions are more subtle. If the surface had been merely etched

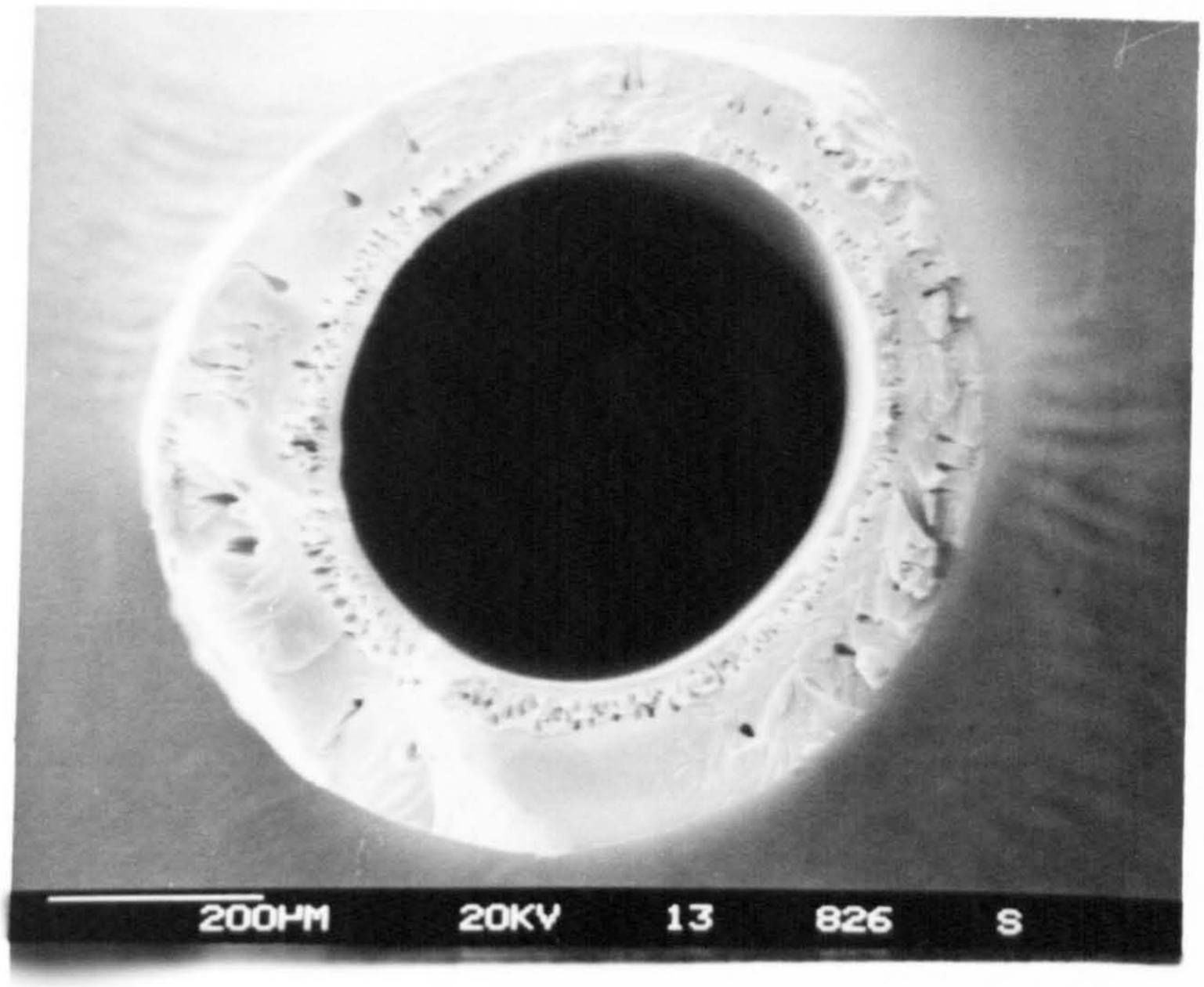

Plate 3.26 Cross-section of sulphonated poly(ether sulphone)[78]

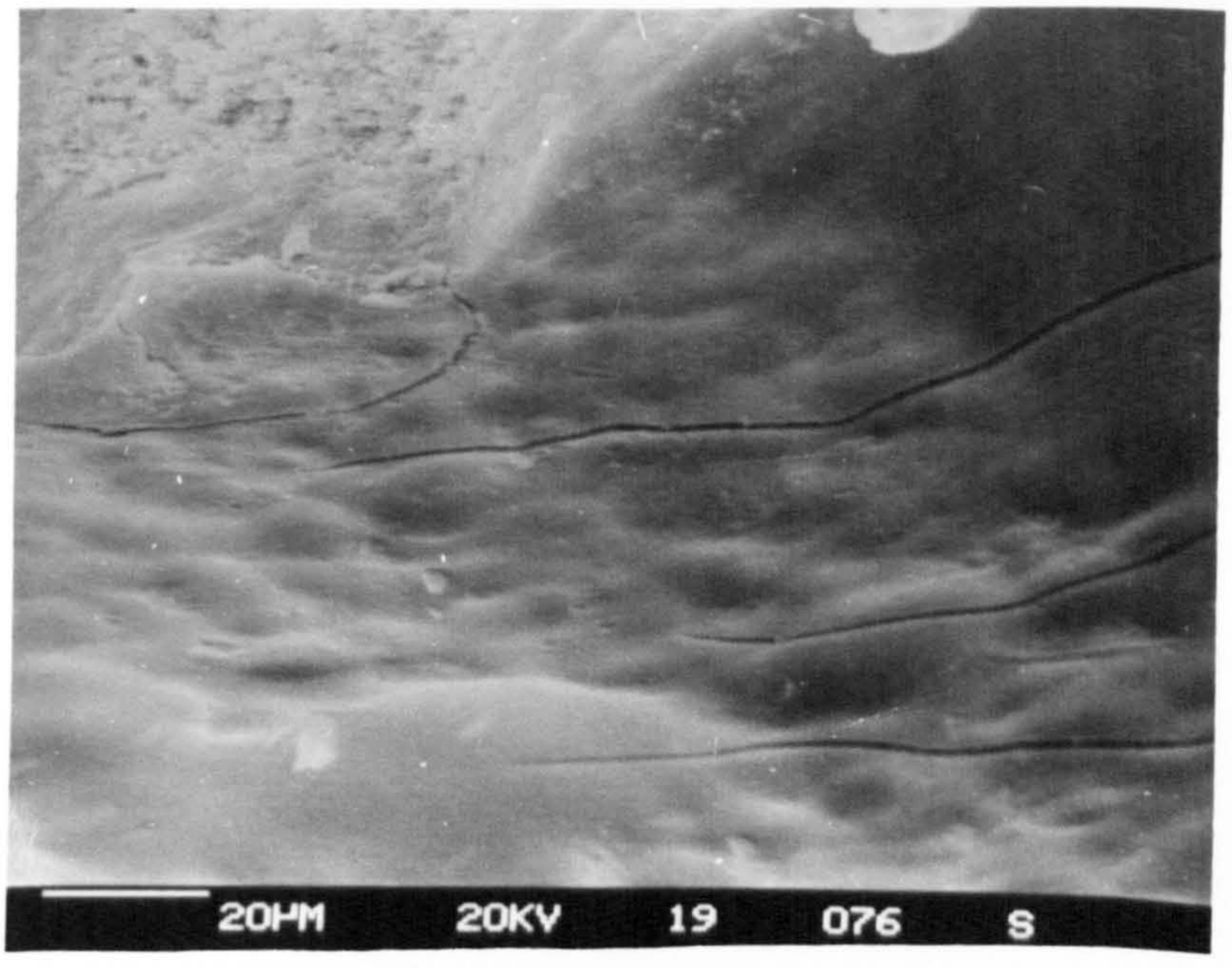

Plate 3.27 Sulphonated fibre.

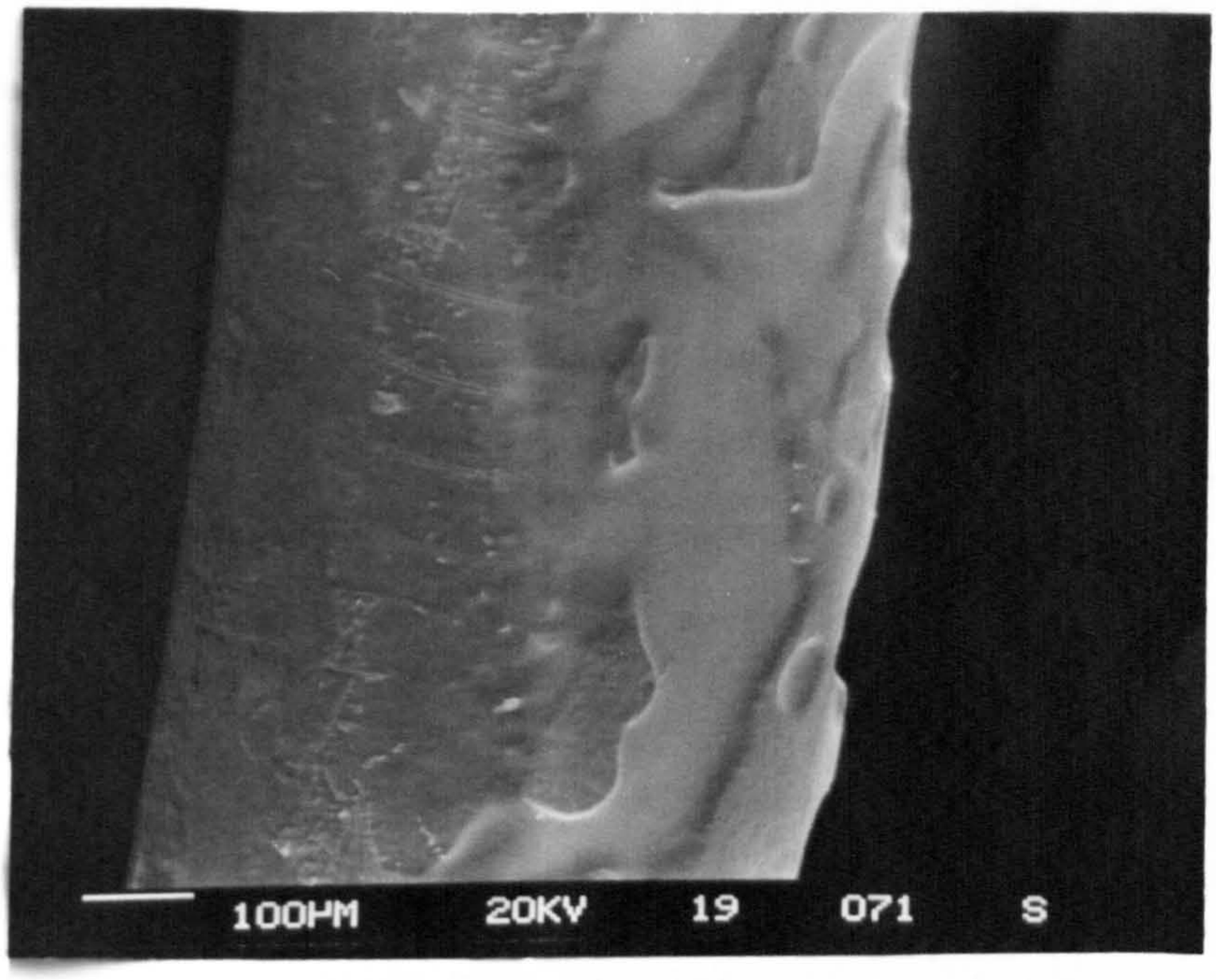

Plate 3.28 Sulphonated fibre

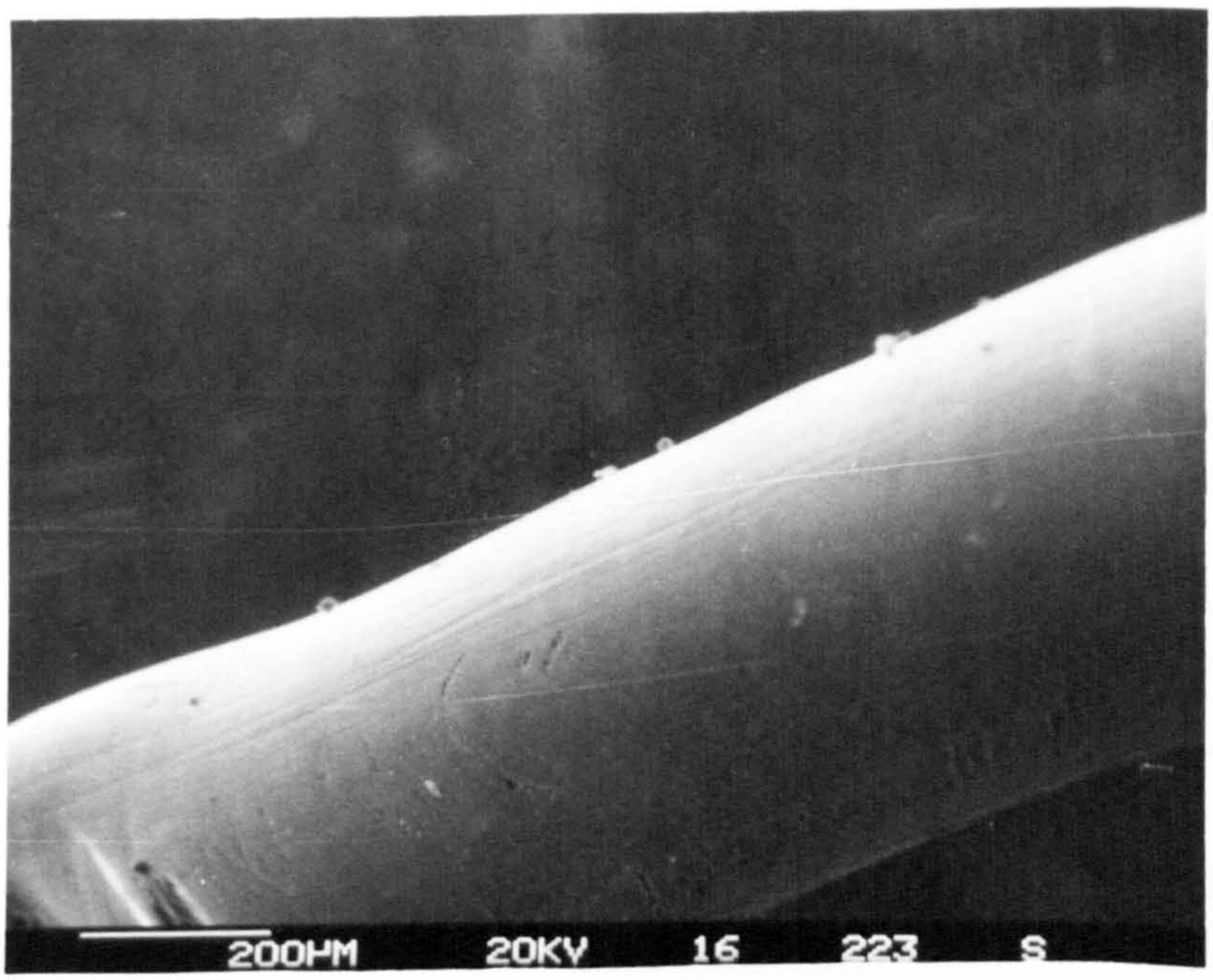

Plate 3.29 Fibre before sulphonation

away then the porous structure of the underlying B_o zone would be observed. This is clearly not the case as the 'etched' zone has a smooth surface. A more likely explanation is that the SO_3 has transformed the surface into a region of very dense polymer. This is consistent with the results obtained in the permeation experiments. The other structural features of note are the deep cracks which appear in the surface orthogonally to the fibre axis. These cracks would be deleterious in gas separation situations as they would provide pathways of low resistance to flow, bypassing the selective surface layer. Cracks such as these probably account for the high permeation rates observed in the sodium sulphonate type modules.

In conclusion, the aims of these surface sulphonation experiments cannot be said to have been fully achieved. However, these preliminary experiments do provide some encouragement. The fact that the separation factors were increased without a drop in the permeation rate of the faster permeating species tends to suggest that further achievements in this direction may be possible. Progress probably lies in the refinement of the sulphonating technique. At present the method is crude. The exposure times are too short to be controlled with any useful degree of accuracy. The controlled release of vapour into the sulphonating chamber was very primitive as was the circulation of the vapour within the chamber. If, after modification of the technique, the vapour phase sulphonation is still considered too severe then it may be necessary to use a sulphonation technique involving a liquid phase (e.g. using the SO_3 / $(C_2H_5O)_3PO$ complex as described by Noshay and Robeson). The number of sulphonic acid groups introduced to the membrane was unknown. In future it may be possible to quantify this by measuring the dye uptake of the fibres during staining.

In addition, the introduction of acid groups may permit subsequent chemical modification by further reactions with the in-situ acid groups.

CHAPTER FOUR

Conclusions

4.1 General summary and conclusions.

(a) Elimination of macrovoids.

The elimination of macrovoids from the morphology of the hollow fibre membranes was sucessfully achieved. The methods described by Frommer et al. [43,48] were generally effective. The inclusion of the nonsolvent formamide, as used by Monsanto [56], was found to be the most effective solution in terms of complete elimination and in being a method which did not involve an increase in the % polymer in dope formulations.

The precise mechanism in which the formamide acts to prevent the formation of macrovoids remains unclear, but the observations made on the mixing of formamide with the main precipitant (water) suggest a competitive interaction takes place which results in a reduced rate of precipitation.

In comparison to the above methods the presence of solvent in the coagulation bath (even at high concentrations) had a negligible effect on the morphology of the membranes precipitated.

The elimination of macrovoids was expected to improve the ability of the membranes to withstand high differential pressures. Certainly, the 1-Fp:Fa membranes had a much improved pressure tolerance, but the membranes spun from the higher % polymer DMAc type dopes showed no improvement in collapse pressure.

(b) Prediction of fibre dimensions from spinning parameters.

The relationships between the spinning parameters studied and the hollow fibre dimensions were successfully determined. Precise equations for predicting the fibre dimensions were not produced due to the

inability to predict or even determine the porosity of the membrane. The % void volume parameter, discussed in Sections 2.4.5 and 3.2.4, did not produce useful results. Too many errors combined to produce results with too great a variability for any constructive evaluation of the membrane porosity to be made.

The model derived for the prediction of fibre dimensions, although inoperable at the present time, should be of use in a modified form in the future if the drying shrinkage and fibre porosity elements can be successfully determined.

(c) Observations on fibre morphology.

The concentration of polymer in the dope formulation was known to affect the permeation rate constants of the membranes spun from the dopes. Observations made on the morphology of the membranes led to the conclusion that the discrete nature of the voids, produced from the higher concentration dopes gave rise to an increased effective thickness of the membrane resulting in the lower permeation rate constants.

It was thought that the difference in mean microvoid size of the 1-Fp:Fa type fibres, compared to the DMAc type, arose from the difference in coagulation rate, a slower coagulation produces larger voids (discounting macrovoids). This conclusion could be seen to support Strathmann's [42] analogy to crystal growth.

The 9:1 1-Fp:Fa type fibres were found to have skin layers consisting of polymer nodules, which were generally of a coarser size than those observed in the skins of the 1-Fp and DMAc type fibres. This observation was thought to account for the much greater permeabilities encountered in the uncoated 1-Fp:Fa type fibres in comparison to the DMAc type.

(d) Effect of coating.

A considerable improvement in performance can be achieved using the silicone elastomer coating material, as used by Monsanto [56]. The other coating material tested did not result in any improvements in the gas transport properties of the membrane to which it was applied. The reasons for this were considered to be two fold. Firstly, the coating material must be post-cured to allow the small pre-cured elements to be drawn into the surface defects during the impregnation stage. Secondly, the permeability of the material must be as high as possible. Only when both criteria are satisfied can the coating material be expected to improve membrane performance.

(e) Prediction of the gas transport properties of the membranes.

Two approaches were made toward this aim, i.e. from information about the spinning parameters and from information about the fibre dimensions. Some useful relationships were established, but the understanding of the system remains insufficient to produce a model to allow predictions to be made.

(f) Gas mixture studies.

Examination of the gas transport properties of a membrane subjected to a gas mixture revealed different values in comparison to those predicted by the single gas studies. The enrichment factors were

consistently lower than the predicted separation factors, but as they were lower by more or less a constant amount it was concluded that the simple gas measurements were of value for evaluating the membrane performance.

The lower rate constant values recorded in the gas mixture studies were not expected, but the rather simplistic model derived for a hypothetical membrane showed a possible explanation for these lower values.

No evidence was found from the mixture studies to show that CO_2 plasticizes the membrane causing enhanced pseudo permeation rate constants, in contrast to the observations made using a succession of single gases in the single gas studies.

The flow rate of feed gas through the permeator chamber proved to be of importance in the mixture studies. Low flow rates were shown to improve the raffinate purity at the cost of a high degree of slippage whilst a high flow rate produced a higher purity permeate, but little difference in the composition of the raffinate from the feed.

(g) Effect of pressure on the gas transport properties.

It was concluded that for a membrane with no surface defects the permeation rate constant could rise as a result of increasing differential pressure. The mechanism by which this could occur was thought to be by compaction of the porous membrane resulting in an increased effective thickness of the membrane. Where a membrane contained defects in the surface layer it was concluded that the permeation rate constant could decrease as a result of increasing differential pressure.

(h) Improved permeation performance.

The difficulties in finding suitable phase inversion conditions for a polymer to produce a hollow fibre membrane of correct porosity, etc. suggest that the most time effective method of trying to improve permeation performance lay in the chemical modification of the surface layer of an already spun polysulphone hollow fibre.

Sulphonation of polysulphone was predicted to produce some improvement following the work of Noshay and Robeson [65]. Modifications were made to the surface without the usual large decrease in the permeation rate constants which was characteristic of the blending, coating and sulphonated poly(ethersulphone) experiments. It was, therefore, concluded that the method was of value either in a modified form or as an intermediate step in a reaction sequence.

4.2 The results in comparison to those of the Monsanto Co.

The procedure detailed by Monsanto [56] for the production of asymmetric hollow fibre membranes was used as the basis for the fibres produced for this research. Therefore, the membranes which were produced are of a comparable nature. Sufficient details are given in the patent examples, reproduced in Appendix 5, to allow a graph of membrane performance to be produced. Fig 4.1 shows the performance characteristics of the 1-Fp:Fa type membranes compared to those of Monsanto. It is immediately evident that the fibres spun by Monsanto exhibited the better performance. Fig 4.1 suggests that the Monsanto fibres generally have both better separation factors and better permeation rate constants. Though the membranes are spun in almost an

Fig 4.1 Comparison of performance with Monsnto's published results.

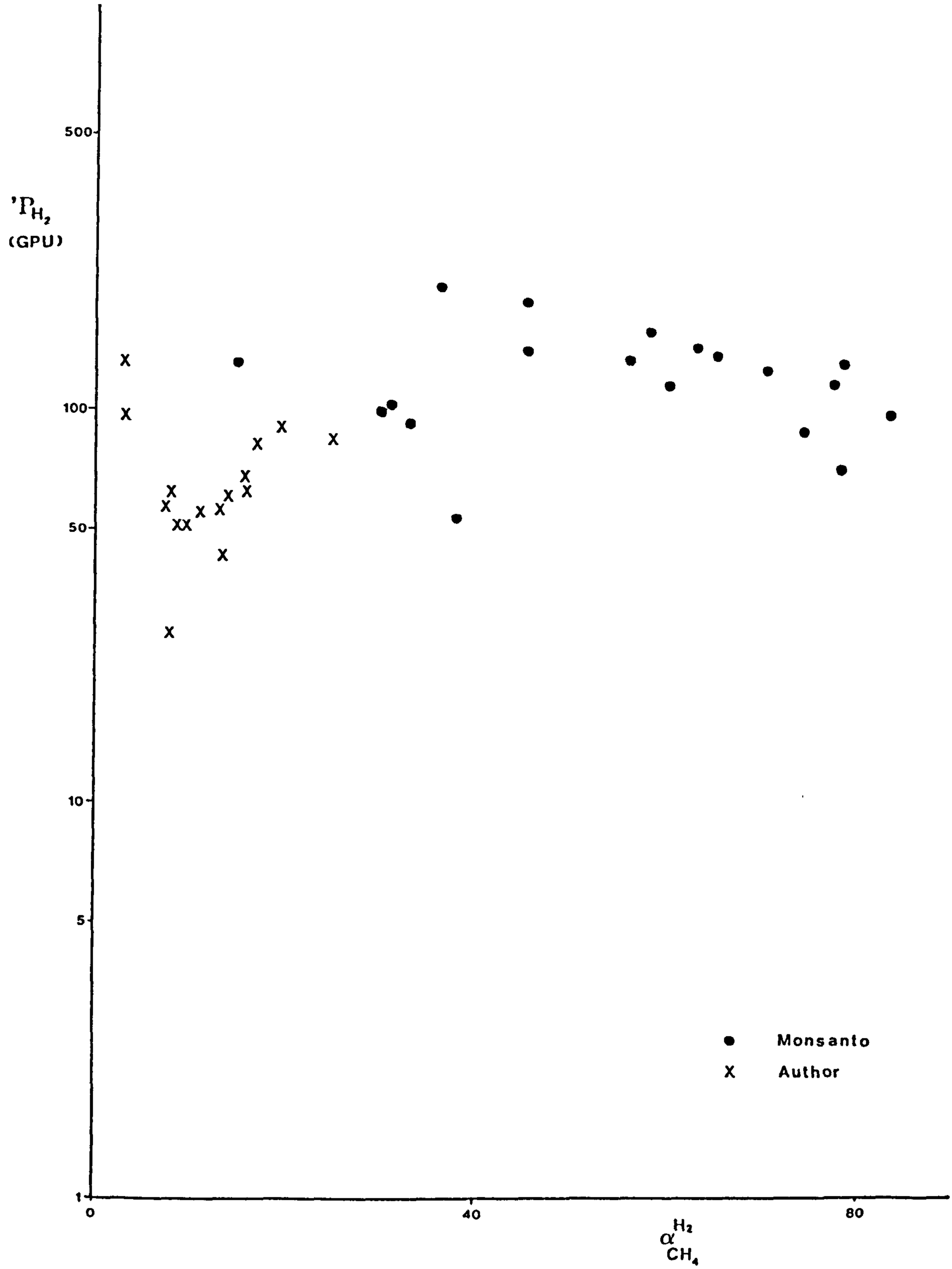

identical manner, it is not known under what conditions the fibres were tested. All that is known is that the operating differential pressure was above 7 MPa (1000 psi). However, it is difficult to believe that the differences in operating procedure could account for the large difference in the separation factors. Therefore, the reason for Monsanto's better performance is unknown.

It is interesting to note that the upward trend which was thought to exist in Fig 3.19 seems to have been followed in Fig 4.1 if the Monsanto data are considered as an extension to the 1-Fp:Fa data.

4.3 Suggestions for future work.

In discussing the results of Chapter 3 a few suggestions for future work have already been made. In this section suggestions are given for the direction in which the research work as a whole could continue.

(a) Hollow fibre membrane production.

It has already been mentioned that finding phase inversion conditions for a new polymer is a difficult process. Therefore, if the emphasis of future research is to be based on modification of polysulphone hollow fibres then what work needs to be done to improve the basic spinning process? The major spinning parameters have been evaluated. However, lack of information concerning the porosity of the membrane prevented a working model from being produced in order that membranes could be produced to pre-specified dimensions. Porosity characterisation could be achieved using mercury intrusion methods or by sophisticated image analysis. Given that characterisation is possible it is then necessary to discover what factors control the porosity of the

membrane. It seems likely that the porosity of the membrane is linked to the kinetics of the precipitation process and thus studies of the effects of dope and coagulation temperature, etc. could yield some useful correlations. Information of this type might then enable the ideal phase inversion conditions to be found for new polymers with less difficulty.

(b) Gas transport characteristics.

If an effective model could be produced to predict hollow fibre dimensions then the next step would entail the production of membranes to enable a better understanding of the gas transport characteristics and their relation to membrane structure.

Understanding of the interaction of gases in a mixture undergoing membrane separation is not well documented. The majority of membrane gas separation research appears to be conducted using single gases. The model produced in Section 3.3.8 is obviously a crude representation of mixture separation. Future workers might produce a more refined model using the well documented mathematical understanding of the permeation process.

As a result, the membranes could be assessed for a specific separation process. Only by setting down the requirements for a physical separation can the true effective performance of the membranes be realised.

(c) Improved permeation performance.

The results of the sulphonation experiments were encouraging. Future work could be concentrated on refining the sulphonation process and examining the possibility of subsequent reactions, possibly in the

gas phase, to further modify the permselective layer.

So far only sulphonation of the surface layer has been considered. Other reactions are possible. The use of plasma polymerization techniques appear to be a potentially productive direction for modification.

APPENDICES

Appendix One. Calculation of the solubility parameters of 1-formylpiperidine.

The total solubility parameter, ∂_T, and subparameters ∂_h, ∂_p and ∂_d were calculated using Small's method as described by Hoy [74] thus:-

$$\partial_T = \frac{\sum F_T + 135.1}{V_m} \qquad (A1.1)$$

where F_T = molar cohesion constant for a functional group in the solvent,

V_m = molar volume of the solvent.

A total solubility parameter of 11.6 (cal cm^{-3})$^{\frac{1}{2}}$ was obtained for 1-Formylpiperidine. The subparameters were then calculated by first calculating the Aggregation number (a):-

$$\log a = 3.39066 \frac{T_b}{T_c} - 0.15848 - \log V_m \qquad (A1.2)$$

where T_b = boiling point of the solvent,

T_c = critical temperature of the solvent.

The function T_b/T_c was estimated from Hoy's [74] tables of group constants and equation (A1.3):-

$$\frac{T_b}{T_c} = 0.567 + \sum \Delta_T - (\sum \Delta_T)^2 \qquad (A1.3)$$

where Δ_T = Lynderson atomic and group constant for critical temperature.

The subparameters were then calculated using equations (A1.4 - A1.6)

$$\partial_h = \partial_T \sqrt{\frac{a - 1}{a}} \qquad \text{(A1.4)}$$

$$\partial_p = \partial_T \sqrt{\frac{\sum F_P}{a \sum F_T}} \qquad \text{(A1.5)}$$

where F_p = polar molar cohesion constant for a functional group.

$$\partial_d = \sqrt{\partial_T^2 - \partial_p^2 - \partial_h^2} \qquad \text{(A1.6)}$$

For 1-formylpiperidine the subparameters were calculated to be:-

$$\partial_d = 8.67 \quad (\text{cal cm}^{-3})^{\frac{1}{2}}$$

$$\partial_p = 5.77 \quad (\text{cal cm}^{-3})^{\frac{1}{2}}$$

$$\partial_h = 5.17 \quad (\text{cal cm}^{-3})^{\frac{1}{2}}$$

From these values the fractional contributions were calculated:-

$$F_d = \frac{\partial_d}{\partial_d + \partial_p + \partial_h} \times 100 = 44\% \qquad \text{(A1.7)}$$

$$F_p = 29\%$$

$$F_h = 26\%$$

Appendix Two. Measurements of dope viscosity.

In order for a polymer solution to be spinnable by the wet-spinning (or dry-jet wet-spinning) process, it must fulfil various criteria of which viscosity is one of the more important. Monsanto [55] state that spinning solutions should have a viscosity within the range of 10 - 500 Pa s (100-5000 Poise). This viscosity range is important as solutions with too low a viscosity will not form a continuous filament during the extrusion/coagulation period, whilst too high a viscosity leads to problems in pumping the solution from the dope reservoir to the spinneret.

Measurements were made on a number of spinning solutions in order to determine viscosity values. It would, perhaps, have been of value to calculate the viscosity at the level of shear encountered during the extrusion from the tube-in-orifice spinnerets. Unfortunately due to the complicated geometry of the spinnerets the shear rates were not easily calculable and so values of viscosity were reported at zero shear rate, estimated by extrapolating back to the y axis on graphs of viscosity against shear rate (see Fig A2.1). All measurements were made using a Haake rotary viscometer (SV I assembly).

A short study on the effect of temperature on the 9:1 1-Fp:Fa type dopes was made in order to examine any correlation between viscosity and morphology. The usual Arrhenius type expression was found to apply (see Fig A2.2) and thus the viscosity of the dope at different temperatures could be easily calculated. At 50 ^{o}C. the 9:1 1-Fp:Fa type dopes (batches 25/1 & 24/3) were observed to have a viscosity of approximately 70 Pa s, lower than the other spinning runs. This facilitated the pumping of the normally highly viscous solution (> 300 Pa s at room temperature).

Fig A2.1 Viscosity / shear rate relationships of spinning dopes.

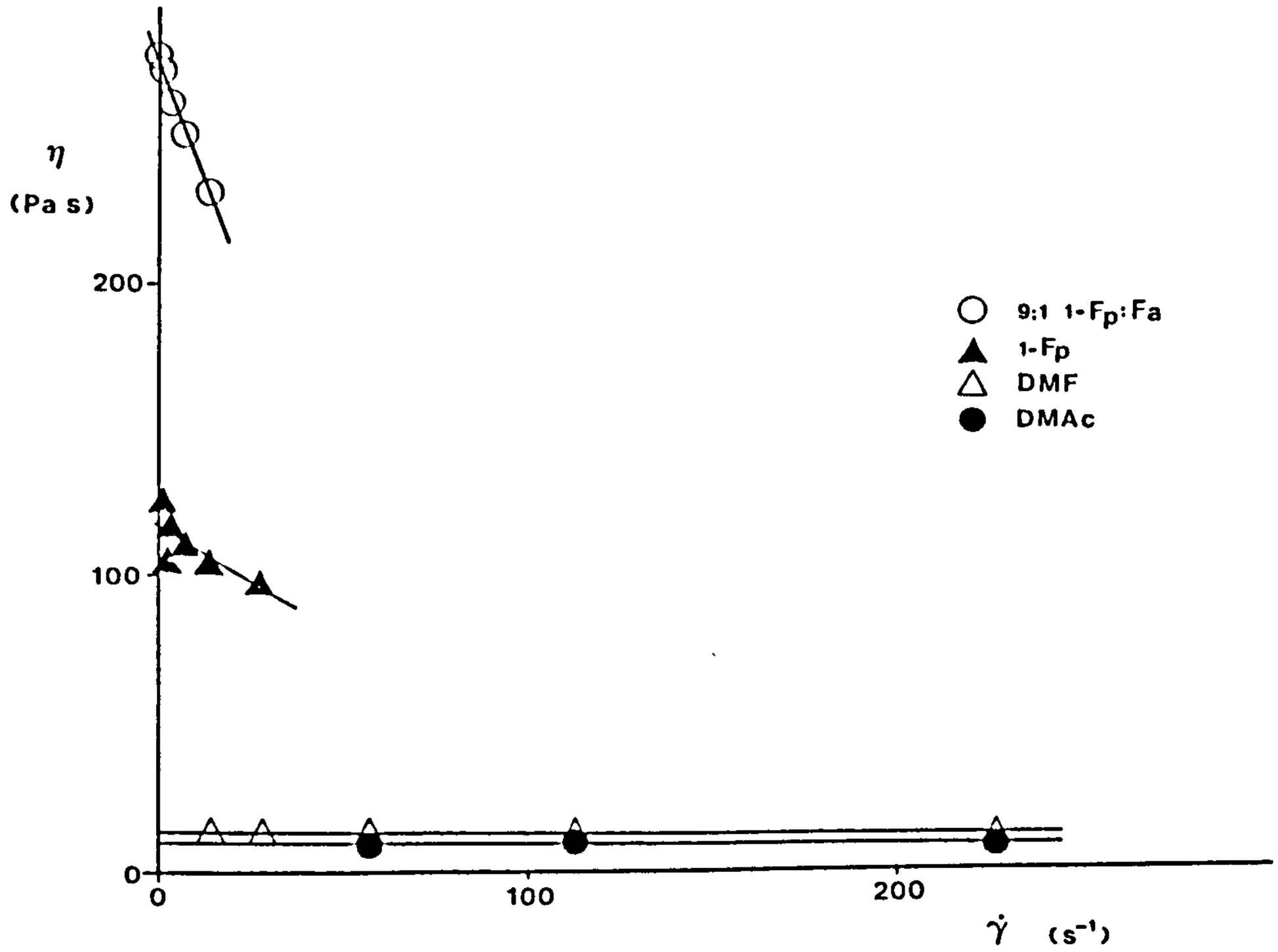

Fig A2.2 Effect of temperature on 9:1 1-Fp:Fa dope viscosity.

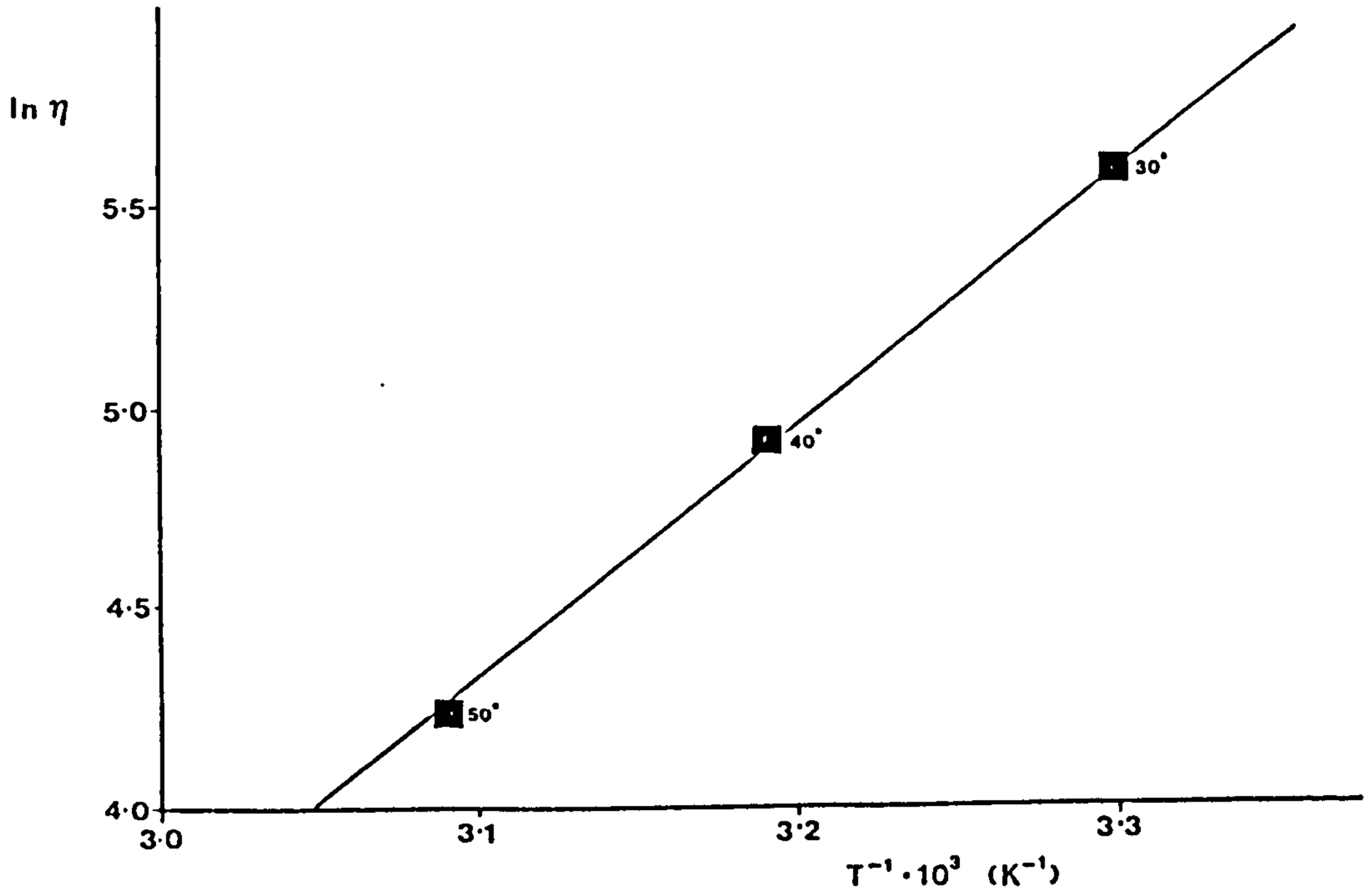

Appendix Three. Collapse of fibre membranes at high pressure.

Hollow fibres are a preferred membrane structure for two main reasons. Firstly, they are self-supporting and secondly, they are better able to withstand a differential pressure. As discussed in Section 3.1.1 the minimum pressure at which the fibres could collapse and still be industrially useful would be around 4 MPa (600 p.s.i.g.). Table A3.1 shows the collapse pressure for certain batches tested.

Table A3.1 Collapse pressure of fibres.

Batch	% Polymer	Liquid Carrier	Collapse Pressure (psi)
29/1a	30	DMAc	450
33/1a	35	DMAc	350
43/1b	40	DMAc	350
35/1g	30	95:5 1-Fp:Fa	>850

It was observed that the hollow fibres could undergo collapse by two different mechanisms. In the first, failure mode A, the permeate flow rate rapidly increases above a certain pressure. This was thought to be a result of holes developing in the surface layer allowing a passage of low resistance to develop between the high and low pressure sides of the membrane. An example of this mode is shown in Fig A3.1. In failure mode B the permeate flow rate fails to increase at a rate in proportion to the increase in differential pressure. This was thought to arise as a result of the membrane structure being compressed resulting in an increase in the effective thickness of the membrane. Fig A3.2 shows an example of failure mode B.

Failure mode B may be less serious in industrial terms as the membranes retain their selectivity after collapse. This means that if a few fibres fail the module can still function effectively, whereas a few fibres failing by mode A would cause a large degree of slippage.

Fig A3.1 Fibre collapse : Mode A.

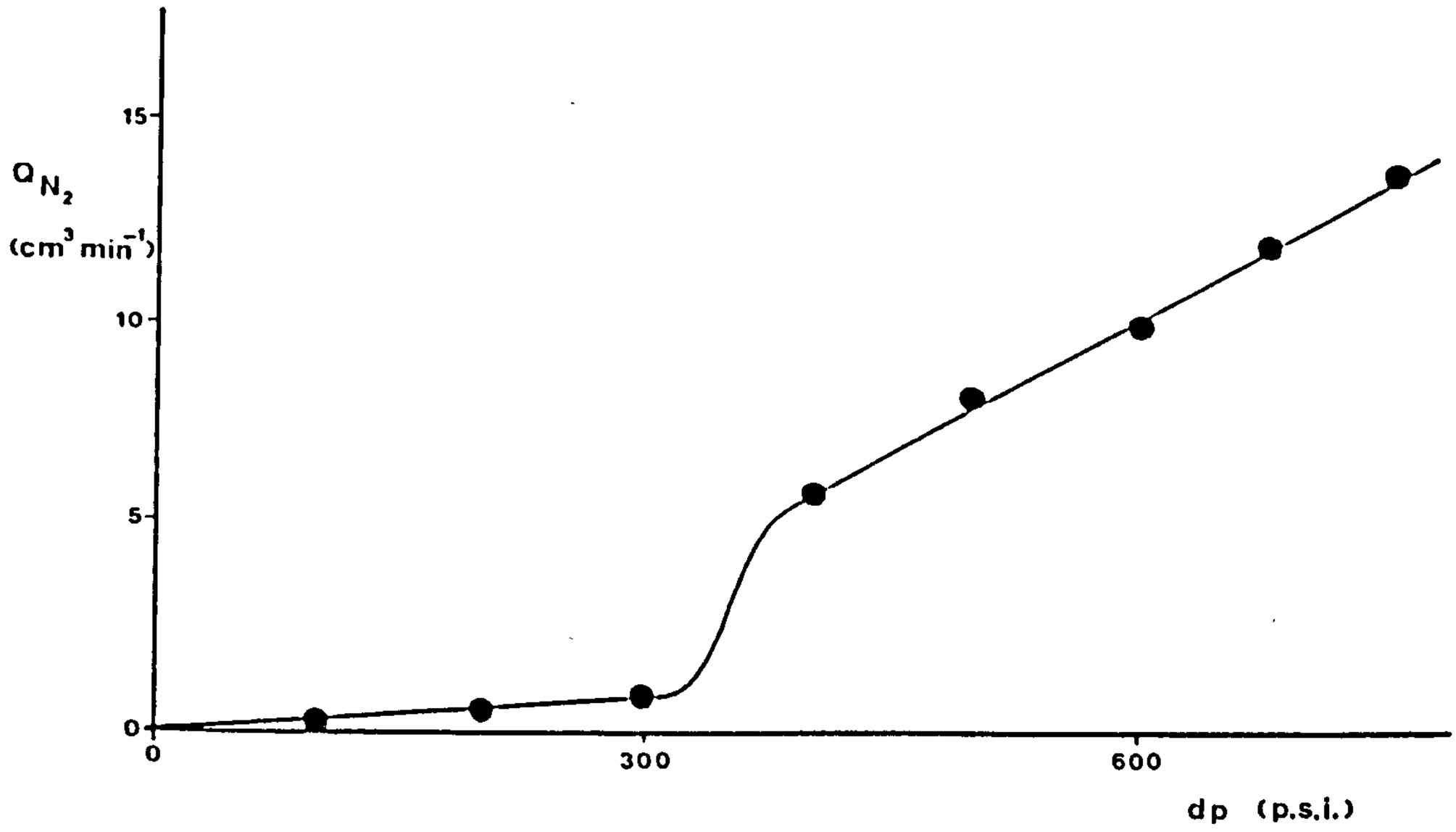

Fig A3.2 Fibre collapse : Mode B.

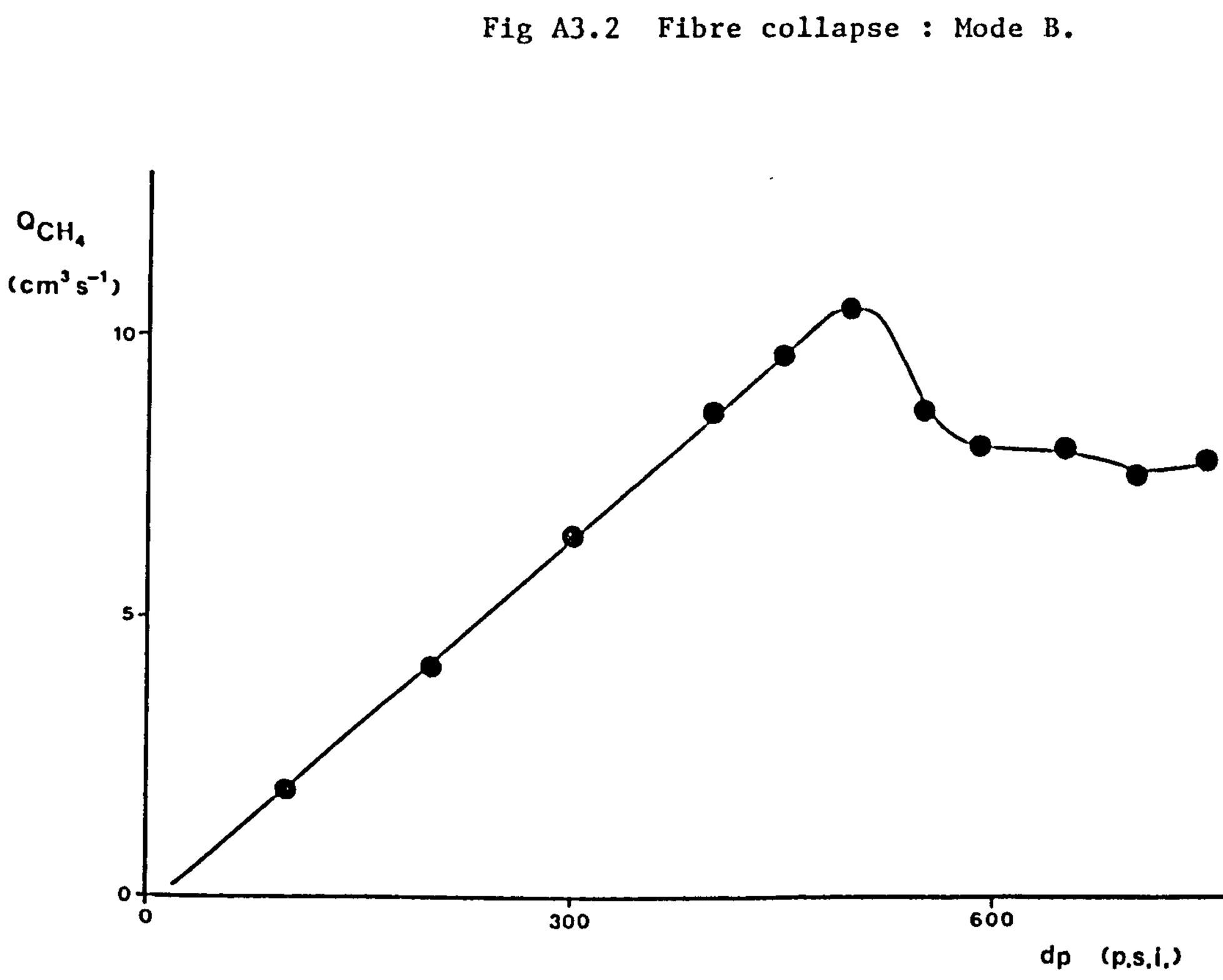

Appendix Four. Details of Spinning runs.

Each batch of fibres produced was identified by a code of the form:-

00/0a

where the first two digits refer to the spinning solution no.; the second number refers to the spinning run in which the dope was used. Usually this number was one, but higher numbers indicate that the preceding spinning runs failed to produce fibre. The final letter in the sequence was used to denote individual batches of fibre which were produced during a spinning run. Certain spinning runs were designed to examine the influence of a specific spinning parameter on the fibre structure and this was achieved by maintaining the other parameters constant.

Batches 11/3 and 11/4 were spun by the previous investigator and were included to provide extra data in order to establish the various relationships discussed in sections 3.2.3, 3.3.6 and 3.3.7.

All dopes were extruded from the spinneret at room temperature except runs 24/3 and 25/1 which were extruded at 50 ^{o}C. The coagulant was maintained below 10 ^{o}C. for all spinning runs conducted after 26/1. Batches 26/1d - 26/1f were the first to be produced with a chilled coagulant.

Table A4.1 lists the details of the fibres produced in the spinning runs and the following abbreviations and units apply to this table.

I.D. = Batch idenification code.
SPT = Spinneret used (see Table 2.1).
POL = % P3500 in dope by weight.
SOLVENT = Liquid carrier composition.
PER = Polymer extrusion rate ($cm^3\ min^{-1}$).
WIR = Water injection rate ($cm^3\ min^{-1}$).
WUS = Wind up Speed ($m\ min^{-1}$).
JS = Jet stretch ratio.
OD = Total diameter (μm).
ID = Lumen diameter (μm).
WT = Wall Thickness (μm).

Table A4.1 Details of spinning runs.

I.D.	SPT	POL.	SOLVENT	PER	WIR	WUS	JS	OD	ID	WT
11/3A	#1	35%	DMAC	4.0	0.75	10.2	0.61	674	335	150
11/3B				5.0	0.75	10.2	0.49	724	350	180
11/3C				2.2	0.75	10.2	1.10	512	310	90
11/3D				1.5	0.75	10.2	1.65	448	295	70
11/4A	#1	35%	DMAC	3.1	0.50	10.2	0.79	558	265	147
11/4B				3.1	1.00	10.2	0.79	621	365	128
11/4C				3.1	1.50	10.2	0.79	651	440	106
11/4D				3.1	2.50	10.2	0.79	719	510	105
11/4G				3.1	0.75	10.2	0.79	575	310	133
21/2A	#2	35%	DMAC	2.65	1.38	14.5	2.8	520	330	95
21/2B				2.21	1.38	14.5	3.4	485	330	70
21/2C				2.02	1.38	14.5	3.6	460	330	65
21/2D				3.10	1.38	14.5	2.3	540	340	100
22/1A	#3	30%	DMAC	3.21	1.38	14.7	1.8	540	340	100
22/1B				3.21	1.38	14.7	1.8	530	320	105
22/1C				3.21	1.38	14.7	1.8	520	310	105
22/1D				3.21	1.38	14.7	1.8	520	340	90
22/1E				2.35	1.38	14.7	2.4	490	310	70
22/1F				1.94	1.38	14.7	2.9	405	--	--
22/1G				1.53	1.38	14.7	3.7	400	--	--
22/1H				1.14	1.38	14.7	4.9	360	--	--
22/1I				3.21	1.38	14.7	1.8	520	320	100
24/3A	#3	30% 9:1 1-FP:FA		2.80	0.42	5.8	0.8	770	410	180
24/3B				2.80	1.38	5.8	0.8	770	530	120
24/3C				1.94	0.42	5.8	1.1	550	310	120
24/3D				1.53	0.42	5.8	1.5	500	260	120
25/1A	#3	30% 9:1 1-FP:FA		1.94	0.42	5.6	1.1	590	330	130
25/1B				1.94	0.42	5.6	1.1	575	325	125
25/1C				1.94	0.42	5.6	1.1	575	325	125
25/1D				2.80	0.42	10.3	1.4	500	260	120
25/1E				3.67	0.42	10.3	1.1	560	210	175
25/1F				1.53	0.42	5.7	1.4	510	280	115
25/1G				1.14	0.42	5.7	1.9	430	260	85
25/1H				1.94	1.38	5.7	1.1	620	450	85
25/1I				1.94	1.12	5.7	1.1	620	400	110
25/1J				1.94	0.69	5.7	1.1	600	340	130
25/1K				1.94	0.14	5.7	1.1	530	160	185
25/1L				1.94	0.42	5.7	1.1	570	300	135
26/1A	#4	30%	1-FP	2.80	0.42	5.6	0.4	620	240	190
26/1B				1.94	0.42	5.6	0.6	520	220	150
26/1C				1.14	0.42	5.6	1.1	450	260	96
26/1D				1.94	0.42	5.6	0.6	540	240	150
26/1E				1.94	0.42	5.6	0.6	500	220	140
26/1F				1.14	0.42	5.6	1.1	320	160	80

I.D.	SPT	POL.	SOLVENT	PER	WIR	WUS	JS	OD	ID	WT
29/1A	#3	30%	DMAC	3.67	1.38	12.0	1.3	608	364	122
32/1A	#5	30%	DMAC	2.80	1.38	12.0	1.0	561	347	107
33/1A	#6	35%	DMAC	3.55	0.42	14.7	1.6	485	210	120
35/1A	#7	30%	95:5 1-FP:FA	3.55	0.69	14.7	0.7	419	192	114
35/1B				2.37	0.69	6.2	0.5	546	286	130
35/1C				2.37	0.98	6.2	0.5	582	347	118
35/1D	#6			2.37	0.69	6.2	1.0	537	246	146
35/1E				1.94	0.42	6.2	1.3	510	244	133
35/1F				4.12	1.38	6.2	0.6	766	383	192
35/1G	#7			1.94	0.42	6.2	0.6	494	242	121
36/1A	#7	30%	95:5 1-FP:FA	2.37	0.56	6.5	0.5	629	375	127
37/1A	#7	30%	9:1 1-FP:FA	7.85	0.84	38.0	0.9	373	120	127
37/1B				0.76	0.84	6.2	0.6	535	273	191
37/1C				1.25	0.42	7.0	0.4	562	191	186
37/1D				1.25	0.14	7.0	0.4	525	157	184
37/1E				1.25	0.69	7.0	0.4	495	227	134
37/1F				1.25	0.98	7.0	0.4	514	261	127
38/1A	#6	30%	9:1 1-FP:FA	1.81	0.42	3.0	0.7	721	328	197
43/1A	#7	40%	DMAC	2.92	0.34	18.7	1.1	459	254	103
43/1B				1.81	1.38	14.4	1.4	395	305	45
43/1C				1.81	1.38	11.5	1.1	465	325	70
43/1D				1.81	1.38	6.9	0.7	580	420	80
43/1E				1.81	1.38	20.0	2.0	357	238	59
43/1F				1.81	1.38	16.8	1.7	365	260	53
43/1G				0.76	1.38	5.4	1.3	522	459	32
43/1H				1.25	0.84	9.0	1.3	424	290	67
43/1I				10.1	0.84	13.0	1.3	381	229	76
43/1J				13.2	0.84	17.0	1.3	362	210	76
43/1K				16.4	0.84	21.0	1.3	369	176	97
43/1L				19.9	0.84	25.0	1.3	357	167	95
43/1M				1.65	1.38	14.7	1.7	400	308	46
43/1N				1.25	1.38	14.7	2.1	369	285	37
43/1O				1.81	1.38	14.7	1.5	409	295	57
43/1P				2.37	1.38	14.7	1.1	447	295	76
43/1Q				2.92	1.38	14.7	0.9	474	289	93
44/3A	#2	30%	DMF	1.81	0.66	6.4	1.6	--	--	--
44/3B				1.81	0.66	11.9	2.9	406	275	66
44/3C				1.81	0.79	11.9	2.9	412	279	67
44/3D				1.81	0.92	11.9	2.9	493	353	70
44/3E				1.81	1.06	11.9	2.9	455	323	66
44/3F				1.81	1.19	11.9	2.9	445	316	70
44/3G				1.81	1.32	11.9	2.9	508	385	62
44/3H				1.81	0.52	11.9	2.9	412	240	91
44/3I				1.81	0.26	11.9	2.9	335	189	73
44/3J				1.81	0.10	11.9	2.9	366	125	120
44/3K				1.81	1.06	7.7	1.9	541	370	86
44/3L				1.81	1.06	11.3	2.8	425	306	60
44/3M				1.81	1.06	14.4	3.6	412	290	61

Appendix 5. Monsanto examples from U.K. Patent 2100181A.

The principal patent describing the work of Monsanto on producing asymmetric hollow fibre membranes for hydrogen / methane separation lists many examples of the process with fairly comprehensive information on the conditions employed. Table A5.1 lists several of these examples together with the gas transport properties of the fibres produced. No information regarding the rate of injection of internal coagulant was given for the examples quoted, merely a statement that it was, "at a rate sufficient to maintain the inside diameter of the hollow fibre." However, in their first example, not quoted in Table A5.1, a rate of 1.2 $cm^3\ min^{-1}$ was used.

The fibres were coated in a 1% solution of Sylgard 184 for ten minutes before the gas transport characteristics were determined. The precise details of the permeability rig and procedure were not given, but an operating pressure of 70 atm was used. The fibre dimensions were measured before drying in all the examples quoted except examples 5/a, 6/a, 7/a and 11/a where the dimensions were measured after drying. Wash times in excess of 190 hours were commonly used. The following abbreviations and units used in Table A5.1 are given below:-

I.D. = Batch idenification code.
SPT = Spinneret used (see Table a5.2).
POL = The grade of polysulphone used.
% POL = % polymer in dope.
SOLV RATIO = % solvent : % formamide in the liquid carrier.
PER = Polymer extrusion rate ($cm^3\ min^{-1}$).
WUS = Wind up Speed ($m\ min^{-1}$).
JS = Jet stretch ratio.
EX T = Extrusion temperature ($^oC.$)
CO T = Coagulant temperature ($^oC.$)
OD = Total diameter (μm).
ID = Lumen diameter (μm).
'PH2 = Hydrogen permeation rate constant (GPU).
H_2/CH_4 = Hydrogen / methane separation factor.

Table A5.1 Monsanto Patent Examples.

I.D.	POL.	% POL	SOLV RATIO	SPT	PER	WUS	EX T.	CO T.	JS	OD	ID	'PH2	H_2/CH_4
2/A	P3500	32	92.5:7.5	2	6.0	36.6	60	3	.96	416	134	124	70
2/B	P3500	32	92.5:7.5	2	6.0	38.1	60	3	.96	410	136	187	45
2/C	P3500	32	92.5:7.5	2	6.0	38.1	60	3	.96	416	136	157	58
2/D	P3500	32	92.5:7.5	1	7.1	42.7	53	2	1.15	425	150	132	56
2/E	P3500	32	90:10	3	8.3	42.7	53	1	.98	456	150	98	101
2/F	P3500	32	90:10	3	8.3	42.7	55	1	.98	448	148	117	77
2/G	P3500	32	87:13	3	8.3	42.7	52	3	.98	456	152	97	83
2/H	P3500	32	87:13	3	8.3	42.7	54	3	.98	448	149	130	78
2/I	P3500	32	90:10	2	6.0	30.5	55	1	.70	479	217	89	74
2/J	P3500	32	90:10	2	6.0	30.5	65	1	.77	445	205	142	63
2/K	P3500	32	92.5:7.5	4	7.1	42.7	64	2	1.75	406	146	131	15
5/A	P3500	36	87:13	2	5.0	45.7	52	3	-	364	165	123	95
6/A	P3500	38	87:13	5	6.0	30.5	70	3	-	444	171	136	65
7/A	P3500	38	87:13	6	6.0	30.5	70	3	-	439	131	205	36
11/A	P1700	40	87:13	5	9.0	30.5	70	4	-	439	154	143	60
13/A	200P	32	90:10	7	7.1	42.4	55	1	-	435	150	41	32
13/B	200P	32	90:10	7	7.1	42.4	50	1	-	435	150	47	47
13/C	200P	32	90:10	7	7.1	42.4	40	1	-	435	150	35	117

Table A5.2 Monsanto spinneret dimensions.

Spinneret	Orifice Diameter (μm)	Capillary Diameter (μm)	Capillary Bore Diameter (μm)
1	533	203	127
2	457	127	76
3	533	203	102
4	635	178	102
5	635	228	152
6	483	152	76
7	533	203	134

Appendix 6 Pressure units conversion table.

	Pa	psi	atm	cm Hg
1 Pa	1	1.450×10^{-4}	9.869×10^{-6}	7.501×10^{-4}
1 psi	6.895×10^{3}	1	0.065805	5.171
1 atm	1.013×10^{5}	14.70	1	75.999
1 cm Hg	1.333×10^{3}	0.1934	0.01316	1

REFERENCES

1 Laverty, B.W., and O'Hair, J.G., "4th BOC Priestley Conference", Royal Society of Chemistry, (1986), 291-311.

2 Kohl, A., and Riesenfeld, F., "Gas Purification", 3rd Edn., Gulf publishing (1979).

3 MacLean, D.L., "4th BOC Priestley Conference", Royal Society of Chemistry, (1986), 382-399.

4 Baldus, W., and Tillmann, D., "4th BOC Priestley Conference", Royal Society of Chemistry, (1986), 26-43.

5 Kirkby, N.F., "4th BOC Priestley Conference", Royal Society of Chemistry (1986), 218-230.

6 Maddox, R.N., Recent Developments in Separation Science, (1971) 1, 129-141.

7 MacLean, D.L., The BOC Group Technology Magazine, N°.5 (Oct. 1986), 38-45.

8 Lonsdale H.K., J.Memb.Sci., (1982) **10**, 81-181.

9 Michaels, A.S., Pure & Applied Chem., (1976) **64**, 193-204.

10 Matson, S.L., Lopez, J., and Quinn, J.A., Chem.Eng.Sci., (1983) **38**, 503-524.

11 Henis, J.M.S., and Tripodi, M.K., Science, (1983) **220**, 11-17.

12 Cooper, A.R., Chem. in Britain, (1984),**20**, 814-818.

13 Cabasso, I., Enc.Chem.Tech., 3rd Edn., Ed. Kirk, R.E., and Othmer, D.F., Wiley Interscience, (1980), **12**, 492-517.

14 Cabasso. I., "Material Science of Synthetic Membranes", Ed. Lloyd, D.R., A.C.S., (1985), 305-323.

15 Vieth, W.R., Howell, J.M., and Hsieh, J.H., J.Memb.Sci., (1976) 1, 177-220.

16 Lloyd, D.R., "Materials Science of Synthetic Membranes", A.C.S. Publ., (1985).

17 Kesting, R.E., "Synthetic Polymeric Membranes - A Structural Perpective", 2nd Edn., J.Wiley & Sons, (1985).

18 Sourirajan, S., "Reverse Osmosis", Logos Press, (1970).

19 Sourirajan, S., "Reverse Osmosis and Synthetic Membranes", Nat.Res.Council Canada, (1977).

20 Lonsdale, H.K., and Podall, H.E., "Reverse Osmosis Membrane Research", Plenum Press, (1972).

21 Lacey, R.E., and Loeb, S., "Industrial Processing with Membranes", Wiley Interscience, (1972).

22 Meares, P., "Membrane Separation Processes", Elsevier, (1976).

23 Crank, J., and Park, G., "Diffusion in Polymers", Academic Press, (1968).

24 Comyn, J., "Polymer Permeability", Elsevier, (1985).

25 Scott, J., "Hollow Fibres - Manufacture and Applications", Noyes Data Corp., (1981).

26 Hoornaert, P., "Reverse Osmosis", EPO.Appl.Tech.Ser., Vol 4, Pergamon Int.Info.Co., (1984).

27 Carman, P.C., "Flow of Gases through Porous Media", Butterworths Sci.Publ., (1956), 139.

28 Graham, T., Philos.Magazine & J. of Science, Ser.4, (1866) 32(218), 401-421.

29 Stern, S.A., "Industrial Processing with Membranes", Ed. Lacey and Loeb, Wiley Interscience, (1972), 279-339.

30 Rogers, C.E., et al., Rec.Dev.Sepn.Sci., (1972) 2, 107-155.

31 Rattee, I.D., and Bruer, M.H., "The Physical Chemistry of Dye Adsorption", Academic Press, (1974), 85-86.

32 Loeb, S., and Sourirajan, S., Adv.Chem.Ser., (1962) 38, 117.

33 Meares, P., "Synthetic Membranes; Science, Engineering and Applications", Ed. Bungay, B.M., et al., D.Reidel Publ., (1986), 155-168.

34 Meares, P., Trans.Faraday Soc., (1958) 54, 40-46.

35 Barrer, R.M., Barrie, J.A., and Slater, J., J.Pol.Sci., (1958) 27, 177.

36 Vieth, W.R., and Sladek, K.J., J.Colloid Sci., (1965) **20**, 1014-1033.

37 Sourirajan, S., and Agrawal, J.P., "Reverse Osmosis and Synthetic Membranes", Ed Sourirajan, S., Nat.Res.Council Canada, (1977).

38 Henis, J.M.S., and Tripodi, M.K., J.Memb.Sci., (1981) **8**, 233-246.

39 Henis, J.M.S., and Tripodi, M.K., Sepn.Sci.Tech., (1980) **15**, 1059-1068.

40 Kesting, R.E., "Synthetic Polymeric Membranes", 2nd Edn., J.Wiley & Sons, (1985), Chapter 7.

41 Strathmann, H., "Materials Science of Synthetic Membranes", Ed. Lloyd, D.R., A.C.S., (1985), Chapter 8.

42 Strathmann, H., Scheible, P., and Baker, R.W., J.Appl.Pol.Sci., (1971), **15**, 811-828.

43 Frommer, M.A., and Messalem, R.M., Ind.Eng.Chem., Prod.Res.Develop., (1973) **12**, 328-333.

44 Cabasso I., ACS.Symp.Ser.N^{O}.153, "Synthetic Membranes: Desalination, Vol 1", (1981), 267-291.

45 Panar, M., Hoehn, H., and Herbert, R., Macromolecules, (1973) **6**, 777.

46 Kamide, K., and Manabe, S.I., "Materials Science of Synthetic Membranes", Ed. Lloyd, D.R., A.C.S., (1985), Chapter 9.

47 Cabasso, I., "Ultrafiltration Membranes and Applications", Ed. Cooper, A., Plenum Press, (1980), 57-78.

48 Frommer, M.A., and Lancet, D., "Reverse Osmosis Membrane Research", Ed. Lonsdale H., and Podall, H.E., Plenum Press, (1972), 85-110.

49 Hwang, S.T., Choi, C.K., and Kammermeyer, K., Sepn.Sci., (1974), **9**, 461-478.

50 Yasuda, H., and Stannett, V., "Polymer Handbook", Ed. Brandrup, J., and Immergut, E.H., 2nd Edn., J. Wiley & Sons, (1975), III - 229-240.

51 Pilato, L.A., et al., ACS Polymer Preprints, (1975) **16**, 41-46.

52 Stannett, V.T., Structural Order Polymer Lecture Int.Symp., (1981), 239-247.

53 Michaels, A.S., and Parker, R.B., J.Poly.Sci., (1959) **41**, 53.

54 Salame, M., "Diffusion in Polymers", Plastics and Rubber Inst.Conf.Preprints, (1986).

55 Kesting, R.E., "Synthetic Polymeric Membranes", 2nd Edn., J.Wiley & Sons, (1985), 106-186.

56 Monsanto Co., G.B.Pat. 2100181A, (1980).

57 Johnson, R.N., Enc.Pol.Sci.Tech., Ed. Mark, H.F., Gaylord, N.G., and Bikales, N.M., (1964), 11, 447-463.

58 Monsanto Co., G.B.Pat. 1212786, (1968).

59 Monsanto Co., G.B.Pat. 1305330, (1970).

60 Monsanto Co., G.B.Pat. 1590813, (1977).

61 Monsanto Co., G.B.Pat. 2047162, (1980).

62 Monsanto Co., U.S.Pat. 4364759, (1980).

63 Nourpanah, P., PhD Thesis, University of Leeds, (1982).

64 Monsanto Co., U.S.Pat. 4214020, (1980).

65 Noshay, A., and Robeson, M., J.Appl.Pol.Sci., (1976) **20**, 1885-1903.

66 Rose, J.B., Private Communication.

67 Cabasso, I., Klein, E., and Smith, J.K., J.Appl.Pol.Sci., (1976) **20**, 2377-2394.

68 Asahi Kasei Kogyo K.K., Eur.Pat. 86235, (1982).

69 Fielding, R., and Dongworth, M.R., Private Communication.

70 Burrell, H., "Polymer Handbook", Ed. Brandrup, J., and Immergut, E.H., 2nd Edn., J. Wiley & Sons, (1975), IV - 348-349.

71 Friedrich, C., et al., Desalination, (1981) **36**, 39-62.

72 Hansen, C.M., J.Paint Tech., (1967) **39**, 104-117.

73 Teas, J.P., J.Paint Tech., (1968) **40**, 19-25.

74 Hoy, K.L., "Tables of Solubility Parameters", 2nd Edn., Union Carbide Corp., (1985).

75 Monsanto Co., U.S.Pat. 4493629, (1985).

76 Meares, P., "4th BOC Priestley Conference", Royal Society of Chemistry, (1986), 1-25.

77 Lai, J-Y, et al., J.Appl.Pol.Sci., (1986) **32**, 4625-4637.

78 Rogers V., Unpublished Results.

79 Yasuda, H.K., "Plasma Polymerization & Plasma Treatment", Appl.Pol.Symp, No.38, J.Wiley & sons, (1984)

80 Yasuda, H.K., Marsh, H.C., and Tsai, J., J.Appl.Pol.Sci., (1975) **19**, 2157-2166.

81 Yamamoto, M., Sakata, J., and Hirai, M., J.Appl.Pol.Sci., (1984) **29**, 2981.